

UNIVERSIDADE DE SÃO PAULO
INSTITUTO DE FÍSICA DE SÃO CARLOS

MARCELO SAITO NOGUEIRA

Fluorescence lifetime spectroscopy for diagnosis of clinically similar skin
lesions

São Carlos

2016

MARCELO SAITO NOGUEIRA

Fluorescence lifetime spectroscopy for diagnosis of clinically similar skin lesions

Dissertation presented to the Graduate Program in Physics to the Graduate Program in Physics at the Instituto de Física de São Carlos, Universidade de São Paulo to obtain the degree of Master of Science.

Concentration area: Applied Physics

Option: Biomolecular Physics

Advisor: Prof. Dr. Cristina Kurachi

Corrected Version

(Original version available on the Program Unit)

São Carlos

2016

AUTHORIZE THE REPRODUCTION AND DISSEMINATION OF TOTAL OR PARTIAL COPIES OF THIS THESIS, BY CONVENCIONAL OR ELECTRONIC MEDIA FOR STUDY OR RESEARCH PURPOSE, SINCE IT IS REFERENCED.

Cataloguing data reviewed by the Library and Information Service
of the IFSC, with information provided by the author

Nogueira, Marcelo Saito
Fluorescence lifetime spectroscopy for diagnosis
of clinically similar skin lesions / Marcelo Saito
Nogueira; advisor Cristina Kurachi - reviewed
version -- São Carlos 2016.
263 p.

Dissertation (Master's degree - Graduate Program
in Biomolecular Physics) -- Instituto de Física de
São Carlos, Universidade de São Paulo - Brasil ,
2016.

1. Fluorescence lifetime spectroscopy. 2. NADH.
3. PAD. 4. Diagnosis. 5. Skin. I. Kurachi,
Cristina, advisor. II. Title.

I dedicate this thesis to my father
Renê de Jesus Nogueira and my mother Maria Sumie Saito.
You have successfully made me the person I am becoming.
You will always be remembered.

Acknowledgments

After an intensive and very instructive period, I would like to thank my parents, family, friends, mentors, colleagues, institutions responsible for my education and work experience, people responsible for the technical support on these institutions, and entities that provided financial support for the performance of the research presented in this work.

I would like to thank my parents for all support, trust, unconditional love, instruction, patience, comprehension, to give me the freedom to choose my own career and all the necessary assistance to make my goals possible to be achieved.

I thank my friend João Victor for the deep friendship on these last six and a half years, the many and valuable advice, funny moments, TRX training, for giving me support and helping me whenever possible.

I would like to thank Ramon and Sebastião for the friendship, personal and intellectual advice, for opening my eyes to new opportunities, for the assistance in the execution of several steps in this work, and for the strong support during the most difficult period in the study development. There were moments during this work in which I deeply considered giving up on the instrumentation field as it usually involves a long, difficult and little prompt-rewarding process; after having worked most of my awaken hours for sixteen months, I only had at that moment something I could not turn into a paper or patent – an assemble of a portable, though previously existing, device. They showed me, by that time, the importance of what I was doing, the relevance for the future studies, and how I could turn all that hard work into “real stuff” as soon as I was able to collect data and validate the system. For this and for everything else, thank you to you both!

I want to thank Bruno Ono for the friendship, funny moments and experiments together.

I thank the professor Cristina Kurachi for the supervision, friendship, trust, advice, teaching, for giving me the opportunity to work in her group, and for always helping me to find new opportunities.

I want to thank the doctor Ana Gabriela for having accepted working with me, and for being an essential person in the development of the clinical research and for being always willing to help.

I thank the team of Amaral Carvalho Hospital for being always willing to help and providing a pleasant work environment in the hospital.

I would like to thank my friends who are or were part of the Biophotonics Lab (Optics Group) for the support in the difficult moments, for being willing to help whenever possible and for being part of my academic and personal life.

I want to thank my friends from my hometown Itu, my colleagues at the grad course (Physical and Biomolecular Sciences), the 2010 classes at IFSC, and from Embrapa. You always gifted me with happy and comfortable moments, even when you were not physically there. I miss you!

I would like to thank Natalia, for always being kind, and for the personal and professional advice in our talks.

I thank José Dirceu, for the friendship, discussions, suggestions, textual corrections, personal and professional advice.

I want to thank professor Janis for his ideas concerning the time-of-flight measurements in scattering media, and for the assistance in performing the experiments.

I would like to thank Alessandro for the friendship, transmitted knowledge about the fluorescence lifetime system operation during my undergraduate project, and professional collaboration.

I thank Camila for the kindness and assistance on the experiments for the system characterization.

I want to thank professor Vanderlei for being inspiring for many people and for allowing me to work in a research group acknowledged worldwide that is the Optics Group, which is composed by many capable people that are willing to help whenever possible.

I would like to thank the staff from the Optics Group (secretaries, LAT, LIEPO and mechanical workshop teams) for the great assistance on the performance of this work.

I thank the IFSC (Sao Carlos Institute of Physics) for providing the infrastructure and support for my education, execution of events organized by students, access to high technology equipments, access to library and print shop services, possibility to produce customized optical components and mechanical parts. I thank also all people who provide this support, especially those from the Mechanical Workshops, since this work would not be feasible without them.

Last but not least, I would like to thank the financial support institutions (CAPES, CNPq and FAPESP) for the financial support to CePOF, INOF and for the project of prof. Janis (FAPESP process 2015/25908-0), and FAPESP, for the financial support for my scholarship during my Master's project (FAPESP process 2014/16154-0).

I don't believe you have to be better than everybody else. I believe you have to
be better than you ever thought you could be.

Ken Venturi

ABSTRACT

NOGUEIRA, M. S. **Fluorescence lifetime spectroscopy for diagnosis of clinically similar skin lesions**. 2016. 263 p. Master's Thesis (Master of Science) – Sao Carlos Institute of Physics, University of Sao Paulo, Sao Carlos, 2016.

The fluorescence spectroscopy and lifetime analysis in biological tissues has been presented as a technique of great potential for tissue characterization for diagnostic purposes. This potential is due to the main advantages of optical techniques based on fluorescence for diagnosis, which includes the possibility of evaluating the tissue metabolism *in situ*, without removal and processing of the biological sample, through a fast and non-invasive response. Skin lesions were the target interrogated tissue in the present study. They can be clinically classified into two major groups: pigmented and non-pigmented lesions. In each group, the clinical discrimination of benign and malignant lesions may be a complex task, especially for non-experienced clinicians. When these lesions have clinically similar features, the choice of the treatment modality becomes difficult. In this context, auxiliary diagnostic techniques are very important to improve the diagnostic resolution as well as treatment planning and success. Gold standard for skin diagnosis is obtained with the biopsy and further histological analysis. The information about these features is invasive and time consuming. When using a non-invasive procedure such as fluorescence lifetime measurements, the main interrogated fluorophores are NADH (nicotinamide adenine dinucleotide) and FAD (flavin adenine dinucleotide), biomolecules involved in cellular respiration that may provide information on the metabolism of the cells. To differentiate each skin lesion, it is necessary to take into account the contribution of endogenous fluorophores emission such as collagen and elastin, and the absorption of chromophores such as melanin and hemoglobin. In addition to fluorescence decay analysis considering the contribution of fluorophores and chromophores, a stable and portable system is desired for clinical measurements and interrogation of biological tissue *in vivo*. In this study, we have assembled, calibrated, and characterized one of the world's first portable time-resolved fluorescence spectroscopy system for single-point measurements. This system was designed to be robust and user-friendly for clinical applications. The system was calibrated and characterized *in vitro* before the clinical application. It was used for evaluation of the photoaging process in sun-exposed and non-exposed skin and for discrimination of clinically similar skin lesions. Significant statistical differences were observed for 10 parameters when comparing normal and photoaged skin (student's t-test, $p < 0.001$), and for all combinations of non-pigmented and pigmented lesions when using tri-exponential decay parameters (Wilcoxon rank sum test, $p < 0.05$). Both *in vivo* measurements showed promising results and have potential for many applications in dermatology, oncology and aesthetics. Next steps include multivariate data analysis and the determination of the diagnostic resolution of fluorescence lifetime spectroscopy. Further investigation of optical processes related to fluorescence decay changes is necessary, since fluorescence lifetime values in biological tissues reported on the literature are very scarce and heterogeneous and not completely understood.

Keywords: Fluorescence lifetime spectroscopy. NADH. FAD. Diagnosis. Skin.

RESUMO

NOGUEIRA, M. S. **Espectroscopia de tempo de vida de fluorescência para o diagnóstico de lesões de pele clinicamente semelhantes**. 2016. 263 p. Dissertação de mestrado (Mestre em Ciências) – Instituto de Física de São Carlos, Universidade de São Paulo, São Carlos, 2016.

A análise da espectroscopia e do tempo de vida da fluorescência em tecidos biológicos vem sendo apresentada como uma técnica com grande potencial para a caracterização tecidual com finalidade diagnóstica. Esse potencial é devido às principais vantagens das técnicas ópticas de diagnóstico baseadas em fluorescência, que possibilitam avaliar o metabolismo *in situ*, sem a necessidade de remoção e processamento da amostra biológica, com uma resposta rápida e não-invasiva. Lesões de pele foram os tecidos investigados no presente estudo. Elas podem ser clinicamente classificadas em dois grandes grupos: pigmentadas e não pigmentadas. Em cada grupo, a discriminação clínica de lesões benignas e malignas pode ser uma tarefa complexa, principalmente para médicos com pouca experiência. Quando essas lesões apresentam características clínicas semelhantes, a escolha do tipo de tratamento torna-se difícil. Nesse contexto, técnicas auxiliares de diagnóstico são de grande relevância para melhorar a resolução de diagnóstico, assim como o planejamento e o sucesso do tratamento. O padrão ouro para o diagnóstico do câncer de pele é obtido por meio da biópsia e posterior análise histopatológica. A obtenção de informações sobre essas características é invasiva e consome bastante tempo. Ao utilizar procedimentos não-invasivos como medidas de tempo de vida de fluorescência, os fluoróforos de mais investigados são o NADH (nicotinamida adenina dinucleotídeo) e o FAD (flavina adenina dinucleotídeo), biomoléculas envolvidas na respiração celular que podem fornecer informação sobre o metabolismo das células. Para diferenciar cada tipo de lesão de pele, é necessário levar em conta a contribuição da emissão de fluoróforos endógenos como o colágeno, elastina e da absorção de cromóforos como melanina e hemoglobina. Além da análise do decaimento de fluorescência considerando a contribuição de fluoróforos e cromóforos, um sistema estável e portátil é desejado para medidas clínicas e investigação de tecidos biológicos *in vivo*. Nesse estudo, nós montamos, calibramos e caracterizamos um dos primeiros sistemas portáteis do mundo para espectroscopia de fluorescência resolvida no tempo para medidas pontuais. Esse sistema foi projetado para ser robusto e amigável ao usuário em aplicações clínicas. O sistema foi calibrado e caracterizado *in vitro* antes das aplicações clínicas. Ele foi utilizado para avaliação do processo de fotoenvelhecimento em pele exposta e não-exposta ao sol e para a discriminação de lesões de pele clinicamente semelhantes. Diferenças estatísticas significativas foram observadas para 10 parâmetros na comparação entre pele normal e fotoenvelhecida (teste t-student, $p < 0.001$) e para todas as combinações de lesões pigmentadas e não-pigmentadas ao utilizar parâmetros do decaimento triexponencial (teste Wilcoxon rank sum, $p < 0.05$). Ambas medidas *in vivo* mostraram resultados promissores e um potencial para muitas aplicações em dermatologia, oncologia e estética. As próximas etapas incluem análise multivariada de dados e determinação da resolução de diagnóstico da espectroscopia de tempo de vida de fluorescência. Uma maior investigação dos processos ópticos relacionados a mudanças nos decaimentos de fluorescência é necessária, pois o número de valores de tempo de vida de fluorescência em tecidos biológicos reportados na literatura é escasso e os valores são heterogêneos e não completamente compreendidos.

Palavras-chave: Espectroscopia de tempo de vida de fluorescência. NADH. FAD. Diagnóstico. Pele.

LIST OF FIGURES

Figure 1 -	Jablonski diagram for the energy levels and spectra related to absorption (violet, blue), fluorescence (green) and phosphorescence (red). Radiative transitions are represented by solid arrows and non-radiative (internal conversion and vibrational relaxation) transitions, by dashed arrows. The dotted arrow represents the intersystem crossing from $S_{1,0}$ to $T_{1,0}$. The spectra for lower energy processes are presented for longer wavelengths.....	38
Figure 2 -	Excitation and emission spectra of the main biological fluorophores in biological tissues. Due to the spectral overlap of many tissue endogenous fluorophores, the extraction of particular information about each one of them remains a challenge for optical diagnostics.....	39
Figure 3 -	Optical window for biological tissues, considering the contribution of the main chromophores in the visible and near-infrared range. The choice of excitation and emission wavelengths in this spectral window allows information extraction or treatment procedures in deeper layers of tissue.	40
Figure 4 -	The apparent absorbance of a 50% relative increase of epidermal keratin in the wavelength regions UVB (280-320 nm), UVA (320-400 nm) and visible (400-700 nm). So, the absorbance in these regions may increase when keratin-rich cells in the epidermis proliferate in order to repair the skin damage due to UV radiation.	40
Figure 5 -	Principle of time-domain fluorescence lifetime techniques. The light pulse excites the sample, and the fluorescence intensity is registered for each time after the excitation pulse. The result is a mono or multiexponential decay. A mono-exponential decay has its lifetime τ and is represented by the red or blue lines, and the green and red dashed curve is a bi-exponential decay resulted from a composition between the mono-exponential decays represented in the same graph.....	43
Figure 6 -	Principle of frequency-domain fluorescence lifetime techniques. The intensity modulated light excites the sample, and the time-resolved intensity is measured for the fluorescence emission of the sample and for a timing reference signal (such as reflected or scattered light). By comparing the detected signals for the sample and reference, the	

modulation m and phase shift ϕ are calculated and compared for each sample. Measured mono-exponential decays are represented by curves in blue or red and bi-exponential decays, by the green and red dashed curve. 43

Figure 7 - Principle of Time-Correlated Single Photon Counting (TCSPC). The sample is excited using a sub-ns pulse for several detection periods, and only the first detected photon is acquired for each pulse. In the end of the measurement, the detected photons are summed for each sampling interval, and time-of-flight signals or fluorescence decays are generated..... 44

Figure 8 - Fundamentals of TCSPC instrumentation. When the light pulse is released, an electrical signal is sent to the CFD, which measures the arrival time of this pulse. The TAC starts to count the time and stops when the CFD measures the arrival time of the first emission photon. The signal can be amplified by using the PGA or suppressed by the WD. Finally, the ADC converts the voltage value to a photon count in a determined sampling interval. This process is repeated many time to generate a temporal photon distribution. 45

Figure 9 - When using the reverse start-stop mode at TCSPC measurements, the principles of this technique remain the same, but the emission signal is used to start the voltage generation by the TAC and the light pulse, to stop the voltage increase. The reverse mode allow the TAC to work only at the rate of photon detection events, which is much better than the classic mode, since the TAC would need to work at rates much higher than excitation pulse rates..... 46

Figure 10 - Multiphoton imaging tool Dermalnspect® 110 and a modified Dermalnspect® instrument that allow the collection of fluorescence lifetime images in four spectral channels and hyperspectral images using an specific spectrometer module. 52

Figure 11 - Experimental setup for multiphoton imaging described at (52). This system is also able to perform two-photon fluorescence, second-harmonic generation and multispectral two-photon emission measurements. The components are: L: lenses, $\lambda/2$: half-wavelength broadband waveplate, PBS: calcite polarizing beam splitter, M: mirrors, S: electronic shutter, G: galvanometer mirrors, CCD: color CCD camera, TL: microscope tube lens, Sm: spherical mirrors, R: metallic

	ring, PZT: piezoelectric stage, OF: multimode optical fiber, and PMT: photomultiplier tube.	54
Figure 12 -	A) A flexible wide-field FLIM endoscope using pulsed blue diode laser, a clean-up filter (F1), a multimode fibre (MMF), steel ferrule (SF), a coherent fibre-optic bundle (CFB), a microscope objective (O), tube lens (L2 or L3), a CCD camera or GOI, a switchable mirror (M). B) Whole-field fluorescence lifetime imaging system, based on a time-gated image intensifier and a solid-state laser oscillator–amplifier.	55
Figure 13 -	A) Optical design and electronic configuration of a simultaneous time-andwavelength-resolved fluorescence spectroscopy system with a single optical fiber as a probe for excitation delivery and fluorescence collection. B) Multispectral FLIM endoscopy system. The system components are: BS: Beam sampler, DM: Dichroic mirror, M: Mirror, F: Filter, L: Lens. C) Combined fluorescence lifetime imaging-reflectance confocal microscopy (FLIM-RCM) system. The abbreviations in the system are: UV: ultraviolet, OL1: 45 mm focal length triplet lens, DM: dichroic mirrors, F: filters, MCP-PMT: micro-channel plate photomultiplier tube, BS: beamsplitter, PD: photodiode, OL2: 1.0 NA objective lens, L: lenses, PH: pinholes, APD: avalanche photodiode, HWP: half wave plate, POL: polarizer, QWP: quarter wave plate, PBS: polarizing beamsplitter. D) A dual-modality optical coherence tomography and fluorescence lifetime imaging microscopy system. The abbreviations of components of this system are: La1-La5: free-space collimation and coupling lenses, Lf1-Lf7: fiber-connected collimation and coupling lenses, NDF: neutral density filter, M1-M4: mirrors, DM1-DM4: dichroic mirrors, and F1-F3: filters.	56
Figure 14 -	Measurement setup assembled over an optical bench used for performing the fluorescence lifetime investigation. The system may be relatively compact but not ideal to be transported with optical, mechanical and electronic stability.	57
Figure 15 -	Optical layout of the time-resolved fluorescence spectrometer that allows measurements of fluorescence decays in 16 channels. The entire dataset for measurements using both lasers consists of two sets of 32 spectrally resolved fluorescence decays.	58

Figure 16 -	Optical setup of the improved time-resolved fluorescence spectrometer system. The system size was reduced and the possibility of diffuse white light reflectance measurements was added.	59
Figure 17 -	Transportable trolley that houses the entire time-resolved fluorescence spectrometer. The trolley has dimensions 182 cm x 70 cm x 55 cm and allow the system transportation with stability, but it remains not compact.....	60
Figure 18 -	Compact Simple-Tau 130 Table-Top TCSPC system from the Becker & Hickl GmbH company in the exposition of SPIE Photonics West conference.	61
Figure 19 -	Schematic drawing of the components for fluorescence spectra and fluorescence lifetime acquisition.....	66
Figure 20 -	A) Previous fluorescence lifetime system assembled over an optical bench. B) System assembly before its complete assembling into the suitcase. C) The system size was reduced for almost half of its previous volume without the computer cabinet. D) System assembly after its encasement provides protection for its components and a user-friendly design for system operator by exhibiting a control panel with access to external controls and the filter holder.	67
Figure 21 -	Last version of the filter holder without the light collimators on the its entrance and exit. The filter holder was designed to be closed, compact, functional, stable, easy to machine, and to ensure a faster filters exchange during measurements.....	70
Figure 22 -	A) Movements of the sliding parts for fast filters exchange during measurements. B) The sliding parts can be opened for filters replacement when it is necessary. C) The step between sliding parts allow their sliding without rub. D) The correction of positions and angles of the light collimators is performed by controlling the depth of the screws in the input part of the front wall of the filter holder.	71
Figure 23 -	The second floor for the system components was designed to support and fix a laser and two external controls and to have a reduced size for air circulation and less weight.	73
Figure 24 -	Air exits for coolers of the power supply, lasers and computer processor are positioned at different sections of the suitcase and the coolers direction was optimized to provide air exchange with external environment or air circulation inside the suitcase.	74

Figure 25 -	Fixation parts (aluminum angles and custom channels) for lasers, and power supply were designed to easy machining and low weight.	75
Figure 26 -	A) Encasement part for system components protection and system operator access to the control panel. B) Protection part for the laser cooler. C) Protection part for the power supply cooler. D) Protection part for the laser exits. All protection parts provide visual comfort for patients and doctor in clinical environment.	76
Figure 27 -	An aqueous solution of 0.5% Lipofundin® was used as scattering medium for determination of the system instrument response function. Measurements were done in a cuvette using a proper support for the optical fiber connection.	77
Figure 28 -	The Rhodamine 6G solution was used to evaluate the calibration of the fluorescence lifetime system, by comparing the obtained lifetime with that reported in the literature. The same support as for the scattering medium was used for Rhodamine measurements.	77
Figure 29-	Optical processes on biological tissues may involve scattering, absorption, fluorescence, phosphorescence, specular and diffuse reflection, direct and diffuse transmission. They are usually complex to be analyzed, since the analysis of each individual interaction is not possible, but only the global resulted effect.	78
Figure 30 -	In order to calibrate the system for determination of the time shift of the maximum intensity of the laser pulse, the optical fiber was positioned at a distance L from a reflective surface. By subtracting the time delay due to the system synchronization and the light travel from the detected pulse and fixing the distance L for all measurements, it is possible to make a correction for the time position of this pulse.	80
Figure 31 -	Measurements in scattering media were performed using a holder to keep a fixed distance between the excitation and collection fibers.	80
Figure 32 -	Clinical measurements using the portable fluorescence lifetime spectroscopy system. The system is very compact and fits well in many places.	82
Figure 33 -	Clinical sites for skin measurements of sun-exposed at dorsal forearm (A) and non-exposed at volar arm (B) regions. The optical probe was designed to allow a more uniform pressure, less external illumination and set angulation during clinical measurements.	83

Figure 34 -	The excitation sources wavelength and spectral window of bandpass filters used on this study are presented by the purple and blue lines and rectangles. The excitation and collection were made for spectral regions where the absorption and emission of targeted endogenous fluorophores are available without many interferences from the other ones. The fluorophores spectra are also shifted at biological tissues, which may make the choice of optical filters more suitable for the targeted fluorophores.....	84
Figure 35 -	Laser pulse compared to IRF curves obtained for 378 nm and 445 nm light backscattering. The observed decay is highly faster than the most of the biological tissues molecules.	87
Figure 36 -	Absorption and fluorescence spectra of Rhodamine 6G at 378 nm and 445 nm excitation. The typical bands of rhodamine indicate that the solution is well standardized.	88
Figure 37 -	Decay curves for Rhodamine 6G, obtained at 378 nm and 445 nm excitations and 20 MHz (left) and 50 MHz (right) repetition rate. The 20 MHz decay can be observed until the intensity returns to background values and may lead to more stable fluorescence lifetime values after the decay curve analysis.....	89
Figure 38 -	Fluorescence lifetime as a function of laser gain at 378 nm excitation and 20 MHz (left) and 50 MHz (right) repetition rate.....	90
Figure 39 -	Fluorescence lifetime as a function of laser gain at 445 nm excitation and 20 MHz (left) and 50 MHz (right) repetition rate.....	90
Figure 40 -	The detected laser pulses for 378 nm (left) and 445 nm (right), 44.0 mm distance between fibers and varying the scatterer concentrations.....	91
Figure 41 -	The FWHM of time-of-flight signals for distances of 14.5 mm (A), 24.4 mm (B), 33.3 mm (C), and 44.0 mm (D) increase with the scatterer concentration. As the scatterer concentration and distances increase, the 378 nm FWHM becomes higher than the 445 nm one, which suggests that the wavelength-dependent scattering effects become relevant for the distances and concentrations where the FWHMs for these wavelengths are separated.	92
Figure 42 -	The time shift of time-of-flight signals for distances of 14.5 mm (A), 24.4 mm (B), 33.3 mm (C), and 44.0 mm (D) increase with the scatterer concentration. The investigated scattering effects may be mostly related to wavelength-independent processes, since there is	

	almost no difference between the time shift values for each wavelength.	92
Figure 43 -	The FWHM of time-of-flight signals for 378 nm low (A) and high (B) photon count rates and 445 nm low (C) and high (D) photon count rates increases with scatterer concentration. The behavior of this increasing is different for each wavelength, and the FWHM did not increase more for distances higher than 33.3 mm and low scatterer concentrations.	93
Figure 44 -	The time shift of time-of-flight signals for 378 nm low (A) and high (B) photon count rates and 445 nm low (C) and high (D) photon count rates, in most of cases, increase almost linearly with the scatterer concentration. An irregular change in the linear tendency was observed for the 0.5% concentration.	94
Figure 45 -	The detected laser pulses for 378 nm (left) and 445 nm (right), 2% of scatterer (Lipofundin®) concentrations and varying the distance between fibers.	94
Figure 46 -	The FWHM of time-of-flight signals for 0.25 % (A), 0.5% (B), 1% (C) and 2% (D) concentration increases with distances between fibers. The FWHM sensitivity for wavelength-dependent scattering processes starts from the 44.0 mm distance for 1% concentration or 24.4 mm distance for 2%.	95
Figure 47 -	The time shift of time-of-flight signals for 0.25 % (A), 0.5% (B), 1% (C) and 2% (D) concentration increases with distances between fibers. The time shift may be more sensitive to wavelength-independent scattering processes, since the time shift values for each wavelength are similar. For the 1% and 2% concentration, a small difference is observed in the time shift for each wavelength.	96
Figure 48 -	Fluorescence spectra of sun-exposed and non-exposed skin for 378 nm (left) and 445 nm (right) excitation. The areas in purple and blue are the spectral window of bandpass filters used in fluorescence lifetime measurements.	97
Figure 49 -	The decay curves of sun exposed and non-exposed skin show some differences for all combinations of excitation sources and optical filters. (A) shows this comparison using 378 nm excitation and a 418 nm longpass filter, B) using 445 nm excitation and 475 nm longpass filter,	

	C) using 378 nm excitation and (440 ± 20) nm bandpass filter and D) using 445 nm excitation and (510 ± 15) nm bandpass filter).	98
Figure 50 -	Boxplots for parameters obtained in the data analysis for 378 nm excitation and longpass filter.	100
Figure 51 -	Boxplots for parameters obtained in the data analysis for 378 nm excitation and bandpass filter.	101
Figure 52 -	Boxplots for parameters obtained in the data analysis for 445 nm excitation and longpass filter.	102
Figure 53 -	Boxplots for parameters obtained in the data analysis for 445 nm excitation and bandpass filter.	103
Figure 54 -	The boxplots for parameters of bi-exponential decay fitting (378 nm excitation) show a good discrimination between the groups, based on the Wilcoxon rank sum test. The tendencies for these parameters show an agreement with studies evaluating metabolic changes for comparisons between BCCs and HNs (a_1 and τ_1 parameters), pigmented BCCs and pigmented SKs (τ_1 and τ_2 parameters), suspected melanomas and pigmented SKs (τ_1 parameter). The tendency for average lifetimes shows an agreement with other studies involving skin measurements only when comparing BCCs and HNs.	109
Figure 55 -	The boxplots for relative coefficients and lifetimes of the tri-exponential decay fitting (378 nm excitation) also show a good discrimination between the groups (Wilcoxon rank sum test). The first lifetime component may be related to the free NADH, collagen and elastin, the second one to bound NADH, collagen and elastin, and the third one to melanin.	110
Figure 56 -	The boxplots for tri-exponential average lifetimes and fractional contribution (378 nm excitation) also show a satisfactory discrimination between the groups (Wilcoxon rank sum test). Compared to the same parameters for the bi-exponential case, the discrimination between some groups of pigmented lesions was possible. The tendency for average lifetimes also shows an agreement with other studies evaluating skin measurements only for the comparison between BCCs and HNs.	111
Figure 57 -	The boxplots for parameters of bi-exponential decay fitting (445 nm excitation) show a good discrimination between the non-pigmented lesions (Wilcoxon rank sum test), and only the pigmented SK and pigmented BCC pair was able to be discriminated among the	

pigmented lesions. The tendencies for these parameters show an agreement with studies evaluating metabolic changes only for the comparison between BCCs and SHs (a_1 and τ_1 parameters). The tendency for average lifetimes shows an agreement with other studies involving skin measurements only when comparing the average lifetime for pigmented SKs and pigmented BCCs. The opposite tendency was observed for intensity lifetimes of BCCs compared to SHs and HNs..... 114

Figure 58 - The boxplots for relative coefficients and lifetimes of the tri-exponential decay fitting (445 nm excitation) show a good discrimination between the groups (Wilcoxon rank sum test). Only the BCC/HN pair was not discriminated with these parameters, but it can be done with the tri-exponential fractional contributions. The first component may be associated to bound FAD, elastin and lipopigments, the second one to free FAD, elastin and lipopigments, and the third one to melanin..... 115

Figure 59 - The boxplots for tri-exponential average lifetimes and fractional contribution (445 nm excitation) also show a satisfactory discrimination between the groups (Wilcoxon rank sum test). Compared to the same parameters for the bi-exponential case, the discrimination between pigmented SKs and suspected melanomas was possible. The tendency for average lifetimes shows an agreement with other studies involving skin measurements only when comparing the average lifetime for pigmented SKs and pigmented BCCs..... 116

Figure 60 - The boxplots for the standard deviation for bi-exponential parameters (378 nm excitation) show discrimination only between the pigmented SK and pigmented BCC groups (Wilcoxon rank sum test). 120

Figure 61 - The boxplots for the standard deviation for tri-exponential relative coefficients and lifetimes (378 nm excitation) show the discrimination between the two groups of non-pigmented lesions and one group of pigmented ones (Wilcoxon rank sum test). 121

Figure 62 - The boxplots for the standard deviation for tri-exponential average lifetimes and fractional contribution (378 nm excitation) show the discrimination only between one group for both pigmented and non-pigmented lesions (Wilcoxon rank sum test). Compared to the standard deviations for the relative coefficients and lifetimes, the discrimination between SHs and HNs was not possible..... 122

Figure 63 -	The boxplots for the standard deviation for bi-exponential parameters (445 nm excitation) show discrimination only between SHs and HNPs, pigmented SKs and pigmented BCCs (Wilcoxon rank sum test).	124
Figure 64 -	The boxplots for the standard deviation for tri-exponential relative coefficients and lifetimes (445 nm excitation) show the discrimination between the two groups of non-pigmented lesions and one group of pigmented ones (Wilcoxon rank sum test).....	125
Figure 65 -	The boxplots for the standard deviation for tri-exponential average lifetimes and fractional contribution (445 nm excitation) show the discrimination only between two groups of non-pigmented lesions (Wilcoxon rank sum test).....	126
Figure 66 -	Main system components (without repetition) to optimize the arrangement and calculation of suitcase volume.....	141
Figure 67 -	Arrangement of the system components taking into account their mechanical, thermal, electronic, optical stability, the system cooling, the feasibility to be used on a clinic, the volume reduction and the weight to be transported into the suitcase.	143
Figure 68 -	When using the reverse start-stop mode, the delay in the reference channel needs to be adjusted to stop the TAC with the correct laser pulse.	145
Figure 69 -	The position of recorded waveform depends on the SYNC and CFD cables length. If the signal is shifted too much for the left, the peak of TAC characteristic may appear or the left part of this waveform may drop abruptly to zero.	146
Figure 70 -	Example of waveform obtained after the cables lengths and TAC parameters are correctly adjusted.....	146
Figure 71 -	Schematic drawing for the connections between the system components.	149
Figure 72-	The fixation of the motherboard in the suitcase wall required spacers that allow the motherboard contacts to be grounded with the metallic shell of the suitcase.	151
Figure 73 -	The structure for the motherboard's fixation allows its electrical grounding and spacing from the suitcase walls.....	152
Figure 74 -	Links between the pins of each DE-15 connector of the wires connecting lasers to external controls, and the external controls to a cable of DCC-100 board.	153
Figure 75 -	Comparison between the length of the cables from the commercial system and the home-made cables.....	154

Figure 76 - Main parts for mounting the support structure for the filter.	155
Figure 77 - First version of the filter holder. It was projected for a fast and easy filter changes during measurements. The optical fiber connectors are threaded to the central parts, so that the distance between them can be changed and a lens can be positioned to focus the input light in the core of the output fiber.	156
Figure 78 - Second version of the filter holder. This version was projected with a support for a beamsplitter that splits the input signal to be detected in the spectrometer and photomultiplier tube. The connections for the output collimators were done after this project.	157
Figure 79 - Third version of the filter holder. In the central input part, the angular position can be optimized to focus the input beam into the core of the collection fiber.	157
Figure 80 - Absorbance for the longpass filters used in this study.	159
Figure 81 - Absorbance for the bandpass filters used in this study.	159

ABBREVIATION AND ACRONYMS LIST

ADC - analog-to-digital converter
AF - autofluorescence
AGE - advanced glycation end products
APD - avalanche photodiode
BCC -Basal cell carcinoma
BiExp – bi-exponential
CCD - charge-coupled device
CFD - constant fraction discriminator
DNA - deoxyribonucleic acid
ECM - extracellular matrix
FAD - flavin adenine dinucleotide
FLIM - Fluorescence Lifetime Imaging Microscopy
FP - fibrous papule
FPGA - field-programmable gate array
FRET - Förster resonance energy transfer
FWHM - full width at half maximum
Hb – deoxyhemoglobin
HbO₂ – oxyhemoglobin
HN - hypochromic nevi
ICCD - intensified charge-coupled device
IRF - instrument response function
IVUS - intravascular ultrasound
LCD - liquid crystal display
MCP-PMT - micro-channelplate photomultiplier tube
NADH - nicotinamide adenine dinucleotide
NA - numerical aperture
Nd:YAG - neodymium-doped yttrium aluminium garnet
PCI - Peripheral Component Interconnect
PGA - programmable gain amplifier
PMT - photomultiplier tube
PpIX - protoporphyrin IX

PVC - poly(vinyl chloride)
SH - sebaceous hyperplasia
SK - seborrheic keratosis
TAC - time-to-amplitude converter
TCSPC - time-correlated single photon counting
TDFL - time domain fluorescence lifetime
TriExp – tri-exponential
USB - Universal Serial Bus
UV –Ultraviolet
UVA – Ultraviolet A
UVB – Ultraviolet B
WD - window discriminator

CONTENTS

1 INTRODUCTION	31
1.1 Clinically similar skin lesions	31
1.2 Non-pigmented skin lesions	32
1.2.1 Fibrous papule	32
1.2.2 Sebaceous hyperplasia	32
1.2.3 Hypochromic Nevus	33
1.2.4 Basal Cell Carcinoma	33
1.3 Pigmented skin lesions	34
1.3.1 Pigmented seborrheic keratosis	34
1.3.2 Melanoma	34
1.4 Oncologic and dermatologic applications of optical diagnosis based on fluorescence techniques	35
1.5 Fluorescence fundamentals and metabolic changes	36
1.5.1 Fluorescence principles	36
1.5.2 Fluorescence spectroscopy, endogenous fluorophores and chromophores	39
1.5.3 Redox Ratio	41
1.6 Fluorescence techniques and molecular interactions	42
1.6.1 Fluorescence lifetime techniques	42
1.6.2 Time domain fluorescence lifetime measurements	47
1.6.3 Fluorescence lifetime and molecular microenvironment sensing	49
2 BIBLIOGRAFIC REVIEW	51
2.1 Clinical fluorescence lifetime imaging systems	51
2.2 Clinical fluorescence lifetime systems for single-point measurements and their portability	57
3 OBJECTIVES	63
3.1 General Objectives	63
3.2 Specific Objectives	63
4 METHODOLOGY	65
4.1 Fluorescence lifetime spectroscopy system	65
4.2 Customizing for clinical measurements	66
4.2.1 Planning, positioning and compacting the fluorescence lifetime system	67
4.2.2 Computer assembling inside a metallic suitcase, system connections and instrumentation synchronization	68
4.2.3 Filter holder	70

4.2.4 Second floor parts	72
4.2.5 Fixation parts and system cooling	73
4.2.6 Enclosing and protection parts	75
4.3 Fluorescence lifetime system characterization and measurements	76
4.3.1 System characterization	76
4.3.2 Measurements at turbid media	78
4.4 Clinical measurements	81
4.4.1 Clinical evaluation	81
4.4.2 Excitation and collection spectral windows	83
4.4.3 Data processing	85
5 RESULTS AND DISCUSSION	87
5.1 Fluorescence lifetime spectroscopy system characterization	87
5.1.1 Instrument Response Function and temporal broadening of laser pulse	87
5.1.2 System calibration	88
5.1.3 Fluorescence lifetime changes as a function of laser gain	89
5.2 Time of flight measurements on scattering media	90
5.2.1 Increasing the scatterer concentration	90
5.2.2 Increasing the distance between excitation and collection fibers	94
5.3 Photoaging process at sun exposed and non-exposed skin	97
5.3.1 Photoaging process and fluorescence lifetime	97
5.3.2 Fluorescence decays	98
5.3.3 Boxplots and data discrimination	99
5.4 Clinically similar skin lesions	105
5.4.1 Fluorophores and chromophores for clinically similar skin lesions	105
5.4.2 Bi-exponential and tri-exponential decay parameters	106
5.4.3 Standard deviation for bi-exponential and tri-exponential decay parameters	119
6 CONCLUSIONS	129
7 PUBLICATIONS AND CONFERENCE PRESENTATIONS	131
REFERENCES	133
APPENDICES	141
Appendix A - System components (without repetition) to optimize the arrangement and calculation of suitcase volume	141
Appendix B - Arrangement of the system components taking into account their mechanical, thermal, electronic, optical stability, the system cooling, the feasibility to be used on a clinic, the volume reduction and the weight to be transported into the suitcase	143
Appendix C - SYNC and CFD Signal Path Length	145

Appendix D - Components of the computer assembled inside the suitcase and of the system instrumentation	147
Appendix E - Connections between the system components	149
Appendix F – Fixation of motherboard in the suitcase wall.....	151
Appendix G - Construction of cables with different lengths for synchronization between electrical and optical signals	153
Appendix H – Versions and components of the filter holder	155
Appendix I – Longpass and bandpass optical filters.....	159
Appendix J – Filter holder base for fixation in suitcase wall.....	161
Appendix K – Correction on the filter holder’s base.....	163
Appendix L – Support (central part) for fiber connector.....	165
Appendix M – SMA 905 fiber connector	167
Appendix N – Sliding part for optical filters – part I.....	169
Appendix O – Sliding part for optical filters – part II.....	171
Appendix P – Sliding part for optical filters – part III	173
Appendix Q – Sliding part for optical filters – part IV	175
Appendix R – Upper part for movement restriction sliding parts.....	177
Appendix S – Lateral supports I	179
Appendix T – Lateral supports II	181
Appendix U – Assembled filter holder – version 1	183
Appendix V – Beamsplitter holder without holes for collimators	185
Appendix X – Enclosing part for beamsplitter holder	187
Appendix Y – Covering part for beamsplitter holder	189
Appendix Z – Assembled filter holder – version 2	191
Appendix AA – Part for adjustment of angular position of collimators.....	193
Appendix BB – Support for angular positioner of fiber collimator.....	195
Appendix CC – Assembled filter holder – version 3	197
Appendix DD – Base part for the suitcase’s second floor.....	199
Appendix EE – Support for the suitcase’s second floor.....	201
Appendix FF – Assembled second floor for the suitcase.....	203
Appendix GG – Custom channels for fixation of power supply	205
Appendix HH – Angles for fixation of TCSPC boards.....	207
Appendix II – Angles for fixation of photomultiplier tube	209
Appendix KK – Angles for fixation of laser in the first floor	211
Appendix LL – Angles for fixation of the computer monitor	213

Appendix MM – Support for fixation of the computer monitor	215
Appendix NN – Support for fixation of the laser in the second floor – part I	217
Appendix OO – Support for fixation of the laser in the second floor – part II.....	219
Appendix PP – Enclosing and protection part – System front panel	221
Appendix QQ – Protection part for laser cooler (first floor)	223
Appendix RR – Protection part for power supply cooler	225
Appendix SS – Protection part for filter holder.....	227
Appendix TT – Protection part for lasers	229
Appendix UU – Assembled protection parts	231
Appendix VV – Protection for the laser cooler (first floor)	233
Appendix XX – Optical fiber connector	235
Appendix YY – Protection part for fiber probe	237
Appendix ZZ – Fixation part for optical fiber inside the fiber probe	239
Appendix AAA – Assembled fiber probe	241
ANNEXES	243
Annex A – 378 nm laser specifications.....	243
Annex B – 445 nm laser specifications.....	245
Annex C – Hybrid photomultiplier tube specifications.....	247
Annex D – SPC-150 Board specifications	249
Annex E – DCC-100 Board specifications.....	251
Annex F – Transmission spectra from bifurcated optical fiber	253
Annex G – Research Ethics Committee approval.....	255
Annex H – Confidentiality Agreement.....	257
Annex I – Letter for the analysis of the project sent to the Research Ethics Committee of Amaral Carvalho Hospital.....	259
Annex J – General data about the research project at Amaral Carvalho Hospital	261
Annex L – Authorization for the development of the proposed research project	263

1 INTRODUCTION

1.1 Clinically similar skin lesions

The incidence of skin cancers (non-melanoma and melanoma) has been increasing over the past decades. According to the World Health Organization (WHO) (1), between 2 and 3 million non-melanoma skin cancers and about 132,000 of cutaneous melanoma lesions occur globally each year. The skin cancer is also the malignant neoplasm with the highest incidence in the Brazilian population, corresponding to about 20% of all diagnosed tumors. 182,130 new diagnosed cases of non-melanoma skin cancer and 5,890 of melanoma cancers were estimated for 2014, according to the Brazilian National Cancer Institute (INCA). (2) For melanoma treatment, the conventional method, i.e., the surgical excision, is only effective on early lesions and its recurrence ranges from 7% to 51%. (3) Diagnosis is one of the most relevant medical factors, especially for cancer, early diagnosis plays a significant role on improving quality of life and decreasing mortality and morbidity rates. Clinically similar lesions reduce the diagnostic resolution, especially for the non-experienced professionals, potentially resulting in a delayed cancer detection and further treatment. One approach to improve diagnostic resolution at clinical site is the use of auxiliary diagnostic techniques to improve the planning and thus increase success of treatment.

Physicians may perform the clinical analysis of skin lesions through palpation and five different methods or combination of them:

- Visual inspection;
- Visual inspection using a manual dermatoscope;
- Visual analysis using a videodermatoscope;
- Computational analysis of skin lesion(s) image on a workstation;
- Remote Analysis by exchange of information (images and clinical data) between medical specialists (telemedicine). (4)

Even with the use of current techniques for skin lesions analysis, benign and malignant lesions with similar clinical features may be confused by professionals with less experience in the dermatology field. These techniques may be complemented by

non-invasive diagnostic techniques to assist the clinicians with an analysis *in situ*, i.e., directly on the patient, without removal and processing of the biological sample.

Clinically similar skin lesions may be divided into pigmented and non-pigmented lesions. The non-pigmented lesions investigated in this study are the fibrous papules, sebaceous hyperplasias, hypochromic nevi (benign lesions) and basal cell carcinomas (malignant lesions) and the pigmented lesions are pigmented seborrheic keratosis (benign) and melanoma (malignant).

1.2 Non-pigmented skin lesions

1.2.1 Fibrous papule

Fibrous papules (FPs) are small and benign protuberances on the skin and are present mainly as a solitary papule or as several dome-shaped, skin-colored, reddish, or pigmented lesions occurring usually on the face, very commonly in the nasal region of adults. They may be confused with basal cell carcinomas and intradermal nevi. (5) When in doubt, a biopsy is performed and the tissue is removed for histopathological analysis. The analyses results indicate whether there is an increase on the blood vessels in the skin dermis and underlying fibrous stroma. Lesion recurrence for FPs is not commonly seen after biopsy removal.

1.2.2 Sebaceous hyperplasia

Sebaceous hyperplasia (SH) is a benign lesion characterized by the increase of the sebaceous glands and is presented as yellowish, small (less than 3 mm in diameter), and solitary or multiple papules on the face, particularly on the forehead of middle-aged individuals and older. SH lesions often reveal a central dell and are often suspected to be basal cell carcinomas due to their similar characteristics, such as telangiectasia. A biopsy may be necessary if the diagnosis is uncertain. (5)

1.2.3 Hypochromic Nevus

The hypochromic nevi (HN) are hypomelanotic lesions that remain stable throughout life and are present in three clinical forms: an isolated, circular or rectangular macule or, less commonly, a dermatomal or quasi-dermatomal pattern or a systematized (unilateral whorls or streaks) form. (5) HN occurs commonly on the trunk and proximal extremities, typically does not cross the midline and may be confused with basal cell carcinoma. Several authors believe that HN belongs to cutaneous mosaicism. (5)

1.2.4 Basal Cell Carcinoma

Basal cell carcinoma (BCC) is a malignant neoplasm derived from nonkeratinizing cells that originate in the basal layer of the epidermis. BCC usually develops on sun exposed areas of the head and neck but it can occur anywhere on the body and, if left untreated, it can become invasive and may result in substantial tissue damage (metastasis is a rare event). BCC features include translucency, ulceration, telangiectasias, and the presence of a rolled border. (5)

There are two subtypes of BCCs that show differential diagnosis with non-pigmented and the pigmented lesions presented in this study: the nodular BCCs and the pigmented BCCs. Nodular BCC is the most common clinical subtype of BCC. It appears as a translucent papule or nodule usually with telangiectasias and often a rolled border. The differential diagnosis of nodular BCC includes dermal nevus and amelanotic melanoma, if it is not pigmented. The pigmented BCC is a subtype of nodular BCC that exhibits increased melanization and appears as a hyperpigmented, translucent papule which may also be eroded. The differential diagnosis includes nodular melanoma. (5)

1.3 Pigmented skin lesions

1.3.1 Pigmented seborrheic keratosis

Seborrheic keratoses (synonyms: senile wart, senile keratosis, seborrheic verruca, basal cell papilloma) are benign skin tumors most commonly found in the over-30 age group. These lesions typically begin as flat, sharply demarcated, brown macules and can appear on any part of the body except the mucous membranes. As they progress, they become polypoidal, with an uneven surface. Their usually dull or lackluster surface commonly shows a “warty” topography with multiple plugged follicles and fronds. Seborrheic keratoses have the follicular prominence as one of their hallmarks. These lesions have colors which may vary from a pale brown with pink tones to dark brown or black, depending on their pigmentation degree. (5)

The confusion between seborrheic keratoses and dysplastic nevi, and the potential malignant progression in the case of the nevi, is a major concern, due to the poor treatment response and low survival rates when melanoma is not detected at early stage. (5)

1.3.2 Melanoma

Melanoma results from the malignant transformation of melanocytes, which are located in the basal layer of the epidermis and, less frequently, in the dermis and sebaceous glands, and produce melanin. It can arise from melanocytes located in these sites and from altered melanocytes called nevus cells in certain precursor lesions.

Cutaneous melanoma is an increasingly common, enigmatic, potentially lethal malignancy of melanocytes, characterized by pigmented lesions with high metastatic potential. In Brazil, its incidence is of about 6,000 lesions diagnosed per year, but it is responsible for between 80 and 85% of all deaths caused by skin cancer. For melanoma, the surgical resection is only effective for initial lesions, and its recurrence can vary from 7 to 51%. (6) Melanoma's early detection is extremely important to patient outcomes and to decreased mortality rate, as early diagnosis and surgical excision of *in situ* or early invasive melanomas are curative in most patients. The

success in the treatment of advanced melanoma remains limited, and the prognosis of metastatic disease is poor, despite the advances in chemotherapy and immunotherapy.

Clinicians challenge is to diagnose and excise melanoma in its earliest stage. Tumor thickness, remains the most important prognostic indicator for primary cutaneous melanoma. Clinical examination is based on the lesion characteristics of asymmetry, border, color, diameter and evolving (ABCDE rule), and other diagnostic techniques such as optical spectroscopy and imaging have the potential to improve the diagnostic efficacy at the clinical site.

1.4 Oncologic and dermatologic applications of optical diagnosis based on fluorescence techniques

Medical diagnosis is a very important procedure to determine the lesion type and to provide enough information for the treatment planning. Early diagnosis, especially for oncology, improves the patient prognosis and decreases the mortality and morbidity rates. Diagnosis may be classified into clinical and laboratory-based diagnosis. In clinical diagnosis, the doctor performs the examination of the patient's general condition and of the lesion(s), searching for information about the macroscopic morphology, color, surface texture, tissue resistance and fixation. Such information is obtained through visualization or inspection, usually under white light illumination, and palpation of the lesion. These procedures are subjective and the clinical diagnosis resolution depends on the health professional experience and skills to recognize the early features of neoplasia.

In Brazil and other countries, there is a lack of dermatologists at many locations outside the large centers, which causes a delay on the skin cancer diagnosis. In some of these places, an appointment with a dermatologist is only available once a month and the biopsy result may take even longer to be obtained. The development of high resolution and more direct diagnostic methods for early detection of cancer biological and biochemical changes is essential to improve the public healthcare systems and patient prognosis. The diagnostic methods using

optical techniques have been demonstrating satisfactory effectiveness for this application.

Other interesting application is the monitoring of the skin photoaging degree. Photoaging is the skin premature aging due to frequent exposure to ultraviolet light, which damage the collagen and elastin, two major structural components that give skin a smooth and youth appearance. The chronic exposure of skin to the sunlight can also induce an accumulation of alterations on the DNA of the epithelial cells. In this way, photoaging ranges from wrinkled and discoloured skin through precancerous lesions. Optical diagnosis may be useful to assess the skin photoaging degree, resulting in many applications at dermatology and aesthetics. These applications may include the estimation of the risk of developing precancerous lesions or estimation of the moment when an aesthetic procedure is needed.

Fluorescence is one of the most investigated optical phenomena for clinical applications, because it has high sensitivity to biochemical changes in biological tissues and fluorescence clinical systems are simpler of lower cost to assemble when compared to systems based on other phenomena. The fluorescence spectra and fluorescence lifetime analysis in biological tissues has been presented as a technique of great potential for tissue characterization for diagnostic purposes. This potential is due to the main advantages of optical techniques based on fluorescence for diagnosis, which include the possibility of evaluating the tissue metabolism *in situ*, without removal and processing of the biological sample, and fast and non-invasive responses. These advantages make the fluorescence spectroscopy and lifetime very suitable techniques for clinical applications such as skin photoaging process and diagnosis of clinically similar skin lesions.

1.5 Fluorescence fundamentals and metabolic changes

1.5.1 Fluorescence principles

Fluorescence is a luminescence process related to the light emission of molecules when they decay from one of the excited states by physical (e.g., light absorption), mechanical (e.g., rubbing) or chemical mechanisms. The luminescence generation due to molecules excitation by absorption of photons is called

photoluminescence and it may be divided into fluorescence and phosphorescence, depending on the electronic configuration of the substance on the excited and ground states, resulting in distinct lifetimes.

When the photoluminescence is the result of a radiative transition between two electronic states of same spin multiplicity ($M_S = 2S+1$), where S is the total spin), it can be called fluorescence. In an example case, if we assume a molecule with two electrons, the spin of the electron in the excited state is still paired with the ground state electron. As the excited electron decays to the ground state, spin multiplicity returns to 1 and a photon of lower energy in comparison with the absorbed photon is emitted. The fluorescence process often involves transitions between the first excited singlet state (S_1) and the ground state (S_0), but decays from higher excited singlet states can lead to fluorescence. (7)

Fluorescence lifetimes are much shorter than phosphorescence lifetimes. Phosphorescence occurs when there is a transition between states of distinct spin multiplicity. Typically, for a triplet-singlet transition, the excited and ground state electrons are unpaired and have the same spin orientation and, then, the decay requires a spin flip. But the excited triplet states, in this case, is considerably more stable than excited singlet states, because the phosphorescence transition is forbidden. While fluorescence lifetimes usually occurs at 10^{-7} - 10^{-9} seconds, phosphorescence lifetimes ranges from 10^{-4} - 10^2 seconds. Population of triplet states are done significantly by intersystem crossing, i.e., a spin-dependent internal conversion process, which involve vibrational coupling between the excited singlet state and a triplet state. The following Jablonski (figure 1) diagram shows the phosphorescence, fluorescence, vibrational relaxation, internal conversion and absorption processes.

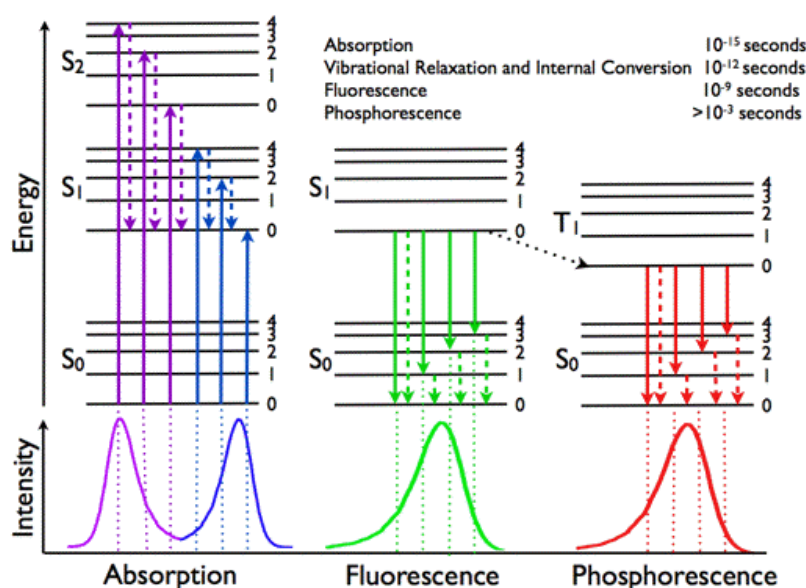


Figure 1 - Jablonski diagram for the energy levels and spectra related to absorption (violet, blue), fluorescence (green) and phosphorescence (red). Radiative transitions are represented by solid arrows and non-radiative (internal conversion and vibrational relaxation) transitions, by dashed arrows. The dotted arrow represents the intersystem crossing from S_{1,0} to T_{1,0}. The spectra for lower energy processes are presented for longer wavelengths.

Source: VISSER; ROLINSK. (8)

After the electrons excitation, they usually decay to the lowest vibrational energy level of the excited state before they decay to the ground state. This happens because vibrational relaxation is a non-radiative process that occurs in order of 10^{-12} seconds, few time scales faster than radiative decay. Another non-radiative process is the internal conversion, i.e., the electrons may also decay non-radiatively from an excited state to a lower energy state with the same multiplicity. Typically, as the energy states become closely spaced, the rate of internal conversion increases. For the major fluorescent molecules, the higher excited states tend to have smaller space in energy, which means that the radiative decay becomes considerable after the excited electron tend to relax to the first excited state.

When a non-radiative transitions occur with a spin inversion of the excited electron, i.e., transitions between states of different spin multiplicity, this is called intersystem crossing (e.g. ISC, figure 1). This type of transition leads to the same spin orientation in the unpaired electrons of ground and excited state and probably a phosphorescence decay. (7)

1.5.2 Fluorescence spectroscopy, endogenous fluorophores and chromophores

The tissue autofluorescence (AF) or endogenous fluorescence is generated by the many fluorophores present in the tissue (figure 2). The fluorophores may be located in the extracellular matrix (ECM) or inside cells. The main endogenous fluorophores present in biological tissues are tryptophan, NADH (nicotinamide adenine dinucleotide), FAD (flavin adenine dinucleotide), collagen, elastin and keratin, and the main absorbers are the water, oxyhemoglobin (HbO_2), deoxyhemoglobin (Hb) and melanin (figure 3).

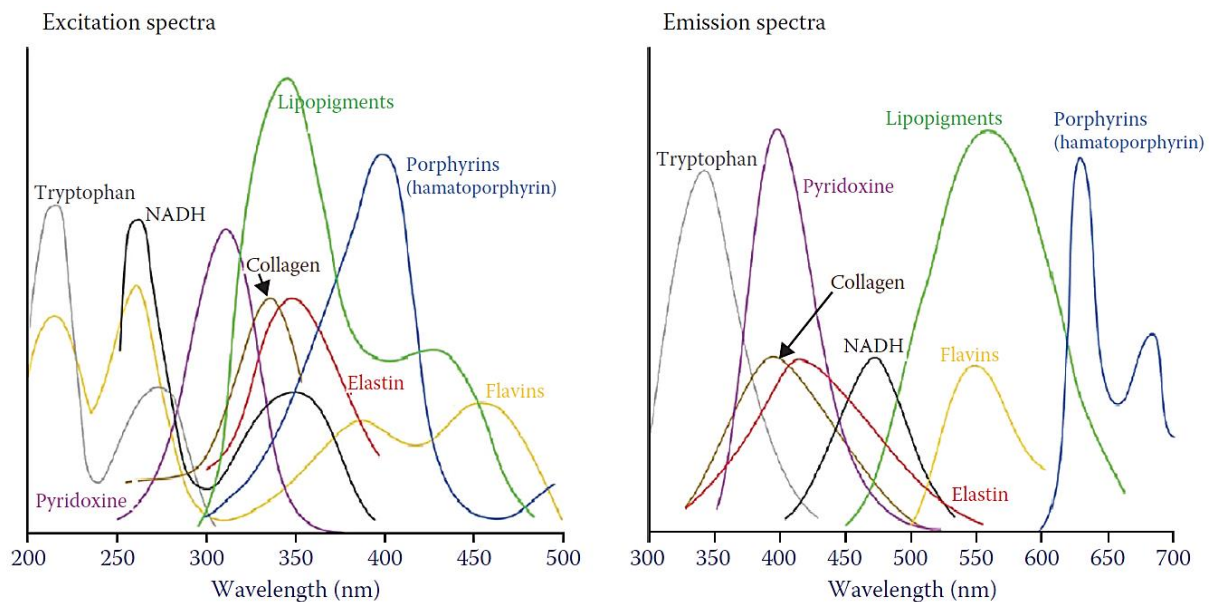


Figure 2 - Excitation and emission spectra of the main biological fluorophores in biological tissues. Due to the spectral overlap of many tissue endogenous fluorophores, the extraction of particular information about each one of them remains a challenge for optical diagnostics.

Source: MARCU et. al. (9)

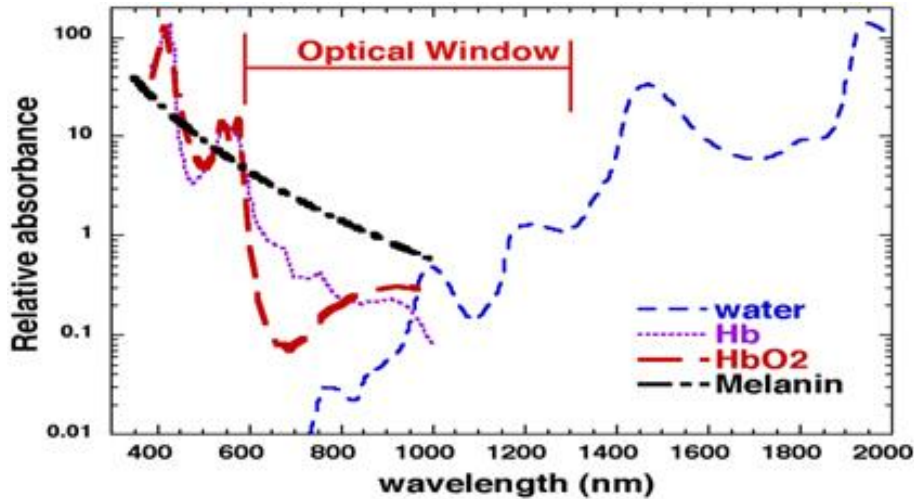


Figure 3 - Optical window for biological tissues, considering the contribution of the main chromophores in the visible and near-infrared range. The choice of excitation and emission wavelengths in this spectral window allows information extraction or treatment procedures in deeper layers of tissue.

Source: HUANG; CHEN; HAMBLIN. (10)

Cellular structures such as membranes, organelles, and collagen fibers also contribute to the light scattering, which may affect indirectly the intensity and shape of the tissue fluorescence spectrum. Other important absorbers are lipids, which present in biological tissues with spectral absorption occurring mainly at the infrared region (11), and keratin, which has an absorption at UV and initial part of visible region of spectrum (figure 4).

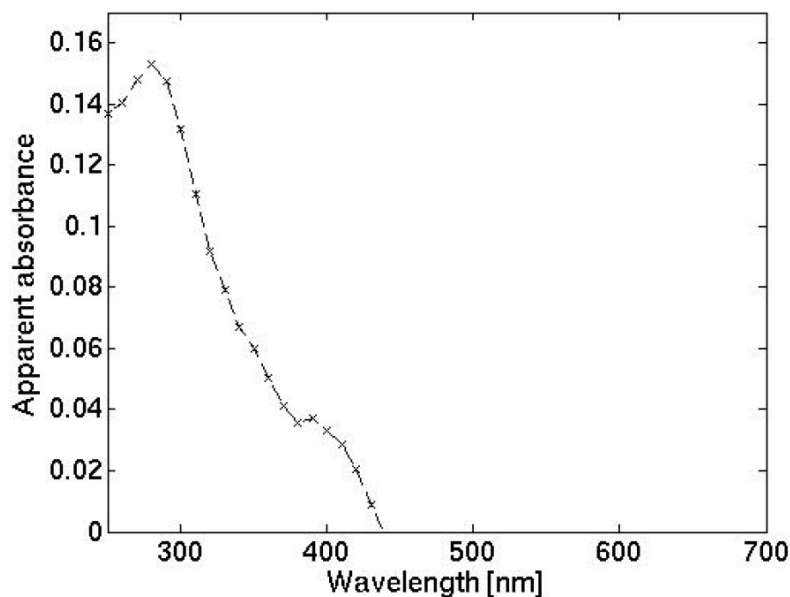


Figure 4 - The apparent absorbance of a 50% relative increase of epidermal keratin in the wavelength regions UVB (280-320 nm), UVA (320-400 nm) and visible (400-700 nm). So, the absorbance in these regions may increase when keratin-rich cells in the epidermis proliferate in order to repair the skin damage due to UV radiation.

Source: NIELSON et. al. (12)

The most important AF fluorophores in cells and tissues are the aminoacids, phenylalanine, tyrosine and tryptophan, which are essential for proteins and enzymes building, flavin and nicotinamide, that regulate cellular metabolism; porphyrins, participant in the transport of gases in the respiratory system; structural proteins (collagen and elastin), responsible for tissue rigidity and flexibility; and fluorescent pigments (melanin, lipofuscin), which are biomarkers for various diseases related to aging. In this case, the fluorescence intensity of NADH is higher than its oxidized form (NAD^+), whereas the opposite occurs for FAD. These endogenous fluorophores may also vary, for example, for different skin lesions or different stages of the same lesion. This variation can be evaluated for the skin lesions diagnostics using fluorescence techniques. (13)

1.5.3 Redox Ratio

The most used optical method for metabolic interrogation is the redox ratio. The redox ratio is the ratio between the fluorescence intensity of NADH and FAD and provides information about the relative changes in redox state inside the cells. The redox ratio is sensitive to changes on the cellular metabolic rates and on the vascular oxygen supply. The increase in the cellular metabolic activity, observed in cancer cells, is usually related to a decrease in the redox ratio. This ratio is commonly assessed by *ex vivo* measurements comparing normal and neoplastic tissues. (14)

The redox ratio has also been used to monitor the oral cancer tissue levels in mice cheek cells or tissues and to check the concentration and incubation time effects of glycolysis and oxidative phosphorylation inhibitor compounds in cell culture studies. (15) The metabolic ratio may be also assessed by measuring the fluorescence lifetime of NADH and FAD free and bound states. Most of fluorescence lifetime measurements for the calculus of redox ratio are performed in cell cultures. So, more investigation of this ratio in tissues is necessary, especially for *in vivo* tissues.

1.6 Fluorescence techniques and molecular interactions

1.6.1 Fluorescence lifetime techniques

The fluorescence lifetime of a molecule is defined as the average time that a molecule remains in the excited state prior to its decay to the ground state. The determination of the molecules lifetime in biological tissues provides important information about the intrinsic condition of the tissue, especially the cells metabolic state, as well as its nearby microenvironment conditions. (14,16)

The first fluorescence lifetime measurements were performed by Gaviola in 1927 (17), but this technique was established for biological molecules only in the late 1980s. (18,19) In the early 1990s, the fluorescence lifetime technique was added to the microscopy and resulted in the Fluorescence Lifetime Imaging Microscopy (FLIM). This technique was already been demonstrated using wide field (20), confocal (21) and multiphoton microscopy. (22)

There are two modalities of techniques for fluorescence lifetime measurements: time-domain (figure 5) and frequency-domain measurements (figure 6). (23) In the time-domain, the excitation is performed by ultrashort laser from few hundred femtoseconds to few hundred picoseconds pulses, and using a fast photon counting electronics. Time-domain techniques are based on the temporal distribution of the photon arrival time after each excitation pulse. This temporal response is determined by the laser pulse shape, the photodetector response, the response of the digitizer electronics, and the data processing methods. Frequency-domain techniques consist in determining the phase shift and fluorescence amplitude modulation as a function of the modulation for the laser excitation.

In the last decade, endoscopes have been developed for fluorescence lifetime measurements for *in vivo* evaluation of endogenous molecules on human tissues using optical fibers in the frequency-domain (24) and time-domain techniques. (25) The fiberoptic time-domain fluorescence lifetime (TDFL) technique has already been used for clinical studies for the detection of the degree of skin glycation (26), early cancer at bronchi (27) and Barrett's esophagus. (28) TDFL has also been used in endoscopy FLIM measurements. (29,30) Due to the requirements for a fast detector and digitization electronics instruments the used pulse sampling methods are

typically based on non-imaging single-point detectors. (9) Single-point measurements using fiber probes are often compatible with the working channel of endoscope systems for investigation of colon (31), esophagus (32) and other organs. Scanning instruments have been reported for arterial samples and oral carcinoma in animal models. (33–35)

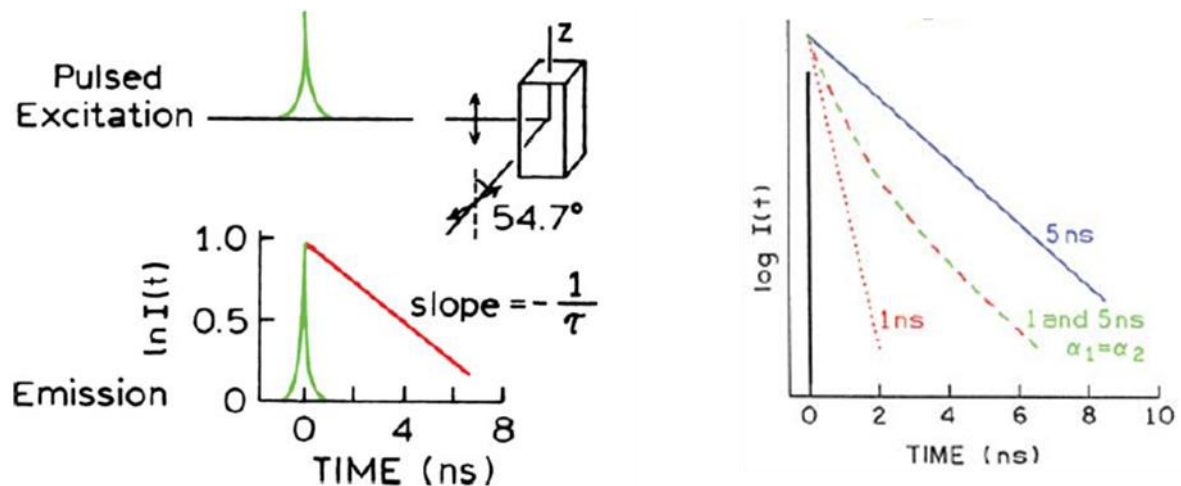


Figure 5 - Principle of time-domain fluorescence lifetime techniques. The light pulse excites the sample, and the fluorescence intensity is registered for each time after the excitation pulse. The result is a mono or multiexponential decay. A mono-exponential decay has its lifetime τ and is represented by the red or blue lines, and the green and red dashed curve is a bi-exponential decay resulted from a composition between the mono-exponential decays represented in the same graph.

Source: LAKOWICZ. (36)

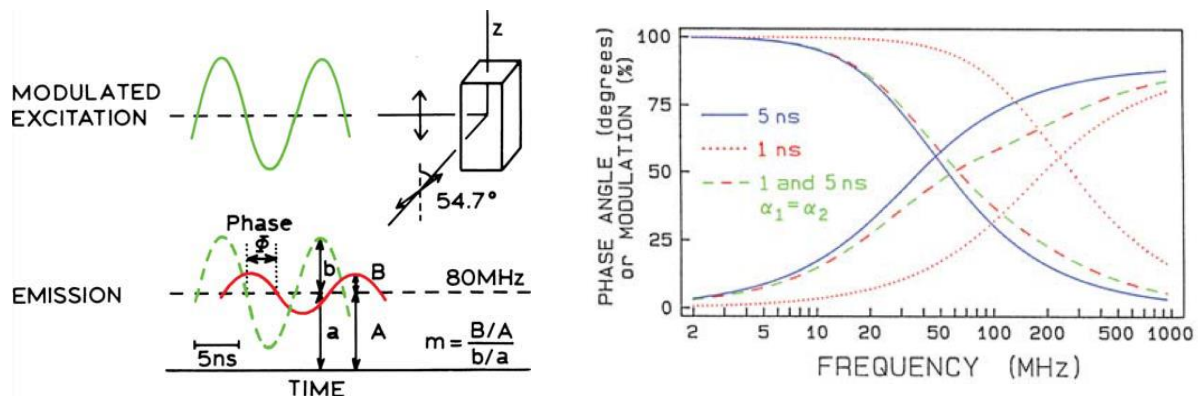


Figure 6 - Principle of frequency-domain fluorescence lifetime techniques. The intensity modulated light excites the sample, and the time-resolved intensity is measured for the fluorescence emission of the sample and for a timing reference signal (such as reflected or scattered light). By comparing the detected signals for the sample and reference, the modulation m and phase shift ϕ are calculated and compared for each sample. Measured mono-exponential decays are represented by curves in blue or red and bi-exponential decays, by the green and red dashed curve.

Source: LAKOWICZ. (36)

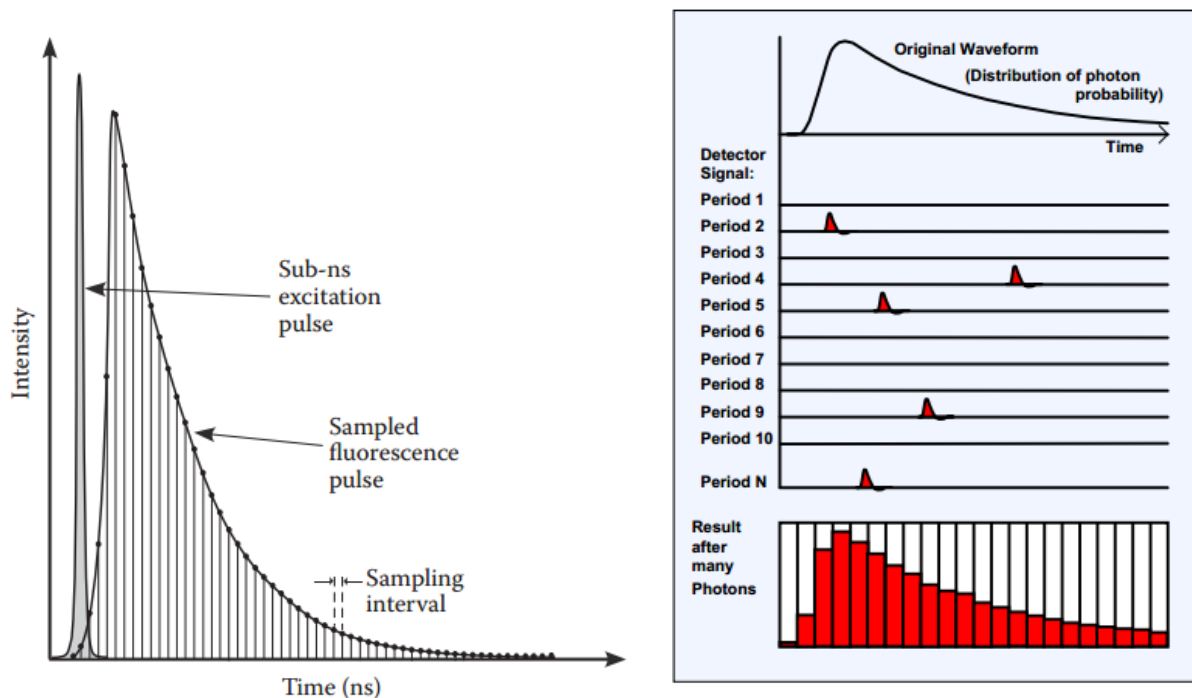


Figure 7 - Principle of Time-Correlated Single Photon Counting (TCSPC). The sample is excited using a sub-ns pulse for several detection periods, and only the first detected photon is acquired for each pulse. In the end of the measurement, the detected photons are summed for each sampling interval, and time-of-flight signals or fluorescence decays are generated.

Source: MARCU et al. (9); BECKER. (37)

One of the most used TDFL techniques is the Time-Correlated Single Photon Counting (TCSPC). The principle of TCSPC is to count the time between the pulse of light and the first photon which arrives in the detector as many times as possible (figure 7). This time delay (difference) is used to construct a histogram of the number of detected photons as a function of time. For fluorescence, this histogram should represent the fluorescence decay over time usually in the nanoseconds scale. The original fluorescence decay is observed when the detection rate is lower than the photon pileup limit, i.e., when the excitation rate is much lower than the light pulse repetition rate. The detection count rate is low enough for values below the 5% of the laser repetition rate. (9,37) These values avoid the apparent shorter measured lifetimes than the real ones when more than one photon arrives in a single photon detection period.

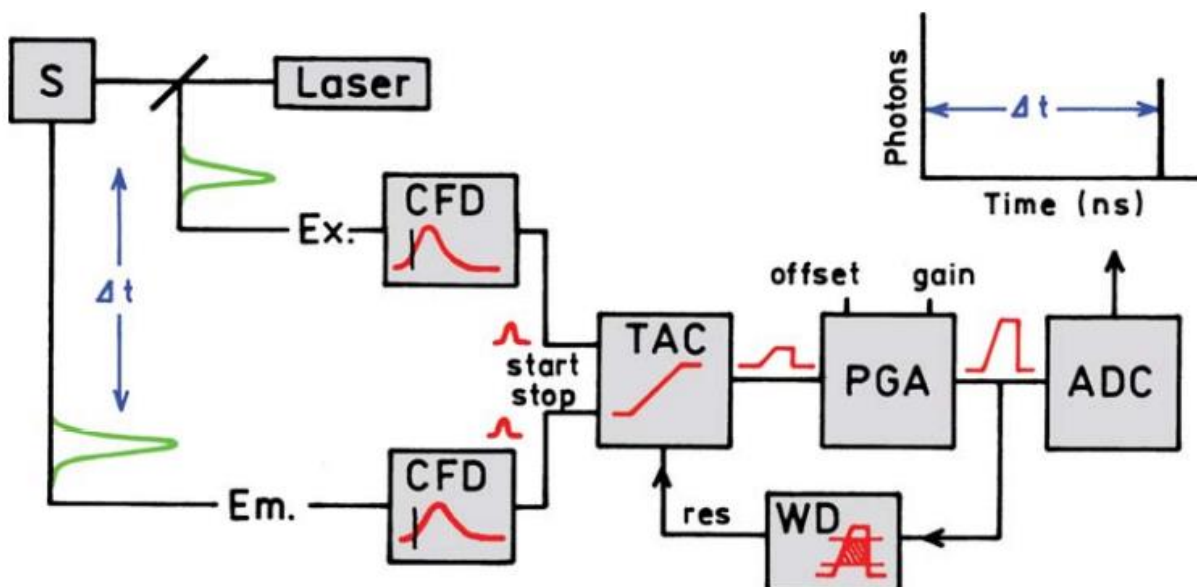


Figure 8 - Fundamentals of TCSPC instrumentation. When the light pulse is released, an electrical signal is sent to the CFD, which measures the arrival time of this pulse. The TAC starts to count the time and stops when the CFD measures the arrival time of the first emission photon. The signal can be amplified by using the PGA or suppressed by the WD. Finally, the ADC converts the voltage value to a photon count in a determined sampling interval. This process is repeated many time to generate a temporal photon distribution.

Source: LAKOWICZ. (36)

The principle of the commonly used method to implement TCSPC electronics is presented in the figure 8. In this method, the measurement starts with the excitation pulse, which will irradiate the sample and induce the fluorescence emission to be detected, typically by a high gain photomultiplier tube (PMT), an avalanche photodiode (APD) or an image intensifier. The excitation electrical signal is sent to a constant fraction discriminator (CFD) for an accurate measurement of the arrival time of the pulse (by minimizing the triggering jitter) and, then, the time-to-amplitude converter (TAC) starts to count the time passed by generating a voltage that increases linearly with the time on the nanosecond scale. The TAC stops to increase the voltage when the arrival time of the first pulse from a single detected photon is determined by another CFD. Now, the TAC contains the voltage ramp from the time difference between the excitation and emission pulse arrival times. This voltage ramp may be amplified by a programmable gain amplifier (PGA) and the voltages out of a pre-determined range can be suppressed by a window discriminator (WD) to minimize false readings. The voltage value is converted to a numerical value by the analog-to-digital converter (ADC) and the latter value is recorded as a single measurement with a determined time interval. After many measurements, the

number of photons is summed up for each time interval and a histogram of the fluorescence decay can be observed. (36)

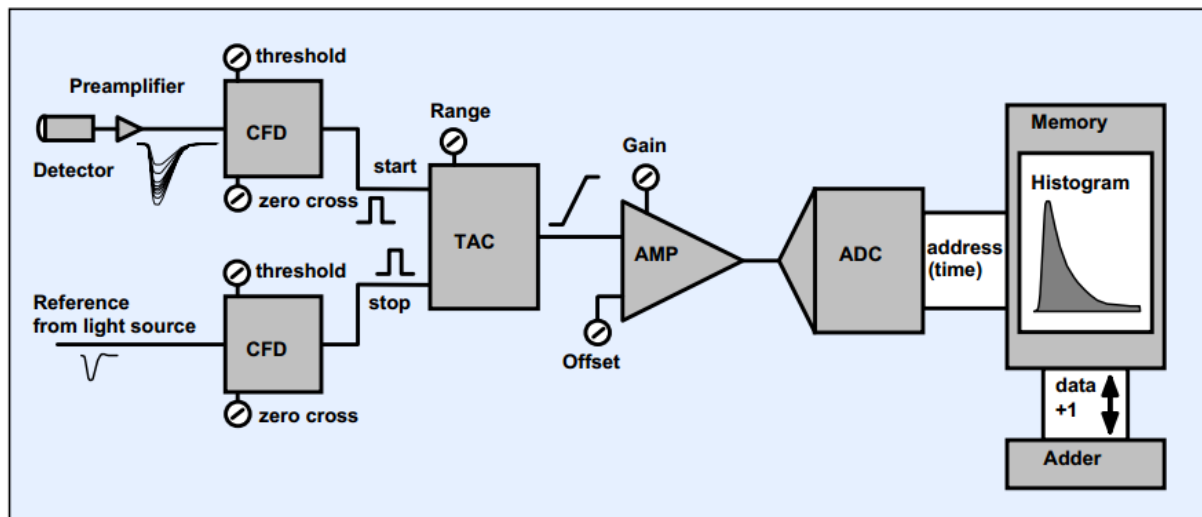


Figure 9 - When using the reverse start-stop mode at TCSPC measurements, the principles of this technique remain the same, but the emission signal is used to start the voltage generation by the TAC and the light pulse, to stop the voltage increase. The reverse mode allow the TAC to work only at the rate of photon detection events, which is much better than the classic mode, since the TAC would need to work at rates much higher than excitation pulse rates.

Source: BECKER. (37)

Most of the TCSPC measurements are performed using the reverse mode (figure 9), which uses the same process described before, except by the TAC's start is determined by the emission pulse and the TAC's stop, by the excitation pulse. The reverse mode is widely used because the TAC takes time to be reset and set to zero voltage before each start pulse. The TAC can be constantly in reset mode if the start signals arrive rapidly, what can be done by modern pulsed-light sources with high repetition rate. This high repetition rate allows the occurrence of around 100 excitation pulses for each emission signal. (36)

The TCSPC is one of the most accurate methods for lifetime determination and may provide high photon saving, shot noise-limited detection, low temporal jitter, high temporal precision, and high dynamic range on the number of recorded photons. The main disadvantage is the low data acquisition rate for single photon detection, which requires that TCSPC instruments operate at low fluorescence intensity levels. Another limitation is the "dead time" between each measurement. This time determines the detection rate and depends mainly on the TAC and CFD reset time. These disadvantages are still less significant than the apparent shorter lifetimes

measured due to the photon pileup effect, i.e., when more than one photon arrives in a single photon detection period. (9)

1.6.2 Time domain fluorescence lifetime measurements

TDFL measurements require signal levels high enough to determine the fluorescence decay with sufficient temporal resolution, and usually subnanosecond pulse widths are desirable to resolve fast decays with fluorescence lifetimes less than 100 ps. The pulse wavelength should be chosen to be within the tissue fluorophores absorption bands and nanojoule pulse energies also ensure the absence of local temperature increase effects, which could modify the sample structure, resulting in a safer interrogation procedure, especially when considering *in vivo* measurements.

The biological tissue AF arises primarily from specific endogenous fluorophores located in mitochondria (NAD(P)H and flavin coenzymes, porphyrins, and lipopigments), structural proteins in ECM (collagen, elastin and keratin), cell lysosomes (lipofuscins), and various aromatic amino acids appearing in many proteins within the living body. (9)

The main targeted tissue fluorophores for the detection of most diseases related to metabolic changes are the NADH and FAD, which have free and bound states, each one with different average lifetimes. The average lifetimes for free and bound NADH and FAD change according to tissue metabolic alterations and may contribute to a non-invasive clinical investigation of injuries such as skin lesions. When NADH or FAD are targeted separately, the decay profiles are usually fitted by a bi-exponential (BiExp) decay function:

$$F(t) = A * a_1 e^{-\frac{t}{\tau_1}} + a_2 e^{-\frac{t}{\tau_2}} \quad (1),$$

where t is the time after the excitation laser pulse, A is the amplitude, a_1 and a_2 are the relative coefficients ($a_1 + a_2 = 100\%$) of each exponential component, and τ_1 and τ_2 are, respectively, the short and long lifetimes.

For NADH, the short lifetime is related to its free state, and the long lifetime, to its bound state. The coefficients a_1 and a_2 provide information about the relative

amounts of molecules on each state. (16) An opposite behavior is observed for FAD, i.e. the short lifetime is related to the bound molecule, and the long one to its free state. These coefficients and lifetimes are very important parameters to monitor the cellular metabolism because it is possible to measure the percentage of bound NADH, related to phosphorylation, in the mitochondria and free NADH, related to glycolysis and usually increased bound NADH amounts are observed at damaged or cancerous tissue. (14,38)

The Warburg effect describes the energy production by high glycolysis rates of cancer cells compared to the normal ones, even when oxygen is abundant. In the latter situation, normal cells prefer to use the aerobic respiration pathways, including the oxidative phosphorylation. The oxidative phosphorylation takes place in the mitochondria and involves both NADH and FAD molecules, while glycolysis involves only the NADH and takes place in the cell cytoplasm. When oxidative phosphorylation occurs more than glycolysis, NADH and FAD molecules use to be both bound in higher amounts than when glycolysis is the main energy production process. The following behavior was observed for the average fluorescence lifetime of NADH and FAD:

- Free NADH lifetime is about 0.3 ns and bound NADH lifetime is 2 ns, and a_1 is related to the free NADH amounts and a_2 to the bound NADH amounts (39);
- Free FAD lifetime is about 5 ns and bound FAD lifetime is less than 1 ns, and a_1 is related to the bound FAD amounts and a_2 to the free FAD amounts. (39)

Other important fluorophores for aging and photoaging monitoring and changes in connective tissues and in the ECM (in angiogenesis, neoplasia or presence of advanced glycation end products; AGE) are the collagen and elastin. Collagen is the major component of the ECM, which provides structural support for cells and facilitate their communication. The mechanical stability of collagen and elastin fibers is related to the covalent cross-links between their fibers. Collagen cross-linking is related to many processes such as skin photodamage, which may decrease fluorescence lifetimes on skin AF (40), corneal diseases (41), aging of human skeletal muscle (42) and collagen glycation in aging and diabetes. (43) ECM components like elastin fibers can be distinguished from collagen (44) by spectrally resolved lifetime detection, because collagen has much longer lifetime than elastin. (9) Elastin allows tissues to change shape undergoing substantial deformation over the life span of the organism and, then, its monitoring is related to aging. Elastin and

different types of collagen fluorescence lifetimes were measured in skin (44), eye (45), and tumors. In tumors, collagen and elastin are attenuated, leading to better isolation of cancer tissue. (46)

Keratin is an important fluorophore in the hair and skin with fluorescent lifetime of 1.4 ns. (47) Keratin and melanin quantitative measurements using time-resolved fluorescence spectroscopy may gather information about dye accumulation inside hair, or monitor intra-tissue diffusion of pharmaceutical and cosmetic components along hair follicles. (47) Keratinization of epithelial tissues was described in oral, esophageal and cervical tissues. (48)

Porphyrins are also important substances related to serious pathologies when they are present in tissues and in blood. These pathologies include necrotic tumors and oral squamous cell carcinoma for direct tissue analysis and gastric cancer, breast cancer, or Hodgkin's lymphoma for blood analysis of patients. Porphyrin derivatives such as protoporphyrin IX (PpIX) can be also monitored for cancer delimitation, diagnostics, and improvement of photodynamic therapy by using σ -aminolevulinic acid, a nonphotoactivable precursor of PpIX, for selective accumulation of PpIX in cancer cells, a diagnostic technique known as photodynamic detection. (9)

Lipofuscins are yellow/brown AF pigments important particularly in the eye, where they manifest changes in pathological conditions, such as age-related degeneration. (9,45,49,50) Lipofuscins fluorescence was described to have a double exponential decay with 0.39 and 2.24 ns in endogenous eye fundus substances. (45) In neurons, lipofuscin is considered to result from incomplete digestion of mitochondrial products. (9)

1.6.3 Fluorescence lifetime and molecular microenvironment sensing

The fluorescence lifetime depends on the molecular microenvironment and not on the concentration, for reasonable ranges. The molecular effects may be investigated independently on the fluorophores concentration, which makes fluorescence lifetime a complementary information to fluorescence spectroscopy data. Most of the fluorescence lifetime applications are reported to FLIM at cell

culture studies. Some of the observed and interrogated effects at FLIM applications are: ionic strength, hydrophobicity (biopolymers), fluorescence quenching by oxygen (organic complexes of ruthenium, europium, platinum, and palladium), calcium or chloride concentration (neuronal systems), pH (molecules' protonated and deprotonated states), aggregation (internalization of dyes into cells), local viscosity (molecular rotors) and local refractive index (structure information about biological cells and tissues), configuration and binding to macromolecules (dyes bonded to proteins, DNA, or lipids and monitoring of protein activities by their conformational changes), NAD/FAD dynamics, drug delivery or diffusion of nanoparticles, Förster resonance energy transfer (FRET; protein interactions and configuration), equilibrium between several conformational states of the fluorophore and another factors that can deplete the excited state by resonance energy transfer. Many of these effects are also explored by other fluorescence lifetime techniques.

Other effects include internal quenching (internal rotation of the parts of the molecule may lead to photoisomerization, and restriction of the rotation by placement of the fluorophores into a rigid environment or lowering the temperature tends to marginalize the role of the non-radiative pathway and to increase the fluorescence and fluorescence lifetime), external quenching (FRET at organic dyes, fluorescent proteins, lanthanides, quantum dots, fullerenes, carbon nanotubes and their combinations, Dexter electron transfer and dynamic quenching when molecules decrease their fluorescence lifetime as a result of multiple processes at the moment of collision such as the formation of metastable complexes, resonance energy transfer, electron transfer), photon reabsorption, and excimer generation (excited dimer formation when an excited molecule associates with the same molecule in the ground state). (9,17)

By exploiting the capability of molecular microenvironment sensing in studies of biological and biochemical processes in cells and tissues, it is possible to evaluate which of these processes are involved with many diseases and alterations in tissues and organs, and the efficacy of their treatments. Since this evaluation is performed with a nondestructive, noninvasive, and non-ionizing radiation technique, fluorescence lifetime techniques have a great potential to be used for many applications in biology and medicine.

2 BIBLIOGRAPHIC REVIEW

The clinical fluorescence lifetime systems described in the literature are divided into systems for imaging (laser scanning) or single-point measurements. Most of the reported imaging systems are able to perform multimodal optical measurements, but their portability is still a challenge due to the size of their instrumentation. This size limitation makes clinical measurements possible only at the place where the system is located. On the other hand, systems for single-point measurements offer more possibilities for clinical investigation in various places due to their simpler of relatively low size and subsequent portability. Clinical *in vivo* measurements using portable systems are relevant since most of fluorescence lifetime measurements are performed in cell cultures, normal tissues, and *ex vivo* diseased tissues.

This section will describe the instrumentations and applications of various fluorescence lifetime systems reported in the literature. Clinical imaging systems are divided into multiphoton and multispectral systems.

2.1 Clinical fluorescence lifetime imaging systems

One of the first commercially available fluorescence lifetime systems for clinical applications is the DermalInspect® 110 (figure 10). This laser imaging system has a total dimension of 75x120x140 cm³, mounted on a transportable workstation, and is considered a class 1M device according to the European laser safety regulations. The system is able to perform measurements based on second-harmonic generation, fluorescence, fluorescence lifetime and optical tomography and consists of three major modules:

1. A turn on key, solid-state, mode-locked 80-MHz titanium:sapphire laser (Ti:S)(MaiTai, Spectra Physics, Newark, Delaware, United States) with a tuning range of 750 to 850 nm, a 75-fs pulse width, and a maximum laser output of about 900 mW;
2. A scanning module, including a motorized beam attenuator and shutter; a laser power detection module and trigger module for the TCSPC unit; a fast x,y galvoscaner and piezodriven 403 focusing optics with NA 1.3 (oil, 140-μm working

distance) or 20x optics NA 0.9 (water, 1.2 mm working distance); a PMT with a short rise time; and a module with a 0.17- μm glass window for *in vivo* skin studies;

3. A control module with power supplies; a single-photon counting board (SPC 730/830, Becker&Hickl Berlin); and image-processing hardware and software, including such features as online control of laser power and adjustment according to tissue depth, monodirectional and bidirectional scanning, line scan, and single-point illumination. (39)

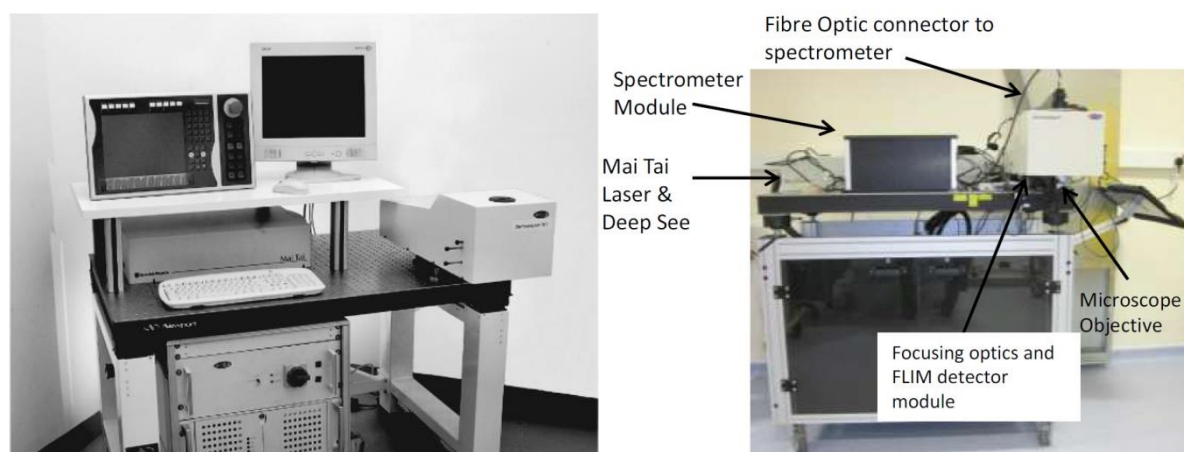


Figure 10 - Multiphoton imaging tool DermalInspect® 110 and a modified DermalInspect® instrument that allow the collection of fluorescence lifetime images in four spectral channels and hyperspectral images using an specific spectrometer module.

Source: KOENIG, RIEMANN (39); PATALAY. (51)

The DermalInspect® (commercially available and modified systems) was used for studies of the fluorescence lifetime of melanin within normal skin *in vivo* and comparison with melanin found in the hair bulb and from melanocytic 3D cell cultures; fluorescence lifetimes from normal skin different body sites and depths; the effect of excision, temperature and the use of culture media on the AF from NAD(P)H in freshly excised human skin; the effects of ischaemia on mouse skin using spectrally resolved images; the variation of tissue AF lifetimes from the dermis with age, sex and body site in the medial and lateral forearms of 47 volunteers; the comparison between normal skin and freshly excised BCCs; the morphological features from 16 *ex vivo* BCCs and their comparison with acquired *in vivo* using reflectance confocal light microscopy; morphological descriptors ('small short-lifetime cells' in the upper and lower epidermal layers, 'edged papillae', 'junctional nests of short-lifetime cells' and 'dermal cell clusters') for 16 *ex vivo* benign naevi; the mean fluorescence lifetimes at three representative cells in the lower layers of 98 healthy

skin lesions and 98 BCC lesions, and the association between these lifetimes and the morphological descriptors. (51)

Other reported multiphoton fluorescence lifetime system is the experimental setup showed in the figure 11 with microscope optics assembled in a custom vertical honeycomb steel breadboard of 60 cm x 90 cm, 070BH0450 (Melles-Griot, Rochester, NY, US), mounted by two square brackets onto an anti-vibrating optical table 100 cm x 200 cm (TMC, Peabody, MA, US) and a wide-field subsystem with two different illumination systems (an halogen lamp KL200 (Schott AG, Mainz, Germany) for thin samples or six superluminescent diodes uniformly mounted on a metallic ring) and color CCD camera COOLPIX 4700 (Nikon, Tokyo, Japan). (52) This system is also able to perform two-photon fluorescence, second-harmonic generation and multispectral two-photon emission measurements. A mode-locked Ti:Sapphire laser CHAMELEON (Coherent Inc, Santa Clara, CA, US) provides the excitation light with 120 fs pulses, repetition rate of 90 MHz and tunable wavelength in the 705-980 nm range. The total dimensions of this system scanning head are 100 mm x 180 mm x 150 mm. A piezoelectric stage PIFOC P-721 (Physik Instrumente GmbH, Karlsruhe, Germany) allows axial displacements of the objective up to 100 mm with 1-nm resolution. The FLIM system includes a detector (Multi-PMT) PML-Spec (Becker-Hickl GmbH, Berlin, Germany) constituted by a diffraction grating with 600 lines/mm and a 16-channel multianode photomultiplier strip with 200 ps FWHM pulses for both spectral and lifetime imaging. The system detection has an upper wavelength limit of 685 nm set by the cut-off optical filter, and a lower limit of 200 nm set by the detector response. The system has an instrument response function (IRF) with FWHM of 280 ps for the overall system. Acquisition and control are performed using a PC and two synchronized I/O boards, a PCI-MIO-16E (National Instruments, Austin, TX, US) and a SPC-730 (Becker-Hickl GmbH, Berlin, Germany). In the FLIM system, the image deconvolution and fluorescence decay analysis are performed using the software SPC-Image 2.8 (Becker-Hickl GmbH, Berlin, Germany). (52) This experimental setup (figure 11) was used for FLIM measurements of 2 samples of malignant melanoma, 1 cutaneous keloid, and 4 nodular BCCs.

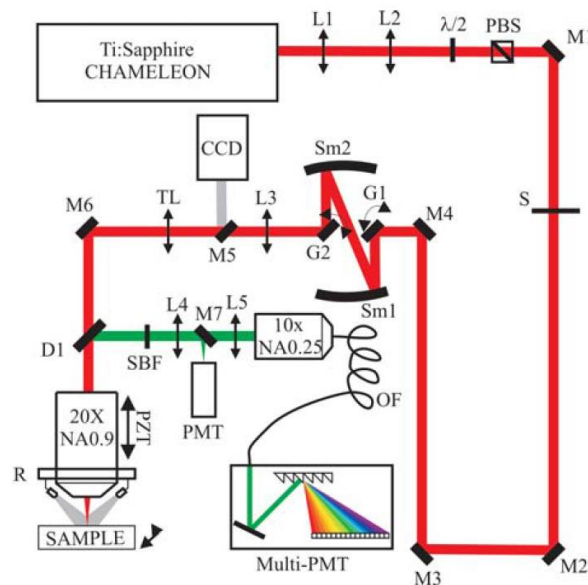


Figure 11 - Experimental setup for multiphoton imaging described at (52). This system is also able to perform two-photon fluorescence, second-harmonic generation and multispectral two-photon emission measurements. The components are: L: lenses, $\lambda/2$: half-wavelength broadband waveplate, PBS: calcite polarizing beam splitter, M: mirrors, S: electronic shutter, G: galvanometer mirrors, CCD: color CCD camera, TL: microscope tube lens, Sm: spherical mirrors, R: metallic ring, PZT: piezoelectric stage, OF: multimode optical fiber, and PMT: photomultiplier tube.

Source: CICCHI. (52)

Other multiphoton FLIM systems are described for flexible wide-field FLIM endoscope (figure 12A) (53) and wide-field time domain FLIM (figure 12B). (54,55) In the endoscope, the excitation is performed by a gain-switched picosecond diode laser operating at 445 nm (PicoQuant, LDHP-C-440M with driver PDL-800-B) or a frequency doubled Ti:Sapphire laser (Newport Spectra-Physics broadband MaiTai), the imaging path consists of a 1 mm diameter, 0.1 NA, 5 mm working distance GRIN objective lens (Grintech, GT-IFRL-100-005-50-CC) directly bonded to a 0.95 mm diameter, 2 m length of coherent optical fibre optic bundle, the sample light emission passes through a 488 nm long pass interference (Semrock, BLP01-488R) and a 475 nm long pass absorption filter, and the fluorescence image is relayed to either a colour CCD camera or to the gated optical intensifier. FLIM endoscopy was used to image diseased human *ex vivo* laryngeal tissue and *ex vivo* neoplastic mouse bowel. The wide-field time domain FLIM used a frequency-doubled mode-locked Cr:LiSAF and Ti:sapphire laser to provide excitation wavelengths above 400 nm, a time-gated optical intensifier to provide a temporal response of around 100 ps and that is able to image lifetime differences as small as 10 ps. The adjustable delay generator scanned the gated detector timing through the fluorescence emission profile in 25-ps steps,

thus permitting a series of time-gated fluorescence images to be recorded on an intensified CCD camera (Photonic Science; ISIS-3).

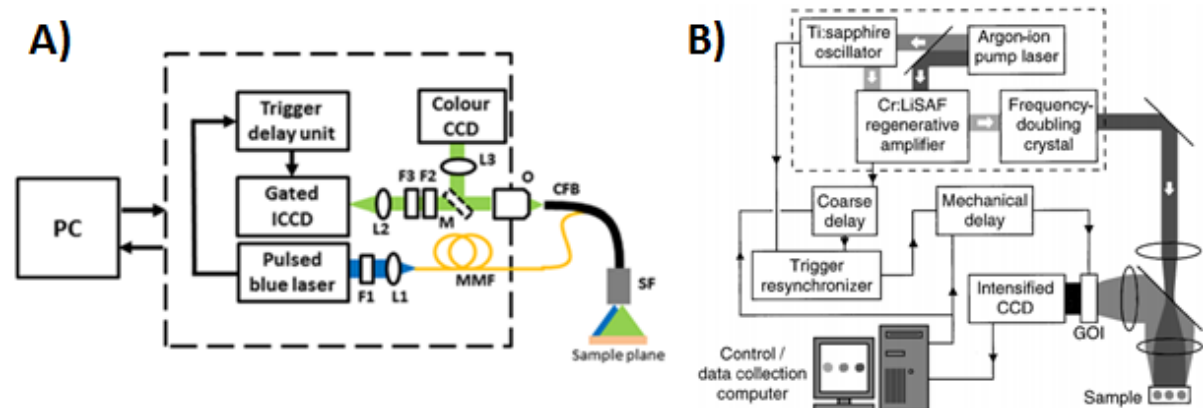


Figure 12 - A) A flexible wide-field FLIM endoscope using pulsed blue diode laser, a clean-up filter (F1), a multimode fibre (MMF), steel ferrule (SF), a coherent fibre-optic bundle (CFB), a microscope objective (O), tube lens (L2 or L3), a CCD camera or GOI, a switchable mirror (M). B) Whole-field fluorescence lifetime imaging system, based on a time-gated image intensifier and a solid-state laser oscillator–amplifier.

Source: SPARKS, et al. (53); DOWLING, et al. (54)

Other clinical systems are reported for multispectral FLIM (34,56–58), including flexible endoscopes (59), optical coherence tomography and FLIM systems (60), and combined fluorescence lifetime imaging and reflectance confocal microscopy systems (figure 13). (61) Most of these systems use an ultraviolet (UV; nitrogen lasers, frequency-tripled Q-switched Nd:YAG lasers) or blue excitation sources (473 nm solid state diode lasers); a set of dichroic mirrors and optical filters for the selection of the emission bands at the multispectral detection module; a set of multimode fibers of different lengths to temporally separate the fluorescence decays for each emission band; an intensified charge-coupled device (ICCD), a PMT or micro-channelplate photomultiplier tube (MCP-PMT) and a high-bandwidth pre-amplifier for fluorescence detection; a digital oscilloscope for signal acquisition and analysis; and a LabVIEW (National Instruments, Austin, Texas) interface to control the instrument, conduct data acquisition, and dynamically display the fluorescence intensities and lifetimes (57), or a set of a high-speed comparator to threshold the pulses, a multiplexer to select between the thresholded signal and an internally generated signal used for calibration purposes, a FPGA with high speed configurable transceivers to de-serialize and convert the serial input signal to introduce a

programmable delay and a FPGA memory controller with a buffer memory to store event times before the transference to the host PC through the USB 2.0 port. (58) The applications of these systems may be extended to operation in an intravascular setting in conjunction with intravascular ultrasound (IVUS) and under blood flow conditions (8 arterial segments of healthy arterial walls of three distinct juvenile Yorkshire pigs), investigation of normal artery and plaque areas (atherosclerotic lesions) of human aorta *ex vivo* samples obtained post-mortem and frozen within 2 hours of autopsy (57) and identification of collagen-rich and lipid-rich plaques of atherosclerotic coronary plaques at human coronary artery segments obtained from 8 autopsy cases within 48 h of the time of death (62), oral normal and malignant tissues at hamster cheek pouch. (56,59)

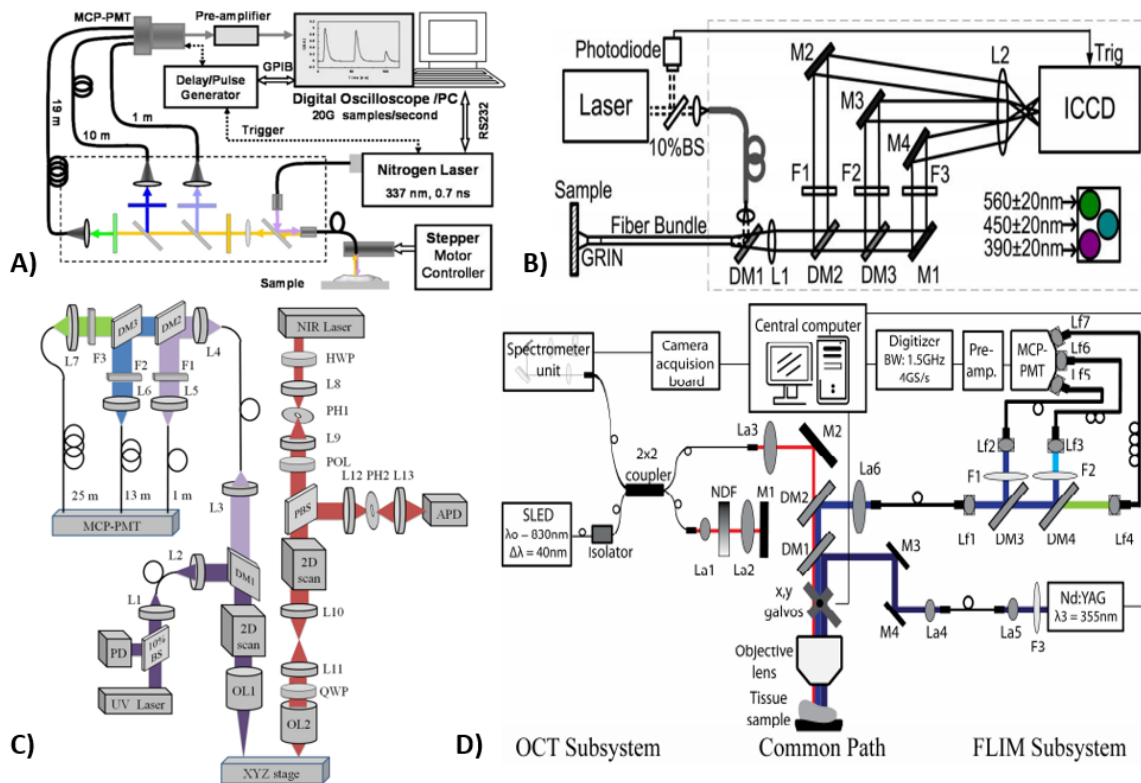


Figure 13 - A) Optical design and electronic configuration of a simultaneous time-and-wavelength-resolved fluorescence spectroscopy system with a single optical fiber as a probe for excitation delivery and fluorescence collection. B) Multispectral FLIM endoscopy system. The system components are: BS: Beam sampler, DM: Dichroic mirror, M: Mirror, F: Filter, L: Lens. C) Combined fluorescence lifetime imaging-reflectance confocal microscopy (FLIM-RCM) system. The abbreviations in the system are: UV: ultraviolet, OL1: 45 mm focal length triplet lens, DM: dichroic mirrors, F: filters, MCP-PMT: micro-channel plate photomultiplier tube, BS: beamsplitter, PD: photodiode, OL2: 1.0 NA objective lens, L: lenses, PH: pinholes, APD: avalanche photodiode, HWP: half wave plate, POL: polarizer, QWP: quarter wave plate, PBS: polarizing beamsplitter. D) A dual-modality optical coherence tomography and fluorescence lifetime imaging microscopy system. The abbreviations of components of this system are: La1-La5: free-space collimation and coupling lenses, Lf1-Lf7: fiber-connected collimation and coupling lenses, NDF: neutral density filter, M1-M4: mirrors, DM1-DM4: dichroic mirrors, and F1-F3: filters.

Source: SUN (57); CHENG (59); PARK (60); JABBOUR (61).

2.2 Clinical fluorescence lifetime systems for single-point measurements and their portability

The optical fiber setup described at (63) represents a relatively simple clinical fluorescence lifetime instrumentation (figure 14). This instrumentation consists in a pulsed diode laser ($\lambda = 415 \pm 5$ nm, $\tau_L = 15$ ns, $P_{\text{peak}} = 1$ W, $f = 1$ MHz), an APD detector (APD120A2, Thorlabs), a fast (1 GHz bandwidth, 50 GS/s for the RIS (Random Interleaved Sampling) mode) digital sampling oscilloscope, a colored glass filter placed in front of the detector (VG09, Zeiss), a microscope lens for coupling the laser light into the fiber, and two multimode silica fibers, one for excitation with 400 μm of core diameter (BFL400, Thorlabs) and another for collection with 600 μm of core diameter (BFH600, Thorlabs). In a preliminary study (63), an IRF of 15.5 ns and a fluorescence spectra and lifetime of healthy and cancerous intestine were measured. The system is assembled in a breadboard, which can be transported to other places, but it should not be optically stable because transport may causes misalignments. The system mobility may also require mechanical stability for the components that are not fixed on the breadboard and the system assembly with all electrical and optical connections working with the same efficiency as it works on the bench.

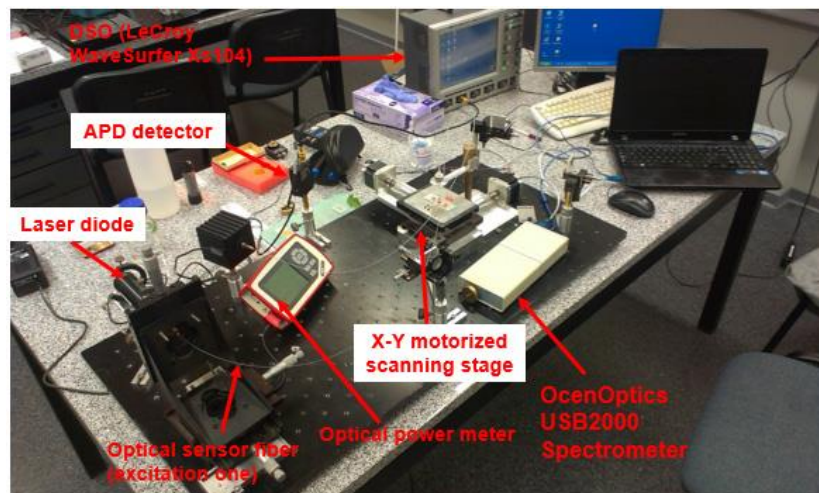


Figure 14 - Measurement setup assembled over an optical bench used for performing the fluorescence lifetime investigation. The system may be relatively compact but not ideal to be transported with optical, mechanical and electronic stability.

Source: POPENDA (63).

Another single-point measurement system is the multispectral fluorescence lifetime system (figure 15) reported in (64). In the time-resolved spectrofluorometer, two pulsed laser sources are used for excitation: a frequency tripled ultrafast Yb: glass fibre laser (UVPower355, Fianium Ltd., UK), which provided 10 ps pulses at 355 nm with a repetition rate of 37.1 MHz; and a diode laser (LDH-P-C- 440B, PicoQuant GmbH, Germany), which emitted 50–150 ps pulses at 445 nm with an adjustable repetition rate of up to 40 MHz. This radiation is coupled into the excitation channel of a custom built fibre-optic probe (FiberTech Optica, Canada) that comprised seven multimode optical fibres with core diameters of 200 μm . The output from the collection optical fibres is imaged onto the input slit of a grating spectrometer (MS125 1/8 m, Lot-Oriel, UK), which is attached to a 16 channel multi-anode PMT detector (PML-16-C, Becker-Hickl GmbH, Germany). The PMT is linked to a computer with a time correlated single photon counting (TCSPC) card (SPC-730, Becker-Hickl GmbH, Germany). The whole system was mounted on a 60 x 60 cm^2 optical breadboard to facilitate transportation and was fully enclosed for safe use in a clinical setting. (64) The system was used for *in vivo* measurements of skin lesions (BCC, squamous cell carcinoma, benign naevus, dysplastic naevus, malignant melanoma, actinic keratosis and other lesions) and *ex vivo* measurements of cartilage degradation (simulating effects of osteoarthritis). (64,65)

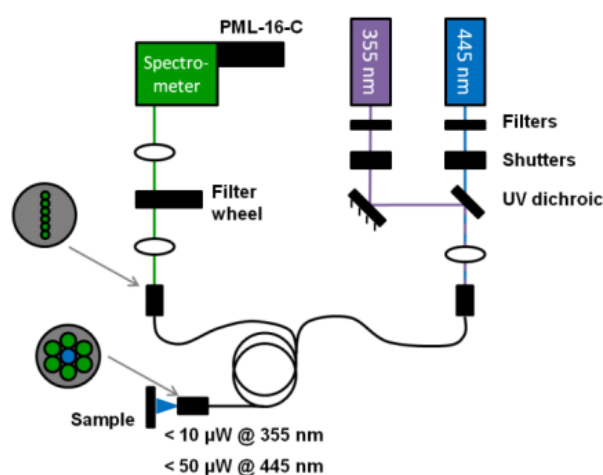


Figure 15 - Optical layout of the time-resolved fluorescence spectrometer that allows measurements of fluorescence decays in 16 channels. The entire dataset for measurements using both lasers consists of two sets of 32 spectrally resolved fluorescence decays.

Source: THOMPSON. (7)

The same single-point fluorescence lifetime system was improved by adding the possibility of diffuse white light reflectance measurements and reducing the

system size by changing the previous excitation sources (in 355 nm and 445 nm; figure 16). For diffuse white reflectance measurements, a white light source (HL-2000-FHSA, Ocean Optics, Dunedin, Florida, USA) and a spectrometer (HR2000CG-UV-NIR, Ocean Optics, Dunedin, Florida, USA) were used. For the size reduction, two diode lasers emitting at 375 nm and 435 nm were used and allowed the optical components to be placed in a 30 cm² x 45 cm² optical breadboard instead of 60 cm² x 60 cm² used before. The optical breadboard and other constituents of the instrument are housed inside a compact, wheeled trolley with dimensions 182 cm x 70 cm x 55 cm to allow easy transportation to (and within) a clinic (figure 17). The breadboard is situated on the top shelf and below this the trolley also contains a driver for the filter wheel (Lambda 10-3, Sutter Instrument Company, USA), a power supply and control unit for the lasers (PDL 828 Sepia II, PicoQuant GmbH, Germany), a USB data acquisition box (USB-DAQ, NI USB-6008, National Instruments, USA), a desktop computer and an isolating medical transformer (REO-MED 600, REO Inductive Components, UK). The trolley was fully enclosed using a stainless steel lid and front, back and side panels made from a black, optically absorbent, rigid foam PVC sheet material (Foamalux®). The panels on the side of the trolley have ventilation holes drilled in to them and two fans are installed on the back. All electrical elements contained within the trolley are connected to the isolating medical transformer. (7) The computer monitor is mounted on a metal post fixed in place at the back of the trolley (figure 17).

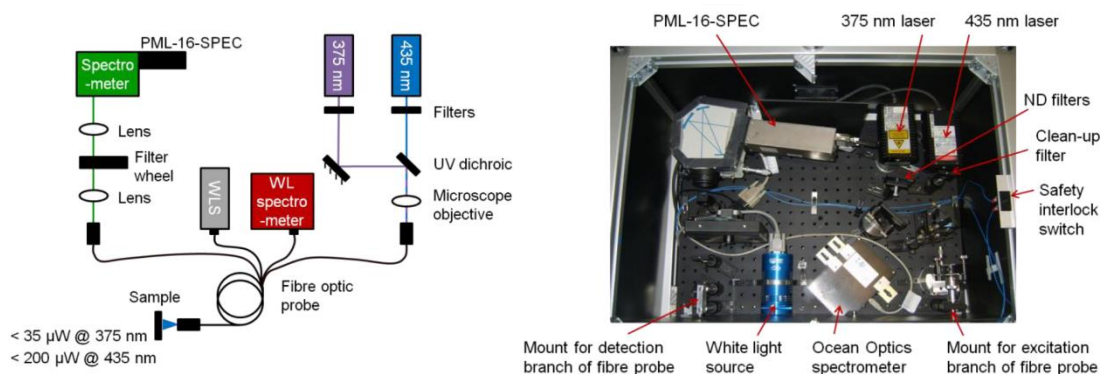


Figure 16 - Optical setup of the improved time-resolved fluorescence spectrometer system. The system size was reduced and the possibility of diffuse white light reflectance measurements was added.

Source: THOMPSON. (7)

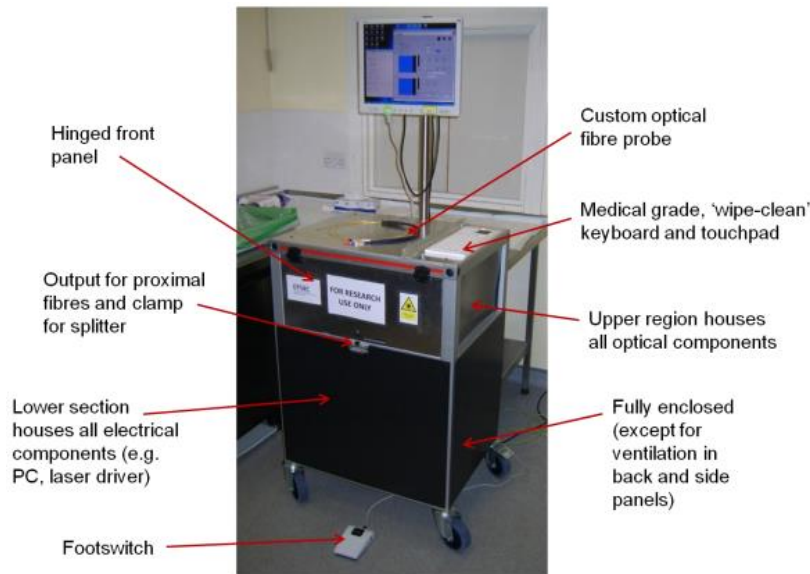


Figure 17 - Transportable trolley that houses the entire time-resolved fluorescence spectrometer. The trolley has dimensions 182 cm x 70 cm x 55 cm and allow the system transportation with stability, but it remains not compact.

Source: THOMPSON. (7)

A recent single-point fluorescence lifetime system was launched by the Becker & Hickl GmbH company. This system is known by “Simple-Tau 130 Table-Top TCSPC system” and work with BDL-SMN lasers (present at 375 nm, 405 nm, 445 nm, 473 nm, 488 nm, 515 nm, 640 nm, 685 nm, 785 nm, 1064 nm wavelengths) and with HPM-100 high speed hybrid detectors (HPM-100-06, HPM-100-40 and HPM-100-50 with detection range of 300 nm to 600 nm, 300 nm to 730 nm, and 400 nm to 900 nm, respectively). The excitation light is delivered to the sample by a bifurcated optical fiber and passes through an optical filter attached to a part of the PMT and goes to the hybrid PMT detector. The data is processed and analyzed in a lap-top computer with an extension box (figure 18). The system is compact, but the components are not fixed, the electrical wires and optical fiber need to be connected again every time the system is assembled, the system transportation requires mechanical stability for the laser(s), detector, computer and extension box, and the optical filter cannot be changed quickly during clinical measurements, it needs to be separated from the part attached to the hybrid PMT and replaced by another one.

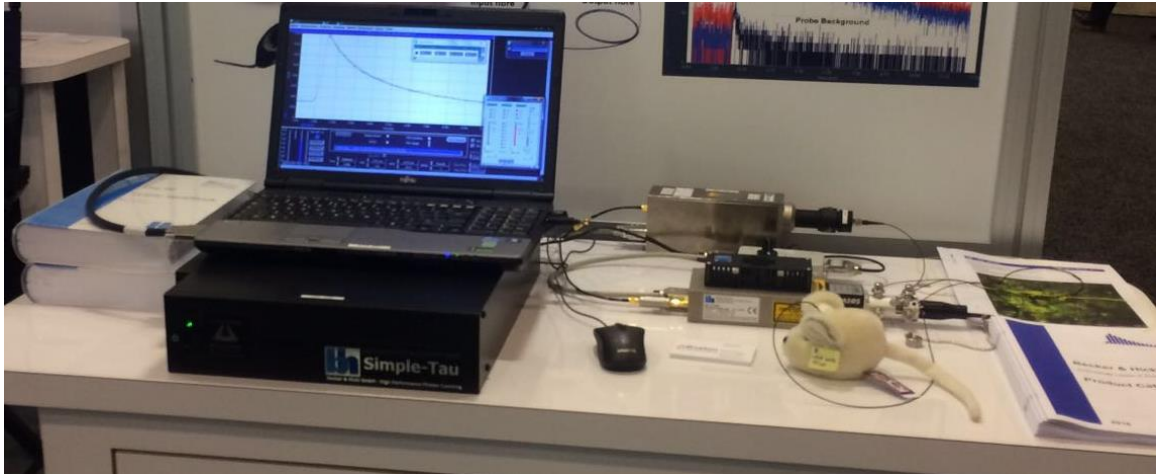


Figure 18 - Compact Simple-Tau 130 Table-Top TCSPC system from the Becker & Hickl GmbH company in the exposition of SPIE Photonics West conference.

Source: By the author.

Although the systems described previously are able to perform multispectral and/or multiphoton fluorescence lifetime imaging and/or a set of second-harmonic generation, single or multiphoton fluorescence, optical tomography measurements, they are not presently at a reduced size and with mechanical, electrical and optical stability for easy and robust transportation for clinical measurements. In this study, we describe a single-point fluorescence lifetime system capable to perform fluorescence spectroscopy and fluorescence lifetime clinical measurements.

3 OBJECTIVES

3.1 General Objectives

The main objective of the present study was to assemble, calibrate and characterize a portable time-resolved fluorescence spectroscopy system for single-point measurements and to preliminary evaluate its efficacy on the discrimination of clinically similar skin lesions.

3.2 Specific Objectives

- Design and assemble a portable single point fluorescence lifetime spectroscopy system;
- Calibrate the system by synchronizing its electrical and optical signals;
- Characterize the developed system in phantom measurements;
- Evaluate the clinical use of the developed system through *in vivo* measurements at healthy volunteers, and patients with clinically similar skin lesions.

4 METHODOLOGY

4.1 Fluorescence lifetime spectroscopy system

The time-resolved fluorescence system uses two lasers: one emitting at 378 nm wavelength and another at 445 nm (BDL-375-SMC e BDL-445-SMC, Becker and Hickl, Berlin, Germany), which are used for NADH and FAD excitation, respectively. The lasers have a repetition rate of 20, 50 or 80 MHz and the pulse width is around 50 to 100 ps. The excitation laser light was coupled in a bifurcated fiber bundle (BIF400-UV-VIS, Ocean Optics, Dunedin, Florida, USA) with a common end of two 400- μ m-diameter fibers, side-by-side positioned (relative transmission is shown at the Annex F). This optical fiber probe conducts the excitation light to the sample, the collected light passes through bandpass filters and goes to a hybrid PMT detector (HPM-100-50, Becker and Hickl, Berlin, Germany) virtually free after-pulsing effect (detection range 400 – 900 nm). Two different bandpass dichroic filters at (440 ± 20) nm and at (514 ± 15) nm were placed in front of the detector in order to mainly provide detection of NADH and FAD emission regions at 378 nm and 445 nm, respectively. Additionally, longpass filters (405 nm longpass for 378 nm excitation and 475 nm longpass for 445 nm excitation) were used for skin measurements to analyze the signal from a broader range of endogenous fluorophores (transmission spectra of filters are shown at the Appendix I). The fluorescence lifetime measurements are performed using the Time Correlated Single Photon Counting technique. The same lasers (378 nm and 445 nm) are used for fluorescence spectroscopy measurements. The fluorescence spectrum is collected using a portable spectrometer Ocean Optics USB2000-FLG (Ocean Optics, Dunedin, Florida, USA). Figure 19 shows a scheme of the assembled experimental setup.

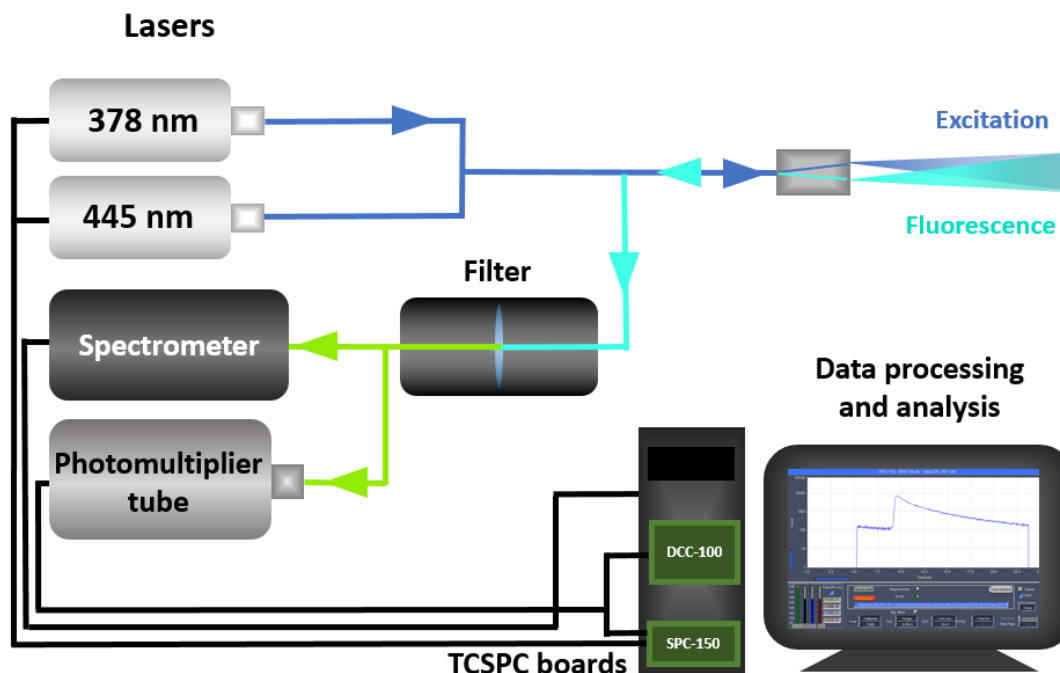


Figure 19 - Schematic drawing of the components for fluorescence spectra and fluorescence lifetime acquisition.
Source: By the author.

4.2 Customizing for clinical measurements

The previous fluorescence lifetime spectroscopy system was assembled over an optical bench and the occupied volume was of approximately $99,990 \text{ cm}^3$ taking into account the desktop computer or $71,628 \text{ cm}^3$ without its cabinet. This volume decreased for around $38,165.75 \text{ cm}^3$, and the present system weight is of approximately 15.9 kg after the assembly into a metallic suitcase with external measurements of 48.5 cm x 38.5 cm x 19 cm (figure 20). Besides the decrease on system volume, its portability improved by fixing each component in a balanced position at the suitcase and by designing the right cooling for each group of system components. It has also mechanical, electrical and optical stability, and allows fast optical filters change during clinical measurements.

The system size and its clinical feasibility were also optimized to do not compromise the hospital routine. The adapted system (figure 20B, 20C and 20D) can be carried to any place and works only with a 110/220 V wall socket.

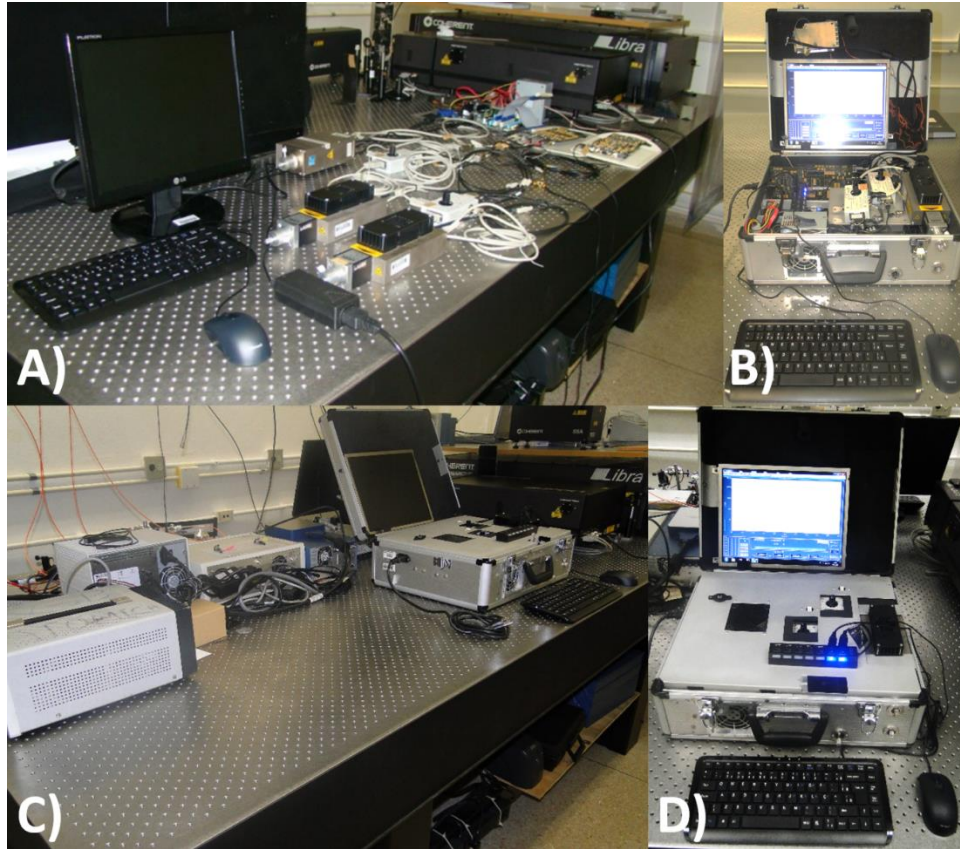


Figure 20 - A) Previous fluorescence lifetime system assembled over an optical bench. B) System assembly before its complete assembling into the suitcase. C) The system size was reduced for almost half of its previous volume without the computer cabinet. D) System assembly after its encasement provides protection for its components and a user-friendly design for system operator by exhibiting a control panel with access to external controls and the filter holder.

Source: By the author.

4.2.1 Planning, positioning and compacting the fluorescence lifetime system

The assembly of a portable system for clinical diagnosis requires planning its configuration, structure and components in a way to allow its transportation without losing performance related to lasers misalignment, scratches at the TCSPC expansion cards, detector exposure to intense light sources for long times, optical elements exposure to dust or chemical substances, and computer's motherboard instability. Mechanical, electronic, optical and thermal stability for the instrumentation and its compartments, the maintenance of connections between equipment pieces and the positions of each piece is also important to keep the system working properly.

The equipment should also be planned to be used any time at clinics. This planning involve the use of only one wall socket for all components of the system and

a quick, easy and accurate change of optical elements such as optical filters along the measurements or when starting a new one. The system was assembled on an aluminum suitcase, which could be drilled or cut without much losses of mechanical stability and it shows durability. This aluminum suitcase has an internal protection layer to avoid damage to instrumentation by shock or vibration.

The estimated system size was calculated by the maximum volume (considering the multiplication of the largest measurements of length, width and height) of each component at an optimum position to fulfill all the requirements planned. Taking into account these features, the best arrangement of the system components (Appendix I) was achieved by measurements of their dimensions and virtual design and reconstruction of each one of them using the Autodesk Inventor Professional 2015 software (San Rafael, California, USA). The same software was used to redesign the positions of the components to ensure the minimum volume required to accommodate the system; suitable refrigeration, support, damping and weight distribution; resistance to mechanical shocks and to minimize potential electrical contacts which could compromise the system operation. More details about the system construction and operation can be found at the Appendix II.

4.2.2 Computer assembling inside a metallic suitcase, system connections and instrumentation synchronization

The fluorescence lifetime spectroscopy system requires a computer to work because the TCSPC boards are PCI expansion cards which need to be directly connected into a PCI slot. This system must to be built using less space as possible and, then, the computer components need to be small enough to provide more space for the connection between the motherboard or TCSPC boards and the other system components. In addition, the cables connecting the external controls and lasers or the DCC-100 board are also important to the system operation and their length needs to be calibrated for the synchronization between the electrical and optical signals. More details about this synchronization, the computer components and the TCSPC boards are found, respectively, at the Appendix III, and Appendix IV and Annexes.

When assembling a computer in a metallic suitcase, careful should be taken in avoiding problems associated to a device operating at high electrical current in a reduced space. These problems are related to electrical grounding of the correct surfaces and the fixation of the motherboard and TCSPC boards in the suitcase walls without undesirable electrical contacts between one another or between boards and connections to the system components (monitor, keyboard, mouse, lasers or monitor power supply, connector attaching the system components and power supplies, SSD, USB2000-FLG spectrometer). In this case, the connections should not change the position of the other system components or its connections, such as the ones between the external controls and lasers or the photomultiplier. More details about these connections can be found in the Appendix V.

The computer was previously built on a computer cabinet with larger computer components (motherboard, power supply and hard disk). Before assembling the computer on the suitcase walls, the computer was assembled outside its cabinet or the suitcase for system operation testing. For this test, we installed the appropriate software for the computer and instrumentation. After both, system and spectroscopic measurements, were working properly the system was enclosed in the metallic suitcase.

For the motherboard fixation, a metallic plate was fixed in the appropriate position, and the suitcase was drilled to screw the appropriate connectors in the metallic plate and suitcase walls. After fixing these connectors, a ring of insulating material was positioned over them to minimize the electrical contact between the motherboard and the connectors. The motherboard was screwed in the positions as specified by the manufacturer (Appendix VI).

When all the system connections were operating properly and the components positions and connections were already set up, the length of the cables connecting the external controls and lasers or the DCC-100 board was minimized by assembling new cables with the necessary length to keep the synchronization. This synchronization also depends on the SYNC and CFD path lengths.

The electrical contacts of each pair of pins and the DE-15 connector shell of the original cables from the Becker and Hickl (Berlin, Germany) company were measured using a multimeter. The new cables were constructed with the appropriate length for the connection of the external controls and the lasers or DCC-100 board

and, to resynchronize the optical and electrical signals of the instrumentation, the SYNC and CFD cables' path length were adjusted. More details about the construction of cables are found in the Appendix VII.

4.2.3 Filter holder

Clinical measurements need to be fast enough to do not compromise the time of the medical appointment and the hospital routine. These measurements were optimized by projecting and constructing an optical filters' holder (figure 21), which was also designed to be closed, compact, functional, stable, easy to machine (each part), and to ensure a faster filters exchange during measurements.

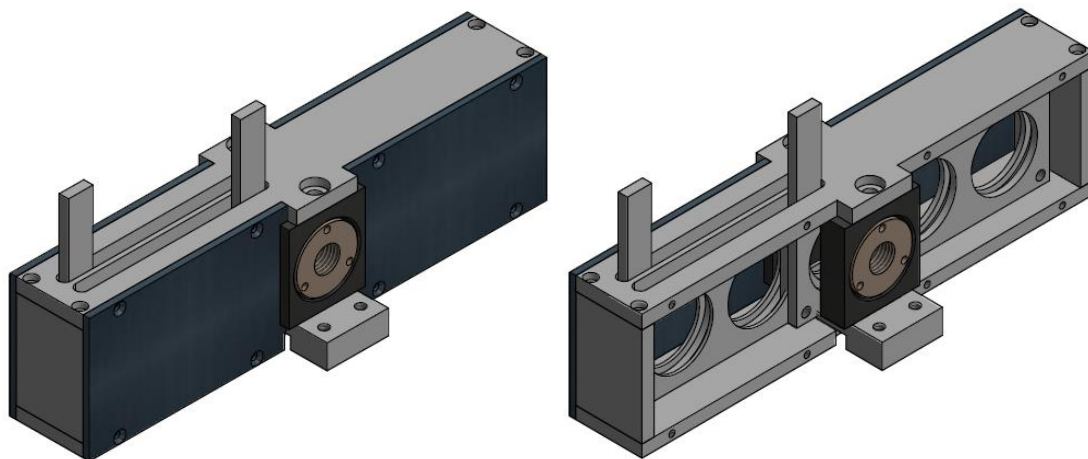


Figure 21 - Last version of the filter holder without the light collimators on its entrance and exit. The filter holder was designed to be closed, compact, functional, stable, easy to machine, and to ensure a faster filters exchange during measurements.

Source: By the author.

The base of the filter holder is fixed to a suitcase wall by using bolts in the edges of the base. In this base, two parts are used to a fast exchange of the filters may slide within the range allowed by the upper part of the filter holder (figure 22A and 22C). Each one of these two filters exchange parts (or sliding parts) may be opened in two units for filter exchange when measurements are not going on (figure 22B). This exchange requires the partial dismantling of the filter holder and may take some time. However, when the filter holder is already assembled, it is possible to use combinations of two among six filters during the measurements.

The steps between each filter exchange parts in the base and the top of the filter holder ensure that these parts will not rub into each other during the fast filters' exchange. The movement of these parts is also restricted by the front wall of the filter holder, which contains a shock absorber material and an adaptive angle input part for the optical fiber collimator (figure 22D). The fiber coupling and the maximum output signal is achieved by finding the correct positions and angles of the front wall, angles of the fiber collimators, and distances between the fibers and the collimators' lenses.

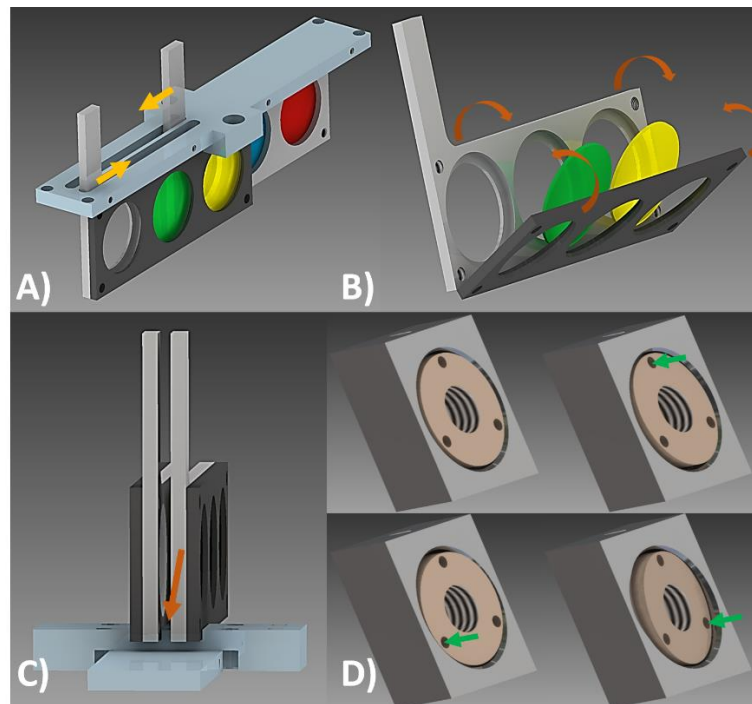


Figure 22 - A) Movements of the sliding parts for fast filters exchange during measurements. B) The sliding parts can be opened for filters replacement when it is necessary. C) The step between sliding parts allow their sliding without rub. D) The correction of positions and angles of the light collimators is performed by controlling the depth of the screws in the input part of the front wall of the filter holder.

Source: By the author.

One of the major challenges on assembling a filter holder for a portable instrumentation is the achievement of high optical precision in a limited space. Some concepts of optical alignment in an optical bench may be applied, but it is not possible to project parts which may easily lose their alignment during the system transportation or may be extremely small to regulate the components' positions and angles. To ensure the stability of this optical alignment, the parts were designed to be fragmented and screwed at many positions. This fragmentation allows more

alignment precision, by varying more degrees of freedom of each part and by making this precision independent on the machining precision of a unique structure. In addition to the alignment, the precision to machine a unique structure decreases because the milling cutter has a limited diameter to mill the edges, and a limited length and precision to machine deep structures. This also happens for other tools and machines that produce deep holes and threads. High precision also requires more time to make each structure and less flexibility to future adaptations and corrections in the filter holder.

In order to achieve the best configuration for the maximum output intensity of the filter holder, three versions were designed and evaluated. Since the first version, the filter holder was closed to allow minimum exposition to external light and possible dust which might accumulate in the filters and other optical components. This minimum exposition to external light is useful for reliable power measurements of the filter holder's output signals with no influence of light from a computer LCD display, for example. More details about the filter holder's version are found on the Appendix VIII.

4.2.4 Second floor parts

The "second floor" was constructed to optimize the volume occupied by the instrumentation at the suitcase. The best configuration based on all the aspects discussed before includes the presence of external controls in the upper part, one of the lasers with the cooler directed to the environmental air, and a hole to air circulation for the motherboard cooler and the TCSPC boards. The support for all these components were projected to be a support plate screwed at three points at one side and fixed on the other side by using the holders described on figure 23 in front of the motherboard coolers.

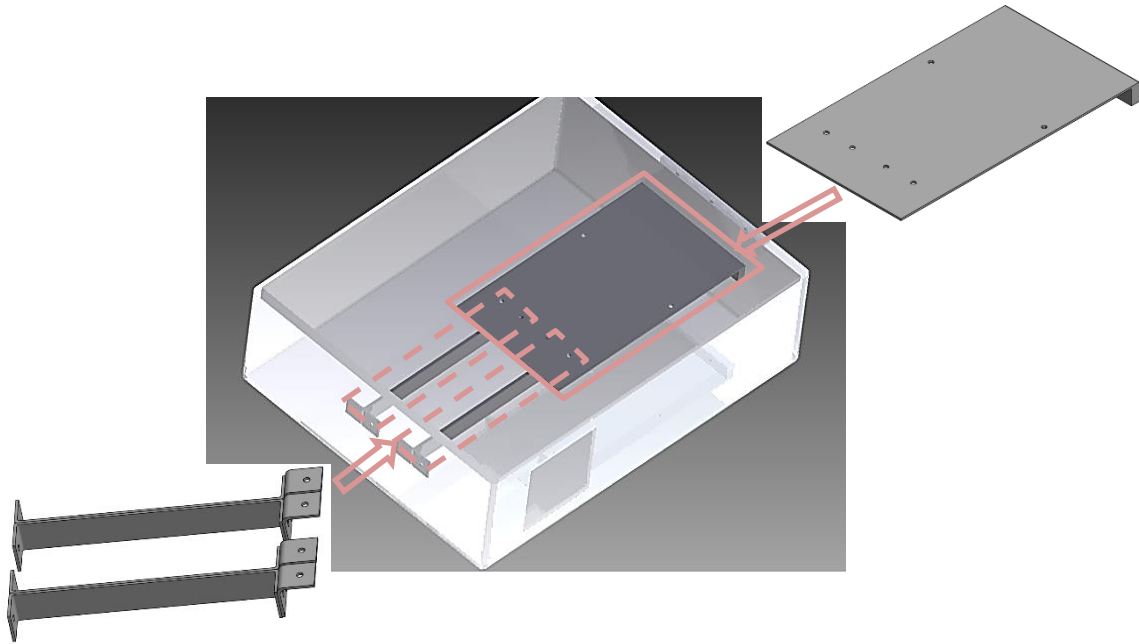


Figure 23 - The second floor for the system components was designed to support and fix a laser and two external controls and to have a reduced size for air circulation and less weight.
Source: By the author.

The volume and weight for the second floor parts was projected to be as less as possible and easy to machine and assemble. The support plate part was used to fix the instrumentation components together with another fixing parts discussed on the next section.

4.2.5 Fixation parts and system cooling

The fixation parts were projected to minimize the system weight and the difficulty of their machining, to ensure the weight distribution along the suitcase structure and their fixation efficiency considering the internal covering for mechanical protection and the contact area with the suitcase walls. In addition to the weight distribution, a number of holes' positions were chosen according to the distances between one another and the cuts on the suitcase structure for the air exits.

The proper system cooling was achieved by positioning the coolers in front of or in contact with the air exits (figure 24), which were made by cutting part of the suitcase walls with a rotating dremel and the suitable cutting wheel. The air exit for the motherboard is 7.5 cm far from the motherboard's cooler, which has an internal volume free for air circulation in front of it.

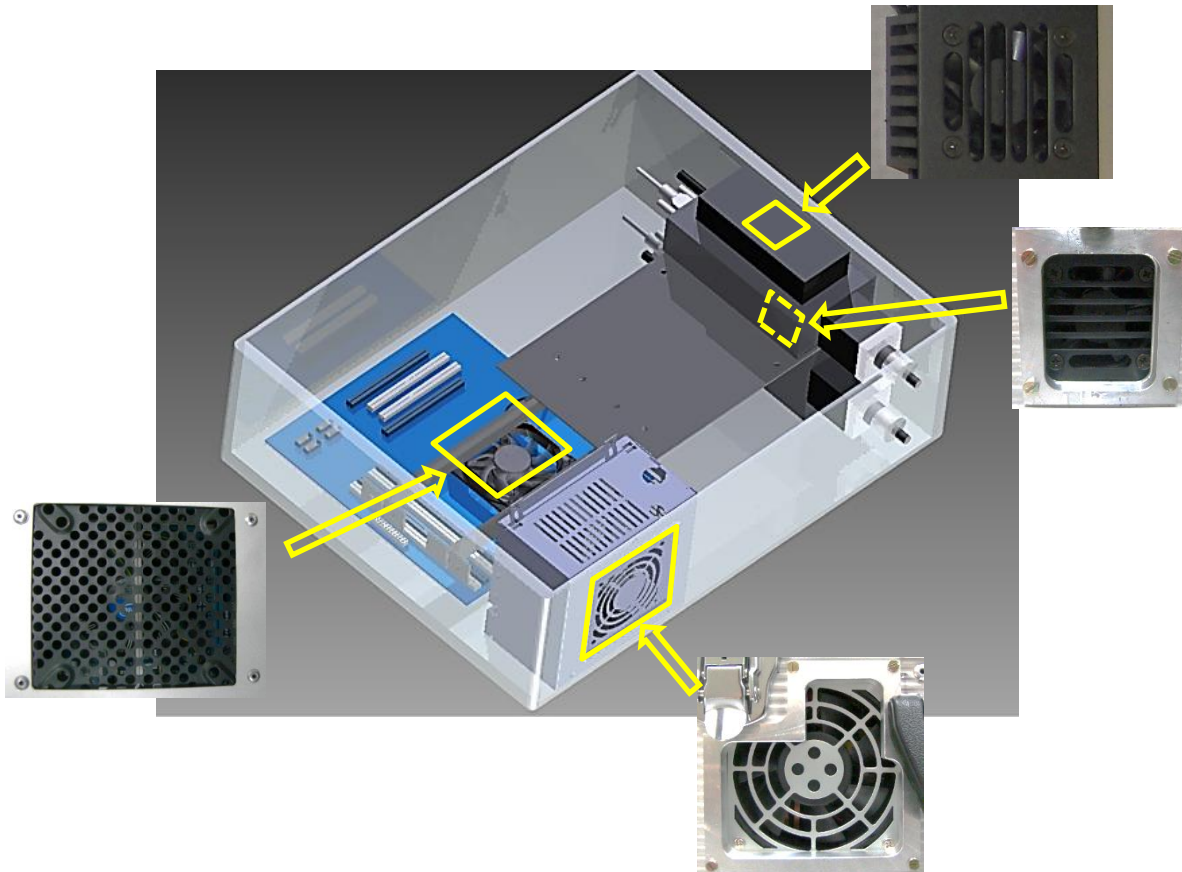


Figure 24 - Air exits for coolers of the power supply, lasers and computer processor are positioned at different sections of the suitcase and the coolers direction was optimized to provide air exchange with external environment or air circulation inside the suitcase.

Source: By the author.

The screws and nuts of the fixation parts (figure 25) were affixed until there was no observed movement and the mechanical stability was evaluated by simulating small vibrations on the system. The mechanical evaluation did not compromise the system operation.

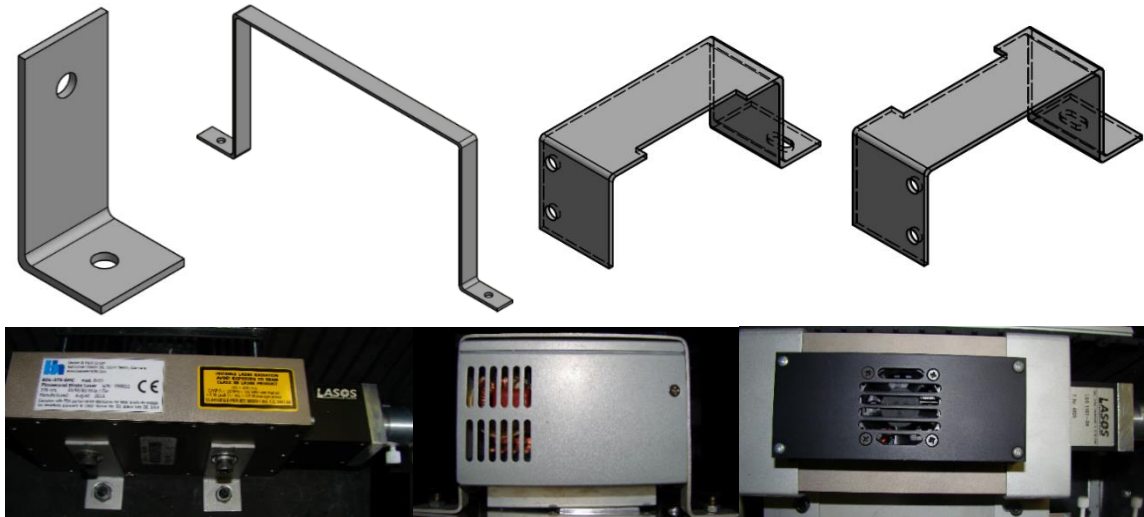


Figure 25 - Fixation parts (aluminum angles and custom channels) for lasers, and power supply were designed to easy machining and low weight.

Source: By the author.

4.2.6 Enclosing and protection parts

The system components are all enclosed in the suitcase by using a covering part (figure 26A) for no contacts between the system operator and electrical components, wires or connections, and optical components. This part contains holes for the air exits, access to the front panel (external controls, filter holder), and allows safety to the use of the system in clinics, an easier way to clean the system in the case of any spillage of clinical liquids, and protection for the system components, which have some fragile parts such as the motherboard, electrical connections and optical filters.

Other parts (figure 26B, 26C and 26D) are used for mechanical protection to the laser and its connections, power supply, and air exits. These parts also provide protection for the system operator, since, without them, the edges of cuts and holes in the suitcase surface are not perfectly smooth. In addition to the protection, they provide visual comfort for clinicians and patients, which are always present in the clinics during the fluorescence lifetime measurements.

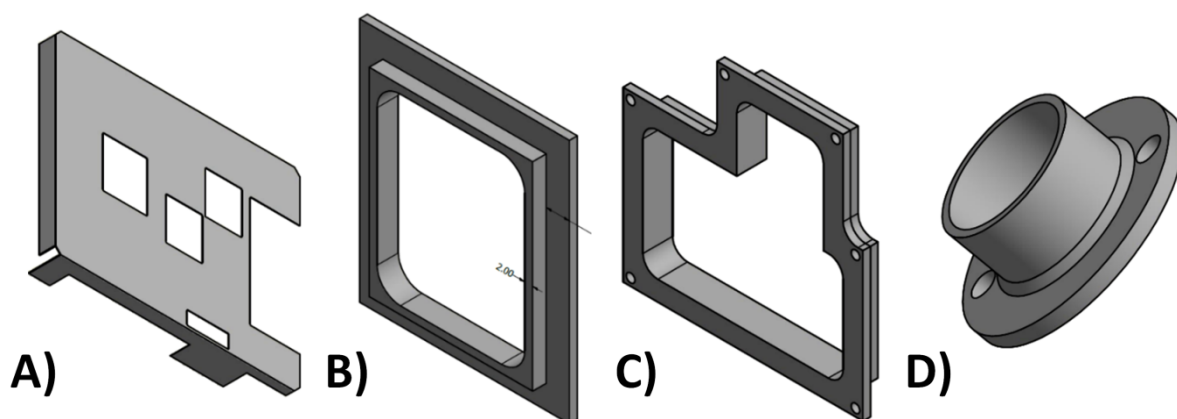


Figure 26 - A) Encasement part for system components protection and system operator access to the control panel. B) Protection part for the laser cooler. C) Protection part for the power supply cooler. D) Protection part for the laser exits. All protection parts provide visual comfort for patients and doctor in clinical environment.

Source: By the author.

4.3 Fluorescence lifetime system characterization and measurements

4.3.1 System characterization

The measurements of the fluorescence lifetime of the standard fluorescent molecule Rhodamine 6G and the IRF, i.e., the temporal pulse width acquired by the detector, are important to determine the fluorescence lifetime resolution of the system and if it is well calibrated. By using an appropriate photon counting rate, the fluorescence decay analysis is expected to result in the same average fluorescence lifetime as reported in the literature.

In order to obtain the temporal broadening due to the use of multimode fibers, the temporal width of the laser pulse was measured after it passes through the excitation and collecting fibers and after it strikes a scattering medium (solution 0.5% Lipofundin® (Laboratories B. Braun S.A., Rio de Janeiro, Brazil) in distilled water; figure 27). A PVC film was used to keep the fiber clean during the measurements. The chosen scatterer concentration is high for immediate scattering of the laser pulses, although the excitation wavelengths (378 nm and 445 nm) do not show high penetration lengths.

A Rhodamine 6G distilled water solution (Sigma Aldrich) 2.5 µg/ml used for calibration of the system was characterized by its absorption and fluorescence spectra using a 475 nm longpass filter, and 378 nm and 445 nm excitation (figure

28). This solution concentration avoids the formation of Rhodamine 6G aggregates in aqueous solution. The calibration of the system was assessed by comparing the measured average lifetime with values for Rhodamine present in the literature.

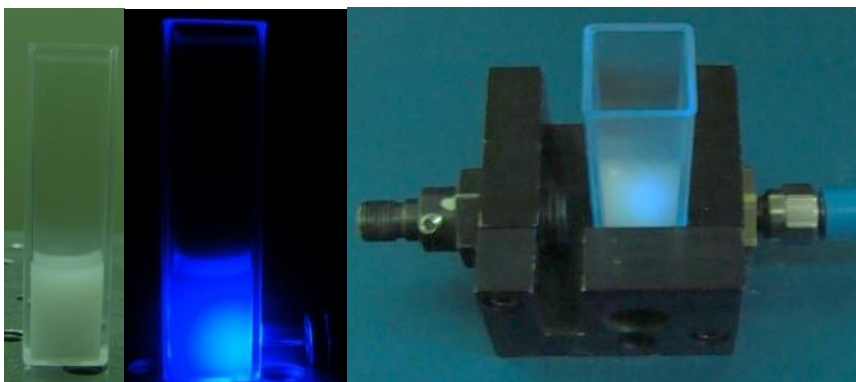


Figure 27 - An aqueous solution of 0.5% Lipofundin® was used as scattering medium for determination of the system instrument response function. Measurements were done in a cuvette using a proper support for the optical fiber connection.

Source: By the author.

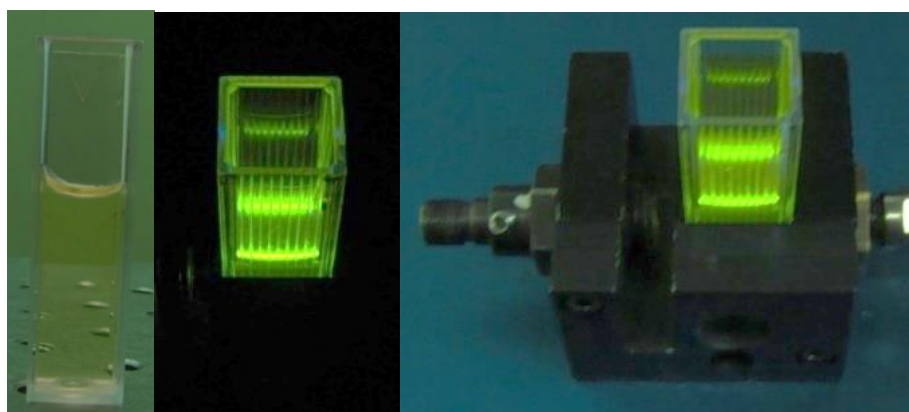


Figure 28 - The Rhodamine 6G solution was used to evaluate the calibration of the fluorescence lifetime system, by comparing the obtained lifetime with that reported in the literature. The same support as for the scattering medium was used for Rhodamine measurements.

Source: By the author.

Each acquired decay profile was processed using the SPCImage software (Becker and Hickl, Berlin, Germany). The fluorescence decay curve was fitted by a mono-exponential decay for both 378 nm and 445 nm excitations. The mean of the average lifetimes τ were compared considering the standard deviation among the measurements.

4.3.2 Measurements at turbid media

The increasing of optical diagnosis and treatment applications resulted in the need for noninvasively determination of the optical properties of living tissues. These properties are related to the scattering and absorption coefficients, which may predict the skin perfusion, blood oxygenation, tissue metabolism, and features of light distribution in tissues for diffuse reflectance measurements, photodynamic therapy and laser surgery planning. (66,67) These coefficients are related to optical processes and light propagation (light/matter interactions; figure 29). By understanding optical processes such as scattering effects in fluorescence lifetime measurements, we may understand how they change the analyzed parameters and determine the scattering coefficient of each sample, which is very useful for many optical applications.

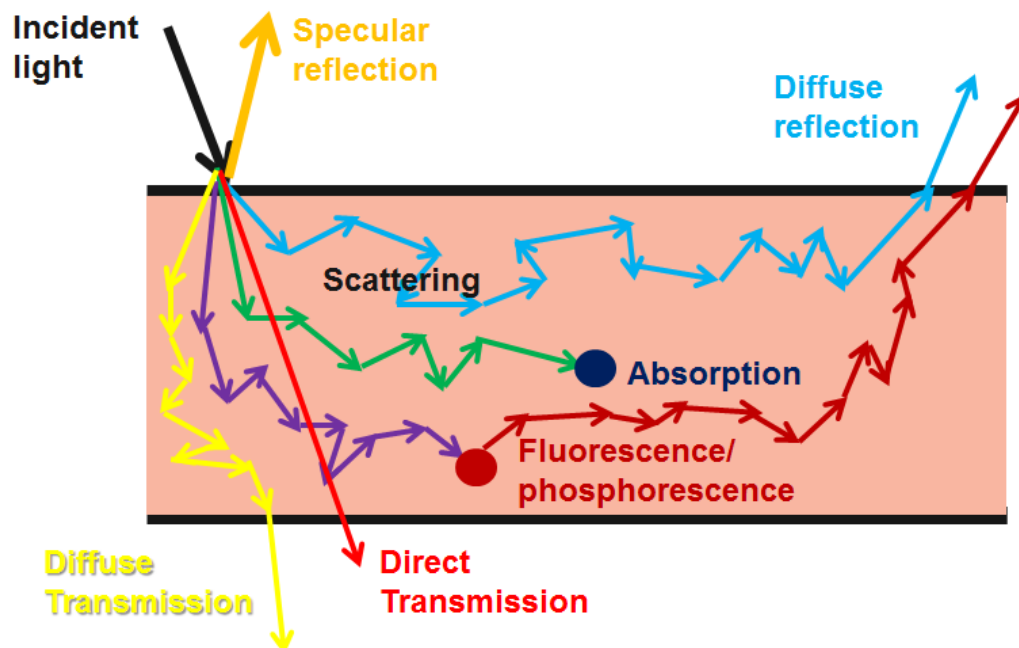


Figure 29- Optical processes on biological tissues may involve scattering, absorption, fluorescence, phosphorescence, specular and diffuse reflection, direct and diffuse transmission. They are usually complex to be analyzed, since the analysis of each individual interaction is not possible, but only the global resulted effect.

Source: By the author.

Information about optical interaction coefficients may be contained on the temporal spreading of a short pulse of light when it passes through a scattering medium. By investigating the relationship between optical interactions and time-

resolved signals, it is possible to create models to describe these interactions and determine the optical properties of biological tissues, and to develop new methods to analyze time-resolved measurements for diffuse reflectance and fluorescence lifetime spectroscopy. In order to understand the effects of light scattering in fluorescence lifetime measurements and the photons diffusion in turbid media, measurements of temporal broadening and time shift of the intensity maximum of the laser pulse were performed.

The temporal broadening was evaluated by measuring the full width at half maximum (FWHM) and the time shift, by collecting the reflection after the laser pulse travels through a fixed distance (L) in air, subtracting the time delay due to the system synchronization and the light travel, and comparing the time position of the intensity maximum measured for various concentrations of scattering media (0.25%, 0.5%, 1% and 2% of aqueous Lipofundin® solution), for various distances between the excitation and collection fibers (14.5 mm, 24.4 mm, 33.3 mm and 44.0 mm) and for photon count rates of around 10^5 and 10^6 (considered as “low” and “high” count rates). The bifurcated fiber (figure 30) was immobilized and used as the detection fiber (figure 31) during measurements in scattering media so that the distance between the fibers changed by moving the excitation fiber, which delivers the laser pulse to the sample. Distilled water was used to prepare the solutions. Measurements with the bifurcated fibers were also performed, but the FWHM and time shift parameters did not change significantly when the scatterer concentration was increased.

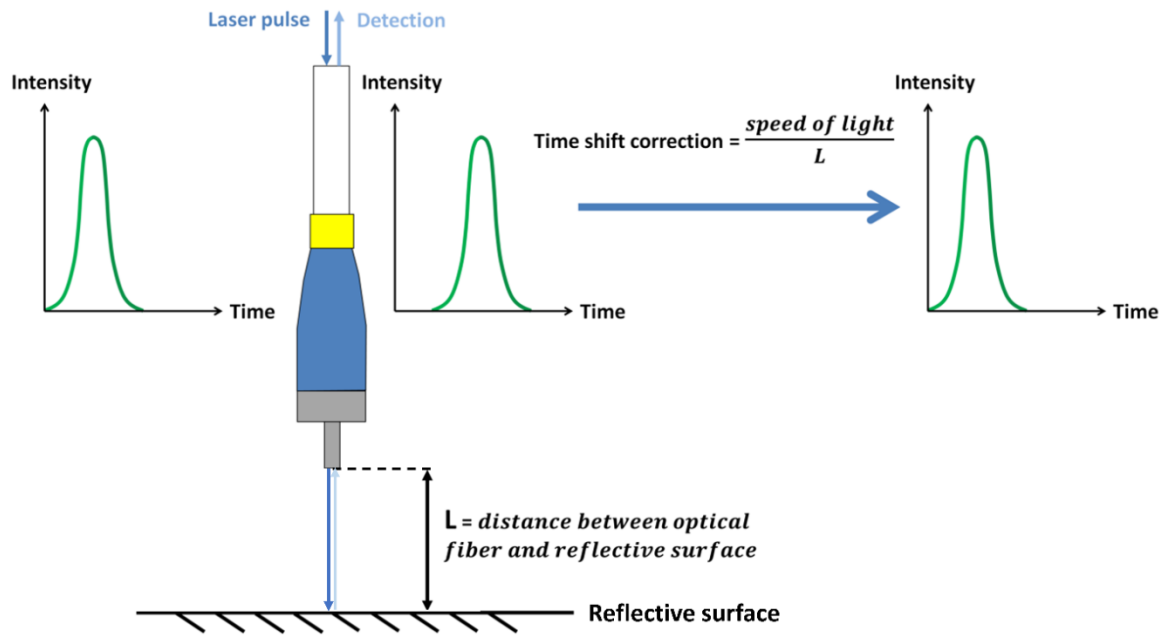


Figure 30 - In order to calibrate the system for determination of the time shift of the maximum intensity of the laser pulse, the optical fiber was positioned at a distance L from a reflective surface. By subtracting the time delay due to the system synchronization and the light travel from the detected pulse and fixing the distance L for all measurements, it is possible to make a correction for the time position of this pulse.

Source: By the author.

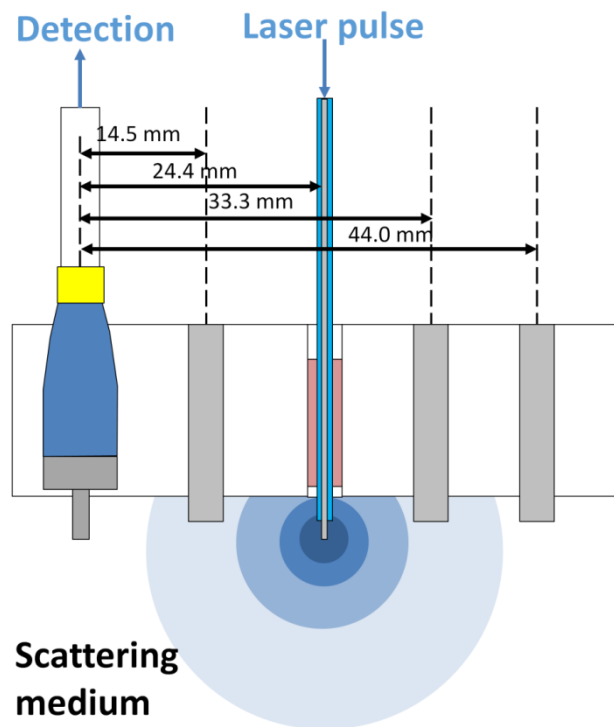


Figure 31 - Measurements in scattering media were performed using a holder to keep a fixed distance between the excitation and collection fibers.

Source: By the author.

4.4 Clinical measurements

4.4.1 Clinical evaluation

The volunteers with skin phototypes from 1 to 4 were evaluated at the Dermatology Ambulatory of Amaral Carvalho Hospital (Jau, Sao Paulo, Brazil) under the supervision of the Dr. Ana Gabriela Salvio, research collaborator in the clinical study. The volunteers were invited to participate in the study after the conventional clinical assessment and lesions classification. The invitation included an explanation about the study, its benefits for science and the improvement of diagnostic tools, the absence of individual and immediate benefits for the volunteer, the potential risks of the optical measurements and the other topics required by the Research Ethics Committee of Amaral Carvalho Hospital and presented in the participation agreement form. The informed written consent form was signed by the volunteers and the patients who accepted to participate in the study.

The investigated lesions were delimited by the dermatologist and cleaned with colorless detergent solution (alcoholic solution of 0.5% clorexidin) without any fluorescence emission at the excitation wavelengths used in this study. For each measurement, the optical fiber coupled to a 378 nm or 445 nm laser was gently positioned at the top of the lesion, and the fluorescence emission was collected using the adequate optical filters for the desired fluorophores selection in fluorescence spectroscopy or lifetime measurements (figure 32). The fiberoptic probe was protected using a PVC film, and changed before each lesion interrogation.

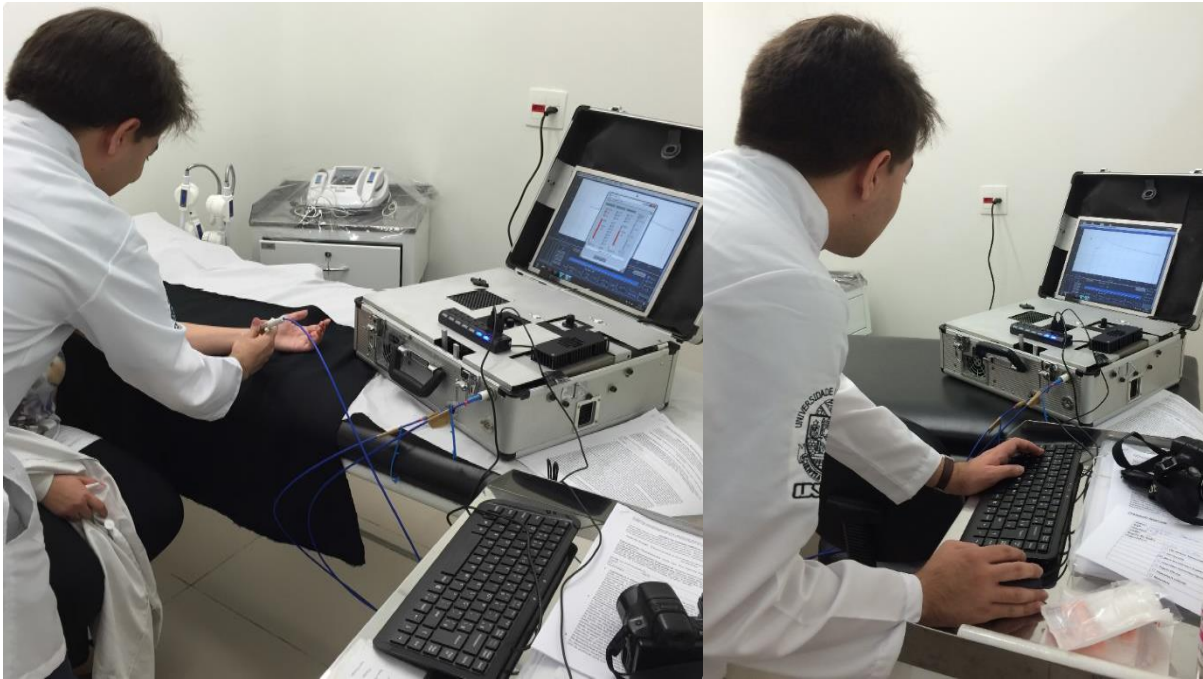


Figure 32 - Clinical measurements using the portable fluorescence lifetime spectroscopy system. The system is very compact and fits well in many places.

Source: By the author.

Among the investigated lesions, six SHs, twenty-five HNs, twelve BCCs, nineteen pigmented seborrheic keratosis (pigmented SK), four highly suspected melanomas and three pigmented basal cell carcinomas (pigmented BCCs) were evaluated. Skin lesions measurements were performed at five sites inside each lesion area and at five sites in normal tissue regions close to each lesion (in the same anatomical site). For skin lesions measurements, 48 volunteers participated in this study (ages range from 38 to 88 years).

For the comparison between the skin sun exposed and non-exposed areas, thirteen normal volunteers were involved in this preliminary study (the ages ranged from 20 to 37 years old). The dorsal forearm was chosen for the sun-exposed skin measurements and the volar arm, for the sun non-exposed skin measurements (figure 33).

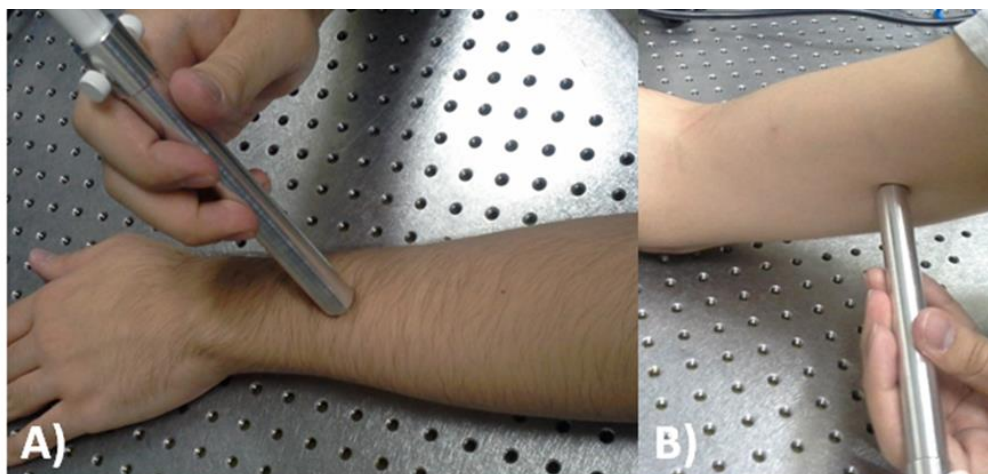


Figure 33 - Clinical sites for skin measurements of sun-exposed at dorsal forearm (A) and non-exposed at volar arm (B) regions. The optical probe was designed to allow a more uniform pressure, less external illumination and set angulation during clinical measurements.

Source: By the author.

4.4.2 Excitation and collection spectral windows

Both fluorescence spectroscopy and lifetime signals depend on which endogenous fluorophores are being interrogated by the combinations of excitation sources and optical emission components. Fluorescence emission of those fluorophores almost always overlap even using suitable excitation sources and optical filters to select the spectral window of the desired molecules (figure 34).

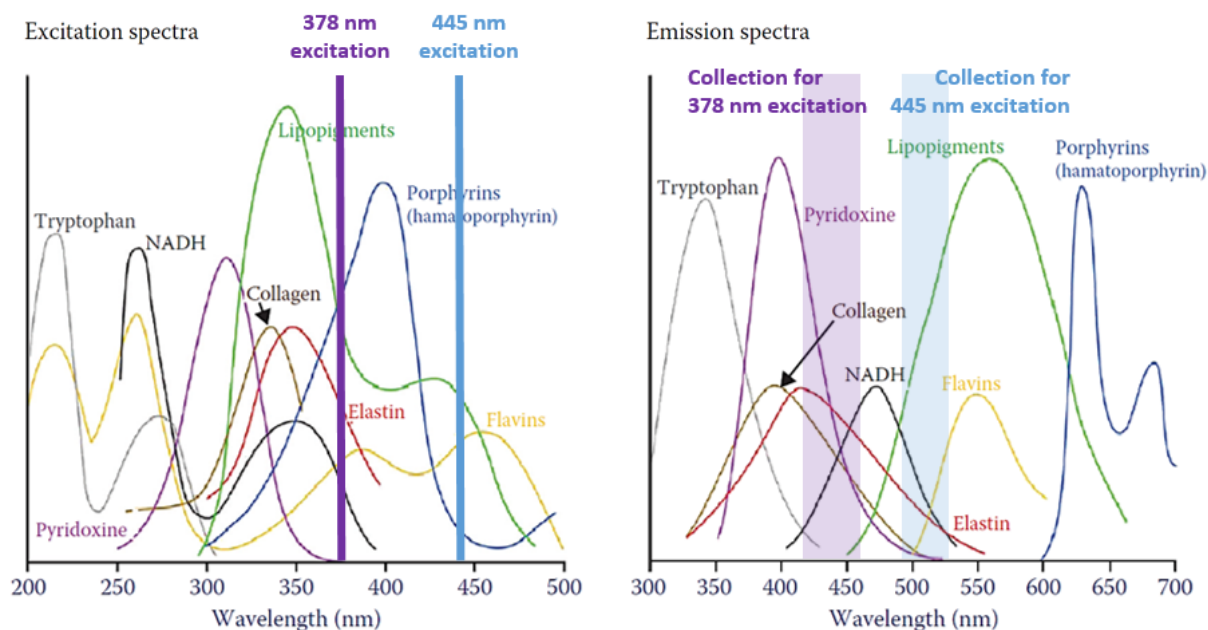


Figure 34 - The excitation sources wavelength and spectral window of bandpass filters used on this study are presented by the purple and blue lines and rectangles. The excitation and collection were made for spectral regions where the absorption and emission of targeted endogenous fluorophores are available without many interferences from the other ones. The fluorophores spectra are also shifted at biological tissues, which may make the choice of optical filters more suitable for the targeted fluorophores.

Source: Adapted from MARCU. (9)

The excitation sources (lasers) and bandpass filters used in this study were chosen in order to excite the NADH and FAD at wavelengths they have sufficient absorption and the other fluorophores have as less absorption as possible. The wavelengths of these lasers are limited to options available for diode lasers, which are more compact and easier to be part of a portable system. Among the picosecond diode laser options from Becker & Hickl GmbH company, only the 375 nm, 405 nm, 445 nm, 473 nm and 488 nm wavelengths are available so far in the 300 nm-500 nm range. It is also important to remember that the absorption and fluorescence spectra in the figure 32 may be also shifted when the endogenous fluorophores are in the microenvironment inside the cells.

When investigating the fluorescence lifetime of living systems, the use of 378 nm excitation combined to a (440 ± 20) nm bandpass filter at fluorescence emission or 445 nm excitation combined to (510 ± 15) nm bandpass filter may allow the selection of a fewer number of fluorophores (figure 32; NADH, collagen and elastin for 378 nm excitation and FAD, elastin and lipopigments for 445 nm excitation). The contribution of these fluorophores and fluorophores at the entire spectrum may be compared by using a longpass filter (418 nm longpass for 378 nm excitation and 475

nm longpass for 445 nm excitation). This comparison may also indicate which fluorophores should be targeted for a better discrimination of abnormal tissues at optical diagnostics and for understanding of the biological and biochemical tissue alterations. For the longpass filters, many fluorophores may contribute to the fluorescence lifetime (NADH, flavins, collagen, elastin, lipopigments and porphyrins for 378 nm excitation, and elastin, flavins, lipopigments and porphyrins for 445 nm excitation). In this study, the AF of sun exposed (photoaged) skin and non-exposed (normal) skin was collected by using combinations of bandpass and longpass filters, while measurements of clinically similar skin lesions were performed using only the bandpass filters.

4.4.3 Data processing

For the skin photoaging evaluation, the BiExp fit of the experimental fluorescence decay $F(t)$ was performed in a MATLAB (R2012a version, Mathworks, Natick, Massachusetts, USA) homemade routine. We obtained the relative coefficients and fluorescence lifetimes by fitting the experimental fluorescence decay $F(t)$ to the convolution between the instrument response function with a multiexponential decay function:

$$F(t) = IRF * \sum a_i e^{-\frac{t}{\tau_i}} \quad (2)$$

where t is the time after the excitation pulse of light, i is the number of exponentials, a_i are the relative coefficients of each exponential component and τ_i are the lifetimes for each component, respectively.

First analyses were performed by calculating the intensity and amplitude average lifetime (equations 3 and 4) for sun exposed and non-exposed skin for each excitation and optic filter.

$$\text{Intensity average lifetime} = \frac{\sum a_i \tau_i^2}{\sum a_i \tau_i} \quad (3)$$

$$\text{Amplitude average lifetime} = \frac{\sum a_i \tau_i}{\sum a_i} \quad (4)$$

The Student's t-test were performed using Microsoft Excel 2013 software (Microsoft Corporation, Redmond, Washington, USA). Significant statistical differences for $p < 0.001$ are represented by the (*) symbol at the boxplots.

For skin lesions measurements, each acquired decays were processed using the SPCImage 5.4.0 software (Becker and Hickl, Berlin, Germany). The fluorescence decay curve was fitted by a BiExp and a tri-exponential (TriExp) decay for both 378 nm and 445 nm excitations. In addition to the intensity and amplitude average lifetimes, the fractional contributions (equation 5) and the standard deviation for each parameter among the five measurements in the same region (inside each lesion or at each the normal tissue area) were evaluated.

$$\text{Fractional contribution } i = \frac{a_i \tau_i}{\sum a_j \tau_j} \quad (5)$$

The Wilcoxon rank sum test were performed using the MATLAB software. Significant statistical differences for $p < 0.05$ are represented by the (*) symbol at the boxplots.

5 RESULTS AND DISCUSSION

5.1 Fluorescence lifetime spectroscopy system characterization

5.1.1 Instrument Response Function and temporal broadening of laser pulse

The IRF was obtained by measurements of the temporal pulse width after the laser pulse passes through the scattering medium (figure 35). A medium with high scatterer concentration should induce an immediate scattering of the laser pulse and the detection of ballistic photons would be minimal, since the used photon counting rate does not lead to a pile-up effect, and the excitation and emission fibers are very close to each other. Figure 33 shows the pulse widths of the 378 nm and 445 nm lasers after their traveling through the excitation and collecting fibers.

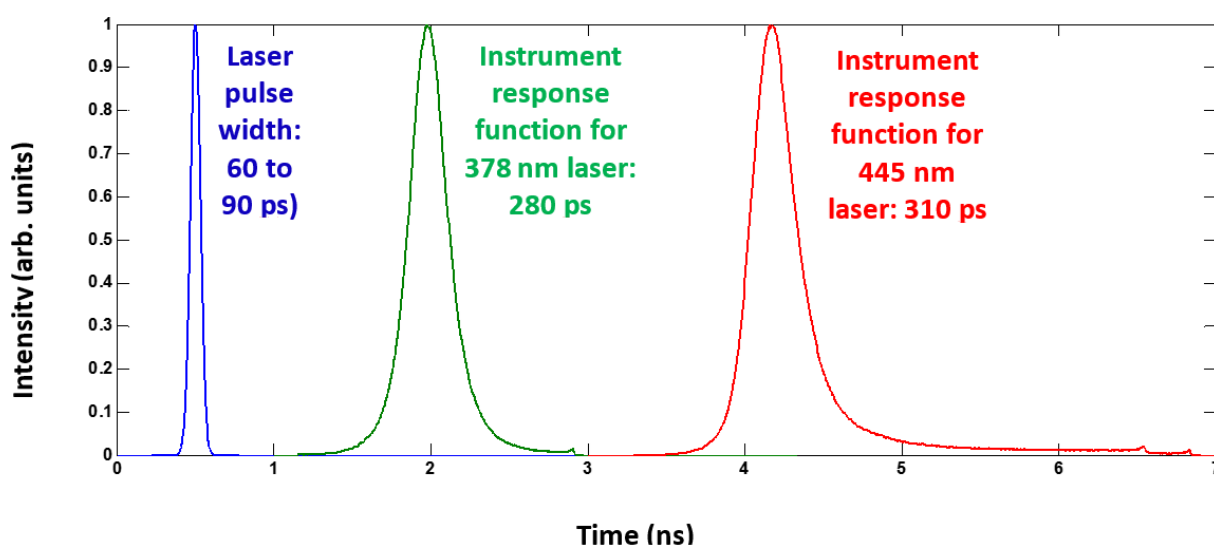


Figure 35 - Laser pulse compared to IRF curves obtained for 378 nm and 445 nm light backscattering. The observed decay is highly faster than the most of the biological tissues molecules.

Source: By the author.

IRF measurements showed that the laser pulse temporal width is around 300 ps. So, it is possible to have accurate measurements for lifetimes greater than 300 ps, which includes the most of the average lifetimes of molecules present in biological tissues (200-5000 ps). In addition, this temporal width allows a satisfactory

fluorescence lifetime resolution to distinguish the shortest lifetime among the fluorophores to be monitored in future biological tissues (NADH and FAD), which can reach between 300 and 400 ps.

5.1.2 System calibration

The Rhodamine 6G absorption, fluorescence spectra, and the presence of Soret band showed that the solution is well standardized (figure 36). The Rhodamine 6G fluorescence decay was measured using 20 MHz and 50 MHz laser repetition rates (figure 37), since the signal acquired using 50 MHz provides less signal to noise rates, but does not correspond to the complete decay for fluorophores with high fluorescence lifetimes such as the Rhodamine 6G. The average lifetime obtained for Rhodamine was of (4.1 ± 0.3) ns. In the literature, the average lifetime for Rhodamine diluted in water is reported to be about 4.1 ns (68–71).

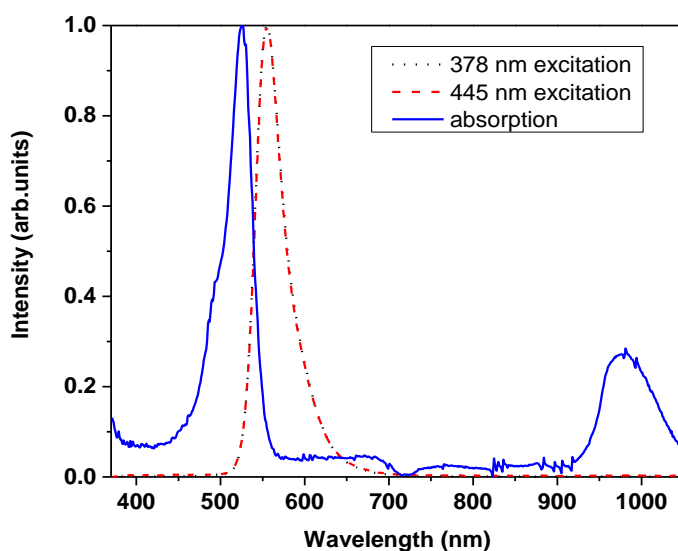


Figure 36 - Absorption and fluorescence spectra of Rhodamine 6G at 378 nm and 445 nm excitation. The typical bands of rhodamine indicate that the solution is well standardized.

Source: By the author.

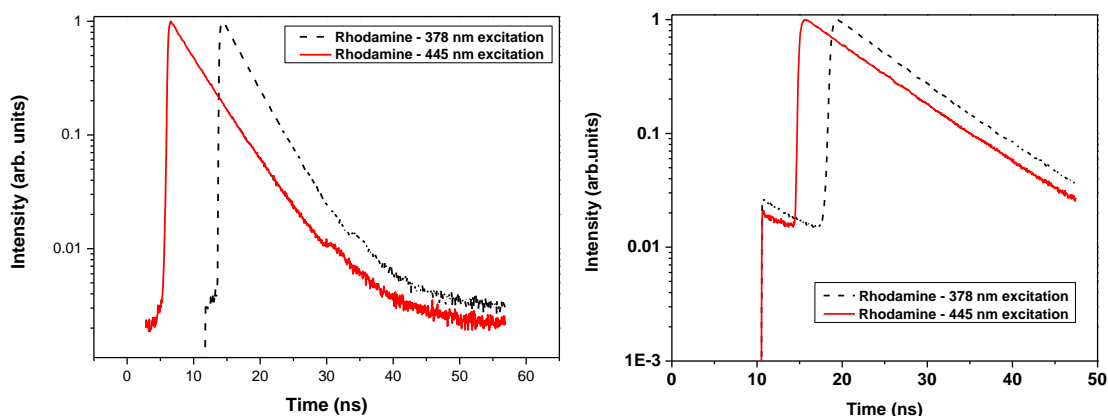


Figure 37 - Decay curves for Rhodamine 6G, obtained at 378 nm and 445 nm excitations and 20 MHz (left) and 50 MHz (right) repetition rate. The 20 MHz decay can be observed until the intensity returns to background values and may lead to more stable fluorescence lifetime values after the decay curve analysis.

Source: By the author.

The agreement between the measured and the reported values of the fluorescence lifetime (4.1 ns) for Rhodamine 6G indicates that our fluorescence lifetime spectroscopy system was properly calibrated with respect to other systems described in the literature, especially the systems that use the same fluorescence lifetime analysis method as SPCImage software uses.

5.1.3 Fluorescence lifetime changes as a function of laser gain

The fluorescence lifetimes of Rhodamine 6G were measured with different laser gains (parameter that controls the laser power) and a photon count rate between 10^5 and 10^6 photons/sec (figures 38, 39). The use of these photon count rate values increase the signal to noise ratio of the collected fluorescence decay curve and decrease the standard deviation for the measurements, reducing possible errors in its exponential decay fitting.

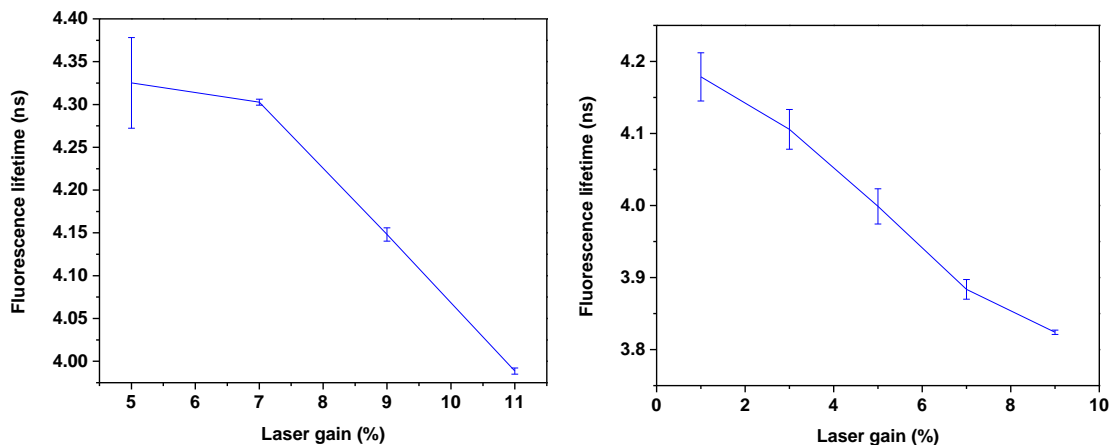


Figure 38 - Fluorescence lifetime as a function of laser gain at 378 nm excitation and 20 MHz (left) and 50 MHz (right) repetition rate.

Source: By the author.

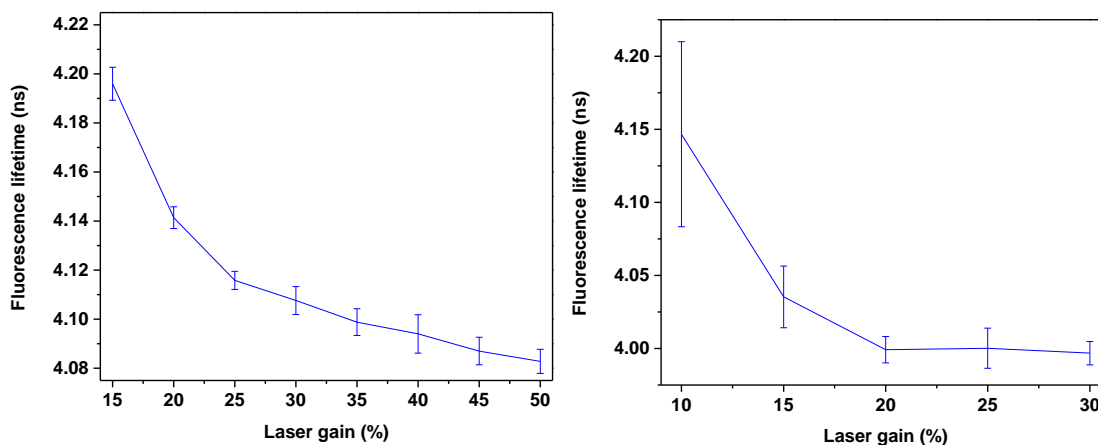


Figure 39 - Fluorescence lifetime as a function of laser gain at 445 nm excitation and 20 MHz (left) and 50 MHz (right) repetition rate.

Source: By the author.

The standard deviation and the fluorescence lifetime change in function of laser gain and are minimized for greater laser powers that keep the photon rate at 10^5 to 10^6 photons/s range.

5.2 Time of flight measurements on scattering media

5.2.1 Increasing the scatterer concentration

As the scatterer concentration increases, the detected signal became broader and a tail similar to a decay appeared due to the increased diffusion of photons in the scattering medium (figure 40). This behavior was similar for both 378 nm and 445 nm

wavelengths and the detected signal for 378 nm was broader than the same for 445 nm when using high scatterer concentrations. This broadening was already expected, since the 378 nm wavelength has less penetration when compared to 445 nm, considering only scattering processes.

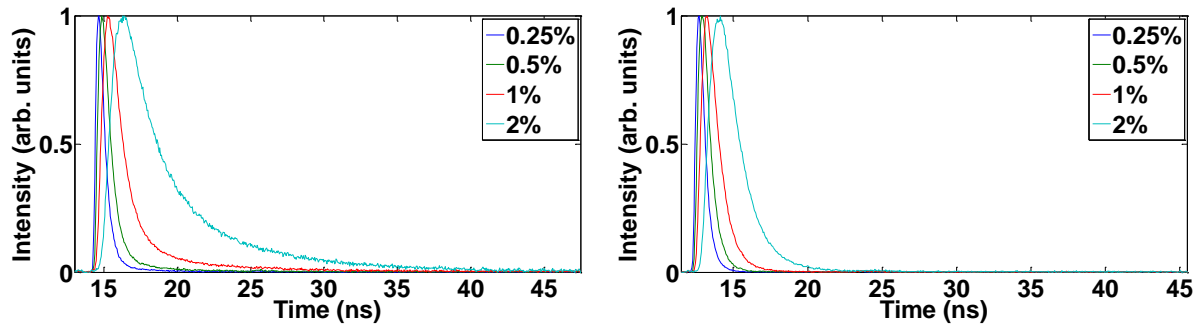


Figure 40 - The detected laser pulses for 378 nm (left) and 445 nm (right), 44.0 mm distance between fibers and varying the scatterer concentrations.

Source: By the author.

When comparing the FWHM and the time shift of the intensity maximum for each distance between the excitation and collection fibers (figures 41, 42), an increase in both parameters was observed as the scatterer concentration increased. For the 14.5 mm distance, the signals of low photon count rate had 0.1 ns more of FWHM for concentrations equal or above 1%, and approximately 0.05 ns less of time shift for concentrations equal or below 1%. This behavior was not observed for the other distances measured. For the 24.4 mm, 33.3 mm and 44.0 mm distance and above, the FWHM for 378 nm was, respectively, around 0.5 ns, 1 ns and 1.5 ns above the 445 nm signal. When considering the 44.0 mm distance, this FWHM difference became observable at 1% concentration. By comparing the FWHM and time shift behavior for both wavelengths, we observed the FWHM may be sensitive to wavelength-dependent effects due to scattering processes, while the time shift is mainly sensitive to wavelength-independent scattering processes.

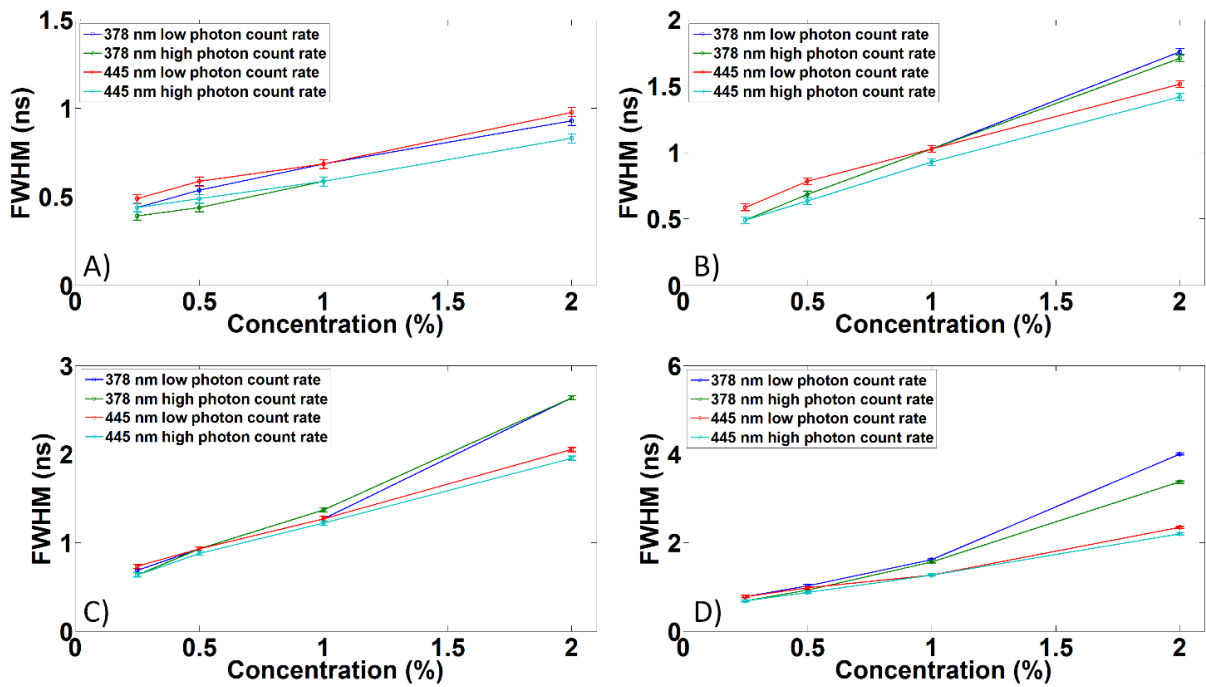


Figure 41 - The FWHM of time-of-flight signals for distances of 14.5 mm (A), 24.4 mm (B), 33.3 mm (C), and 44.0 mm (D) increase with the scatterer concentration. As the scatterer concentration and distances increase, the 378 nm FWHM becomes higher than the 445 nm one, which suggests that the wavelength-dependent scattering effects become relevant for the distances and concentrations where the FWHMs for these wavelengths are separated.

Source: By the author.

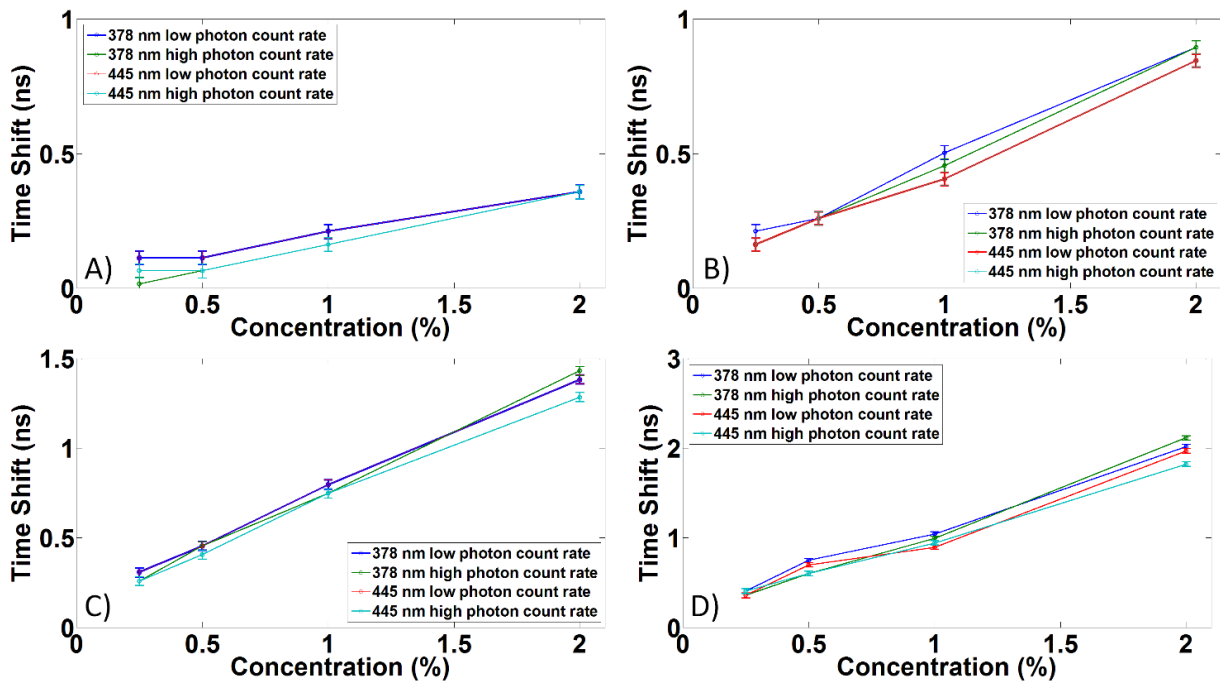


Figure 42 - The time shift of time-of-flight signals for distances of 14.5 mm (A), 24.4 mm (B), 33.3 mm (C), and 44.0 mm (D) increase with the scatterer concentration. The investigated scattering effects may be mostly related to wavelength-independent processes, since there is almost no difference between the time shift values for each wavelength.

Source: By the author.

For fixed wavelengths and power, the FWHM and time shift increased with the scatterer concentration and the distance between excitation and collection fibers (figures 43, 44). The time shift, in most of cases, depend almost linearly on the scatterer concentration, except by the time shift value for 0.5% concentration in both 378 nm and 445 nm wavelengths. The FWHM for 378 nm did not show great differences when using 33.3 mm and 44.0 mm distances for concentrations equal or below 0.5%, while, for 445 nm, it did not show these differences for the same distances and concentrations equal or below 1%. The behavior for FWHM curves was also different when comparing 378 nm and 445 nm wavelengths because the FWHM and its variation increase more rapidly with concentration for 378 nm.

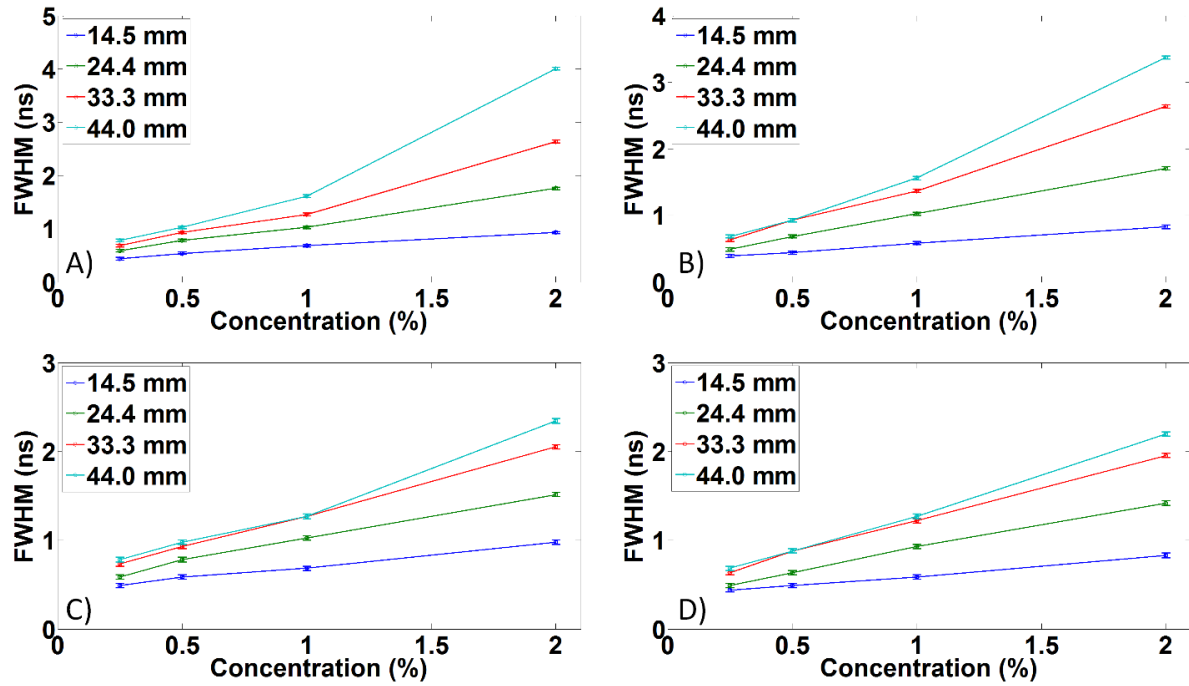


Figure 43 - The FWHM of time-of-flight signals for 378 nm low (A) and high (B) photon count rates and 445 nm low (C) and high (D) photon count rates increases with scatterer concentration. The behavior of this increasing is different for each wavelength, and the FWHM did not increase more for distances higher than 33.3 mm and low scatterer concentrations.

Source: By the author.

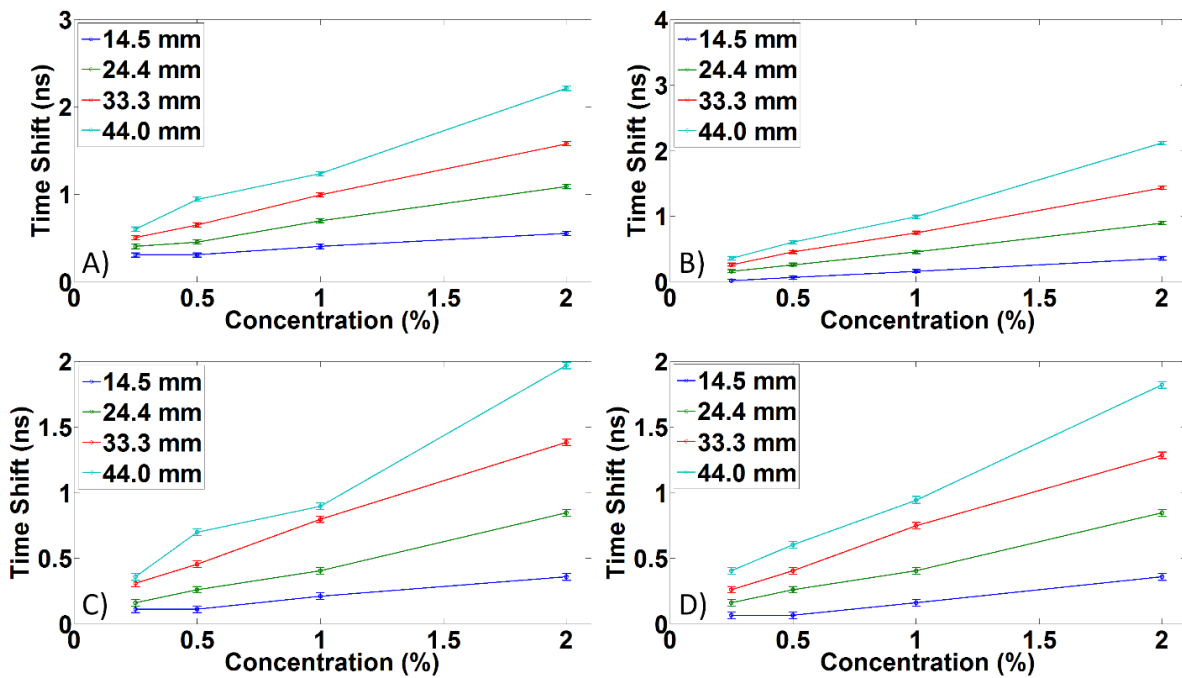


Figure 44 - The time shift of time-of-flight signals for 378 nm low (A) and high (B) photon count rates and 445 nm low (C) and high (D) photon count rates, in most of cases, increase almost linearly with the scatterer concentration. An irregular change in the linear tendency was observed for the 0.5% concentration.

Source: By the author.

5.2.2 Increasing the distance between excitation and collection fibers

By measuring the detected signals for various distances between excitation and collection fibers, a similar behavior compared to the scatterer concentration was observed. In this case, the detected signal for 378 nm was also temporally broader than 445 nm signals, confirming again what was expected by these wavelengths penetration on scattering media (figure 45).

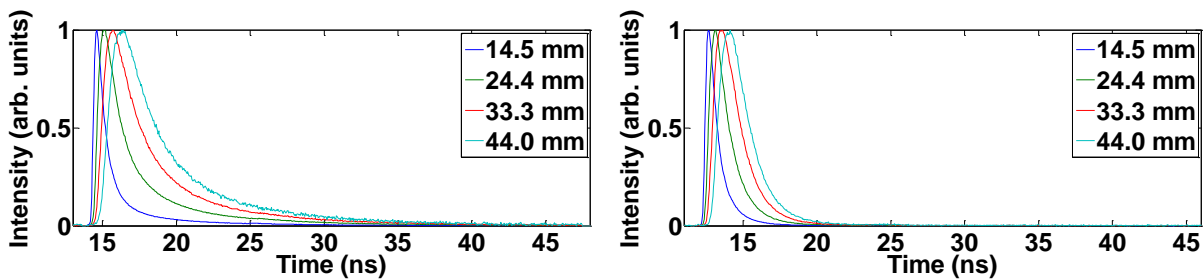


Figure 45 - The detected laser pulses for 378 nm (left) and 445 nm (right), 2% of scatterer (Lipofundin®) concentrations and varying the distance between fibers.

Source: By the author.

When considering 0.25% or 0.5% concentrations, and the appropriate distances, we observed that measured FWHMs and time shifts for low photon count rate were larger than the same parameters for high photon count rate (figures 46, 47). This behavior was observed for FWHMs at distances equal or above 24.4 mm for 0.25% concentration and distances below 33.3 mm for 0.5% concentration, and, for time shifts, at the 44.0 mm distance for 0.5% concentration. The tendencies concerning photon count rates changed for 1% and 2% concentration, since the 378 nm FWHMs and time shifts were larger than the same parameters for the 445 nm wavelength, when considering the 1% and 2% concentration, and 44.0 mm. By monitoring the FWHM for 2% concentration (figure 46D), we have observed that the FWHM difference between 378 nm and 445 nm wavelengths starts from the 24.4 mm distance between fibers.

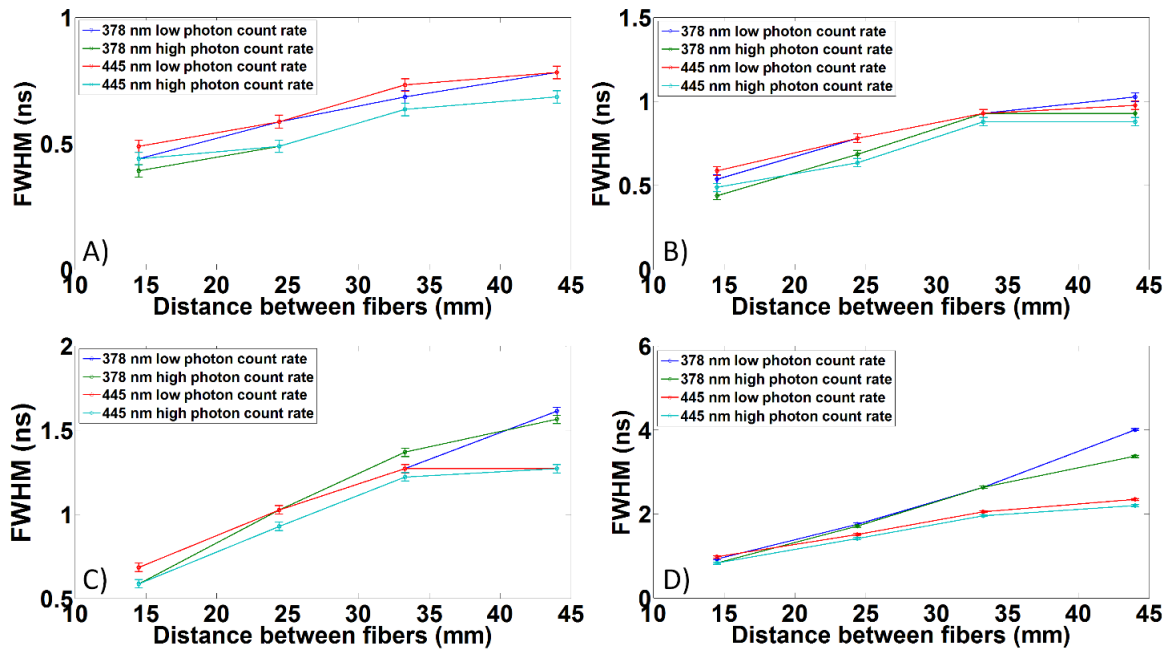


Figure 46 - The FWHM of time-of-flight signals for 0.25 % (A), 0.5% (B), 1% (C) and 2% (D) concentration increases with distances between fibers. The FWHM sensitivity for wavelength-dependent scattering processes starts from the 44.0 mm distance for 1% concentration or 24.4 mm distance for 2%.

Source: By the author.

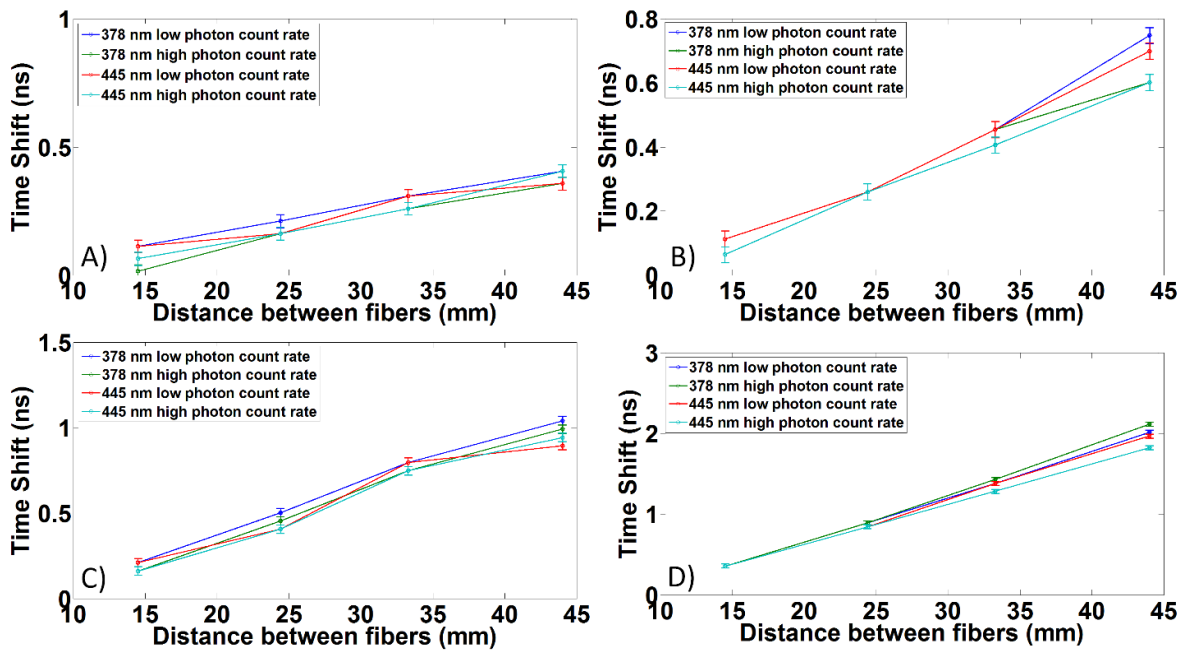


Figure 47 - The time shift of time-of-flight signals for 0.25 % (A), 0.5% (B), 1% (C) and 2% (D) concentration increases with distances between fibers. The time shift may be more sensitive to wavelength-independent scattering processes, since the time shift values for each wavelength are similar. For the 1% and 2% concentration, a small difference is observed in the time shift for each wavelength.

Source: By the author.

The observed scattering effects on the FWHM of time-of-flight measurements may be present on fluorescence lifetime measurements and may change the obtained lifetime values by changing the IRF broadening depending on the scattering coefficient of each probed region. Since we do not know the IRF and its broadening for each measurement, the best we can do is to suppose the best IRF for each measurement. For the SPCImage software, the synthetic IRF is supposed to be the first derivative of the rising edge of the experimental curve. To improve the IRF determination, more investigation about the relationship between time-of-flight signals and the optical properties of biological tissues is necessary.

Next steps include the implementation of Monte Carlo simulations to model the light scattering and describe the performed measurements. The investigation of these measurements may allow the determination of optical properties of turbid media and biological tissues, and the understanding about optical processes related to fluorescence decay changes, which are very important for this study.

5.3 Photoaging process at sun exposed and non-exposed skin

5.3.1 Photoaging process and fluorescence lifetime

In our study, photoaged (sun-exposed) and normal (non-exposed) skin were investigated by using the fluorescence lifetime analysis, since their fluorescence spectra are very similar (figure 48). Photodamage caused to the collagen and elastin fibers may induce abnormal production of elastin and degradation of collagen by metalloproteinases; skin regeneration or development of precancerous lesions may also induce NADH and FAD metabolic changes at photoaged skin; and melanin production is also increased. All these endogenous fluorophores may contribute to the discrimination of normal and photoaged skin.

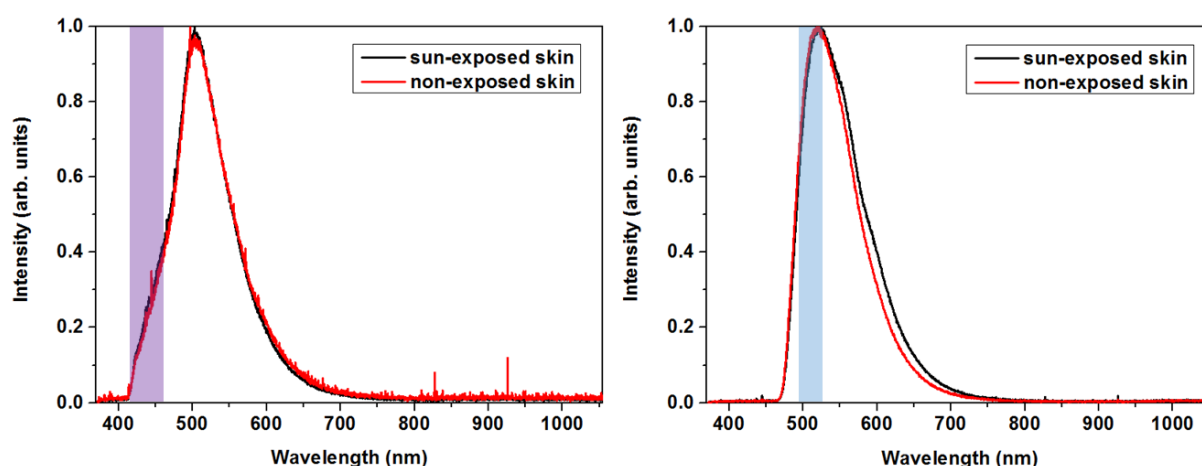


Figure 48 - Fluorescence spectra of sun-exposed and non-exposed skin for 378 nm (left) and 445 nm (right) excitation. The areas in purple and blue are the spectral window of bandpass filters used in fluorescence lifetime measurements.

Source: By the author.

The fluorescence lifetime analysis was based on the targeted fluorophores when using the bandpass and longpass filters. The bandpass filters are not centered at the maximum of fluorescence spectrum because the main targeted fluorophores of this study (NADH, FAD, collagen and elastin) are localized approximately in the spectral windows showed in the figure 48. Analyses comparing the responses for bandpass and longpass filters may contribute to further studies aiming to differentiate normal skin from each skin lesion, since they need to be independent of the variability of skin phototypes, and they require information about the possible areas

where a lesion may develop, particularly photoaged regions, and the contribution of endogenous fluorophores emission such as melanin, collagen and elastin.

5.3.2 Fluorescence decays

Measured fluorescence decay curves for each configuration of excitation sources (378 nm or 445 nm) and optical filters (longpass or bandpass filter) are shown on figure 49. The fluorescence decays of sun non-exposed skin using 378 nm excitation, on average, decay slower than sun exposed skin, which may indicate that sun non-exposed skin uses to have longer lifetimes. Using 445 nm excitation and the bandpass filter, the opposite occurs and the fluorescence decays are similar when using the longpass filter.

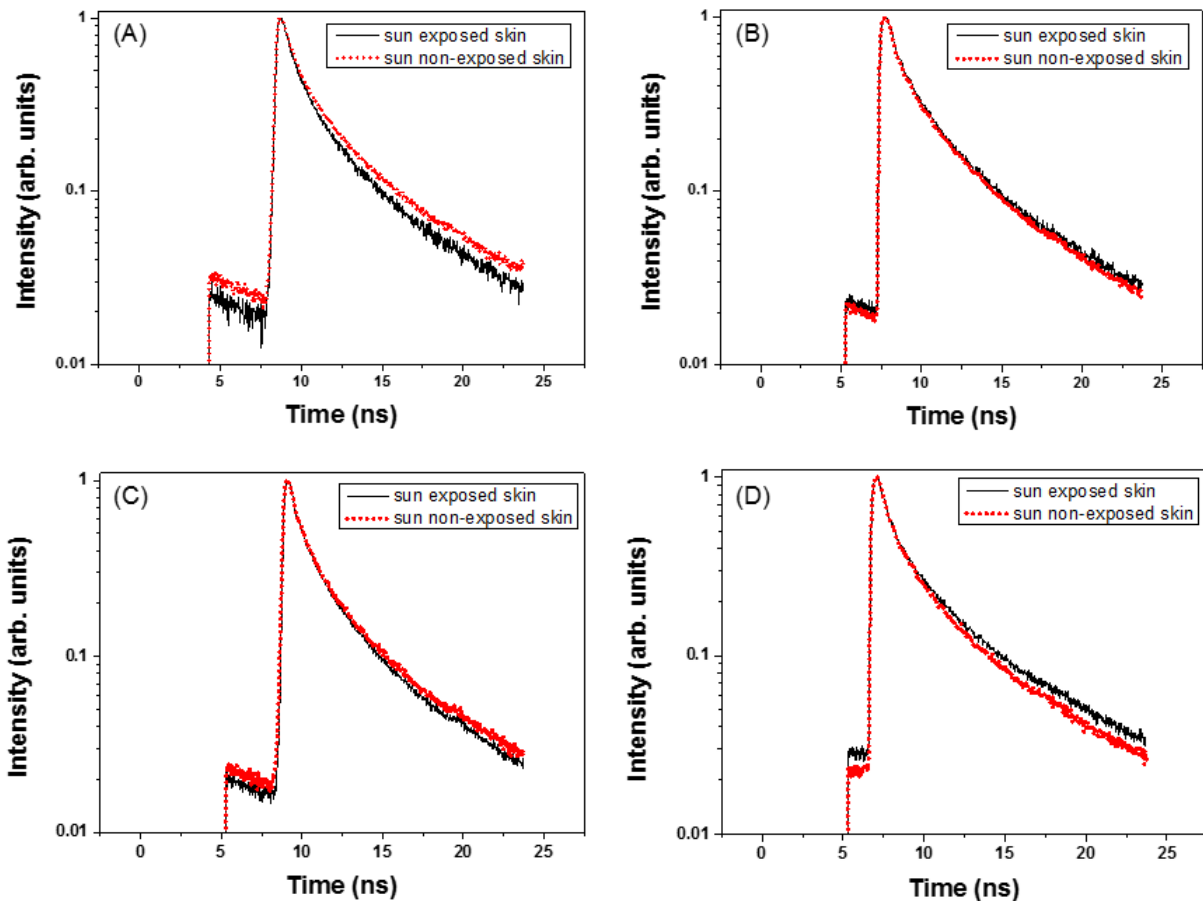


Figure 49 - The decay curves of sun exposed and non-exposed skin show some differences for all combinations of excitation sources and optical filters. (A) shows this comparison using 378 nm excitation and a 418 nm longpass filter, B) using 445 nm excitation and 475 nm longpass filter, C) using 378 nm excitation and (440 \pm 20) nm bandpass filter and D) using 445 nm excitation and (510 \pm 15) nm bandpass filter).

Source: By the author.

The use of each longpass filter allows the detection of fluorescence emission of all fluorophores excited by 378 nm or 445 nm wavelength. For 378 nm excitation, they may include NADH, flavins, collagen, elastin, lipopigments and porphyrins and, for 445 nm, elastin, flavins, lipopigments and porphyrins. These molecules may provide information about the global processes of skin metabolism. Some particular processes were investigated by using the bandpass filters, which may provide information about fluorophores emitting only at the filters spectral range. They may include NADH, collagen and elastin for 378 nm excitation and FAD, elastin and lipopigments for 445 nm excitation.

5.3.3 Boxplots and data discrimination

Comparing the boxplots between sun-exposed and non-exposed areas (figures 50-53) of skin for average lifetime, significant statistical differences are only observed for intensity lifetimes using 378 nm excitation and the amplitude lifetime using 378 nm excitation and the longpass filter. However, a_1 , a_2 , τ_1 and τ_2 parameters show a better discrimination between sun-exposed and non-exposed skin, because these parameters show statistical differences with $p < 0.001$ even when the same is not shown for intensity and amplitude average lifetimes. These average lifetimes showed a better discrimination for 378 nm excitation when compared to the 445 nm one.

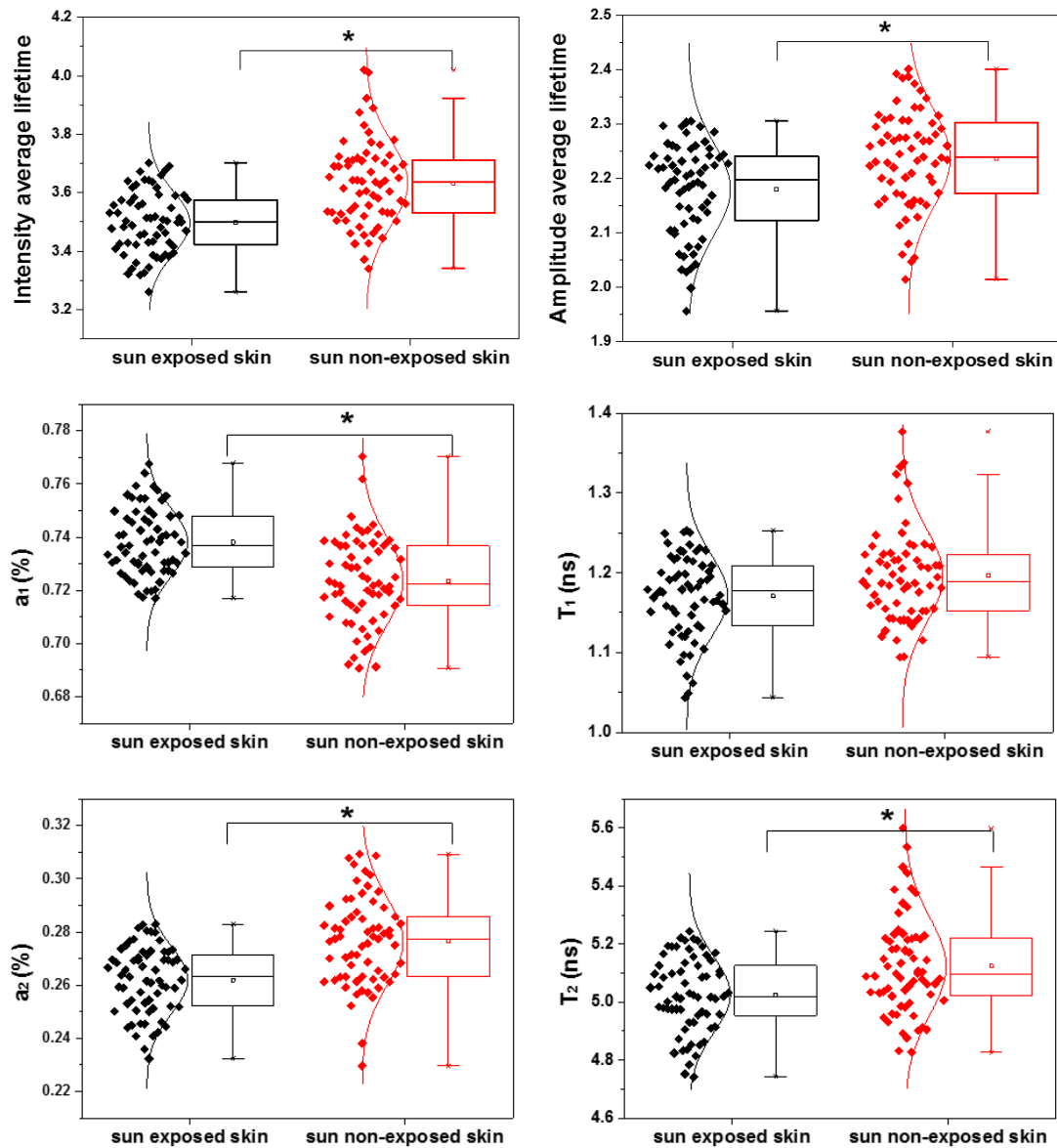


Figure 50 - Boxplots for parameters obtained in the data analysis for 378 nm excitation and longpass filter.

Source: By the author.

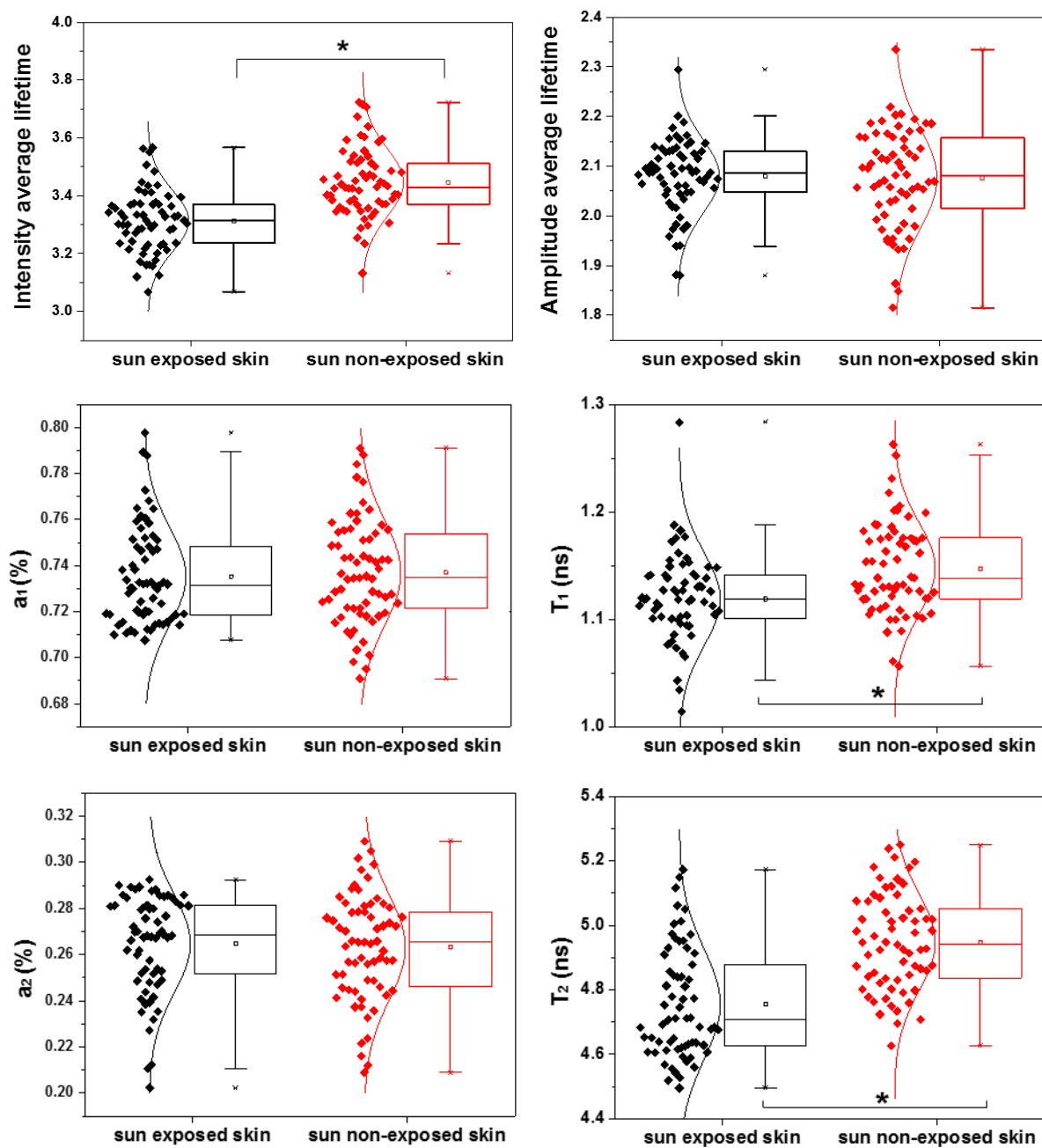


Figure 51 - Boxplots for parameters obtained in the data analysis for 378 nm excitation and bandpass filter.

Source: By the author.

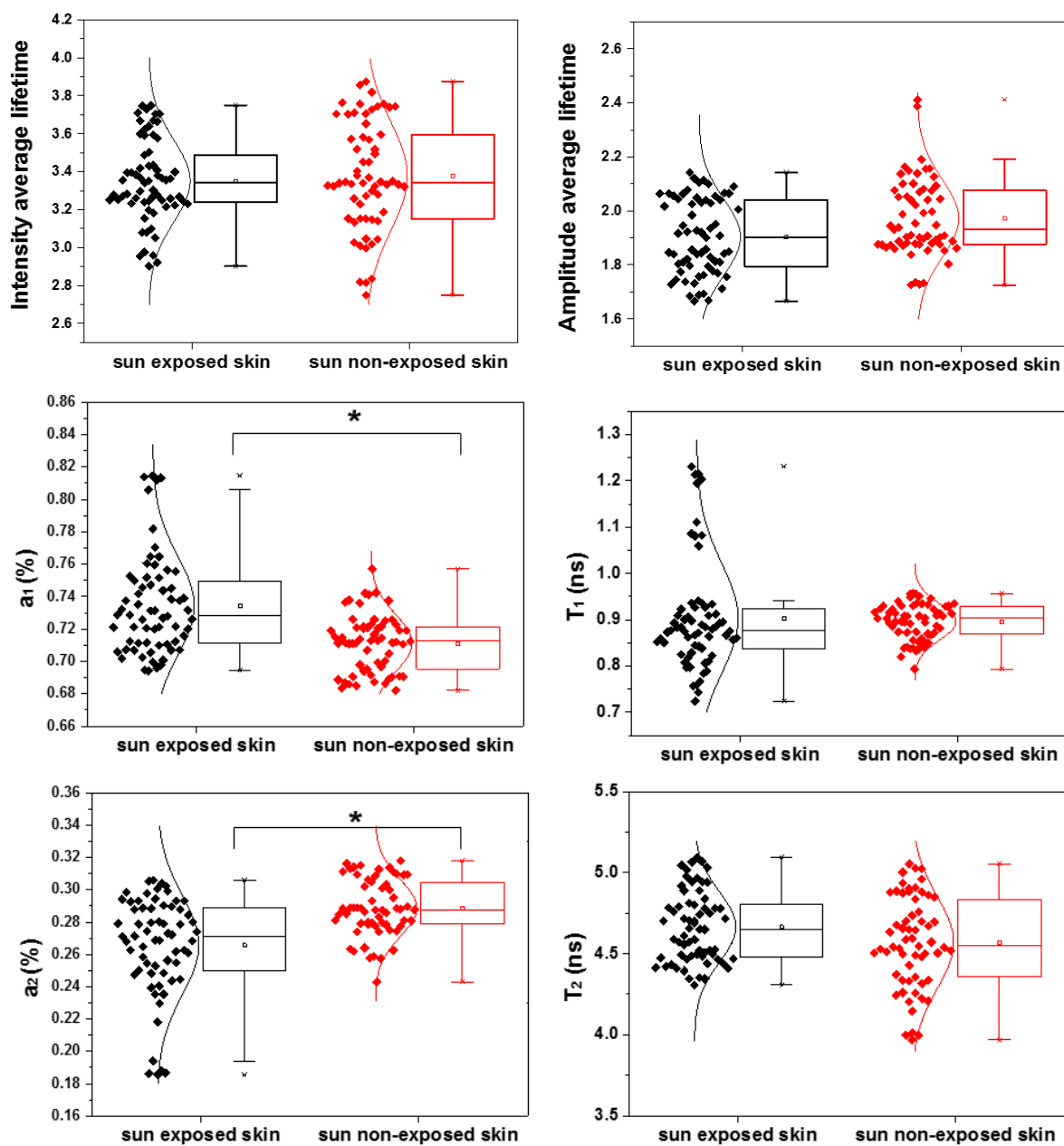


Figure 52 - Boxplots for parameters obtained in the data analysis for 445 nm excitation and longpass filter.

Source: By the author.

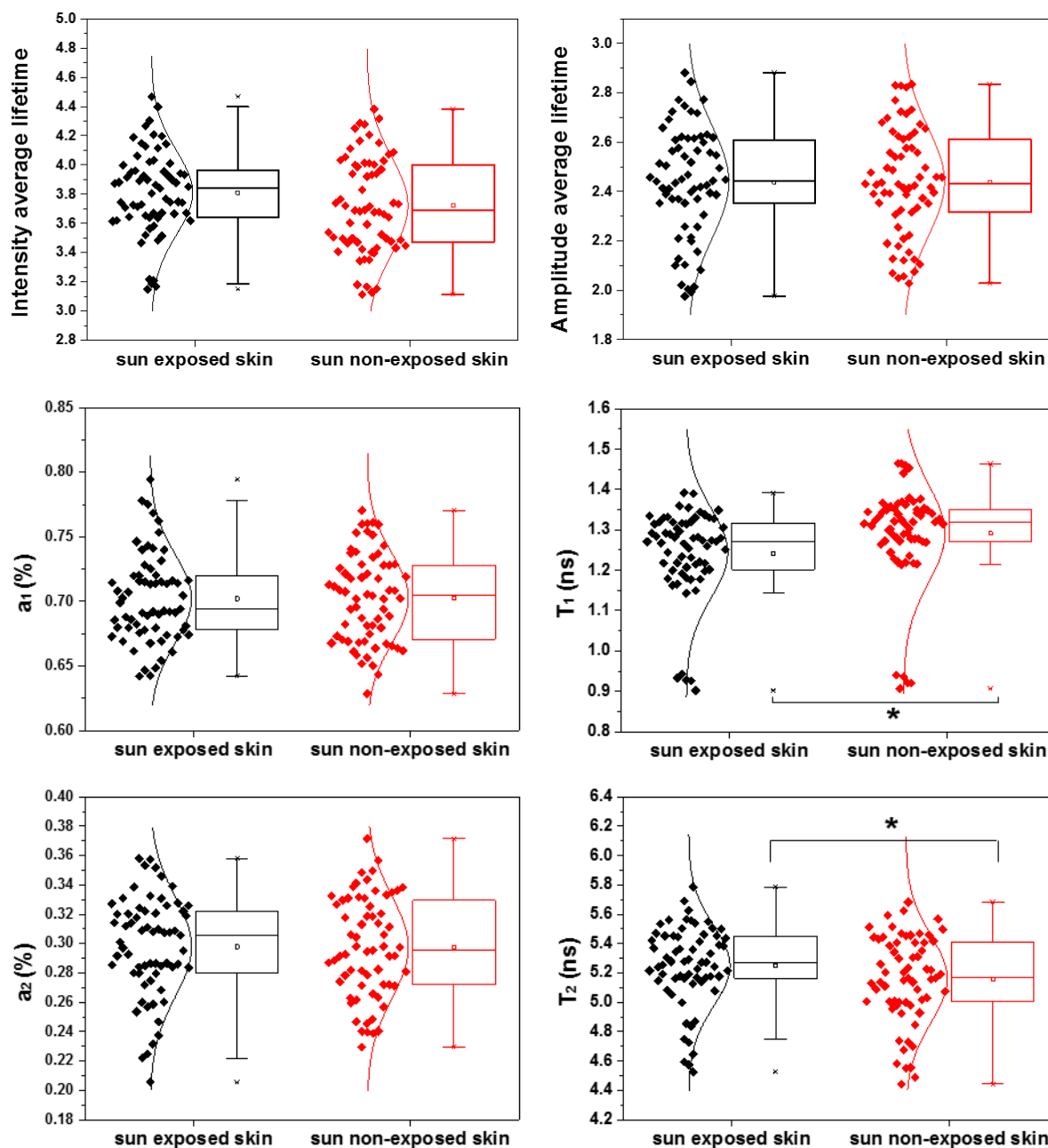


Figure 53 - Boxplots for parameters obtained in the data analysis for 445 nm excitation and bandpass filter.

Source: By the author.

The single coefficients and lifetimes analyzed show a significant statistical difference at relative coefficients a_1 and a_2 for both excitations using the longpass filters, while the short and long lifetimes show this difference for both excitations using bandpass filters.

These results suggest the microenvironment of the endogenous fluorophores selected by the bandpass filters (NADH, collagen and elastin for 378 nm excitation

and FAD, elastin and lipopigments for 445 nm) changes as the fluorescence lifetimes become different for the sun exposed and non-exposed skin areas. But, when the fluorescence contribution of other endogenous fluorophores are included by using longpass filters, changes on the fluorescence lifetimes become insignificant and the relative coefficients can be used to discriminate those areas (table 1). This behavior may be associated with the proportion of fluorophores out of the bandpass filters range (flavins, lipopigments and porphyrins for 378 nm and porphyrins for 445 nm) and the biological processes associated with them.

Table 1 - Main used features of fluorophores and analysis concerning the excitation wavelengths and filters used for sun-exposed and non-exposed skin measurements

Filter's type	Long-pass filters	Band-pass filter
Discrimination	Relative coefficients	Lifetimes
Probable discrimination due to	Proportion between fluorophores	Fluorophores microenvironment
Suspected changes on the following fluorophores (378 nm)	Flavins, lipopigments and porphyrins	NADH, collagen and elastin
Suspected changes on the following fluorophores (445 nm)	Porphyrins	FAD, elastin and lipopigments

Source: By the author.

Considering the fluorescence lifetime values (Table 2) for 378 nm excitation, the melanin, collagen and elastin may be the main targeted fluorophores and, for 445 nm excitation, FAD may be the main target, based on the values described on the literature. (39)

Table 2 - Fluorescence spectral and lifetime characteristics of endogenous skin fluorophores

Fluorophore	Excitation	Emission	Fluorescence lifetime
NAD(P)H	340	450–470	0.3 (free), 2 (bound)
FAD	370, 450	530	5.2 (free), 1 (bound)
Lipofuscins	UV/visible	570–590	Multiexponential
Collagen	300–340	420–460	0.2–0.4/0.4–2.5
Elastin	300–340	420–460	0.2–0.4/0.4–2.5
Melanin	UV/visible	440, 520, 575	0.2/1.9/7.9

Source: Reproduced from KOENIG; RIEMANN. (39)

In general, all combinations of excitation sources and optical filters made the discrimination possible for sun exposed and non-exposed areas, even for young adult volunteers' skin, which have been less exposed to sun over time than middle-aged/senior volunteers. Next steps include the use of multivariate data analysis and data mining tools for classification of sun exposed and non-exposed skin and investigation of aging and photoaging at older voluntaries. This analysis may be useful for applications at dermatology and aesthetics by assessing the photoaging degree, which may suggest the chance to development of precancerous lesions or the moment when an aesthetic procedure is needed.

5.4 Clinically similar skin lesions

5.4.1 Fluorophores and chromophores for clinically similar skin lesions

For measurements on clinically similar skin lesions, the excitation wavelengths may be absorbed by many endogenous molecules (NADH, collagen and elastin for 378 nm excitation and FAD, elastin and lipopigments for 445 nm excitation) or chromophores such as Hb, HbO₂, keratin and melanin. The excitation wavelengths used have a poor penetration into biological tissues and, then, the Hb and HbO₂ absorbance, which might be relevant in cases of inflammation, should not have much interference on the performed measurements. As a non-invasive and fast procedure, keratin layers were not removed from the skin lesions and may contribute to the fluorescence signal by absorbing the excitation and emission light or by emitting

fluorescence at the collection spectral window. (72) This absorbance depends on the stratum corneum thickening when keratin-rich cells proliferate to give some protection against UV damage on skin and to repair this damage. The melanin is also an important chromophore, especially for the pigmented lesions. Melanin is produced in the melanocytes and, depending on the melanocytes concentration and distribution, the signal to noise ratio may decrease to unacceptable levels in some areas and the signal can be highly heterogeneous for the same skin lesion. When the signal to noise ratio is too low, an adequate exponential decay fitting becomes a challenge and can also lead to fluorescence lifetime parameters heterogeneity.

By using the 378 nm and 445 nm excitation, we planned to focus on metabolic changes of tissue, which may lead to a better discrimination of cancerous lesions from normal tissues or benign lesions, due to Warburg effect. Collagen and elastin signals may contribute to the fluorescence decay and this contribution make the fluorescence decay more complex, depending on the abundance of collagen and elastin molecules excited. So, the fluorescence lifetime spectroscopy, in this case, was used to discriminate benign from malignant lesions, to help the clinician in the choice of the best treatment for each lesion, since the clinically similar aspects may confuse clinicians that are not dermatology specialists (which usually first assess the lesion clinically), and to investigate the fluorescence lifetime parameters from skin measurements *in vivo* when using BiExp and TriExp decay fittings.

5.4.2 Bi-exponential and tri-exponential decay parameters

Both BiExp and TriExp parameters were very useful for the discrimination between groups of non-pigmented and pigmented lesions. For 378 nm, this discrimination of all combinations of non-pigmented and pigmented lesions was possible using BiExp or TriExp parameters. For 445 nm, BiExp parameters were able to discriminate between all groups of non-pigmented lesions and the pigmented SK from pigmented BCC, while all combinations of non-pigmented and pigmented lesions were discriminated using TriExp parameters. By comparing the lifetime values obtained in this study when using the TriExp decay fitting with the lifetimes of endogenous fluorophores in the table 2 and the spectra in figure 34, the preliminary results suggest that the 378 nm measurements may be related to the free NADH,

collagen and elastin (first lifetime component), to bound NADH, collagen and elastin (second lifetime component), and to melanin (third lifetime component), and the 445 nm measurements may be associated to bound FAD, elastin and lipopigments (first lifetime component), to free FAD, elastin and lipopigments (second lifetime component), and to melanin (third lifetime component). The tendencies of BiExp parameters for malignant and benign lesions are compared with that expected based on the studies reported at. (14,15) The tendencies of the average lifetimes are compared to that described for fluorescence lifetime skin measurements in the literature. (52,64,73-74)

The BiExp and TriExp decay fittings were performed because, in some cases of non-pigmented lesions and in most cases of pigmented lesions, TriExp ones led to significantly lower values of χ_r^2 (relatively to each measurement) of SPCImage software. These lower values may suggest that a BiExp decay may not be used to describe efficiently the decay processes related to the tissue AF when using 378 nm and 445 nm excitations. Although BiExp decays are not useful for a complete parameterization of the experimental decays described in this study, fitting them demands less parameters (relative coefficients and lifetimes), which may lead to less restrictions concerning the convergence of the fitting solution to a global minimum. The more starting values for these parameters are used, more solutions converging to a local minimum are found. So, the parameterization for TriExp fittings increase the solutions space and allow to find a solution closer to the experimental decay, but the convergence of the final solution to a global minimum may be more difficult due to the increase of local minima that can be close to the starting values of TriExp parameters. The convergence to a global minimum is very important, but it may become difficult when the resolution of multiexponential decays is not enough to describe them precisely using the relative coefficients and lifetimes, since these parameters are correlated. (36) By evaluating both BiExp and TriExp parameters, we may find a better discrimination between the groups and different information about the processes related to the fluorescence decay. The tendencies for BiExp parameters for malignant and benign lesions, which may be different due to the Warburg effect, are compared to the tendencies described in. (14,15) The first study described that the following tendencies for low and high grade precancerous epithelium cells compared to normal tissue cells: for the 780 nm excitation, a_2 , τ_1 and

τ_2 (corresponding to NADH) decrease and, for the 890 nm excitation, a_1 and τ_2 (corresponding to FAD) decrease and τ_1 increase. The second study described that, when using a 780 nm two-photon excitation, high density of cells, and comparing with the control group, the long fluorescence lifetime (τ_2) increase and its relative coefficient (a_2) decrease with glycolysis inhibition by using 3-bromopyruvate, and the same parameters decrease with the oxidative phosphorylation inhibition by using cobalt chloride. The tendencies of the average lifetimes found in our study are also compared to the values described for fluorescence lifetime skin measurements in the literature.

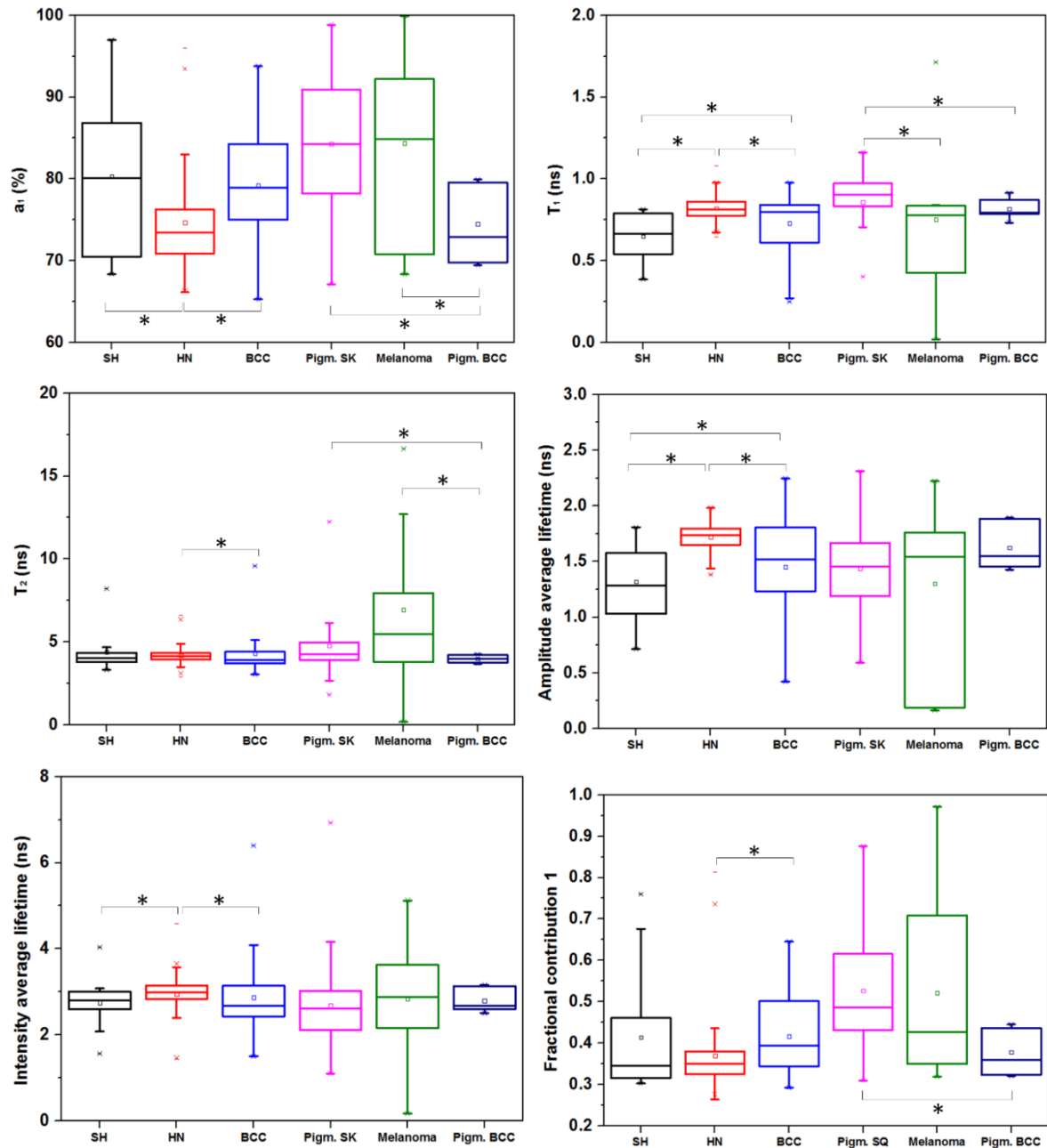


Figure 54 - The boxplots for parameters of bi-exponential decay fitting (378 nm excitation) show a good discrimination between the groups, based on the Wilcoxon rank sum test. The tendencies for these parameters show an agreement with studies evaluating metabolic changes for comparisons between BCCs and HNs (a_1 and τ_1 parameters), pigmented BCCs and pigmented SKs (τ_1 and τ_2 parameters), suspected melanomas and pigmented SKs (τ_1 parameter). The tendency for average lifetimes shows an agreement with other studies involving skin measurements only when comparing BCCs and HNs.

Source: By the author.

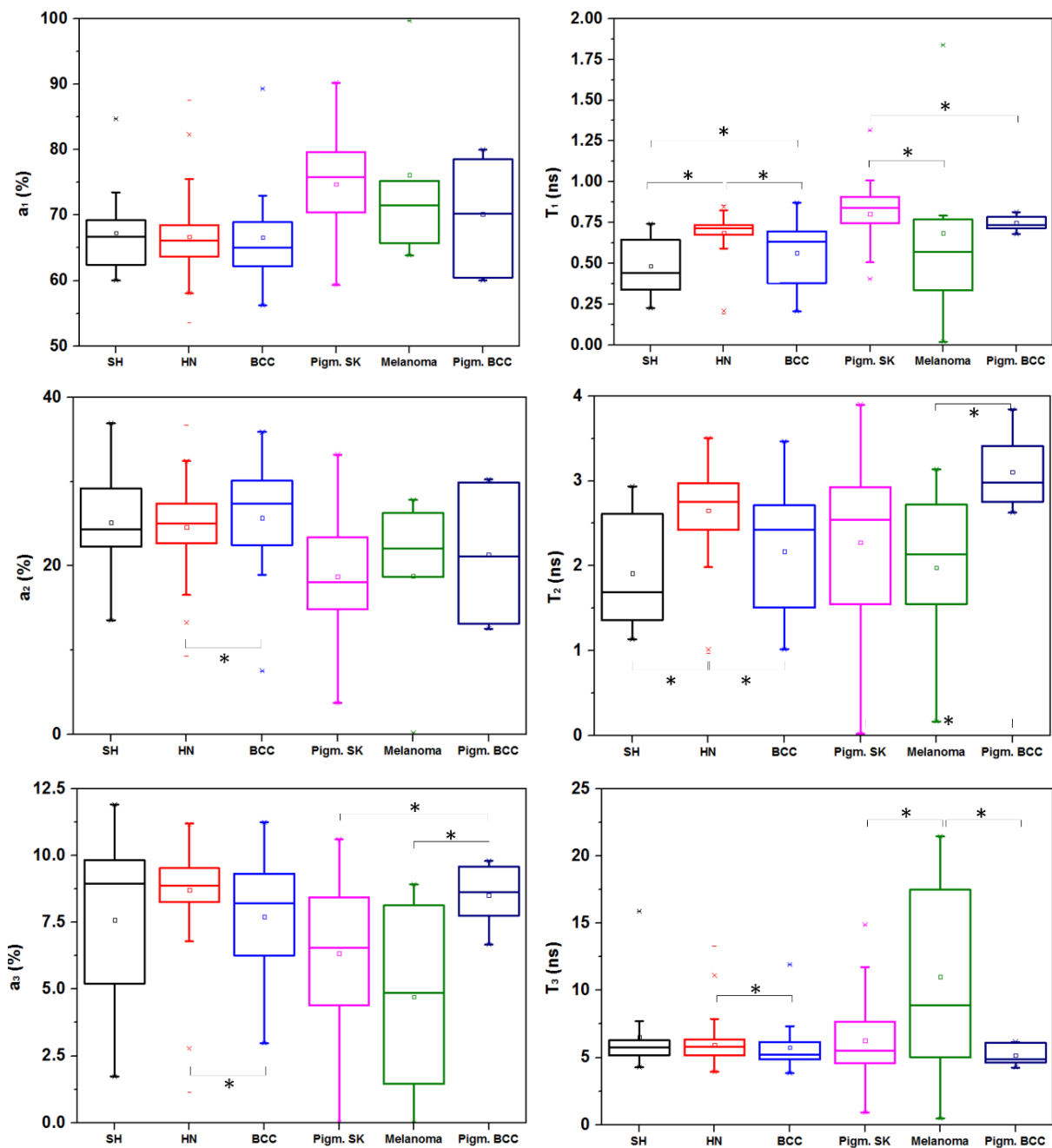


Figure 55 - The boxplots for relative coefficients and lifetimes of the tri-exponential decay fitting (378 nm excitation) also show a good discrimination between the groups (Wilcoxon rank sum test). The first lifetime component may be related to the free NADH, collagen and elastin, the second one to bound NADH, collagen and elastin, and the third one to melanin.

Source: By the author.

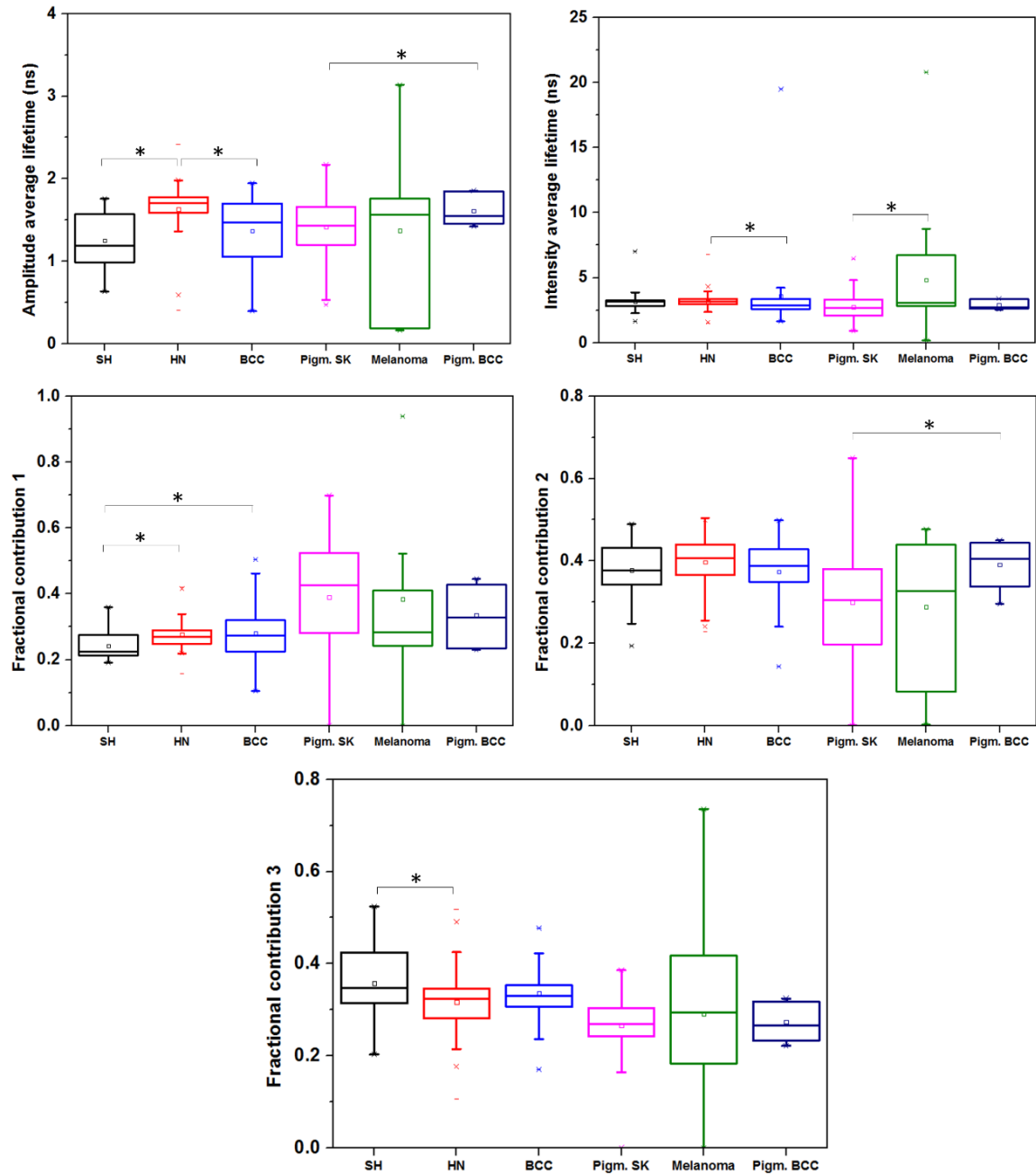


Figure 56 - The boxplots for tri-exponential average lifetimes and fractional contribution (378 nm excitation) also show a satisfactory discrimination between the groups (Wilcoxon rank sum test). Compared to the same parameters for the bi-exponential case, the discrimination between some groups of pigmented lesions was possible. The tendency for average lifetimes also shows an agreement with other studies evaluating skin measurements only for the comparison between BCCs and HNs.

Source: By the author.

Both 378 nm BiExp and TriExp parameters resulted in a discrimination of all combination of non-pigmented and pigmented lesions (figures 54-56). This discrimination is possible when using only the relative coefficients and lifetimes. In the BiExp case, the average lifetimes and fractional contributions allow only the

discrimination of non-pigmented lesions, while the melanoma and pigmented BCC pair cannot be discriminated using these parameters for the TriExp fitting.

The TriExp fitting contains more information concerning the decays of specific endogenous fluorophores of skin, since a_3 values are significant and this fitting provides much better precision compared to the BiExp one. When considering fluorescence lifetime and relative coefficients for the BiExp case, most of the parameters of a more complex decay may be imbued into less components (fluorescence lifetime component = $a_i\tau_i$). For the TriExp fitting, the first lifetime component may be related to the free NADH, collagen and elastin, the second one to bound NADH, collagen and elastin, and the third one to melanin (table 3), based on the lifetime values described on the table 2 and the spectra in figure 34. Although the third component may be related to melanin based on the lifetime values, it only shows some differences between pigmented and non-pigmented lesions for the fractional contribution 3. It is important to remember that chromophores absorption may change lifetimes by filtering selectively wavelengths of fluorophores emission, and scattering effects may increase the fluorescence lifetime values when using the SPCImage software analysis because these effects interfere on its synthetic IRF, which is estimated based on the first derivative of the “rising edge” the recorded signal. (37)

By comparing the tendencies of BiExp parameters for malignant lesions compared to benign lesions, there is an agreement with both (14,15) studies for the following comparisons: BCCs showed a_1 and τ_1 greater and smaller than the same parameters for HN, respectively; pigmented BCCs showed τ_1 and τ_2 smaller than pigmented SKs, and suspected melanomas showed τ_1 smaller than pigmented SKs. In a preliminary analysis, this agreement suggests that these parameters may be related to free and bound NADH or combinations of fluorophores strongly related to them.

When considering the average lifetimes reported in the literature, some studies show that there is a decrease of these lifetimes for malignant lesions (BCCs and melanomas) compared to normal tissues. (52,64,73,74) So, we expected that malignant lesions would present longer average lifetimes compared to benign ones. This tendency was observed only for non-pigmented lesions when comparing both amplitude and intensity average lifetimes between BCCs and HNs. It is not

completely known the lifetime fluorescence spectral effects of the highly absorptive tissues, due to the high melanin concentration, and presently no assumptions have been made or implemented on the conventional spectrum processing. The present knowledge relies on the spectral response in cell culture samples and its direct translation to the tissue interrogation is not possible.

Table 3 – Potential associated fluorophores to each one of the tri-exponential components

	Fluorophores associated to components		
Tri-exponential decay component	First	Second	Third
378 nm	free NADH, collagen and elastin	bound NADH, collagen and elastin	melanin
445 nm	bound FAD, elastin and lipopigments	free FAD, elastin and lipopigments	melanin

Source: By the author.

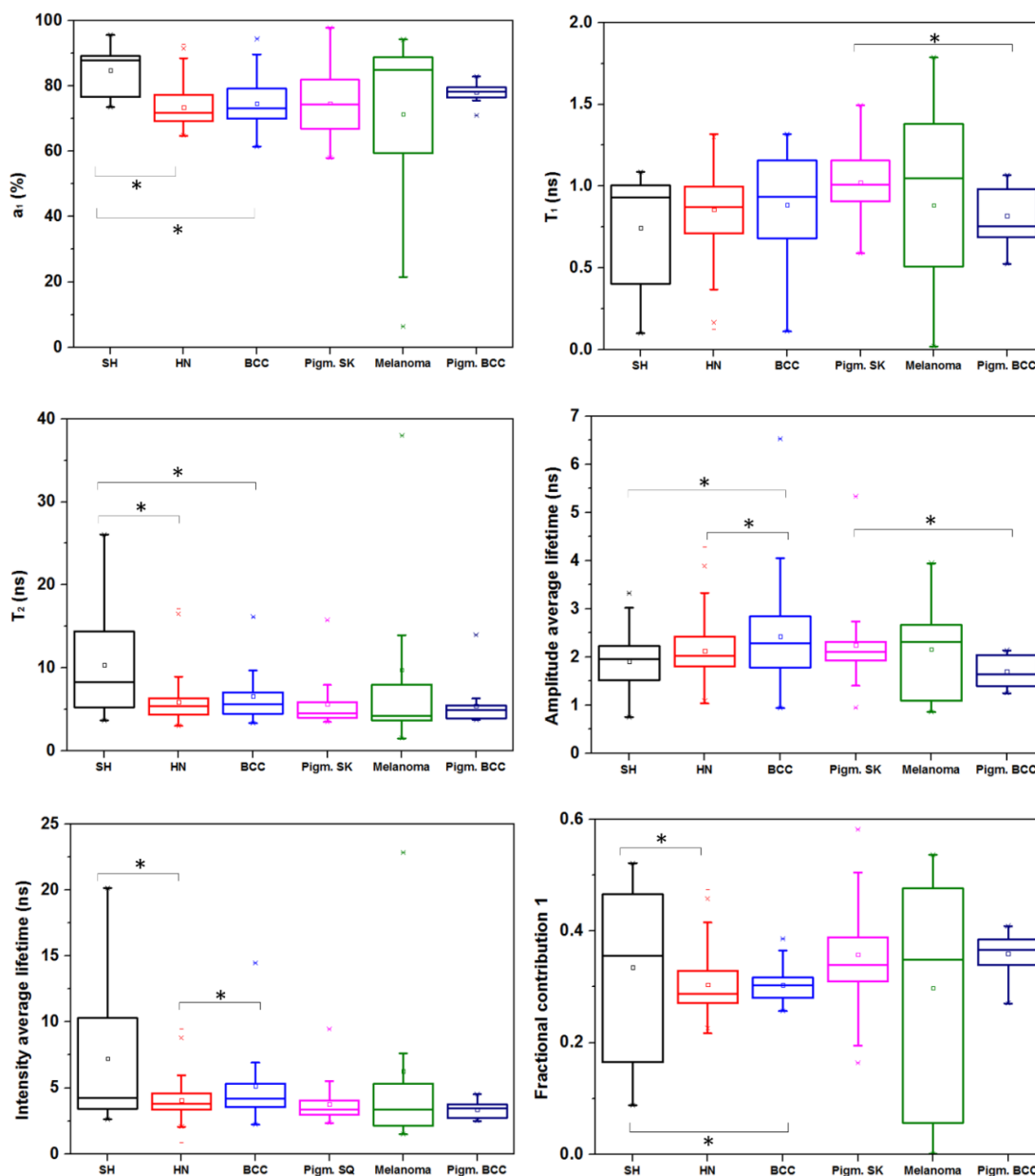


Figure 57 - The boxplots for parameters of bi-exponential decay fitting (445 nm excitation) show a good discrimination between the non-pigmented lesions (Wilcoxon rank sum test), and only the pigmented SK and pigmented BCC pair was able to be discriminated among the pigmented lesions. The tendencies for these parameters show an agreement with studies evaluating metabolic changes only for the comparison between BCCs and SHs (a_1 and τ_1 parameters). The tendency for average lifetimes shows an agreement with other studies involving skin measurements only when comparing the average lifetime for pigmented SKs and pigmented BCCs. The opposite tendency was observed for intensity lifetimes of BCCs compared to SHs and HNs.

Source: By the author.

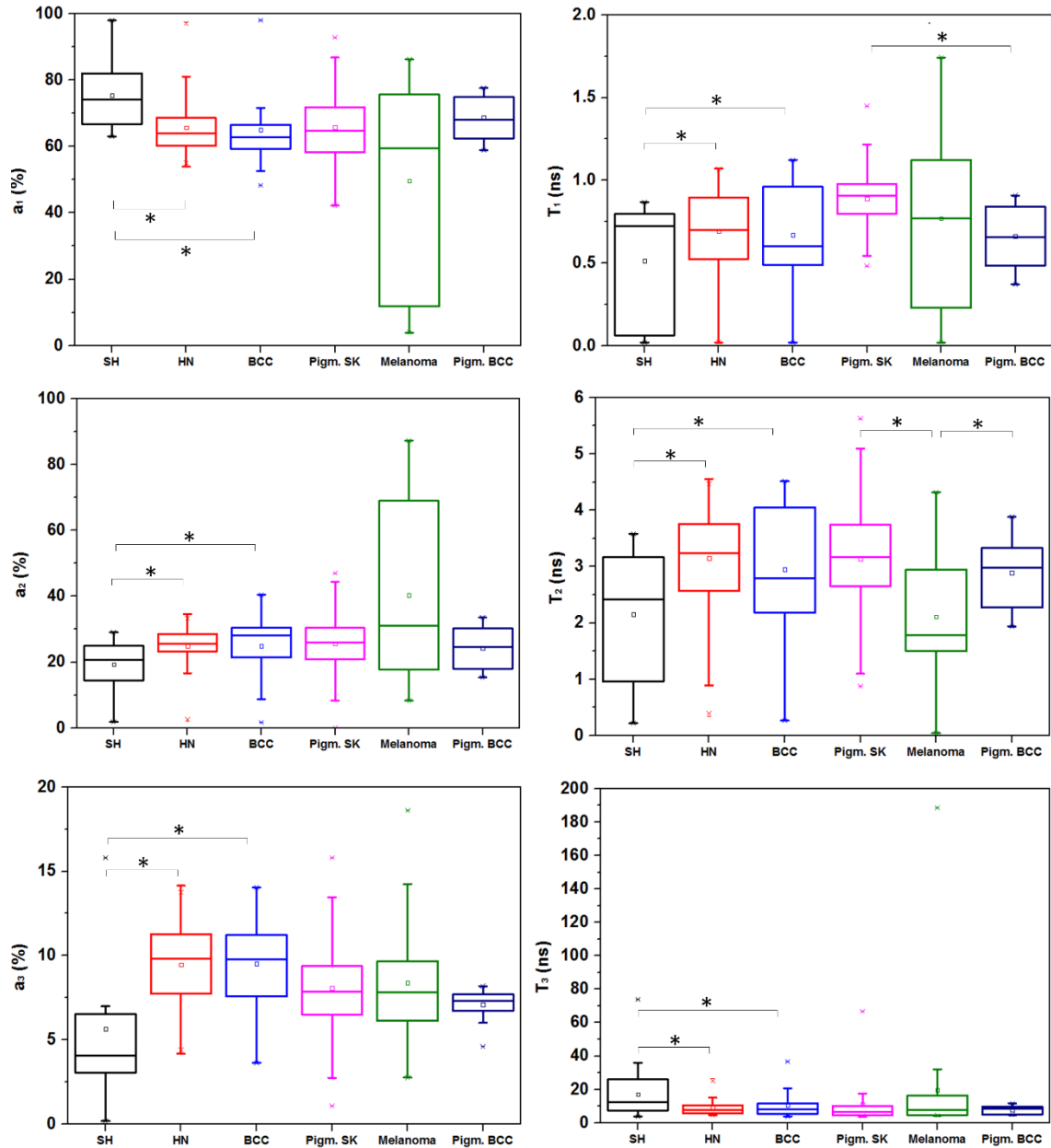


Figure 58 - The boxplots for relative coefficients and lifetimes of the tri-exponential decay fitting (445 nm excitation) show a good discrimination between the groups (Wilcoxon rank sum test). Only the BCC/HN pair was not discriminated with these parameters, but it can be done with the tri-exponential fractional contributions. The first component may be associated to bound FAD, elastin and lipopigments, the second one to free FAD, elastin and lipopigments, and the third one to melanin.

Source: By the author.

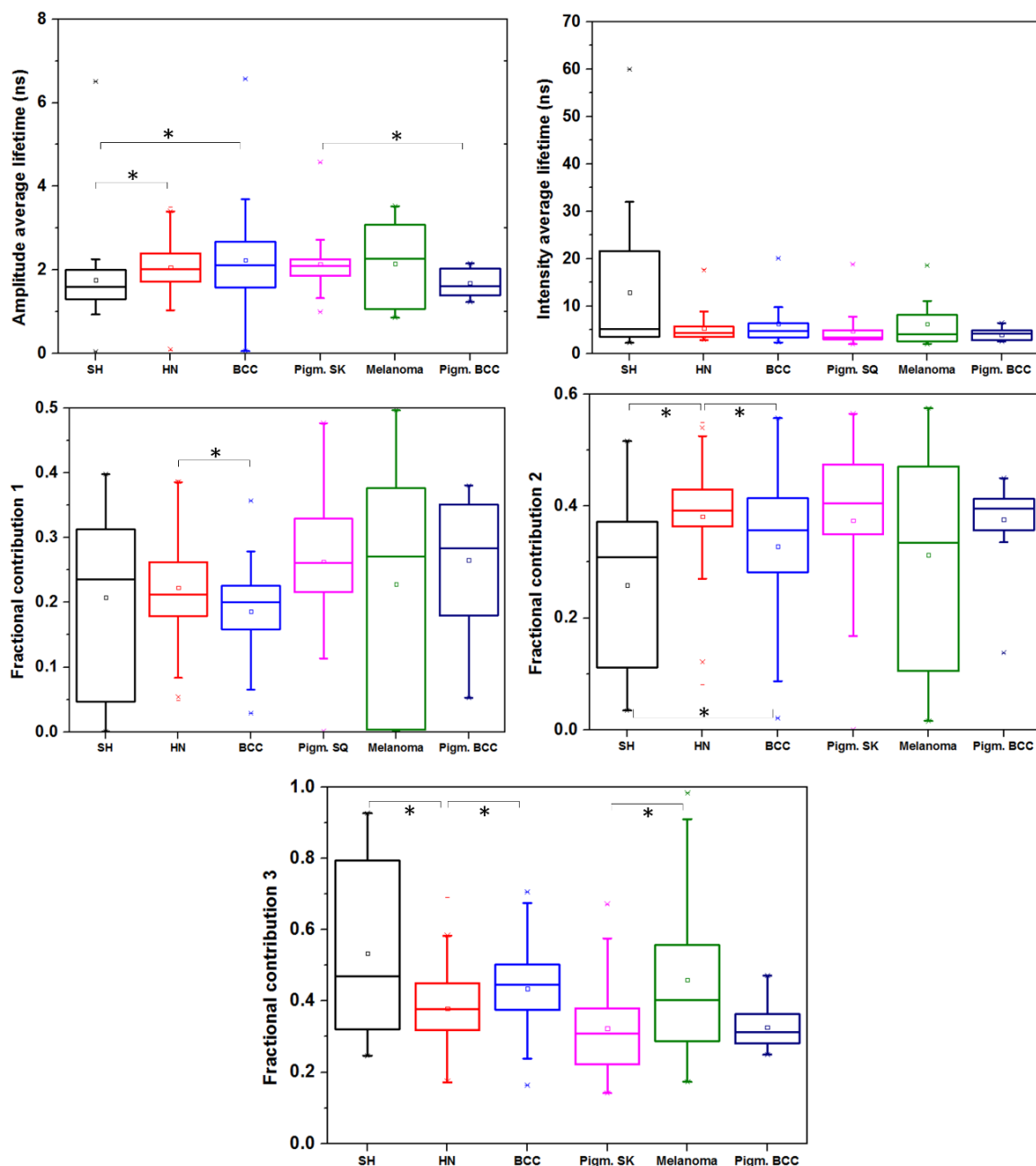


Figure 59 - The boxplots for tri-exponential average lifetimes and fractional contribution (445 nm excitation) also show a satisfactory discrimination between the groups (Wilcoxon rank sum test). Compared to the same parameters for the bi-exponential case, the discrimination between pigmented SKs and suspected melanomas was possible. The tendency for average lifetimes shows an agreement with other studies involving skin measurements only when comparing the average lifetime for pigmented SKs and pigmented BCCs.

Source: By the author.

The 445 nm BiExp parameters provided discrimination of the non-pigmented lesions and the pigmented SK from pigmented BCC, while all combinations of non-pigmented and pigmented lesions were discriminated using TriExp parameters (figures 57-59). In the BiExp case, the relative coefficients and lifetimes resulted in

the discrimination of the same combinations of lesions from average lifetimes and fractional contributions. However, for TriExp parameters, the use of the relative coefficients and lifetimes to discriminate all combinations of skin lesions could be performed, while the average lifetimes and fractional contributions were not able to discriminate only the melanoma from pigmented BCC.

The TriExp fitting for 445 nm also contains more information about the endogenous fluorophores related to the fluorescence decay changes compared to the BiExp one, since, as for the 378 nm, the first one provides less error and a_3 values are significant. Furthermore, the τ_3 shows the same tendency for the τ_2 for the BiExp fitting, even the a_3 value is lower than the other relative coefficients and indicates a smaller contribution of the third component to the fluorescence decay. By comparing the obtained lifetimes values with that described in the table 2 and based on the fluorophores spectra in figure 34, we may associate the first component to bound FAD, elastin and lipopigments, the second one to free FAD, elastin and lipopigments, and the third one to melanin. The fractional contribution 3 shows some differences between pigmented and non-pigmented lesions, but another fluorophore(s) may be involved with the fluorescence of SHs, since its third component parameters, particularly a_3 and fractional contribution 3, do not show the same tendency (absolute values and variance) for the non-pigmented lesions.

The BiExp parameters for 445 nm show an agreement with the study described at (14) when considering the a_1 and τ_2 for BCCs compared to SHs. In this case, the small number of agreements is due to less statistically significant differences between lesions and, then, fewer tendency for malignant lesions compared to benign ones.

By comparing the tendencies of average lifetimes, an agreement with (52,64,73,74) was shown for the comparison of amplitude lifetimes between pigmented SKs and pigmented BCCs. The opposite behavior was observed for intensity lifetimes of BCCs compared to SHs and HNs.

Table 4 – Ratio of useful parameters for a significant statistical difference between each pair of lesions considering 378 nm or 445 nm excitation and bi-exponential or tri-exponential parameters

	Number of parameters useful for discrimination / total number of parameters					
	SH and HN	SH and BCC	HN and BCC	Pigm SK and Melanoma	Pigm. SK and Pigm. BCC	Melanoma and Pigm. BCC
378 nm (Bi-exponential parameters)	4/6	2/6	6/6	1/6	3/6	2/6
378 nm (Tri-exponential parameters)	5/11	2/11	7/11	3/11	5/11	3/11
445 nm (Bi-exponential parameters)	4/6	4/6	2/6	0/6	2/6	0/6
445 nm (Tri-exponential parameters)	9/11	7/11	3/11	2/11	2/11	1/11

Source: By the author.

Finally, the table 4 summarizes the number of parameters that allowed a discrimination between each pair of lesions using bi- or tri-exponential parameters for 378 nm or 445 nm excitations. We observed that, in general, more parameters led to a discrimination between non-pigmented lesions when compared to the pigmented ones. On average, a higher ratio of parameters useful for discrimination was observed for bi-exponential parameters when using 378 nm excitation, and tri-exponential parameters when using 445 nm excitation. In addition, the number of useful 378 nm tri-exponential parameters are not so higher when compared to the bi-exponential ones, and the tendencies on their ratio among total are almost the same, suggesting that the extracted information may be redundant. Conversely, these tendencies are different for the number of useful 445 nm parameters. In this case, the tri-exponential parameters may improve the discrimination between each pair of lesions, and bring new information about their endogenous fluorophores. In order to check this, the next step involves the use of parameters for classification and

determination of sensitivity and specificity of fluorescence lifetime technique for the discrimination of clinically similar skin lesions.

5.4.3 Standard deviation for bi-exponential and tri-exponential decay parameters

The standard deviation for each parameter may provide information about the heterogeneity among different regions of the same lesion. This intralesion heterogeneity is useful to estimate if the variability of each parameter is due to variations of the same lesion or variations between lesions of different volunteers.

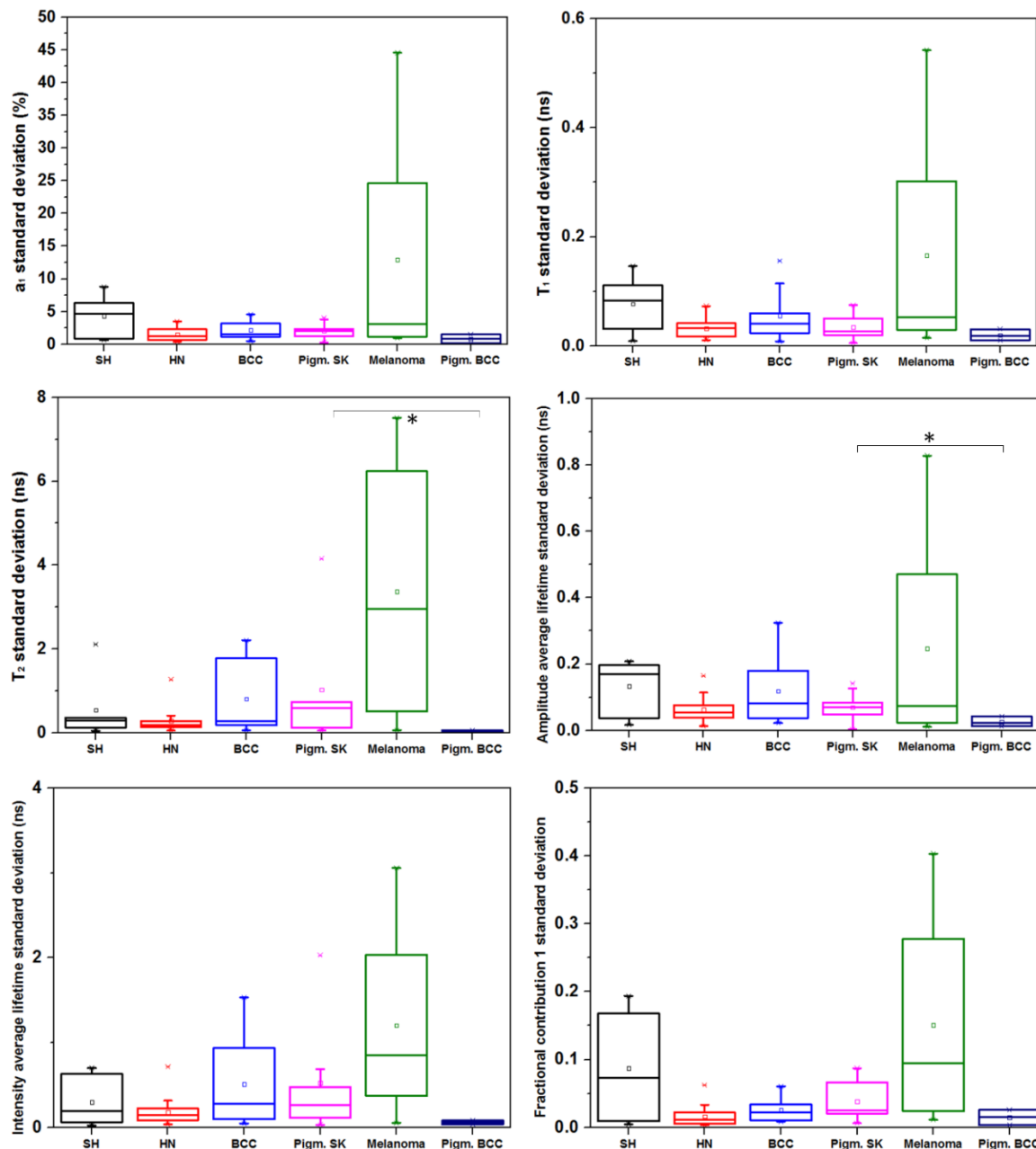


Figure 60 - The boxplots for the standard deviation for bi-exponential parameters (378 nm excitation) show discrimination only between the pigmented SK and pigmented BCC groups (Wilcoxon rank sum test).

Source: By the author.

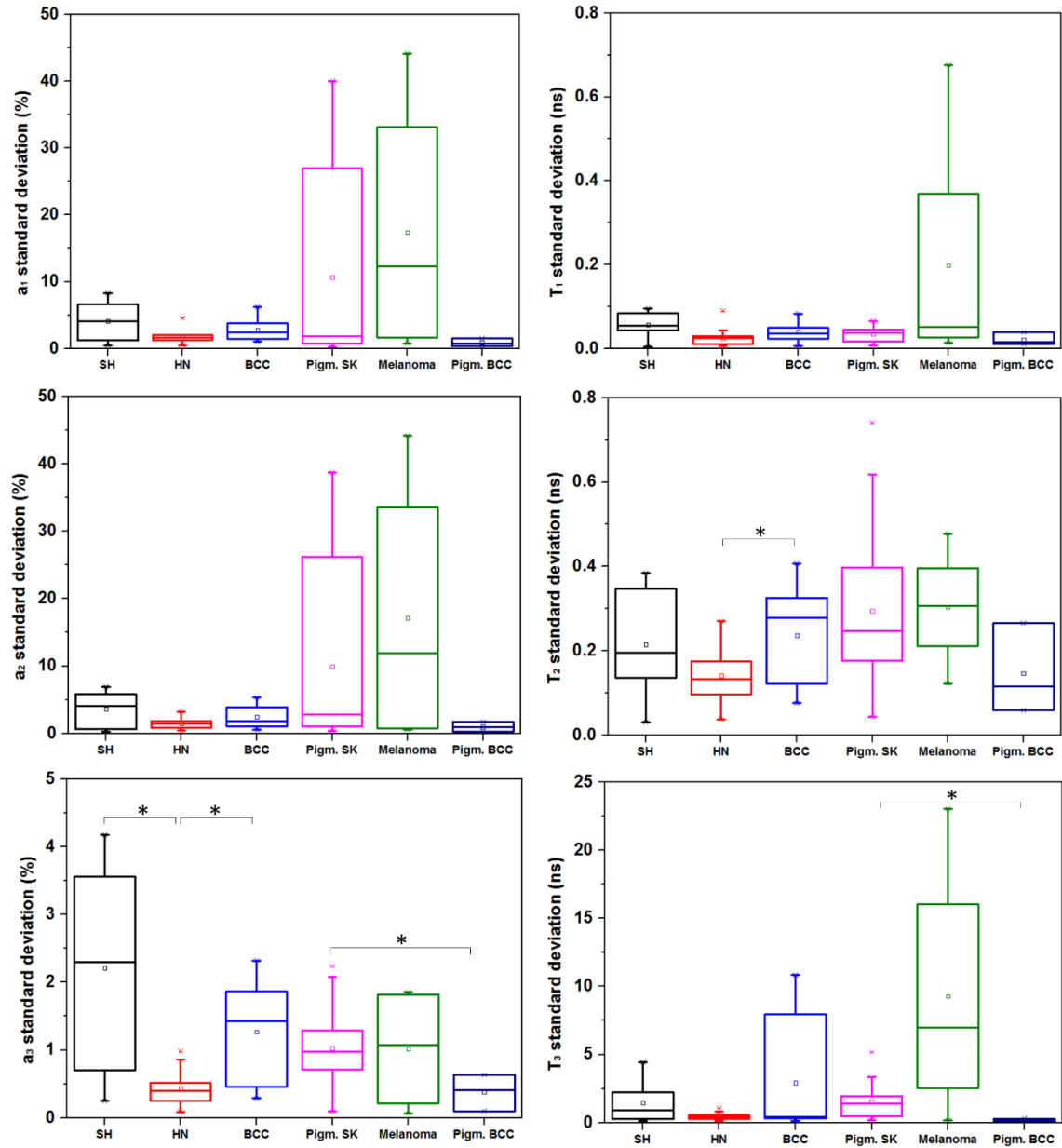


Figure 61 - The boxplots for the standard deviation for tri-exponential relative coefficients and lifetimes (378 nm excitation) show the discrimination between the two groups of non-pigmented lesions and one group of pigmented ones (Wilcoxon rank sum test).

Source: By the author.

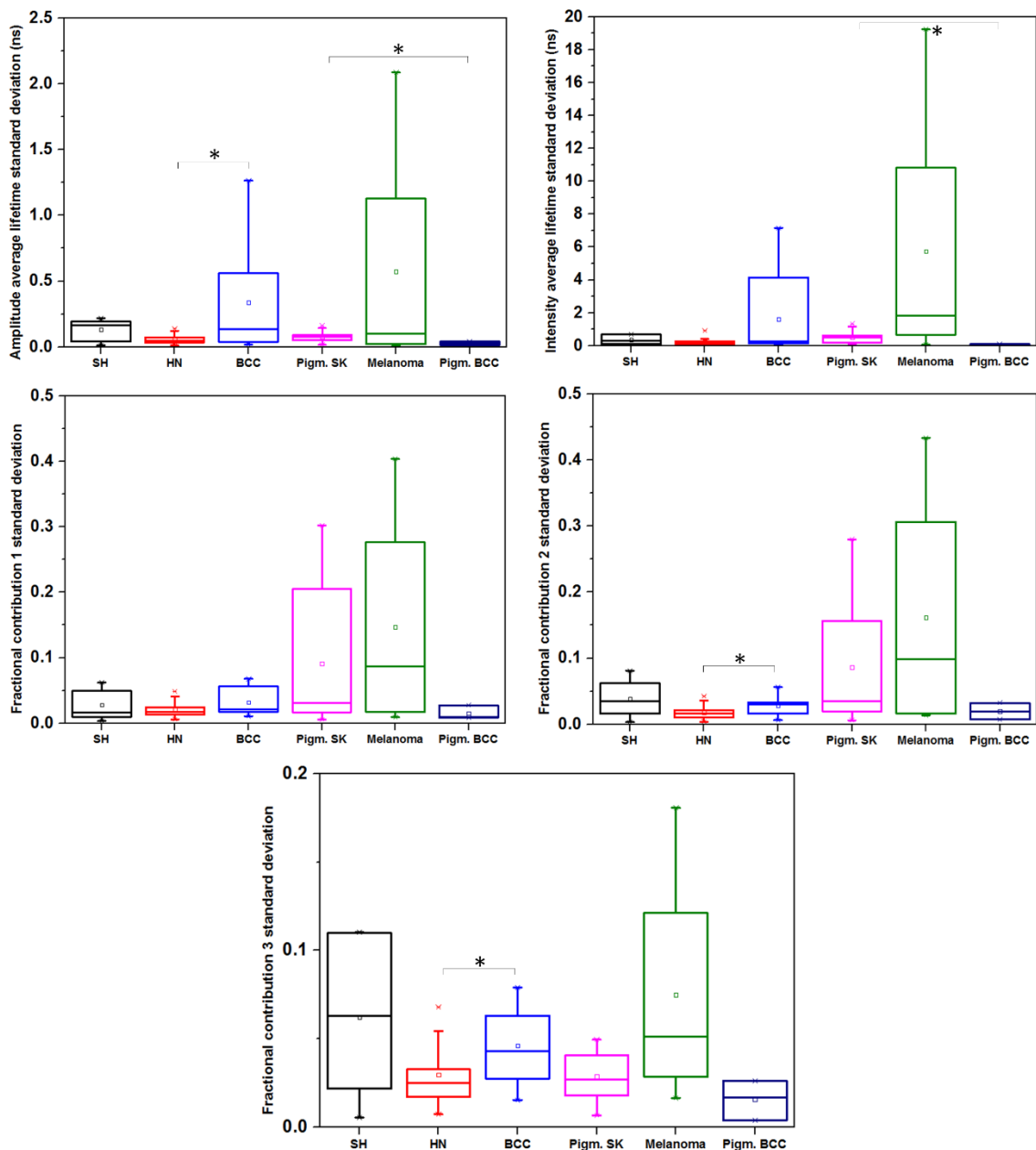


Figure 62 - The boxplots for the standard deviation for tri-exponential average lifetimes and fractional contribution (378 nm excitation) show the discrimination only between one group for both pigmented and non-pigmented lesions (Wilcoxon rank sum test). Compared to the standard deviations for the relative coefficients and lifetimes, the discrimination between SHs and HNs was not possible.

Source: By the author.

By comparing the parameters standard deviation using a 378 nm BiExp and a 378 nm TriExp fitting, we can observe that the TriExp parameters standard deviations allow the discrimination between more groups of skin lesions (figure 60-62). BiExp standard deviations only discriminate between the pigmented SK and pigmented BCC and, except for melanoma and, in some cases, SH and BCC, most of parameters do not show a high intra or interlesion variance. The opposite occurs

for TriExp standard deviations, which exhibit high variances that may be comparable to the TriExp parameters and discriminate between more groups of lesions (SH and HN, HN and BCC, pigmented SK and pigmented BCC). On average, especially for the non-pigmented lesions, 378 nm TriExp parameters showed a higher ratio of parameters useful for discrimination (table 5). This result may suggest that the TriExp parameters standard deviations are more sensitive to each skin lesion heterogeneity, which may improve the diagnostic resolution when combining them with TriExp parameters.

Table 5 – Ratio of useful parameters for a significant statistical difference between each pair of lesions considering 378 nm or 445 nm excitations and standard deviations of bi-exponential or tri-exponential parameters

Discrimination between	Number of standard deviations of parameters useful for discrimination / total number of parameters					
	SH and HN	SH and BCC	HN and BCC	Pigm SK and Melanoma	Pigm. SK and Pigm. BCC	Melanoma and Pigm. BCC
378 nm Biexponential standard deviations	0/6	0/6	0/6	0/6	2/6	0/6
378 nm Triexponential standard deviations	1/11	0/11	5/11	0/11	4/11	0/11
445 nm Biexponential standard deviations	2/6	0/6	0/6	0/6	1/6	0/6
445 nm Triexponential standard deviations	4/11	1/11	1/11	4/11	0/11	0/11

Source: By the author.

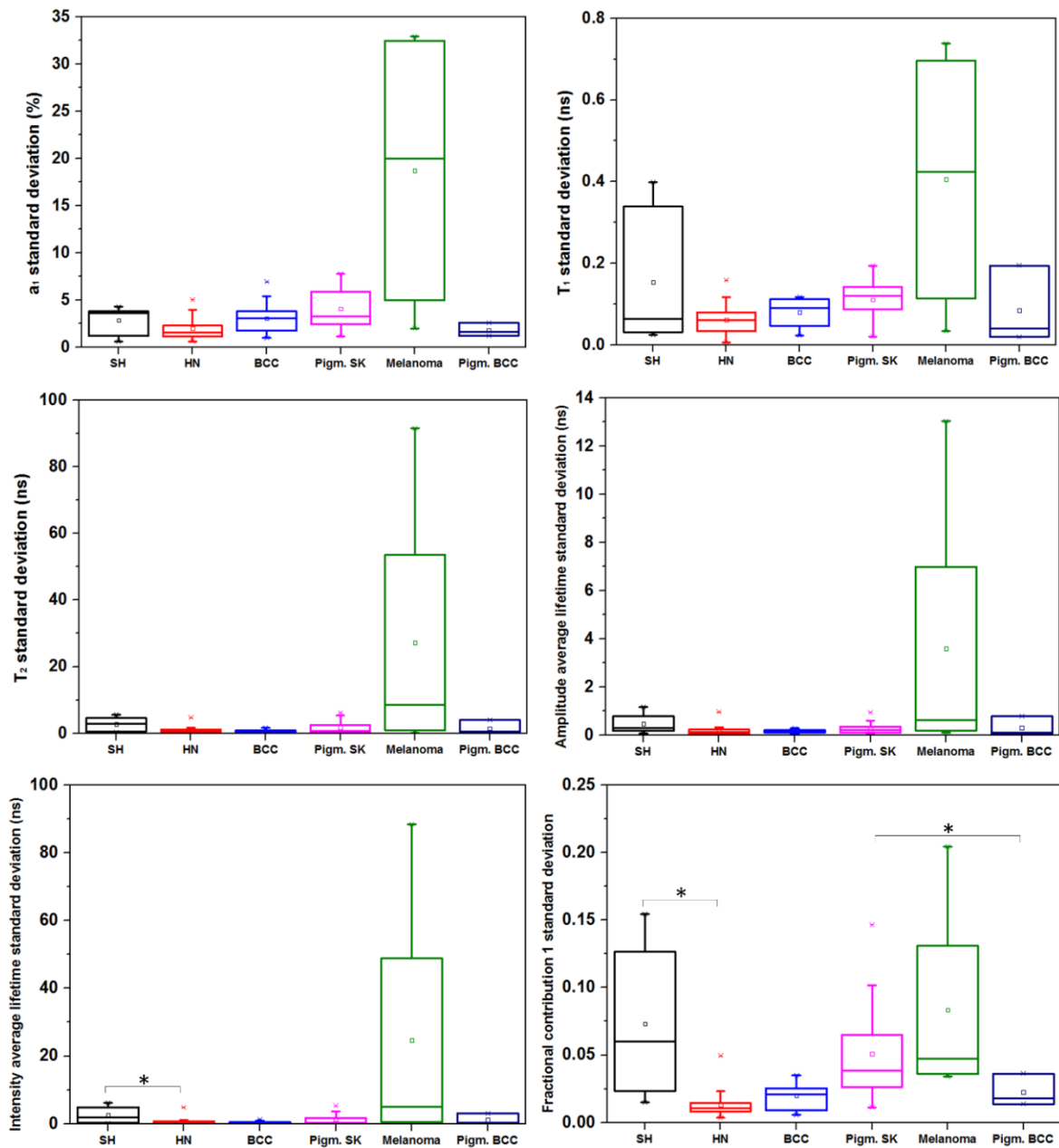


Figure 63 - The boxplots for the standard deviation for bi-exponential parameters (445 nm excitation) show discrimination only between SHs and HNs, pigmented SKs and pigmented BCCs (Wilcoxon rank sum test).

Source: By the author.

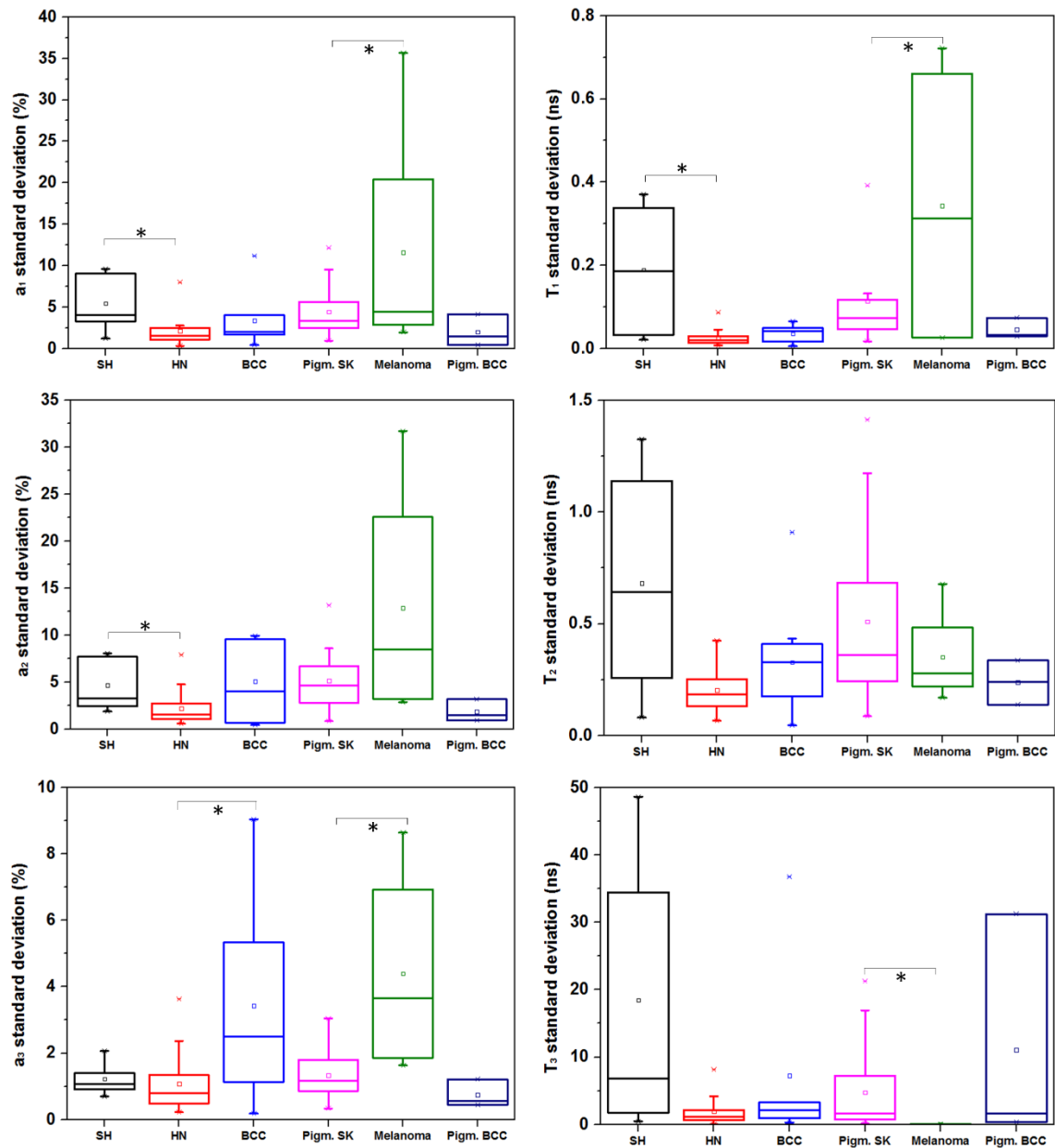


Figure 64 - The boxplots for the standard deviation for tri-exponential relative coefficients and lifetimes (445 nm excitation) show the discrimination between the two groups of non-pigmented lesions and one group of pigmented ones (Wilcoxon rank sum test).

Source: By the author.

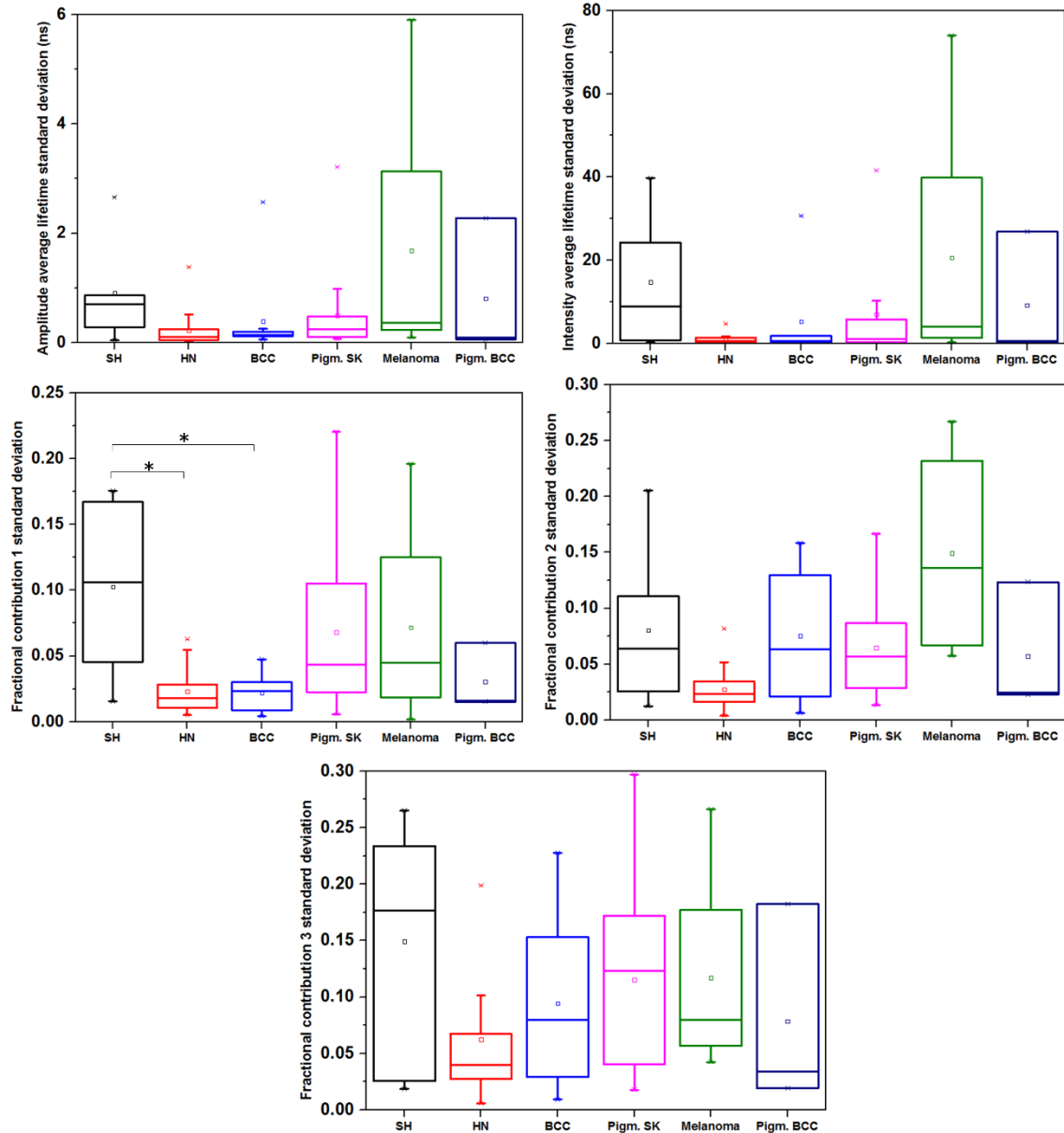


Figure 65 - The boxplots for the standard deviation for tri-exponential average lifetimes and fractional contribution (445 nm excitation) show the discrimination only between two groups of non-pigmented lesions (Wilcoxon rank sum test).

Source: By the author.

The standard deviations for 445 nm BiExp parameters were useful to discriminate the SH from HN and pigmented SK from pigmented BCC, while 445 nm TriExp ones were able to discriminate more groups of lesions (SH from HN, HN from BCC, pigmented SK from melanoma). Most of TriExp standard deviations useful for discrimination between skin lesions are related to the relative coefficients and lifetimes (figures 63-65). Among the average lifetimes and fractional contributions, the fractional contribution 1 standard deviation allow the discrimination of SH from HN in both BiExp and TriExp cases, but the discrimination of pigmented SK from

pigmented BCC only occurs for the BiExp case, even when considering the other TriExp standard deviations.

The standard deviations for 445 nm TriExp parameters were more useful to discriminate between groups of lesions than the BiExp ones. In addition, pairs of groups with no useful parameters for discrimination in the BiExp case showed that some parameters led to a significant statistical difference when using TriExp parameters (table 5). This result suggests that TriExp parameters are more sensitive to variations on the same lesion and/or more information may be extracted when using these parameters. Because of the predominant interlesions variability compared to the intralesions one, most of the standard deviations of the BiExp and TriExp parameters did not show a good discrimination between the skin lesions in this study. However, the parameters that were useful for this discrimination can be used to improve the diagnostic resolution in the next steps, which include multivariate data analysis for classification of each group of skin lesions.

6 CONCLUSIONS

In this study, we assembled, calibrated, and characterized and one of the world's first portable systems for time-resolved fluorescence spectroscopy. This system can be transported with mechanical, electrical and optical stability, allow fast optical filters change during clinical measurements, and has 38,165.75 cm³ of occupied volume. Its size and feasibility to be used in clinics are optimized to do not compromise the hospital routine and to allow the system to be carried to any place and to work just with a wall socket. These features make possible the performance of clinical measurements, diseases diagnostic, evaluation of treatment procedures, and investigation of biochemical processes at biological tissues with a portable equipment. The developed device showed to be robust enough and user-friendly at the *in vivo* measurements tested.

The evaluation of the photoaging process in sun exposed and non-exposed body areas showed discrimination between these areas, even for young adult volunteers' skin, which have been less exposed to sun over time than middle-aged/senior volunteers, even though these results should be further evaluated at larger clinical trials. Next steps include the investigation of aging and photoaging at skin of older volunteers and multivariate data analysis and data mining tools for classification. This analysis has potential to be useful for applications at dermatology and aesthetics by assessing the photoaging degree, which may also suggest the chance to development of precancerous lesions or the moment when an aesthetic procedure is needed.

The measurements of clinically similar skin lesions showed promising results for the discrimination of benign from malignant lesions, which has a great impact in their treatment planning and success, since the patient prognosis and the treatment modality depend on the histological type and the evolution of the lesion. This discrimination may also help clinicians to decide the correct clinical procedures for differential diagnosis. In the future, further data will be collected to improve our fluorescence lifetime database and multivariate data analysis and data mining tools will be used for classification. In addition to this analysis, the collected fluorescence spectra will be processed and analyzed, and the redox ratio will be calculated for

each lesion. This preliminary study may be useful as a pilot study for investigation of the sources of the fluorescence lifetime signal and the potential of the fluorescence lifetime spectroscopy for clinically similar skin lesions diagnostic.

The fluorescence lifetime investigation in biological tissues, particularly for *in vivo* measurements, is also important for fundamental knowledge concerning the optical processes related to changes in the fluorescence decay (such as absorption, scattering, biochemical reactions, biological processes, anisotropy, etc.). By understanding these processes, the fluorescence decay data may be analyzed using improved methods to extract information about each one of these processes separately, and the effect of each process on the information extracted by each type of analysis method may be discovered. Further investigation of these processes is necessary, as it can be observed by the heterogeneity of fluorescence lifetime values reported on the literature, depending on the optical techniques used or different types of analysis methods in cellular and tissue studies.

7 PUBLICATIONS AND CONFERENCE PRESENTATIONS

1 PIRES, L.; **NOGUEIRA, M. S.**; PRATAVIEIRA, S.; MORIYAMA, L. T.; KURACHI, C. Time-resolved fluorescence lifetime for cutaneous melanoma detection. **Biomedical Optics Express**, v. 5, n. 9, p. 3080, 2014.

2 COSCI, A; **NOGUEIRA, M. S.**; PRATAVIERA, S; TAKAHAMA JR., A; AZEVEDO, R. S.; KURACHI, C. Time-resolved fluorescence spectroscopy for clinical diagnosis of actinic cheilitis, **Biomedical Optics Express**, v.7, n.10, p. 4210-4219, 2016.

3 SILVA, A. P.; **NOGUEIRA, M. S.**; JO, J. A.; BAGNATO, V. S.; INADA, N. M. Optical based diagnosis and treatment of onychomycosis. In: **Biomedical Optics 2016**. Washington, D.C.: OSA, 2016, p. JTU3A.37. doi:10.1364/CANCER.2016.JTU3A.37.

4 **NOGUEIRA, M. S.**; KURACHI, C. Assessing the photoaging process at sun exposed and non-exposed skin using fluorescence lifetime spectroscopy. **Proceedings of SPIE**, v. 9703, p. 97031W, 2016. doi:10.1117/12.2209690.

5 **NOGUEIRA, M. S.** et al. Evaluation of actinic cheilitis using fluorescence lifetime spectroscopy. **Proceedings of SPIE**, v. 9703, p. 97031U, 2016. doi:10.1117/12.2209689.

6 ANDRADE, C. T.; **NOGUEIRA, M. S.** et al. Optical spectroscopy of radiotherapy and photodynamic therapy responses in normal rat skin shows vascular breakdown products. **Proceedings of SPIE**, v. 9694, p. 969410, 2016. doi:10.1117/12.2210988.

7 **NOGUEIRA, M. S.** et al. Assembly and characterization of a fluorescence lifetime spectroscopy system for skin lesions diagnostic. **Proceedings of SPIE**, v. 9531, p. 95313D, 2015. doi:10.1117/12.2180599.

8 D'ALMEIDA, C. P.; CAMPOS, C.; **NOGUEIRA, M. S.**; PRATAVIEIRA, S.; KURACHI, C. Time-resolved and steady-state fluorescence spectroscopy for the assessment of skin photoaging process. **Proceedings of SPIE**, v. 9531, p. 953146, 2015. doi: 10.1117/12.2180975.

9 KURACHI, C.; PIRES, L.; **NOGUEIRA, M. S.**; PRATAVIEIRA, S. Lifetime fluorescence for the detection of skin lesions. **Biomedical Optics 2014**. Washington, D.C.: OSA, p. BS4B.3, 2014. doi:10.1364/BIOMED.2014.BS4B.3.

REFERENCES

- 1 WORLD HEALTH ORGANIZATION. **Ultraviolet radiation and the INTERSUN Programme:** skin cancers. 2016 Available from: <http://www.who.int/uv/fag/skincancer/en/index1.html>>. Accessible at: 15 June 2016.

- 2 INSTITUTO NACIONAL DO CANCER. **Estimativa 2014:** incidência de câncer no Brasil. Rio de Janeiro: INCA, 2014

- 3 LEITER, U. et al. Hazard rates for recurrent and secondary cutaneous melanoma: an analysis of 33,384 patients in the German Central Malignant Melanoma Registry. **Journal of the American Academy of Dermatology**, v. 66, n. 1, p. 37–45, 2012.

- 4 SOARES, H. B. **Análise e classificação de imagens de lesões da pele por atributos de cor, forma e textura utilizando máquina de vetor de suporte.** 2008. 160 p. Tese (Doutorado) - Universidade Federal do Rio Grande do Norte, Natal, 2008.

- 5 THAI, K. Fitzpatrick's dermatology in general medicine. **Australasian Journal of Dermatology**, v. 49, n. 3, p. 175–175, 2008.

- 6 PIRES, L. et al. Time-resolved fluorescence lifetime for cutaneous melanoma detection. **Biomedical Optics Express**, v. 5, n. 9, p. 3080, 2014.

- 7 THOMPSON, A. J. **Developing endoscopic instrumentation and techniques for in vivo fluorescence lifetime imaging and spectroscopy.** 2013. Thesis (Doctoral) - Imperial College of London, London, 2013.

8. VISSER, A. J. W. G.; ROLINSKI, O. J. Basic photophysics. **American Society for Photobiology.** 2014 Available from: <http://www.photobiology.info/Visser-Rolinski.html>>. Accessible at: 1 June 2016.

- 9 MARCU, L. et al. **Fluorescence lifetime spectroscopy and imaging.** Boca Raton: CRC Press, 2014. 570 p.

- 10 HUANG, Y. Y. Low-level laser therapy: an emerging clinical paradigm. **SPIE Newsroom**, 2009. doi: 10.1117/2.1200906.1669 Available from: <http://spie.org/newsroom/1669-low-level-laser-therapy-an-emerging-clinical-paradigm>>. Accessible at: 1 June 2016.

11 VEEN, R. L. et al. Determination of visible near-IR absorption coefficients of mammalian fat using time- and spatially resolved diffuse reflectance and transmission spectroscopy. **Journal of Biomedical Optics**, v. 10, n. 5, p. 054004, 2005.

12 PRATAVIEIRA, S. et al. Optical imaging as auxiliary tool in skin cancer diagnosis. In: LA PORTA, C. **Skin Cancers** - risk factors, prevention and therapy. 2011. 272 p. Available from: <<http://www.intechopen.com/books/skin-cancers-riskfactors-prevention-and-therapy/optical-imaging-as-auxiliary-tool-in-skin-cancer-diagnosis>> Accessible at: 1 June de 2016.

13 NIELSON, K. P. et al. The optics of human skin: aspects important for human health. **Solar Radiation and Human Health**. Oslo: Norwegian Academy of Science and Letters, p. 35–46, 2008. Available from: <http://www.dnva.no/geomed/solarpdf/Nr_3_Nielsen.pdf>. Accessible at 23 Jan. 2016.

14 SKALA, M. C. et al. In vivo multiphoton microscopy of NADH and FAD redox states, fluorescence lifetimes, and cellular morphology in precancerous epithelia. **Proceedings of the National Academy of Sciences**, v. 104, n. 49, p. 19494–19499, 2007.

15 SKALA, M. C. et al. In vivo multiphoton fluorescence lifetime imaging of protein-bound and free nicotinamide adenine dinucleotide in normal and precancerous epithelia. **Journal of Biomedical Optics**, v. 12, n. 2, p. 024014, 2007.

16 VISHWASRAO, H. D. et al. Conformational dependence of intracellular NADH on metabolic state revealed by associated fluorescence anisotropy. **Journal of Biological Chemistry**, v. 280, n. 26, p. 25119–25126, 2005.

17 BEREZIN, M. Y.; ACHILEFU, S. Fluorescence lifetime measurements and biological imaging. **Chemical Reviews**, v. 110, n. 5, p. 2641–2684, 2010.

18 ELOVE, G.A. et al. Early steps in cytochrome c folding probed by time-resolved circular dichroism and fluorescence spectroscopy. **Biochemistry**, v. 31, n. 30, p. 6876–6883, 1992.

19 DIAMANDIS, E. P. Immunoassays with time-resolved fluorescence spectroscopy: principles and applications. **Clinical Biochemistry**, v. 21, n. 2, p. 139–150, 1988.

20 WANG, X. F. et al. A Two-dimensional fluorescence lifetime imaging system using a gated image intensifier. **Applied Spectroscopy**, v. 45, n. 3, p. 360–366, 1991.

- 21 SANDERS, R. et al. Quantitative pH imaging in cells using confocal fluorescence lifetime imaging microscopy. **Analytical Biochemistry**, v. 227, n. 2, p. 302–308, 1995.
- 22 FRENCH, T. et al. Two-photon fluorescence lifetime imaging microscopy of macrophage-mediated antigen processing. **Journal of Microscopy**, v. 185, n. 3, p. 339–353, 1997.
- 23 GRATTON, E. et al. Fluorescence lifetime imaging for the two-photon microscope: time-domain and frequency-domain methods. **Journal of Biomedical Optics**, v. 8, n. 3, p. 381–390, 2003.
- 24 MIZERET, J. et al. Instrumentation for real-time fluorescence lifetime imaging in endoscopy. **Review of Scientific Instruments**, v. 70, n. 12, p. 4689, 1999.
- 25 FANG, Q. et al. Time-domain laser-induced fluorescence spectroscopy apparatus for clinical diagnostics. **Review of Scientific Instruments**, v. 75, n. 1, p. 151, 2004.
- 26 BLACKWELL, J. et al. In vivo time-resolved autofluorescence measurements to test for glycation of human skin. **Journal of Biomedical Optics**, v. 13, n. 1, p. 014004, 2008.
- 27 UEHLINGER, P. et al. In vivo time-resolved spectroscopy of the human bronchial early cancer autofluorescence. **Journal of Biomedical Optics**, v. 14, n. 2, p. 024011, 2009.
- 28 PFEFER, T. J. et al. Temporally and spectrally resolved fluorescence spectroscopy for the detection of high grade dysplasia in Barrett's esophagus. **Lasers in Surgery and Medicine**, v. 32, n. 1, p. 10–16, 2003.
- 29 SIEGEL, J. et al. Studying biological tissue with fluorescence lifetime imaging: microscopy, endoscopy, and complex decay profiles. **Applied Optics**, v. 42, n. 16, p. 2995, 2003.
- 30 FRUHWIRTH, G. O. et al. Fluorescence lifetime endoscopy using TCSPC for the measurement of FRET in live cells. **Optics Express**, v. 18, n. 11, p. 11148, 2010.
- 31 MYCEK, M.-A. et al. Colonic polyp differentiation using time-resolved autofluorescence spectroscopy. **Gastrointestinal Endoscopy**, v. 48, n. 4, p. 390–394, 1998.

32 PFEFER, T. J. et al. Temporally and spectrally resolved fluorescence spectroscopy for the detection of high grade dysplasia in Barrett's esophagus. **Lasers in Surgery and Medicine**, v. 32, n. 1, p. 10–16, 2003.

33 BEC, J. et al. Design, construction, and validation of a rotary multifunctional intravascular diagnostic catheter combining multispectral fluorescence lifetime imaging and intravascular ultrasound. **Journal of Biomedical Optics**, v. 17, n. 10, p. 106012, 2012.

34 SUN, Y. et al. Simultaneous time- and wavelength-resolved fluorescence spectroscopy for near real-time tissue diagnosis. **Optics Letters**, v. 33, n. 6, p. 630, 2008.

35 XIE, H. et al. Multispectral scanning time-resolved fluorescence spectroscopy (TRFS) technique for intravascular diagnosis. **Biomedical Optics Express**, v. 3, n. 7, p. 1521, 2012.

36 Lakowicz, J. R. **Principles of fluorescence spectroscopy**. 3rd ed. Boston, MA: Springer, 2006. 954 p.

37 BECKER, W. **The bh TCSPC handbook**. Berlin: Becker & Hickl GmbH, 2010. 566 p.

38 SKALA, M. C. et al. In vivo multiphoton fluorescence lifetime imaging of protein-bound and free nicotinamide adenine dinucleotide in normal and precancerous epithelia. **Journal of Biomedical Optics**, v. 12, n. 2, p. 024014, 2007.

39 KOENIG, K.; RIEMANN, I. High-resolution multiphoton tomography of human skin with subcellular spatial resolution and picosecond time resolution. **Journal of Biomedical Optics**, v. 8, n. 3, p. 432, 2003.

40 LUTZ, V. et al. Impact of collagen crosslinking on the second harmonic generation signal and the fluorescence lifetime of collagen autofluorescence. **Skin Research and Technology**, v. 18, n. 2, p. 168–179, 2012.

41 ASHWIN, P. T.; MCDONNELL, P. J. Collagen cross-linkage: a comprehensive review and directions for future research. **British Journal of Ophthalmology**, v. 94, n. 8, p. 965–970, 2010.

42 HAUS, J. M. et al. Collagen, cross-linking, and advanced glycation end products in aging human skeletal muscle. **Journal of Applied Physiology** (Bethesda, Md. : 1985), v. 103, n. 6, p. 2068–2076, 2007.

43 REISER, K. M. Nonenzymatic glycation of collagen in aging and diabetes. **Experimental Biology and Medicine**, v. 218, n. 1, p. 23–37, 1998.

44 KÖNIG, K. et al. Multiphoton autofluorescence imaging of intratissue elastic fibers. **Biomaterials**, v. 26, n. 5, p. 495–500, 2005.

45 SCHWEITZER, D. et al. Towards metabolic mapping of the human retina. **Microscopy Research and Technique**, v. 70, n. 5, p. 410–419, 2007.

46 PROVENZANO, P. P. et al. Collagen reorganization at the tumor-stromal interface facilitates local invasion. **BMC Medicine**, v. 4, n. 1, p. 38, 2006.

47 EHLERS, A.; RIEMANN, I.; et al. Multiphoton fluorescence lifetime imaging of human hair. **Microscopy Research and Technique**, v. 70, n. 2, p. 154–161, 2007.

48 WU, Y.; QU, J. Y. Autofluorescence spectroscopy of epithelial tissues. **Journal of Biomedical Optics**, v. 11, n. 5, p. 054023, 2006.

49 DELORI, F. C. et al. Age-related accumulation and spatial distribution of lipofuscin in RPE of normal subjects. **Investigative Ophthalmology & Visual Science**, v. 42, n. 8, p. 195–1866, 2001.

50 SCHWEITZER, D. et al. In vivo measurement of time-resolved autofluorescence at the human fundus. **Journal of Biomedical Optics**, v. 9, n. 6, p. 1214, 2004.

51 PATALAY, R. **The clinical application of multispectral fluorescence lifetime imaging of human skin using multiphoton microscopy**. 2013. 261 p. Thesis (Doctoral) - Imperial College of London, London, 2013.

52 CICCHI, R. et al. Nonlinear laser imaging of skin lesions. **Journal of Biophotonics**, v. 1, n. 1, p. 62–73, 2008.

53 SPARKS, H. et al. A flexible wide-field FLIM endoscope utilising blue excitation light for label-free contrast of tissue. **Journal of Biophotonics**, v. 8, n. 1-2, p. 168–178, 2015.

54 DOWLING, K. et al. Fluorescence lifetime imaging with picosecond resolution for biomedical applications. **Optics Letters**, v. 23, n. 10, p. 810, 1998.

55 ELSON, D. et al. Time-domain fluorescence lifetime imaging applied to biological tissue. **Photochemical & Photobiological Sciences**, v. 3, n. 8, p. 795, 2004.

56 SHRESTHA, S. et al. High-speed multispectral fluorescence lifetime imaging implementation for in vivo applications. **Optics Letters**, v. 35, n. 15, p. 2558, 2010.

57 SUN, Y. et al. Dynamic tissue analysis using time- and wavelength-resolved fluorescence spectroscopy for atherosclerosis diagnosis. **Optics Express**, v. 19, n. 5, p. 3890, 2011.

58 FEREIDOUNI, F. et al. High speed multispectral fluorescence lifetime imaging. **Optics Express**, v. 21, n. 10, p. 11769, 2013.

59 CHENG, S. et al. Flexible endoscope for continuous in vivo multispectral fluorescence lifetime imaging. **Optics Letters**, v. 38, n. 9, p. 1515, 2013.

60 PARK, J. et al. A dual-modality optical coherence tomography and fluorescence lifetime imaging microscopy system for simultaneous morphological and biochemical tissue characterization. **Biomedical Optics Express**, v. 1, n. 1, p. 186–200, 2010.

61 JABBOUR, J. M. et al. Fluorescence lifetime imaging and reflectance confocal microscopy for multiscale imaging of oral precancer. **Journal of Biomedical Optics**, v. 18, n. 4, p. 046012, 2013.

62 PARK, J. et al. Biochemical characterization of atherosclerotic plaques by endogenous multispectral fluorescence lifetime imaging microscopy. **Atherosclerosis**, v. 220, n. 2, p. 394–401, 2012.

63 POPENDA, M. et al. Fluorescence lifetime measurements with all-fiber optical setup for non-invasive in-vivo diagnostics. 2015. doi: 10.1109/ICTON.2015.7193676. Available from: <http://ieeexplore.ieee.org.ez67.periodicos.capes.gov.br/stamp/stamp.jsp?arnumber=7193676>. Accessible at: 1 June 2016.

64 THOMPSON, A. J. et al. In vivo measurements of diffuse reflectance and time-resolved autofluorescence emission spectra of basal cell carcinomas. **Journal of Biophotonics**, v. 5, n. 3, p. 240–254, 2012.

65 THOMPSON, A. et al. Hyperspectral fluorescence lifetime fibre probe spectroscopy for use in the study and diagnosis of osteoarthritis and skin cancer. **Proceedings of SPIE**, v. 7895, 2011. doi:10.1117/12.875120.

66 PATTERSON, M. S. et al. Time resolved reflectance and transmittance for the noninvasive measurement of tissue optical properties. **Applied Optics**, v. 28, n. 12, p. 2331, 1989.

67 BREWSTER, M. Q.; YAMADA, Y. Optical properties of thick, turbid media from picosecond time-resolved light scattering measurements. **International Journal of Heat and Mass Transfer**, v. 38, n. 14, p. 2569–2581, 1995.

68 HANLEY, Q. S. et al. Fluorescence lifetime imaging: multi-point calibration, minimum resolvable differences, and artifact suppression. **Cytometry**, v. 43, n. 4, p. 248–260, 2001.

69 HARRIS, J. M.; LYTLE, F. E. Measurement of subnanosecond fluorescence decays by sampled single-photon detection. **Review of Scientific Instruments**, v. 48, n. 11, p. 1469, 1977.

70 MAGDE, D. et al. Solvent dependence of the fluorescence lifetimes of xanthene dyes. **Photochemistry and Photobiology**, v. 70, n. 5, p. 737–744, 1999.

71 LAKOWICZ, J. R.; BERNDT, K. W. Lifetime-selective fluorescence imaging using an rf phase-sensitive camera. **Review of Scientific Instruments**, v. 62, n. 7, p. 1727, 1991.

72 PENA, A. et al. Spectroscopic analysis of keratin endogenous signal for skin multiphoton microscopy: erratum. **Optics Express**, v. 13, n. 17, p. 6667, 2005.

73 GALLETLY, N. P. et al. Fluorescence lifetime imaging distinguishes basal cell carcinoma from surrounding uninvolved skin. **British Journal of Dermatology**, v. 159, n. 1, p. 152–161, 2008.

74 BEULE, P. A. A. et al. A hyperspectral fluorescence lifetime probe for skin cancer diagnosis. **Review of Scientific Instruments**, v. 78, n. 12, p. 123101, 2007.

APPENDICES

Appendix A - System components (without repetition) to optimize the arrangement and calculation of suitcase volume

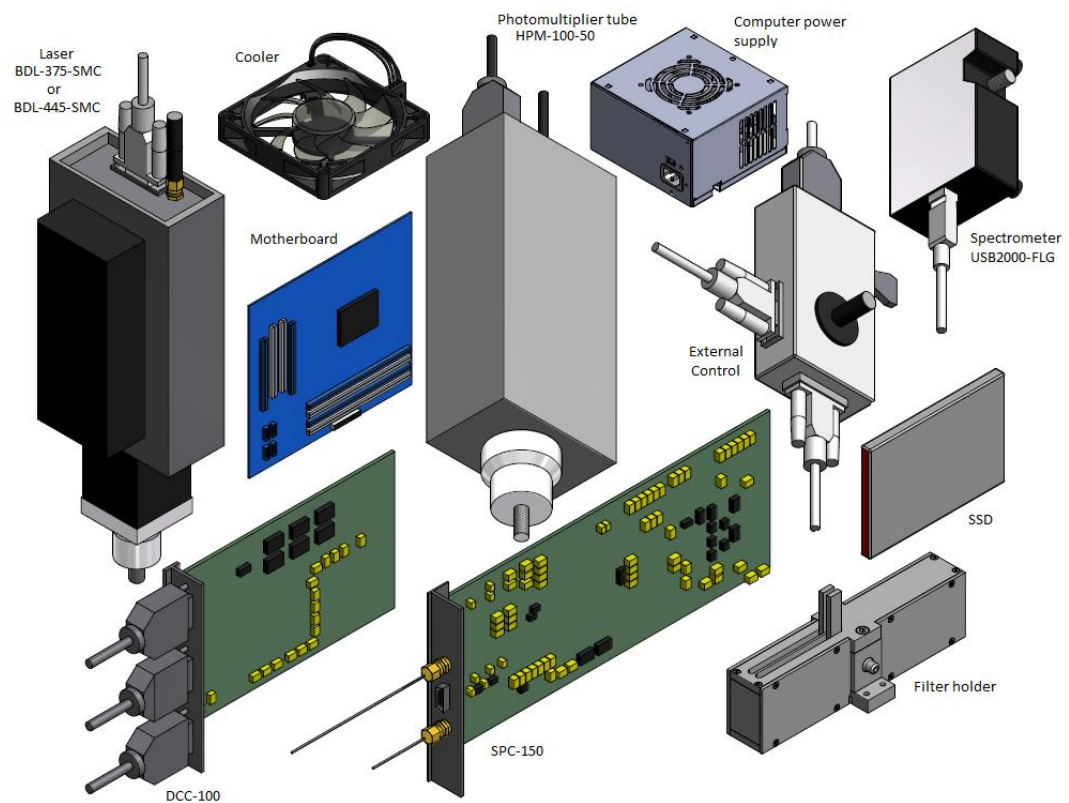


Figure 66 - Main system components (without repetition) to optimize the arrangement and calculation of suitcase volume.

Source: By the author.

Appendix B - Arrangement of the system components taking into account their mechanical, thermal, electronic, optical stability, the system cooling, the feasibility to be used on a clinic, the volume reduction and the weight to be transported into the suitcase

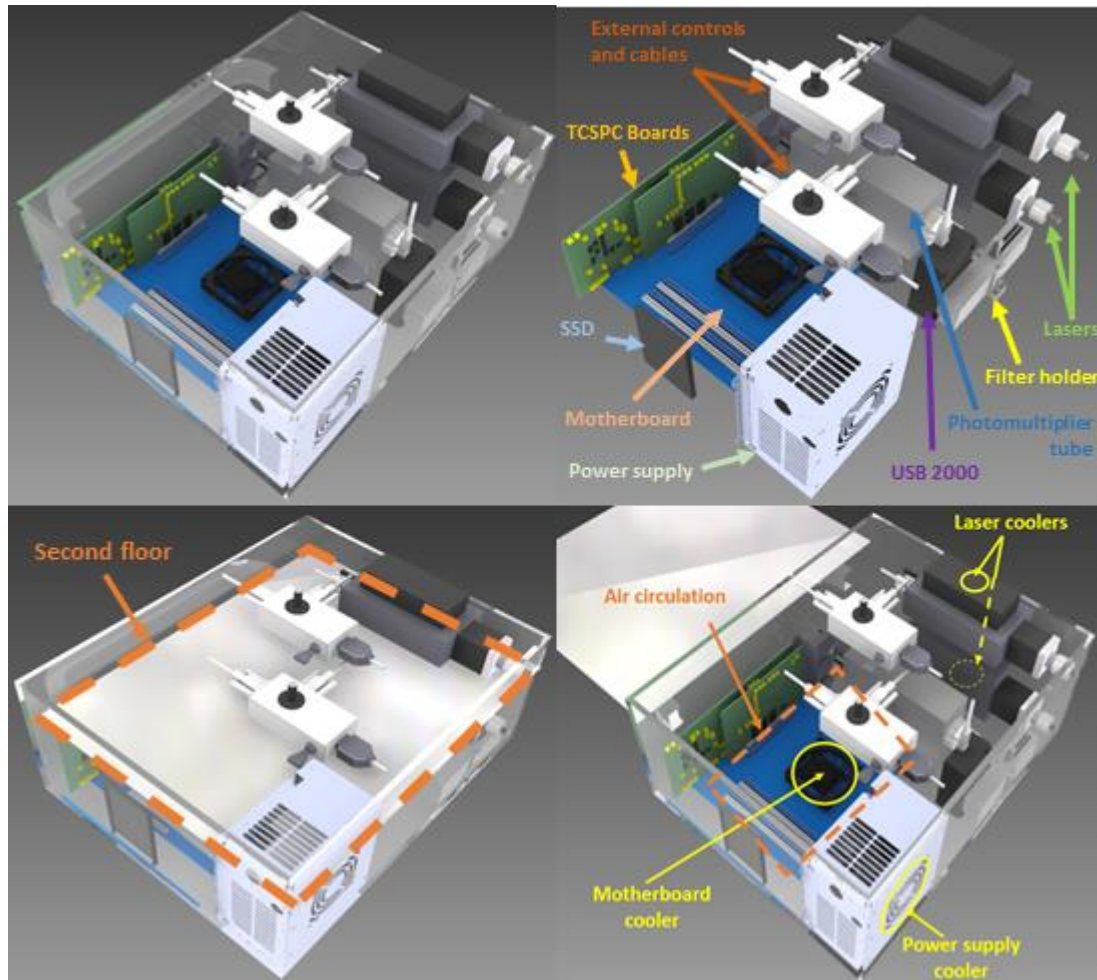


Figure 67 - Arrangement of the system components taking into account their mechanical, thermal, electronic, optical stability, the system cooling, the feasibility to be used on a clinic, the volume reduction and the weight to be transported into the suitcase.

Source: By the author.

The positions of the system components were chosen for no contacts between the system boards (motherboard and TCSPC boards) and wires or conductive surfaces, to keep lasers and power supply at fixed positions at the suitcase by using the less volume possible for the fixing them, to keep the adequate cooling by putting each equipment cooler aiming to different air exits and by providing a large volume for air circulation for internal coolers (motherboard cooler) and to allow the user

access to external controls (on/off switches and repetition rate changes), optical filters and fiber optic connectors (figure 67).

The photomultiplier is only exposed when the optical fiber to perform fluorescence lifetime spectroscopy measurements. Optical filters are allocated on a closed holder, which allows no contact between them and external dust or chemical substances and keeps the collection fiber (fiber connecting the filter's holder and the detector) away the external light during the measurements.

The electrical outlets of each component were combined with proper connectors to allow the equipment operation by using only one wall outlet. The system cables are clustered on places where they cannot be extended or contracted to do not interfere on system connections and on the air circulation.

Appendix C - SYNC and CFD Signal Path Length

TCSPC systems using the reverse start-stop mode require a reference pulse at the end of the signal period or at the end of the recorded time interval. In some cases, the laser pulse that stops the time measurement is not clear and may be a pulse from a period before or after the conventional recording period. If this pulse is in the wrong period, the position of the recorded signal in the TAC range changes with the laser period. These changes are not desired for diode lasers, which may have selectable pulse periods. So, to keep the position of the recorded signal independent on the chosen laser period, it is necessary to delay the reference pulse so that it arrives after the emitted photon pulse for each laser period. This delay should be the sum of the detector transit time, the recorded time interval, the TAC start delay (figure 68).

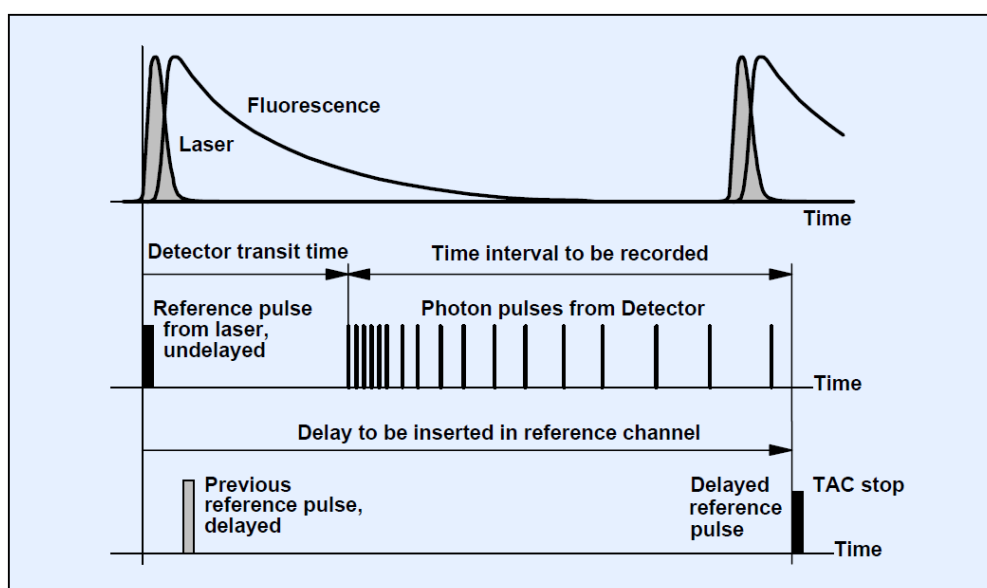


Figure 68 - When using the reverse start-stop mode, the delay in the reference channel needs to be adjusted to stop the TAC with the correct laser pulse.

Source: BECKER. (37)

In order to set the corrected delay for the reference pulse, we tested various cables lengths for the connections the CFD and SYNC channels, between the lasers and external controls, and between the external controls and the DCC-100 board. The location of the recording interval within the signal period depends on the optical path lengths, the cable lengths in the CFD and SYNC channels and on the delays in

the PMT and SYNC detectors. (37) The variations on the recorded signal position due to changes of SYNC and CFD cables are shown in figure 69.

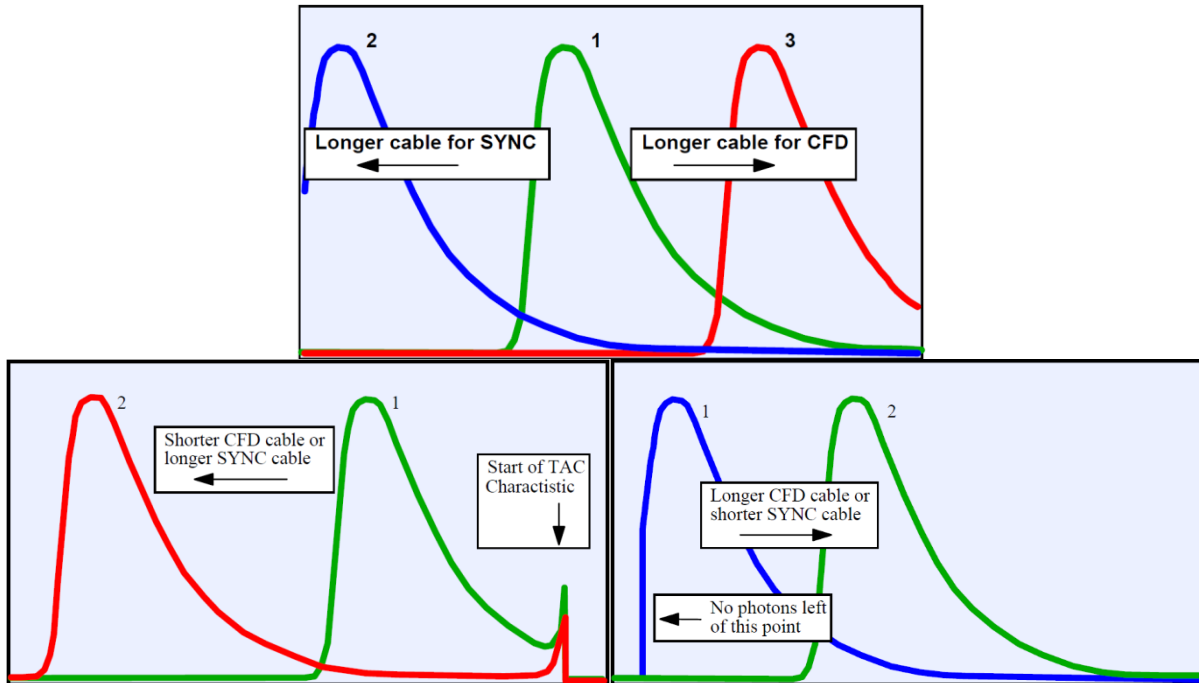


Figure 69 - The position of recorded waveform depends on the SYNC and CFD cables length. If the signal is shifted too much for the left, the peak of TAC characteristic may appear or the left part of this waveform may drop abruptly to zero.

Source: BECKER. (37)

By changing the cable lengths, we may shift the peak at the start of TAC characteristic out of the recorded range or shift the waveform (experimental curve) so that the initial part at the left of the signal does not drop abruptly to zero, since this happens when the signal photons arrive too early. The cables lengths and TAC parameters (37) were adjusted until we obtain a signal as in the figure 70.

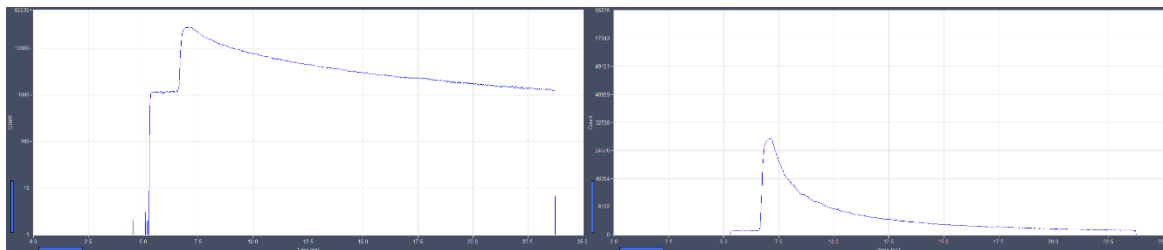


Figure 70 - Example of waveform obtained after the cables lengths and TAC parameters are correctly adjusted.

Source: By the author.

Appendix D - Components of the computer assembled inside the suitcase and of the system instrumentation

Table 6 - Computer and instrumentation components for assembly of the time-resolved fluorescence spectroscopy system

Number of components	Computer and instrumentation components
1	Intel® Gigabyte GA-B75M-D3H Motherboard LGA 1155 DDR3 Chipset B75 - HDMI VGA DVI
1	Intel® Core™ i7-3770 LGA 1155 Intel HD Graphics 4000 Processor (8M Cache, up to 3.40 GHz) - BX80637I73770
2	Kingston® Memory 8GB DDR3 1333 - KVR1333D3N9 / 8G
1	SSD Kingston® SV300S3D7/480G V300 480GB 2.5" SATA III
1	Seventeam power supply 350W (Automatic Bivolt) Real Mini ST-350MAE Dimensions: (125 x 78 x 100) mm
1	Mini LS Keyboard USB standard ABNT low profile keys
1	Black USB Mouse 1405 - (35H-00006) from Microsoft
1	Picosecond Diode Laser BDL-375-SMC from Becker and Hickl company
1	Picosecond Diode Laser BDL-445-SMC from Becker and Hickl company
1	Hybrid photomultiplier tube detector HPM-100-50 from Becker and Hickl company
2	External controls from Becker and Hickl company
1	SPC-150 board from Becker and Hickl company
1	DCC-100 board from Becker and Hickl company
1	Portable spectrometer USB2000-FLG from Ocean Optics company
1	Home-made filter holder
1	Optical fiber BIF-400-UV-VIS from Ocean Optics company
1	Optical fiber SPLIT-400-UV-VIS from Ocean Optics company

Source: By the author.

Appendix F – Fixation of motherboard in the suitcase wall

Since the internal suitcase walls are covered by a mechanical protection layer made of a material that may accumulate electrical charges, the motherboard needed to be spaced from this material. So, the motherboard fixation was achieved by using a metallic plate fixed to the suitcase wall, appropriate connectors screwed on this wall and useful as spacers for no electrical contacts between the metallic plate and the motherboard, screws to the fixation of motherboard over these connectors and electrical insulators between connectors and motherboard.

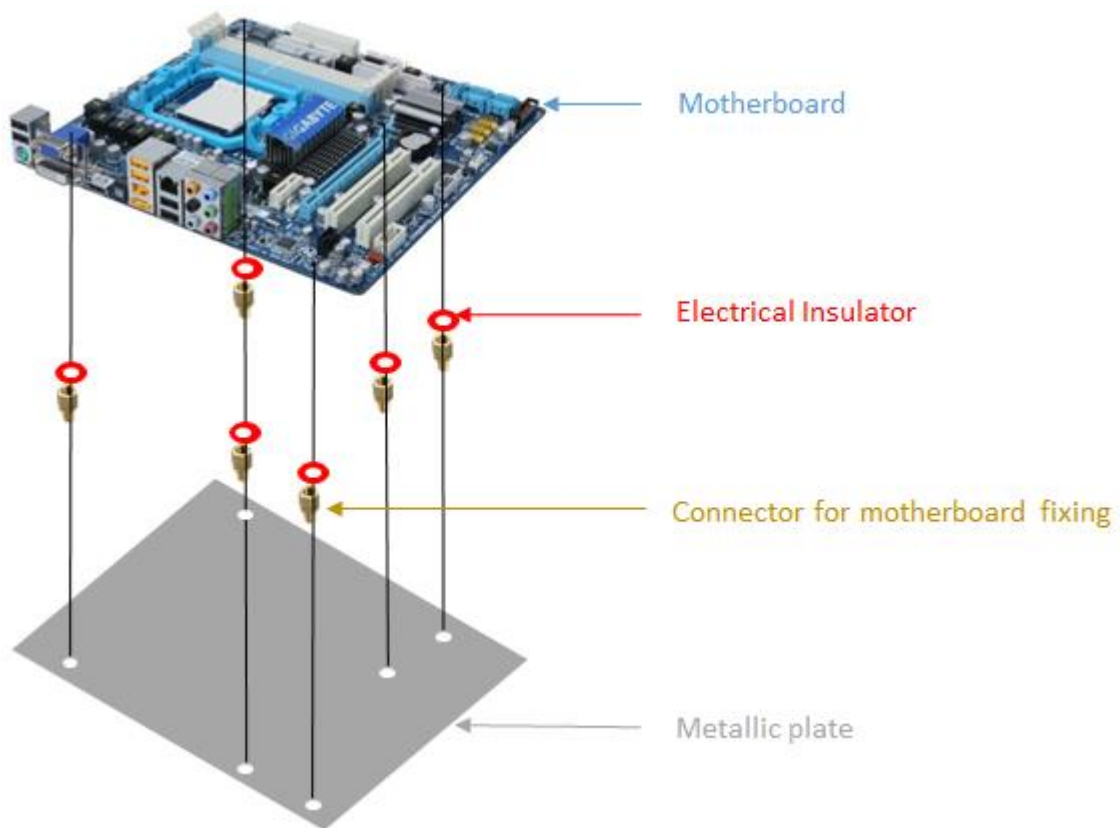


Figure 72- The fixation of the motherboard in the suitcase wall required spacers that allow the motherboard contacts to be grounded with the metallic shell of the suitcase.

Source: By the author.

The fixation procedure included the following steps: the metallic plate was fixed in the suitcase wall, both were drilled in the connectors positions, these connectors were screwed in the suitcase wall over the metallic plate (for a better immobilization due to an increase of rubbing between metallic surfaces), rings of

insulating material were positioned between the connectors and motherboard surfaces, and the motherboard was properly fixed using screws for these connectors.

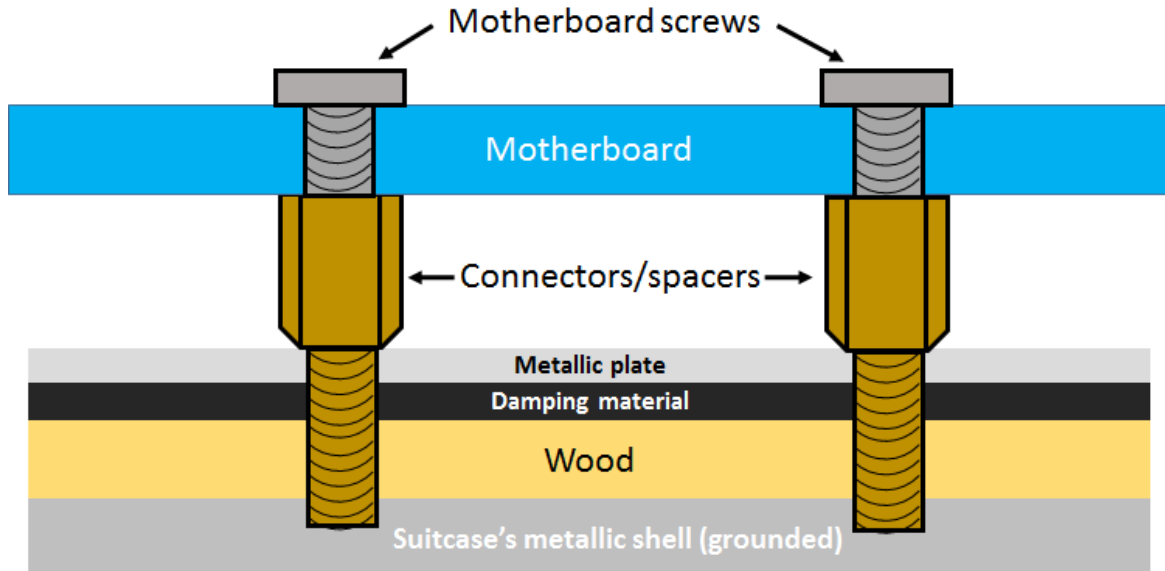


Figure 73 - The structure for the motherboard's fixation allows its electrical grounding and spacing from the suitcase walls.

Source: By the author.

By using the structure in the figure 73, it is possible to ground the motherboard circuit by using the motherboard connections to the computer power supply, which has a plug with a grounding pin connected to the main ground wire for the suitcase) and the structures for motherboard fixation.

Appendix G - Construction of cables with different lengths for synchronization between electrical and optical signals

To construct the new cables, the electrical contacts of each pair of pins (figure 74) and the cable's shell of the original cables from the Becker and Hickl (Berlin, Germany) company were measured using a multimeter. Then, the new cables were constructed using DE-15 connectors, cables with 15 stranded conductors (26 AWG), PVC jacket and overall foil shield, electrical insulating tape and liquid electrical insulating tape. First, each cable (conductor) inside the multiconductor cable was stripped and soldered to each one of the 15 pins and the shell of the DE-15 connectors as the connections in the (figure 74). The electrical contact for each multiconductor cable was checked using a multimeter and, then, the liquid electrical insulating tape was inserted between the conductors to avoid the electrical contact when the cables are handled. The electrical insulating tape covering was also used to provide more mechanical resistance to the ends of the cables.

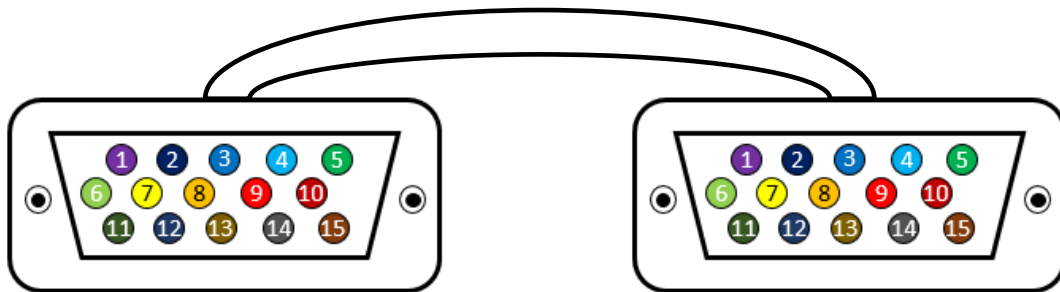


Figure 74 - Links between the pins of each DE-15 connector of the wires connecting lasers to external controls, and the external controls to a cable of DCC-100 board.

Source: By the author.

After the cables' construction, the electrical contacts between the pins and the shell were checked again with the multimeter. Then, the cables were tested on the instrumentation, replacing the original cables (figure 75). This replacing changes on the instrumentation synchronization were calibrated by adjusting the SYNC and CFD cables' path length, which are related to the laser and detector signals (Appendix III).



Figure 75 - Comparison between the length of the cables from the commercial system and the home-made cables.

Source: By the author.

Appendix H – Versions and components of the filter holder

The filter holder's structure was assembled including some main parts for the input connection of the optical fiber, fixation of this connection, light block structures, sliding parts for filters change during measurements and bases for restriction of the movement of the sliding parts (figure 76). The filter holder parts allow its compaction, functionality and easy disassembly for filter combinations changes or modifications on the structure parts.

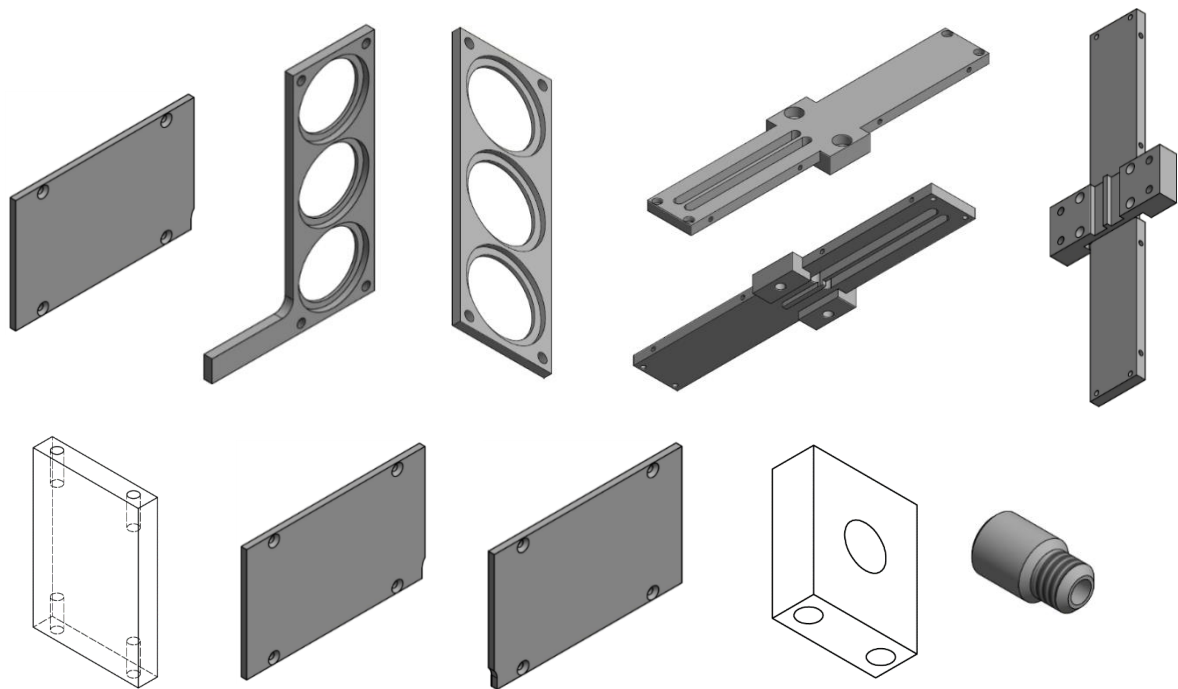


Figure 76 - Main parts for mounting the support structure for the filter.
Source: By the author.

In addition to the main parts of the filter holder's structure, other parts and their combinations were tested to increase the output to input power ratio. To improve this ratio, a high precision on the light focus position is required in a reduced space. This reduction makes difficult the fine tuning of this position, since less degrees of freedom can be adjusted with precision and the optimized position need to be mechanically stable for the portable system transport. Keeping this in mind, some combinations of filter holder parts were tested.

In the first version (figure 77), the input and output SMA 905 connections were projected to allow the adjustment of the distance between them and the presence of

a lens in the central part to focus the input light in the core of the output optical fiber. In the second version (figure 78), the output connection and the central part fixing it were replaced to a holder with a beamsplitter, which separates the filtered beam for the detection in the PMT and the spectrometer. In this case, the positions of the beamsplitter and central parts of the filter holder were not stable enough to keep a good output to input power ratio. In the third and last version (figure 79), the degrees of freedom and fixation problems were solved by allowing an angular tuning in the position of the fiber optic collimators (figure 22D). In this version, the light beam is focused directly in a single core of an output fiber, which splits and delivers the light for both spectrometer and PMT detectors.

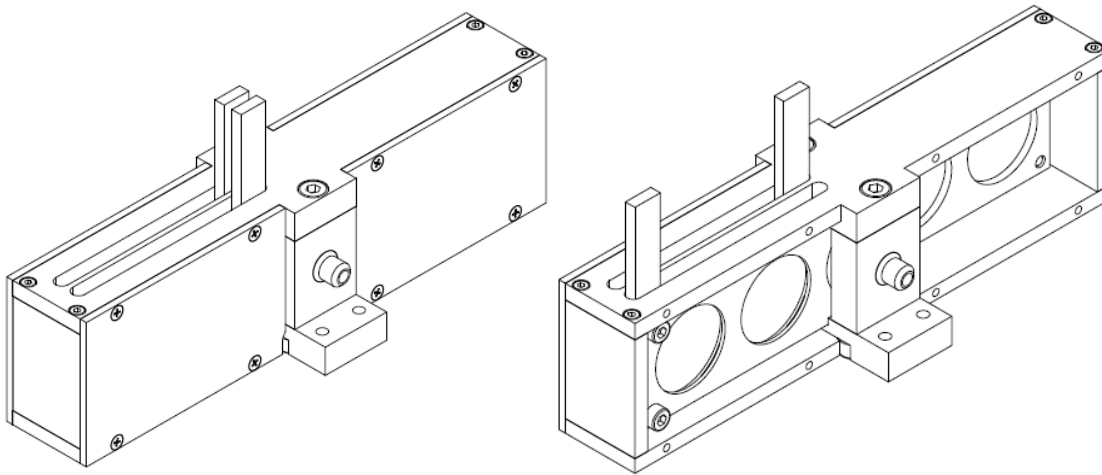


Figure 77 - First version of the filter holder. It was projected for a fast and easy filter changes during measurements. The optical fiber connectors are threaded to the central parts, so that the distance between them can be changed and a lens can be positioned to focus the input light in the core of the output fiber.

Source: By the author.

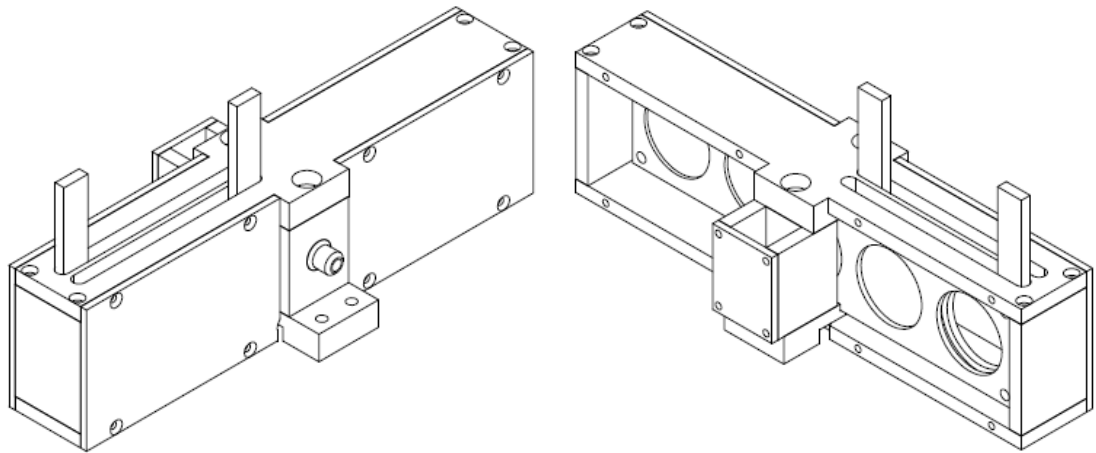


Figure 78 - Second version of the filter holder. This version was projected with a support for a beamsplitter that splits the input signal to be detected in the spectrometer and photomultiplier tube. The connections for the output collimators were done after this project.

Source: By the author.

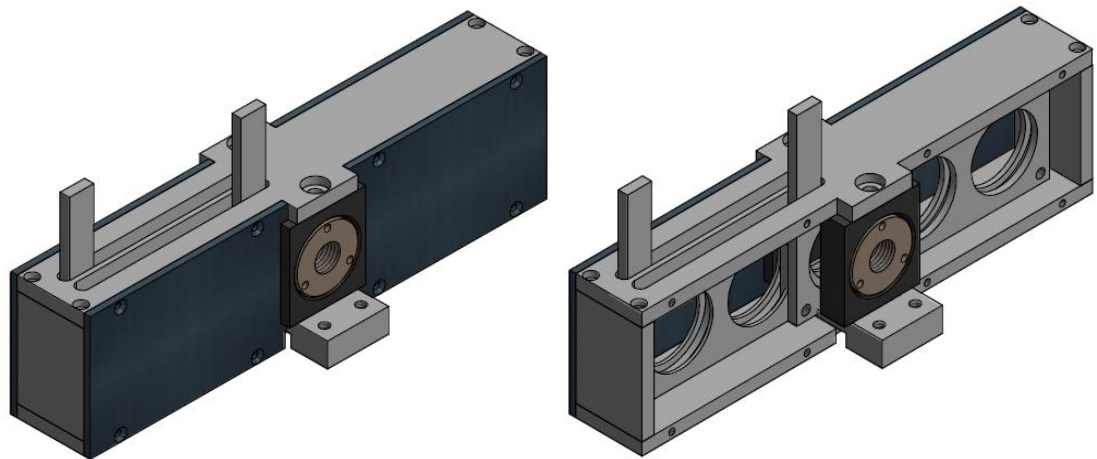


Figure 79 - Third version of the filter holder. In the central input part, the angular position can be optimized to focus the input beam into the core of the collection fiber.

Source: By the author.

Appendix I – Longpass and bandpass optical filters

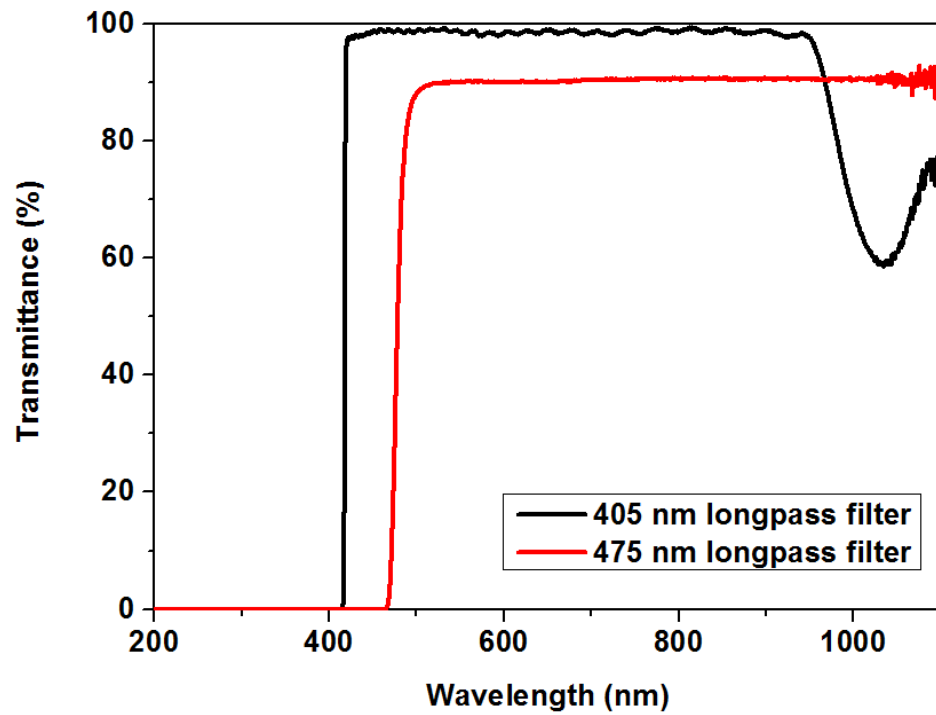


Figure 80 - Absorbance for the longpass filters used in this study.
Source: By the author.

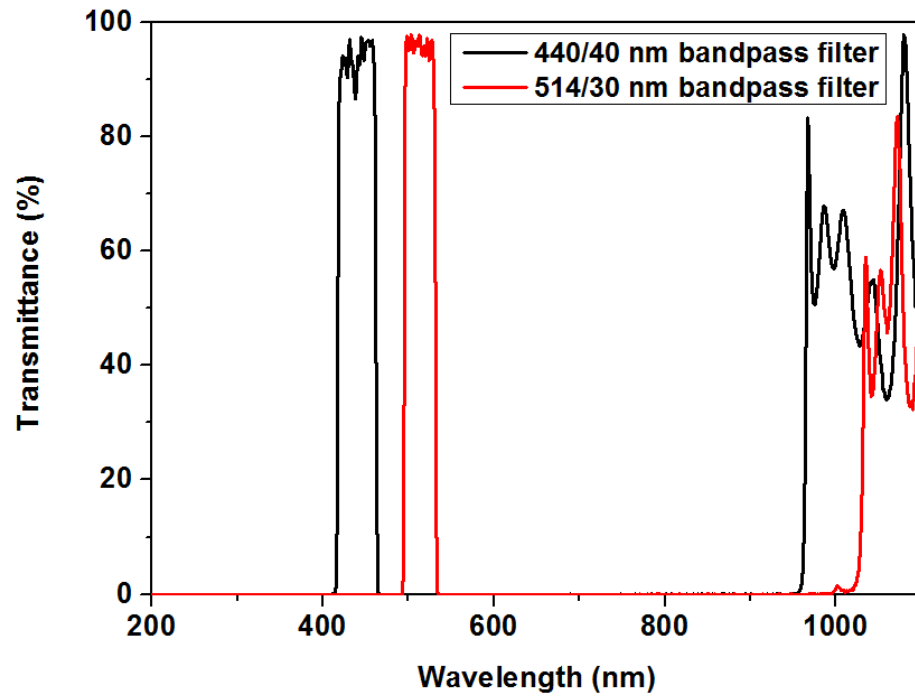
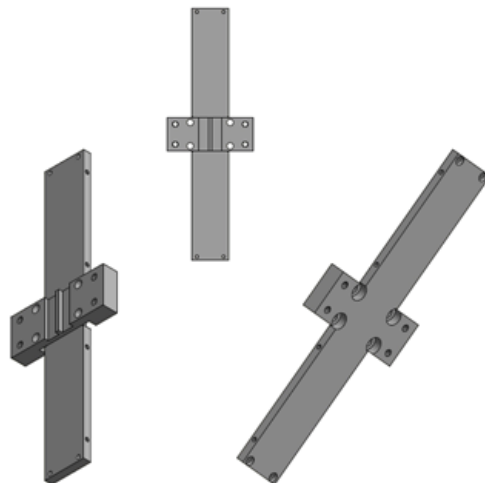
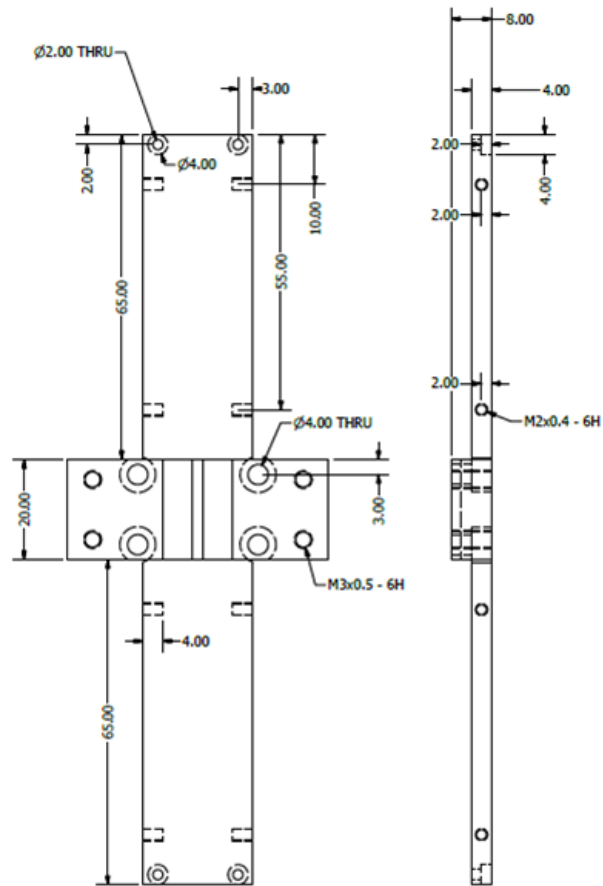




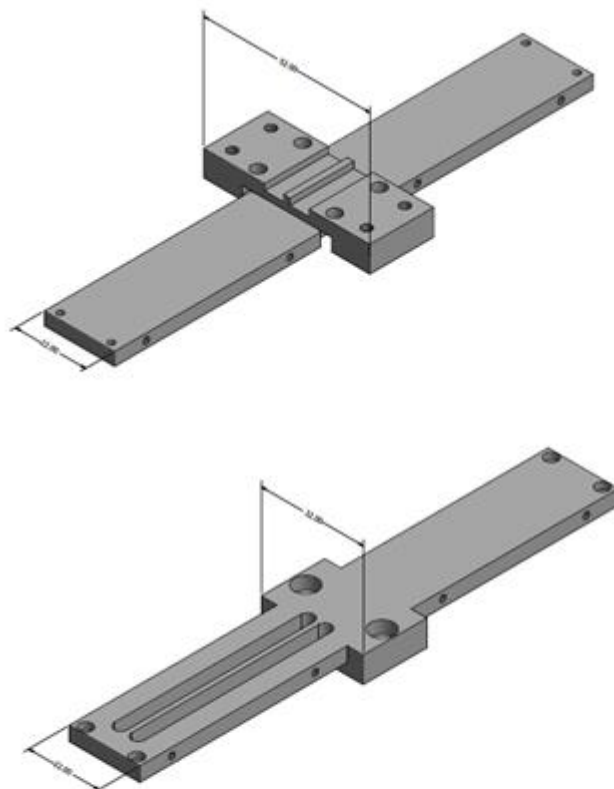
Figure 81 - Absorbance for the bandpass filters used in this study.
Source: By the author.



Appendix J – Filter holder base for fixation in suitcase wall



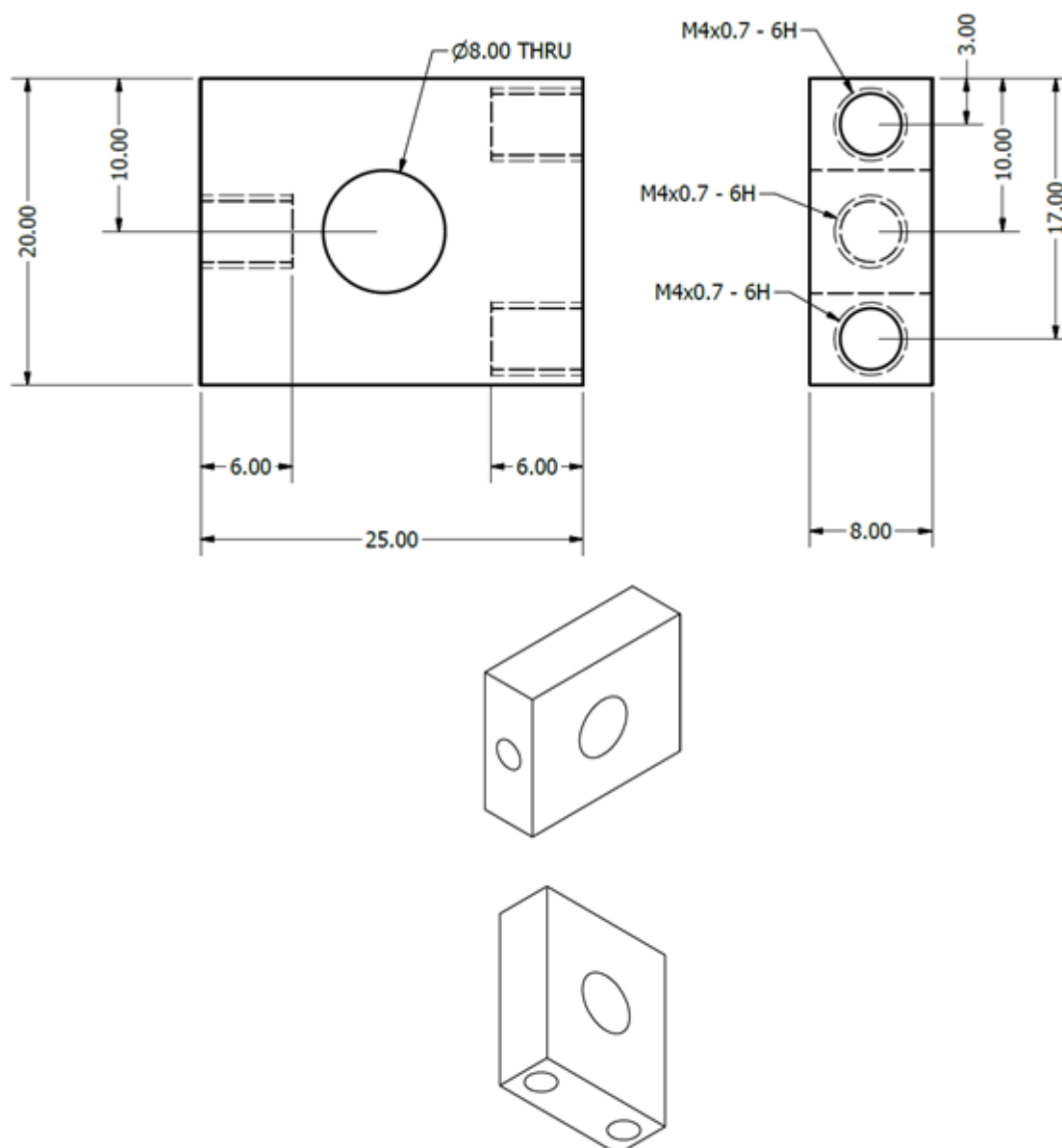
DESIGNED BY Marcelo S. Nogueira		DATE 11/28/2015	ALL DIMENSIONS mm
		Filter holder base for fixation in suitcase wall	
1 part - Aluminum		SHEET 01/12	



Appendix K – Correction on the filter holder's base



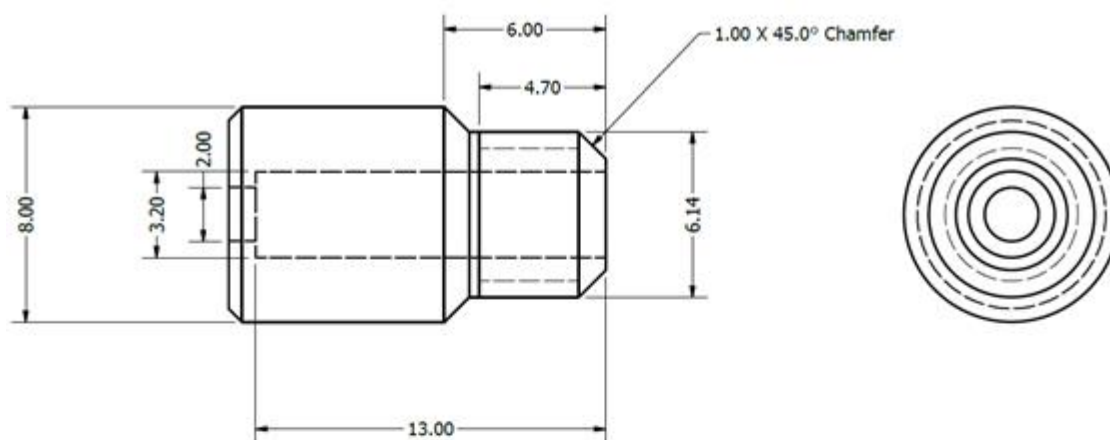
DESIGNED BY Marcelo S. Nogueira		DATE 11/28/2015	ALL DIMENSIONS mm
	Correction on the filter holder's base		SHEET 02/12
1 part- Aluminum			



Appendix L – Support (central part) for fiber connector



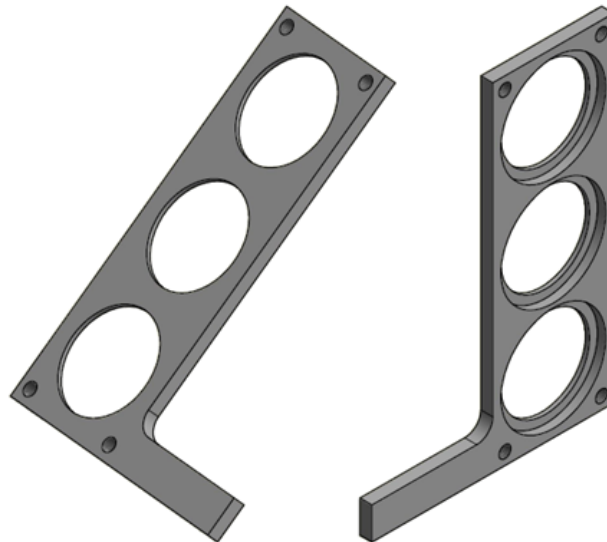
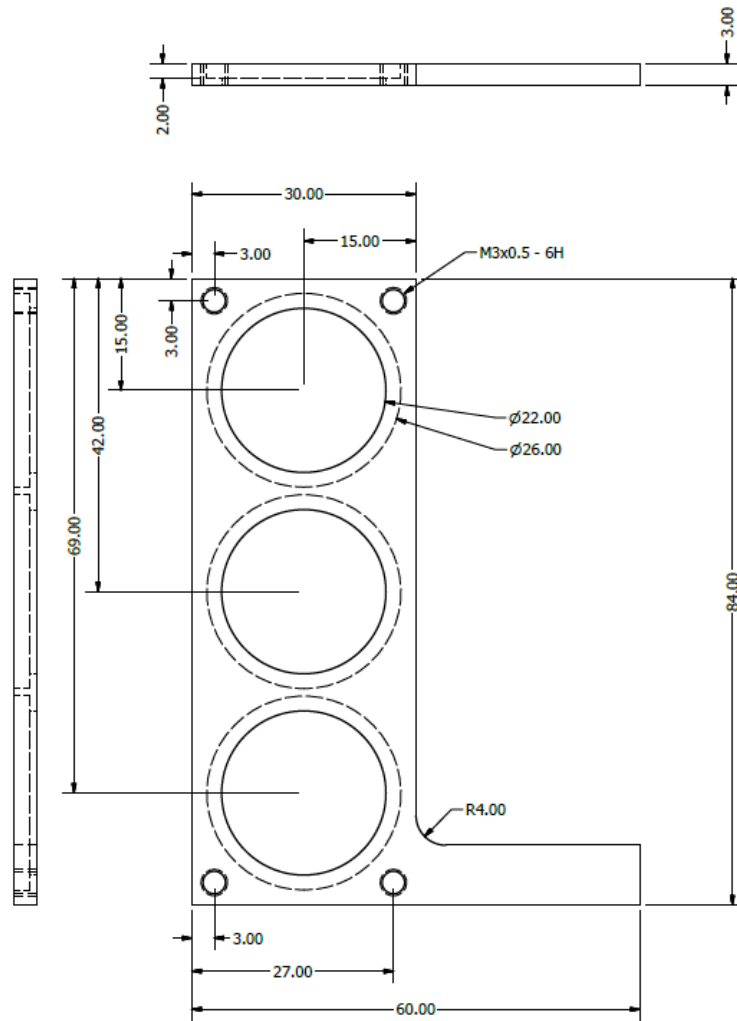
DESIGNED BY Marcelo S. Nogueira		DATE 11/28/2015	ALL DIMENSIONS mm
	Support (central part) for fiber connector		SHEET 03/12
2 parts - Aluminum			


Appendix M – SMA 905 fiber connector



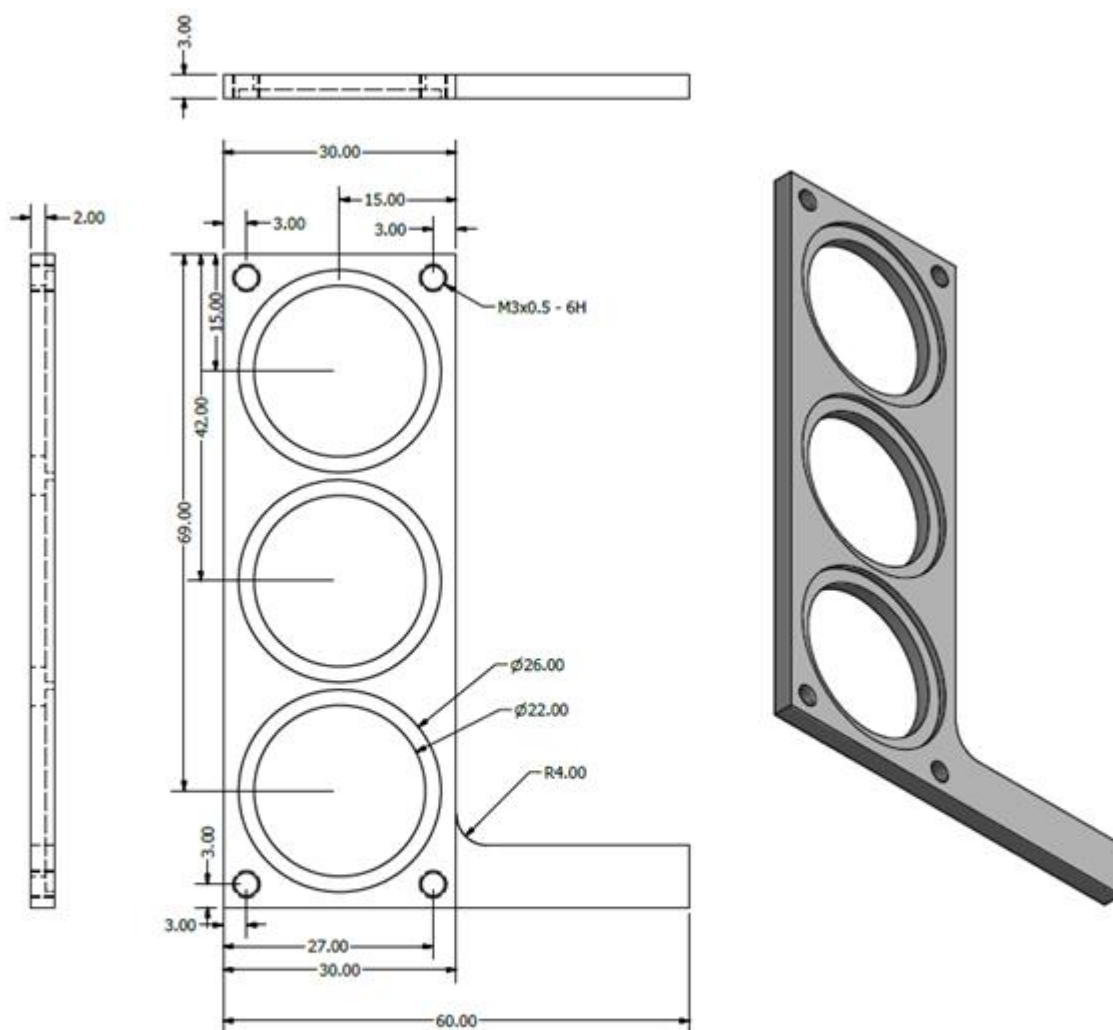
DESIGNED BY Marcelo S. Nogueira		DATE 11/28/2015	ALL DIMENSIONS mm
	SMA 905 fiber connector		SHEET 04/12
	2 parts - Aluminum		



Appendix N – Sliding part for optical filters – part I



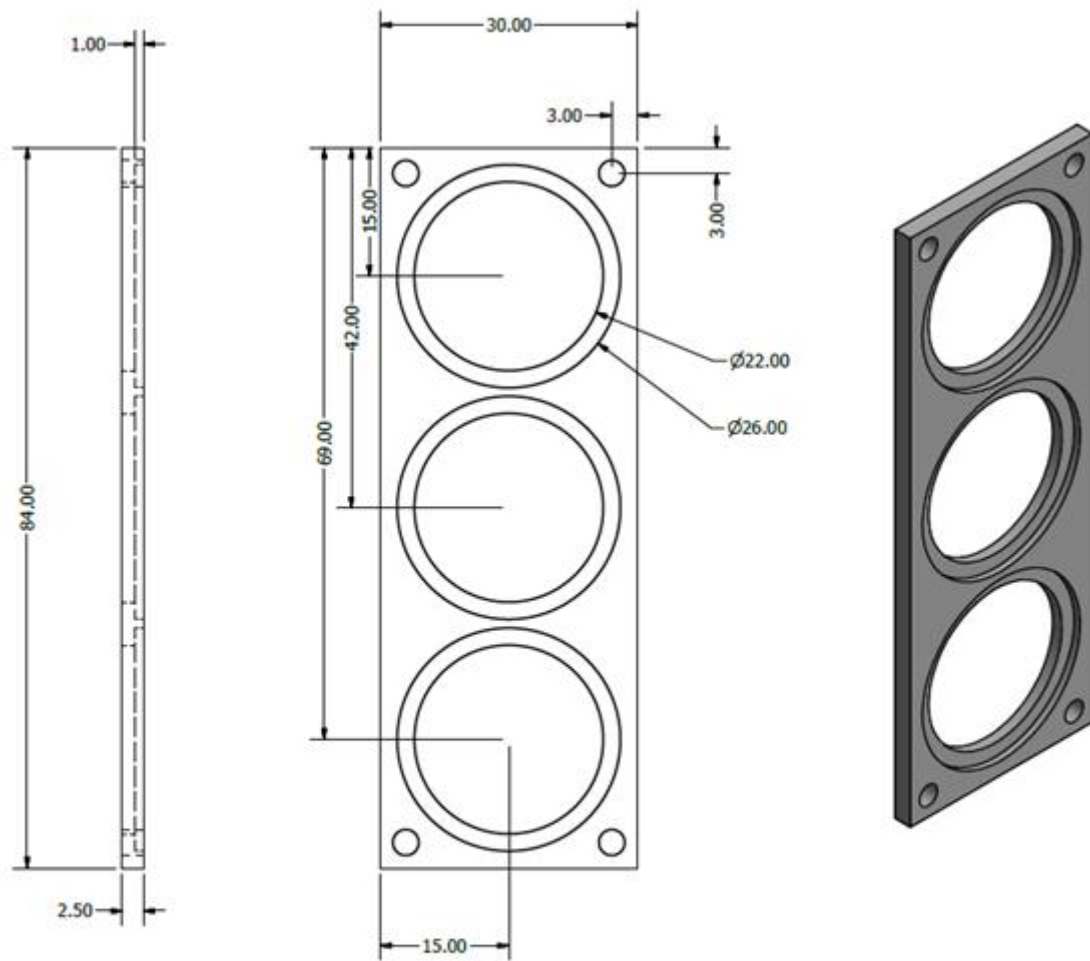
DESIGNED BY Marcelo S. Nogueira	DATE 11/28/2015	ALL DIMENSIONS mm
	Sliding part for optical filters – part I	1 part - Aluminum
		SHEET 05/12



Appendix P – Sliding part for optical filters – part III



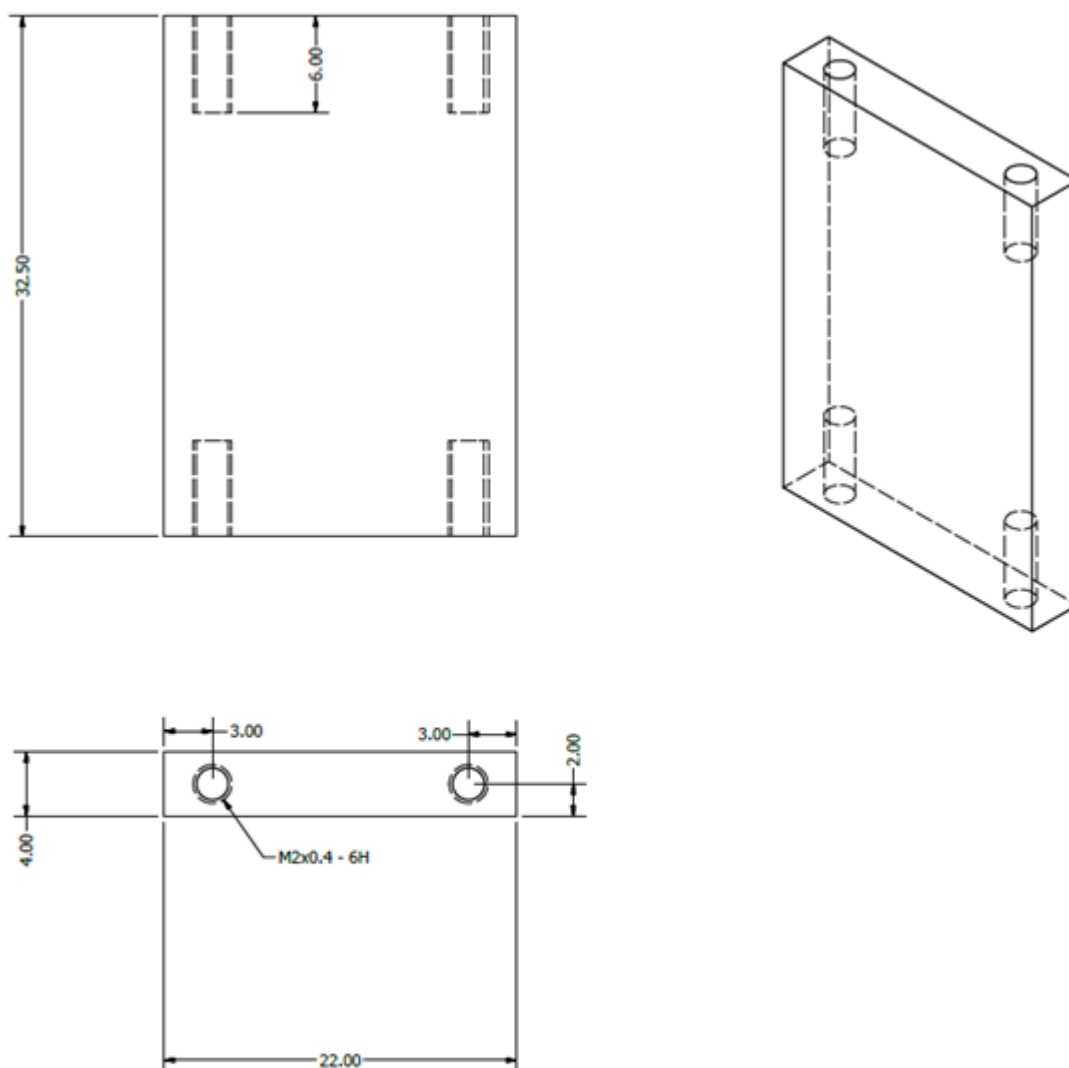
DESIGNED BY Marcelo S. Nogueira		DATE 11/28/2015	ALL DIMENSIONS mm
 CEPOF bio <small>CENTRO DE ESTUDOS DE FÍSICA E ÓPTICA</small>	Sliding part for optical filters – part III		SHEET 07/12
1 part - Aluminum			



Appendix Q – Sliding part for optical filters – part IV



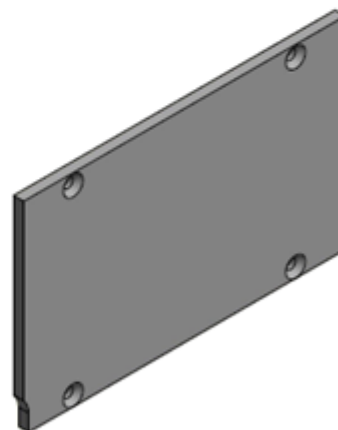
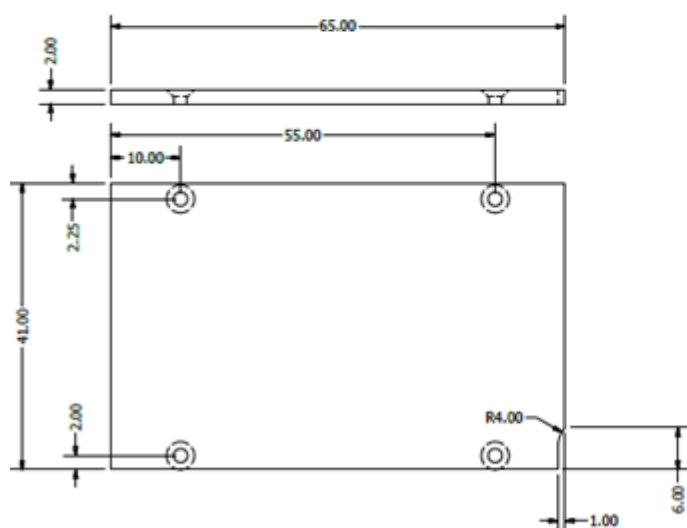
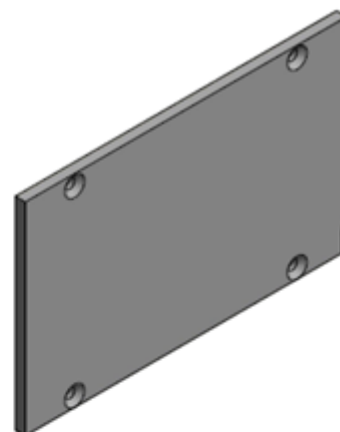
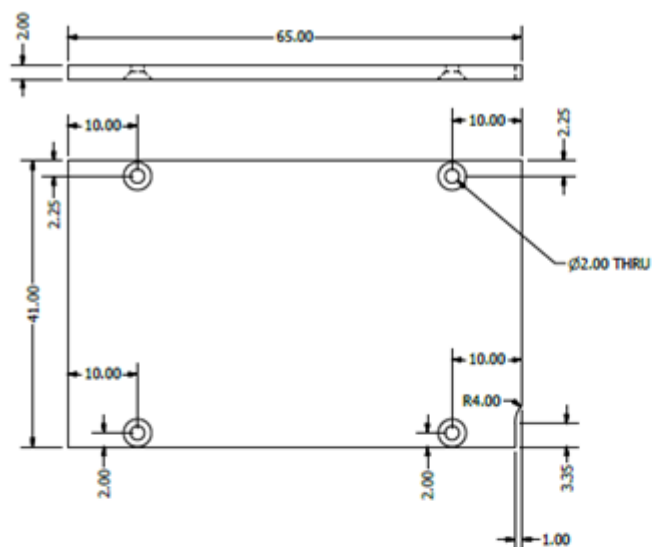
DESIGNED BY Marcelo S. Nogueira		DATE 11/28/2015	ALL DIMENSIONS mm
	Sliding part for optical filters – part IV		SHEET 08/12
1 part - Aluminum			




Appendix S – Lateral supports I



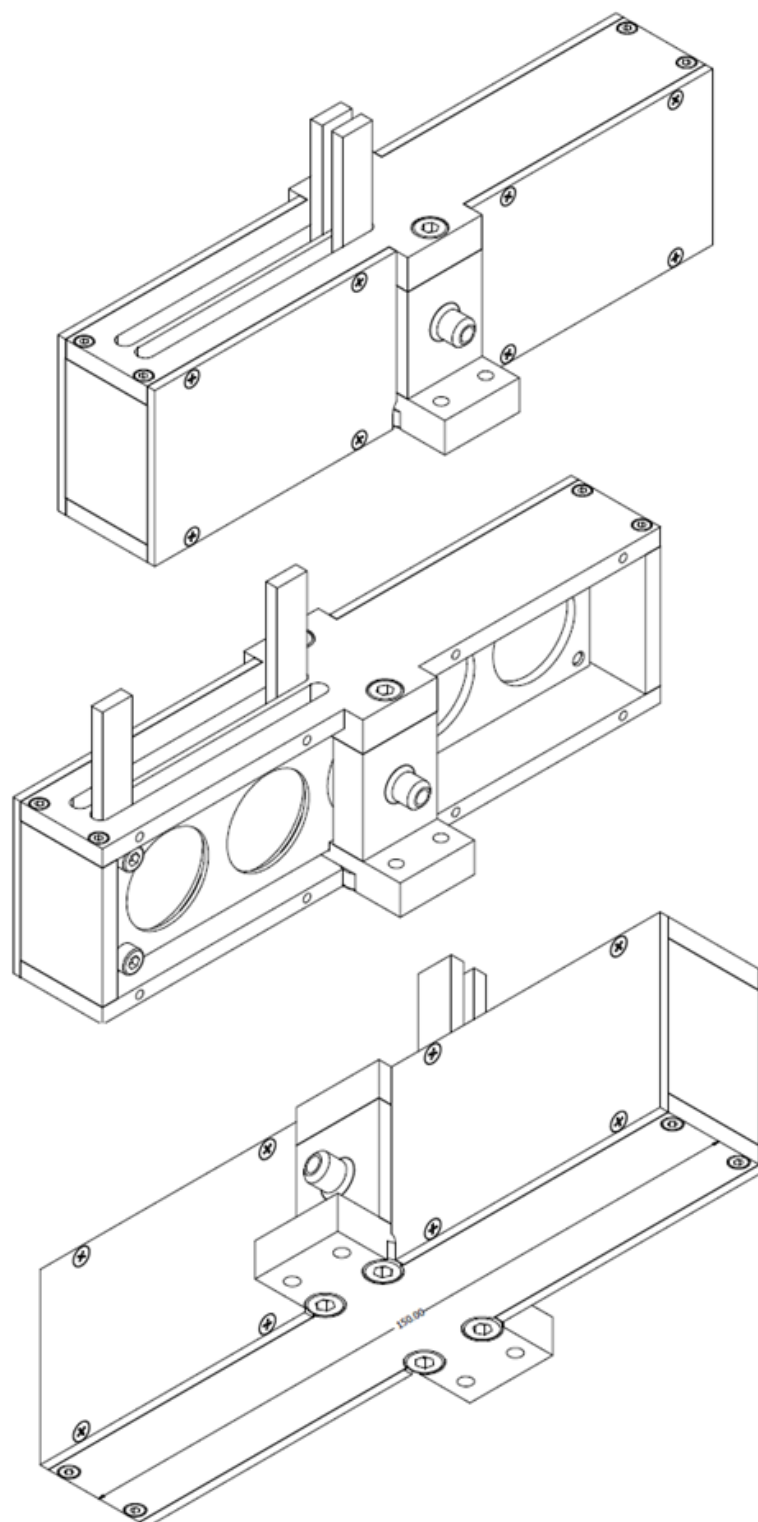
DESIGNED BY Marcelo S. Nogueira		DATE 11/28/2015	ALL DIMENSIONS mm
	Lateral supports I		
	2 parts - Aluminum		SHEET 10/12


Appendix T – Lateral supports II



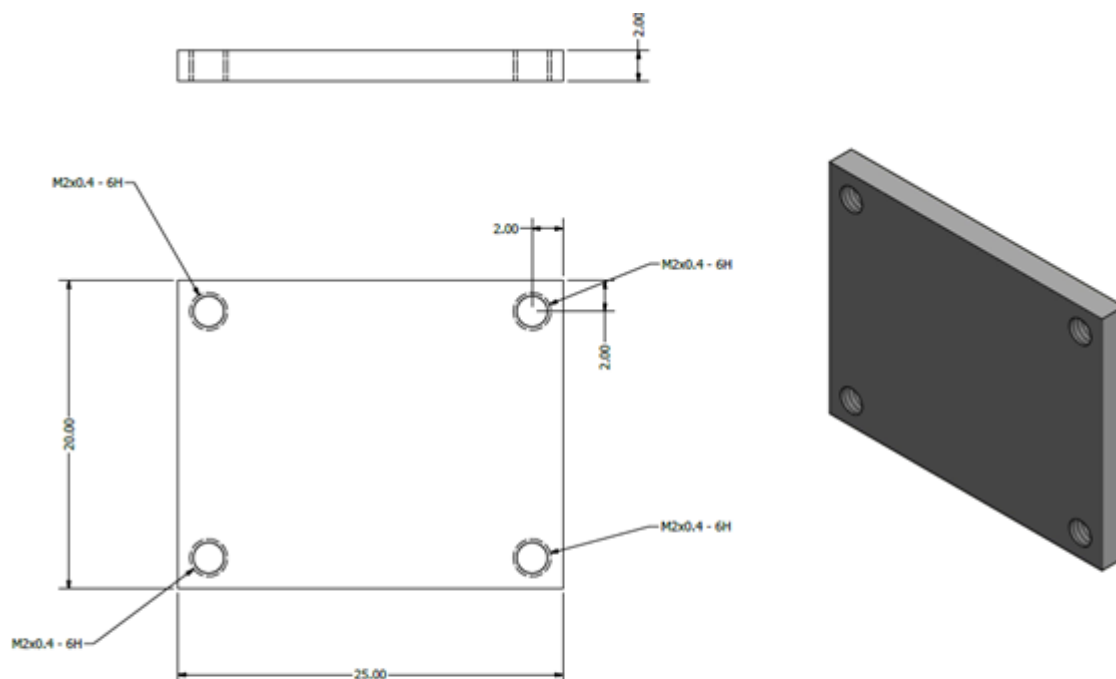
DESIGNED BY Marcelo S. Nogueira	 	DATE 11/28/2015	ALL DIMENSIONS mm
 CEPOF bio CENTRO DE PESQUISAS DE ÓPTICA E FÍSICA	Lateral supports II		
	4 parts - Aluminum		SHEET 11/12

Appendix U – Assembled filter holder – version 1



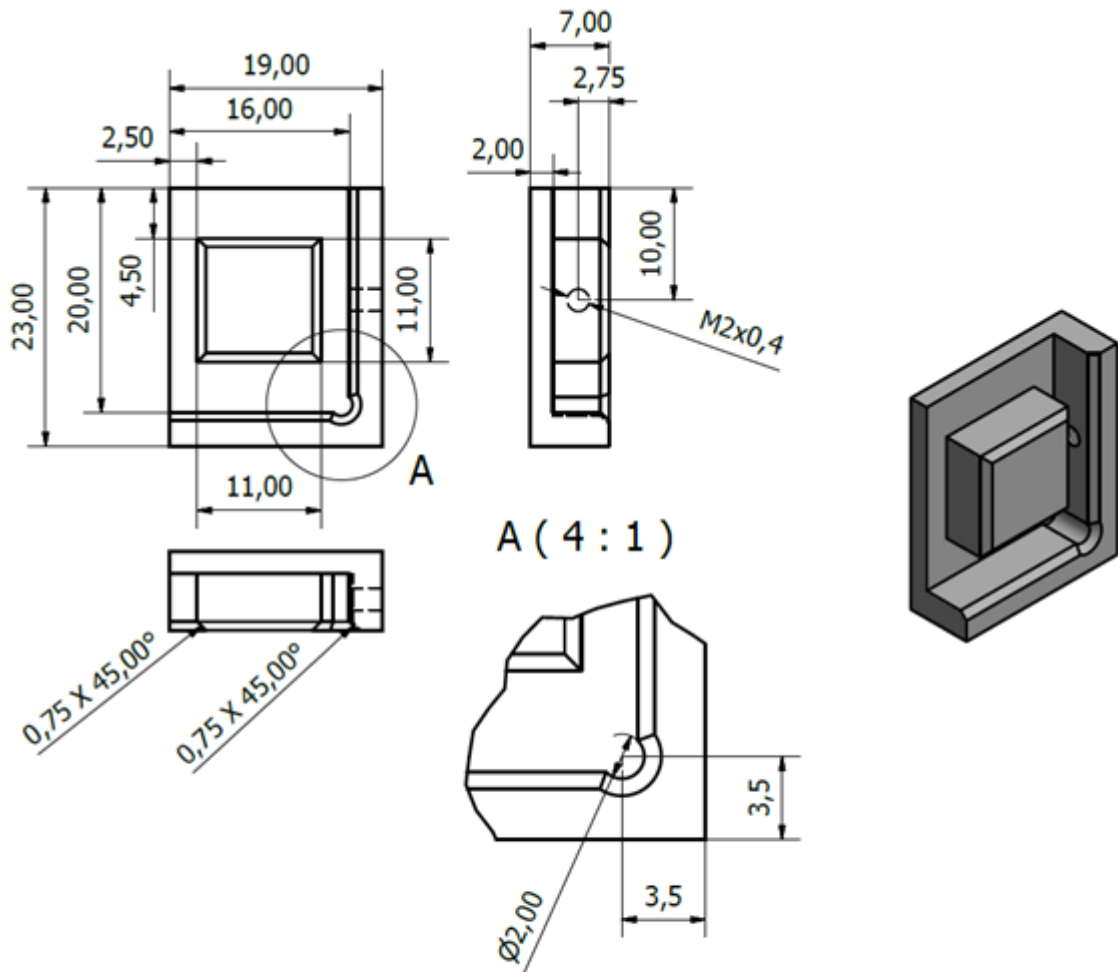
DESIGNED BY Marcelo S. Nogueira		DATE 11/28/2015	ALL DIMENSIONS mm
Assembled filter holder – version 1			SHEET 12/12



Appendix X – Enclosing part for beamsplitter holder

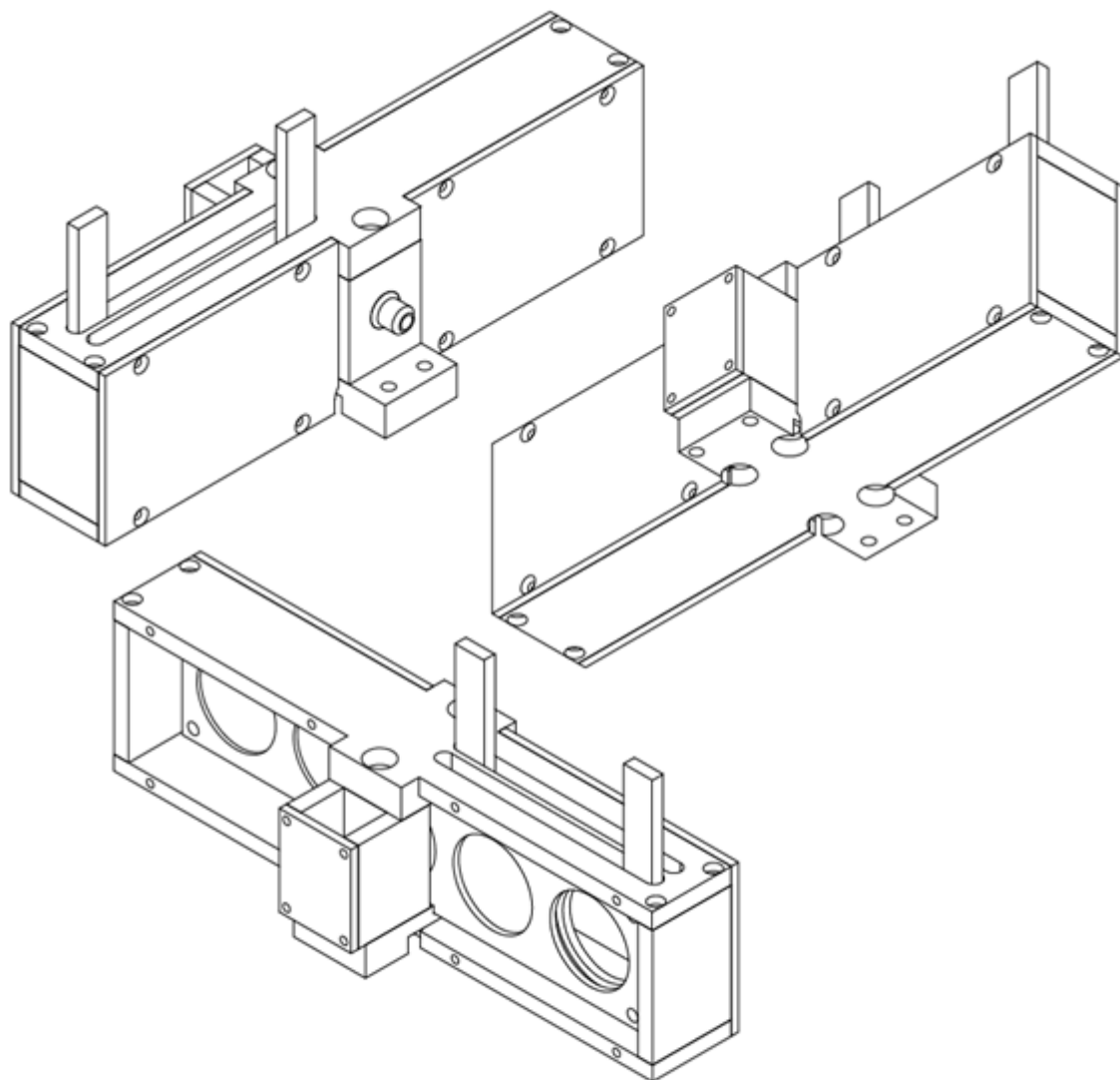




DESIGNED BY Marcelo S. Nogueira		DATE 01/05/2015	ALL DIMENSIONS mm
	Enclosing part for beamsplitter holder		
	1 part - Aluminum		SHEET 2/4

Appendix Y – Covering part for beamsplitter holder

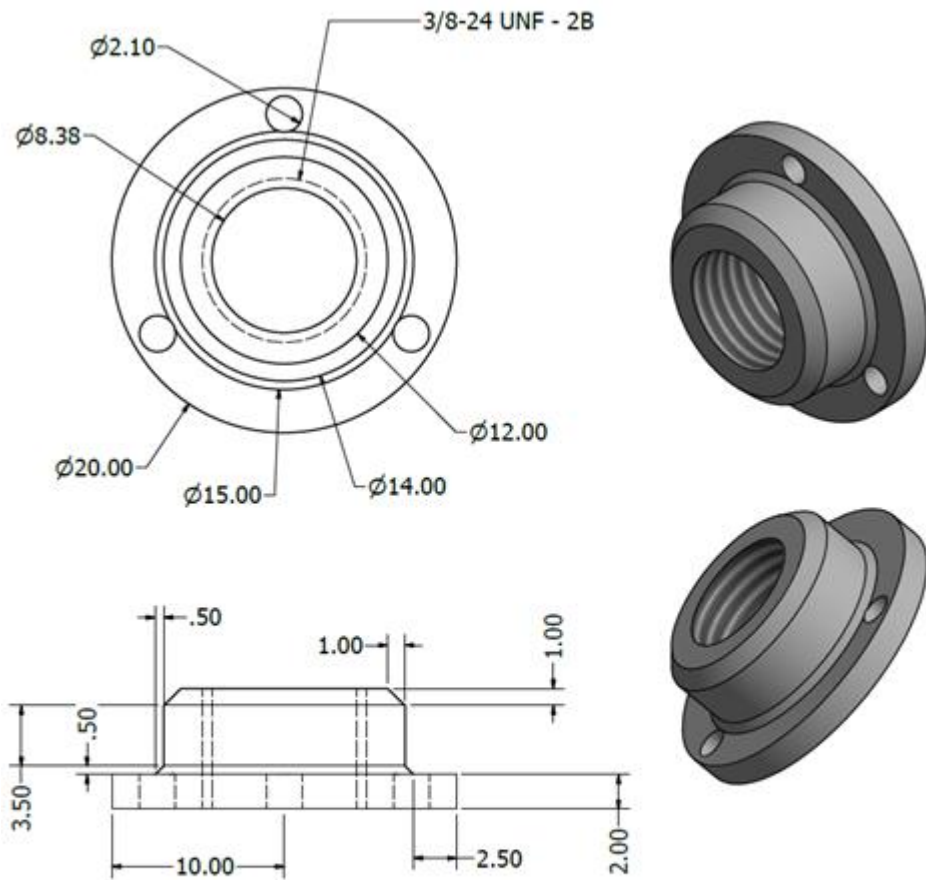




DESIGNED BY Marcelo S. Nogueira		DATE 01/05/2015	ALL DIMENSIONS mm
	Covering part for beamsplitter holder		
	1 part- Aluminum		SHEET 3/4

Appendix Z – Assembled filter holder – version 2

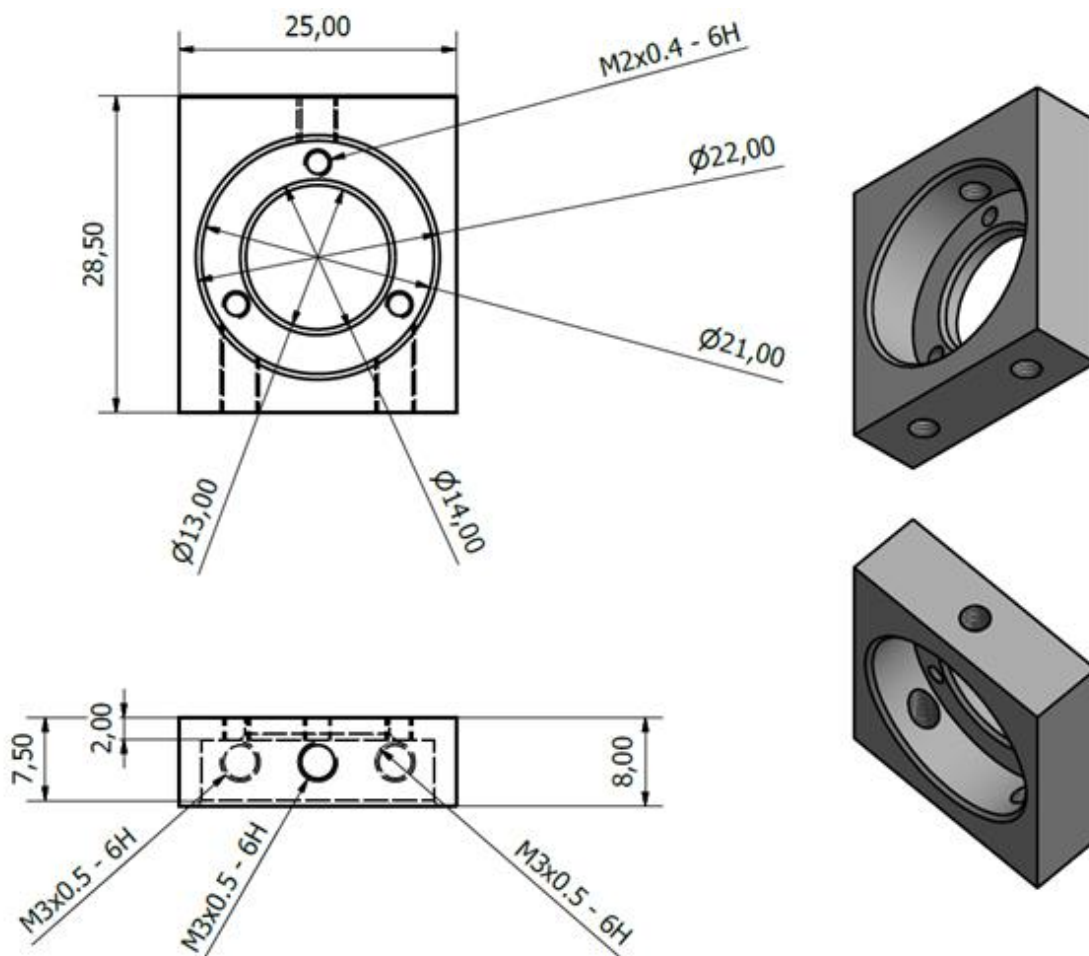
DESIGNED BY Marcelo S. Nogueira		DATE 01/05/2015	ALL DIMENSIONS mm
	Assembled filter holder – version 2		SHEET 4/4


Appendix AA – Part for adjustment of angular position of collimators



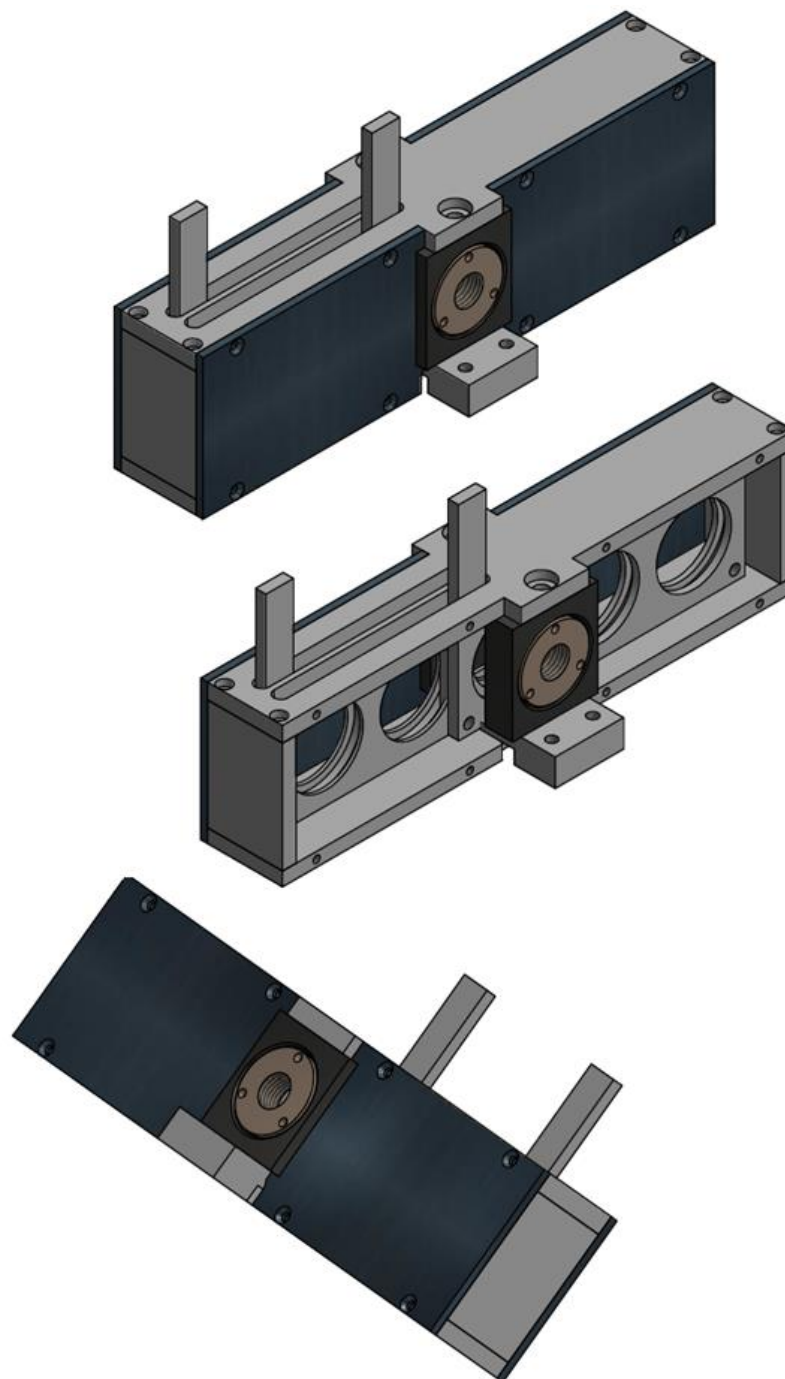
DESIGNED BY Marcelo S. Nogueira		DATE 03/12/2015	ALL DIMENSIONS mm
	Part for adjustment of angular position of collimators		
1 part - Brass			SHEET 1/3



Appendix BB – Support for angular positioner of fiber collimator



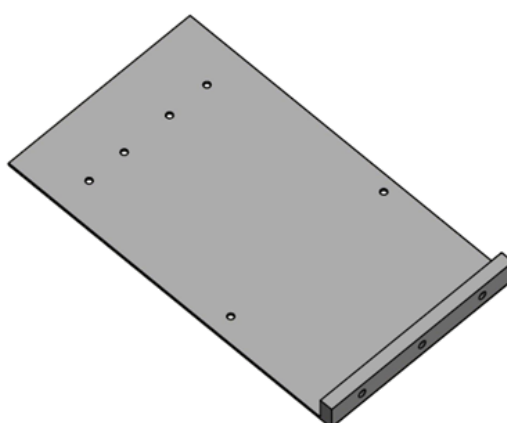
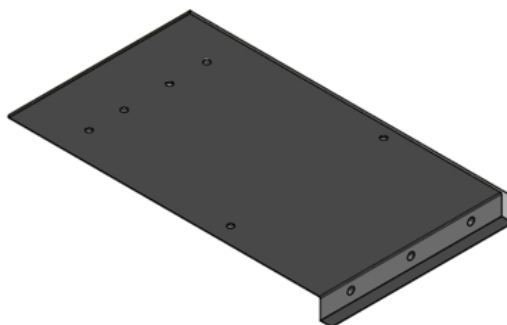
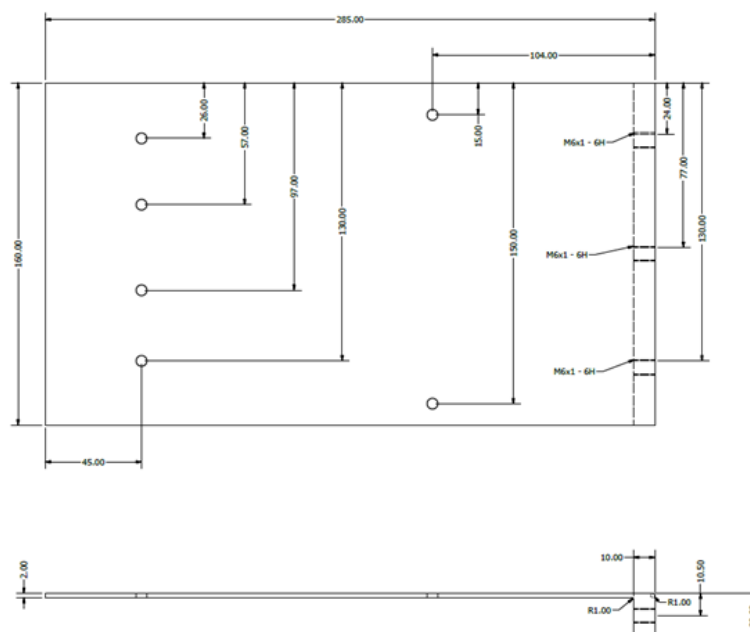
DESIGNED BY Marcelo S. Nogueira		DATE 03/12/2015	ALL DIMENSIONS mm
	Support for angular positioner of fiber collimator		SHEET 2/3
	1 part - Aluminum		



Appendix CC – Assembled filter holder – version 3



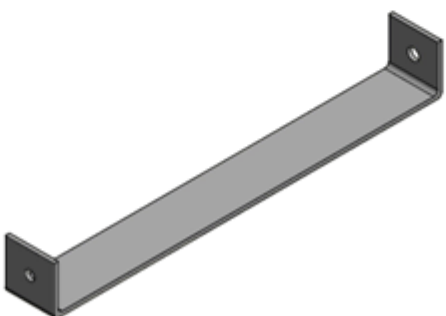
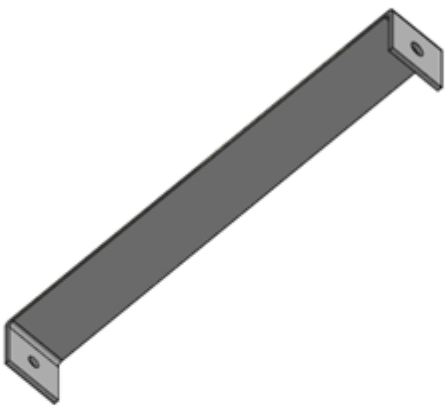
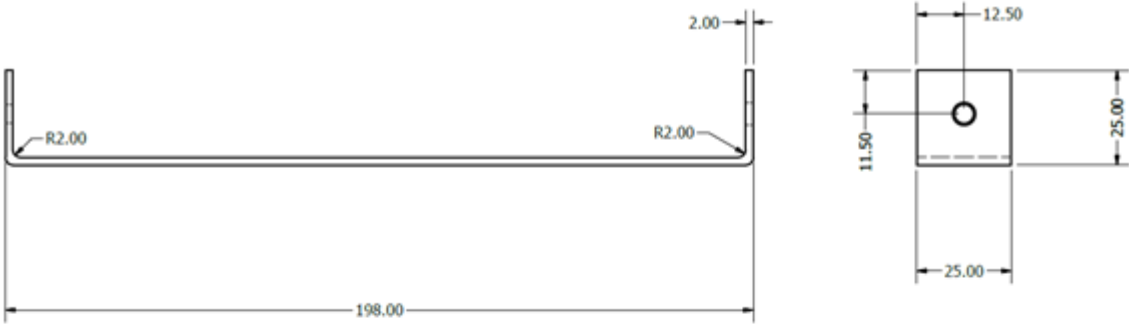
DESIGNED BY Marcelo S. Nogueira		DATE 03/12/2015	ALL DIMENSIONS mm
	Assembled filter holder – version 3		SHEET 3/3



Appendix DD – Base part for the suitcase's second floor



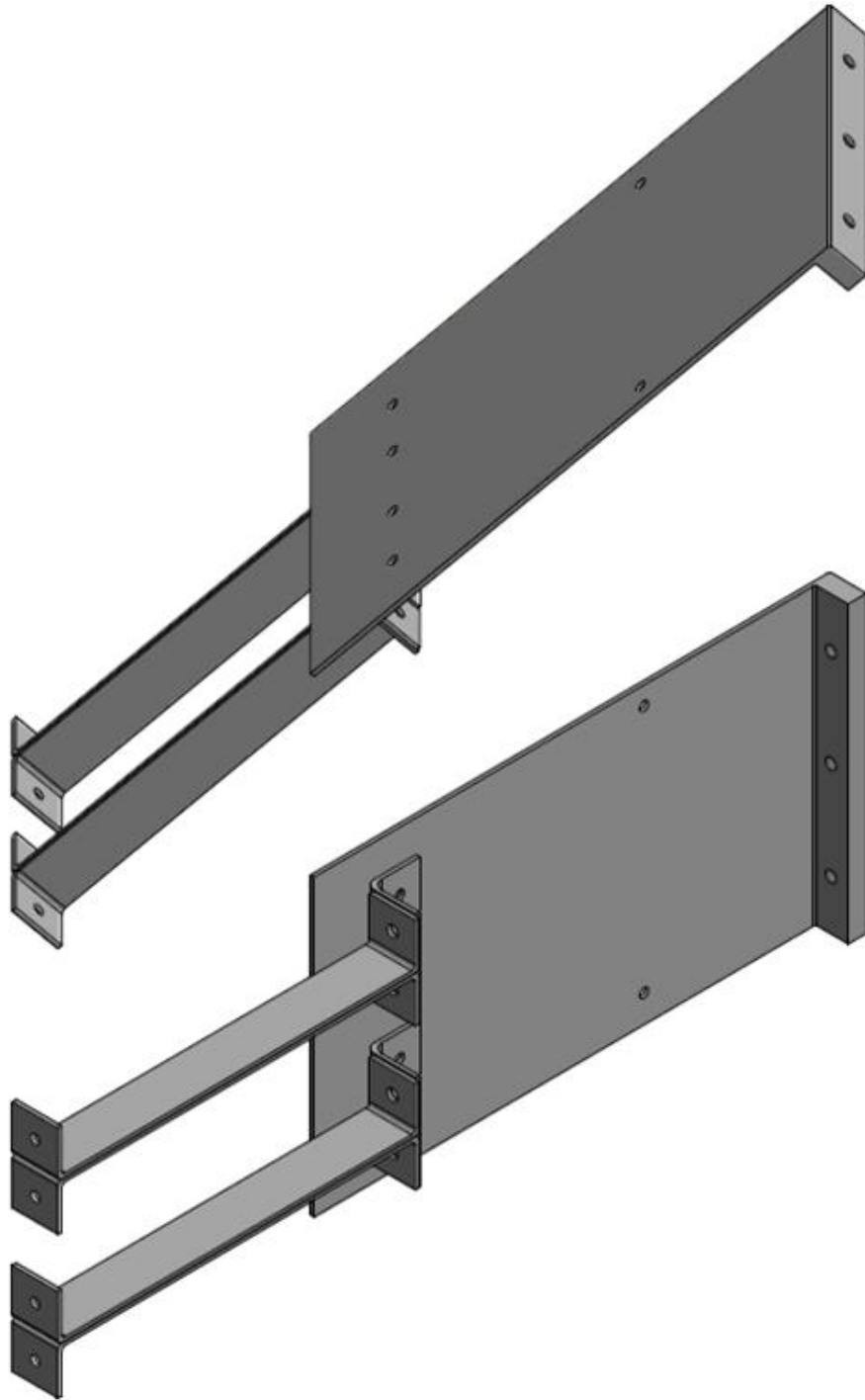
DESIGNED BY Marcelo S. Nogueira		DATE 03/09/2015	ALL DIMENSIONS mm
	Base part for the suitcase's second floor		
	1 part - Aluminum		SHEET 1/3



Appendix EE – Support for the suitcase’s second floor



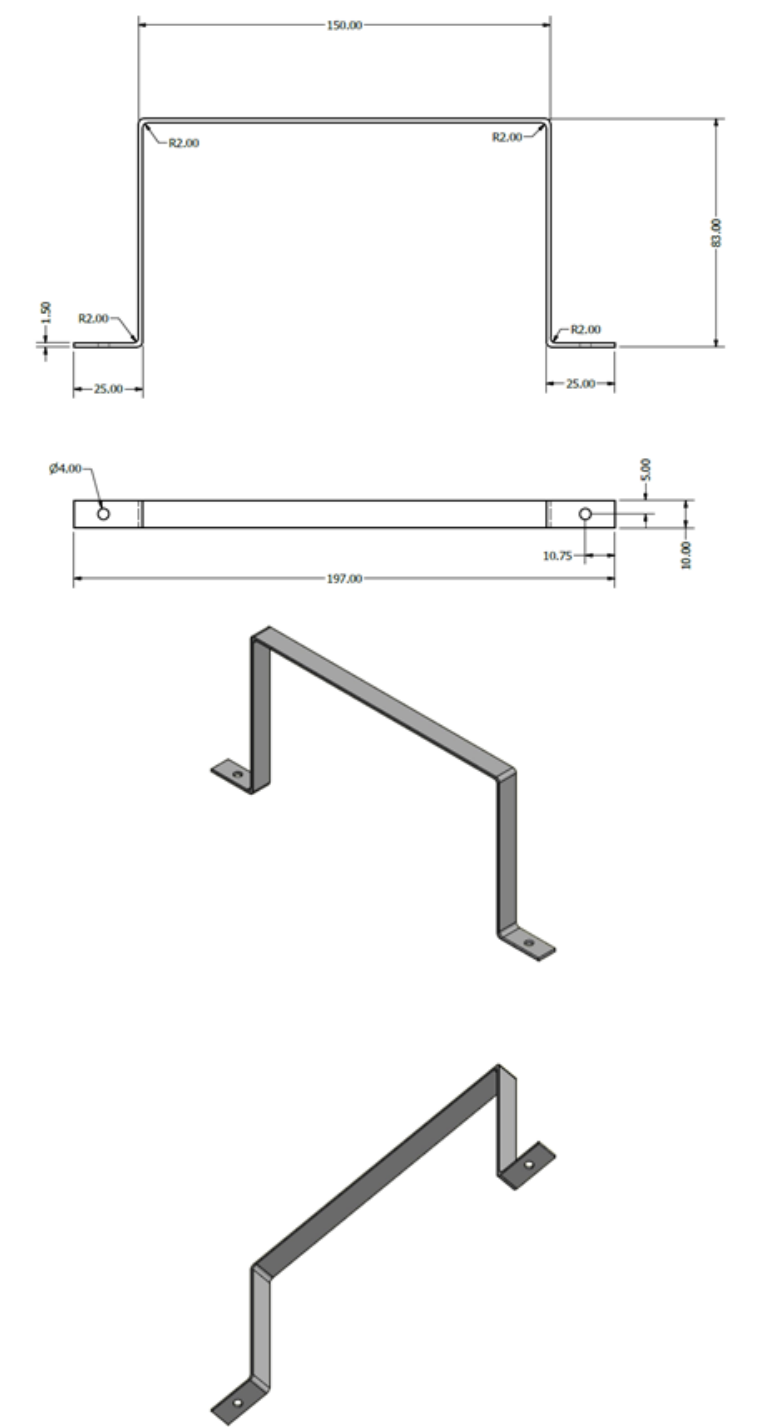
DESIGNED BY Marcelo S. Nogueira		DATE 03/09/2015	ALL DIMENSIONS mm
	Support for the suitcase's second floor		
	4 parts - Aluminum		SHEET 2/3



Appendix FF – Assembled second floor for the suitcase



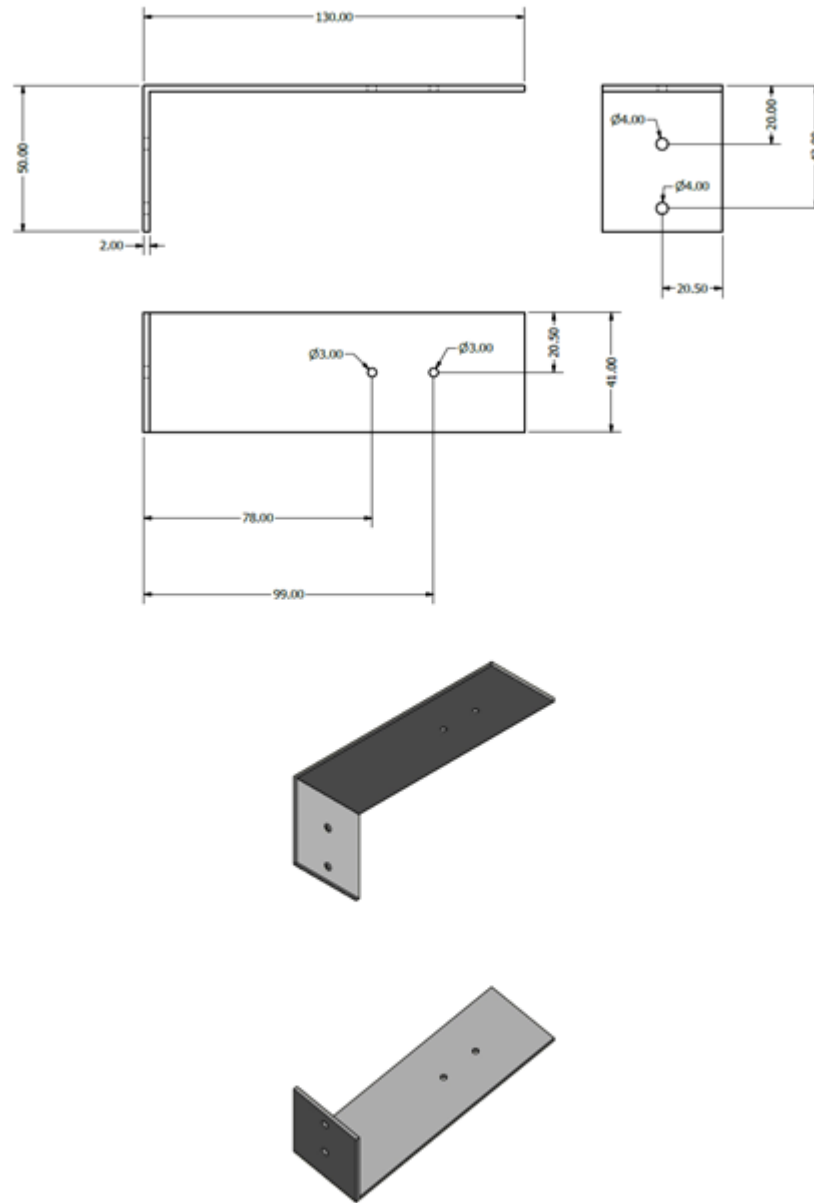
DESIGNED BY Marcelo S. Nogueira		DATE 03/09/2015	ALL DIMENSIONS mm
	Assembled second floor for the suitcase		SHEET 3/3



Appendix GG – Custom channels for fixation of power supply



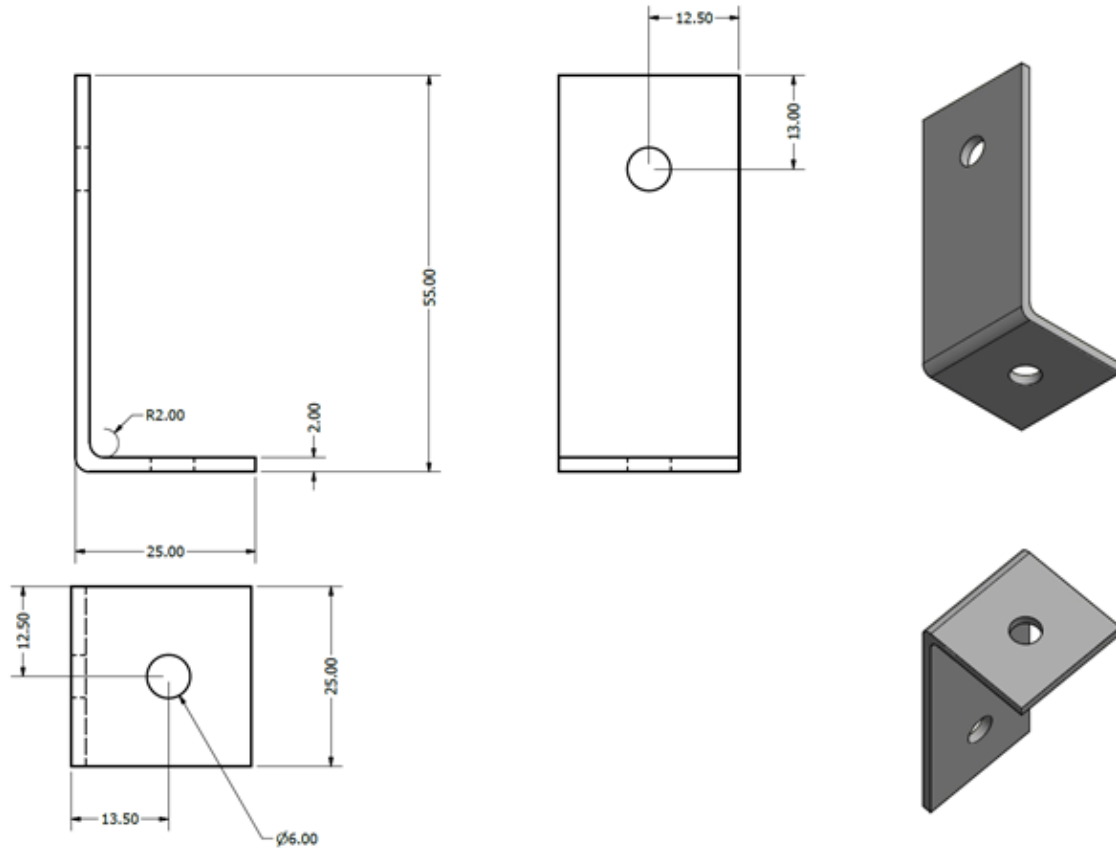
DESIGNED BY Marcelo S. Nogueira		DATE 03/09/2015	ALL DIMENSIONS mm
 CENTRO DE PESQUISA EM OPTICA E FOTONICA	Custom channels for fixation of power supply		
	3 parts - Aluminum		SHEET 1/1

Appendix HH – Angles for fixation of TCSPC boards



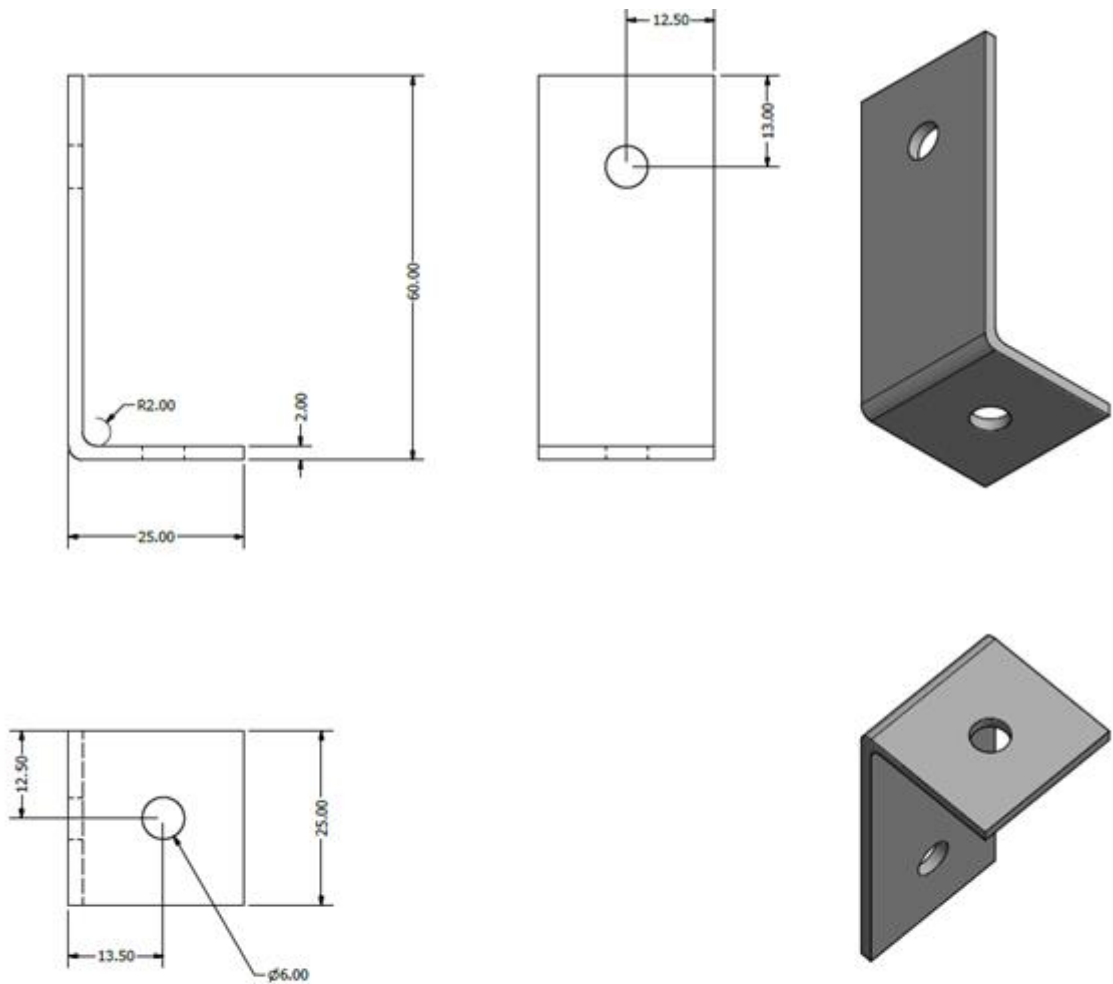
DESIGNED BY Marcelo S. Nogueira		DATE 03/09/2015	ALL DIMENSIONS mm
	Angles for fixation of TCSPC boards		
	1 part - Aluminum		SHEET 1/1



Appendix II – Angles for fixation of photomultiplier tube



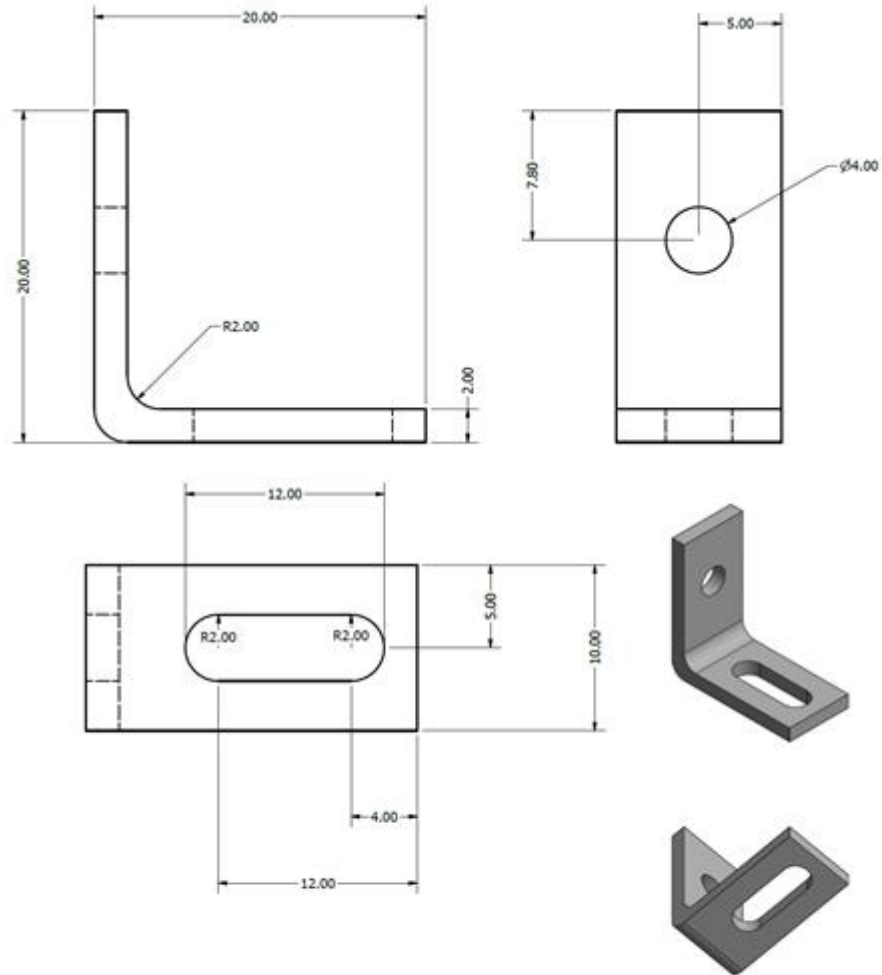
DESIGNED BY Marcelo S. Nogueira		DATE 03/09/2015	ALL DIMENSIONS mm
	Angles for fixation of photomultiplier tube		SHEET 1/1
	2 parts - Aluminum		



Appendix KK – Angles for fixation of laser in the first floor



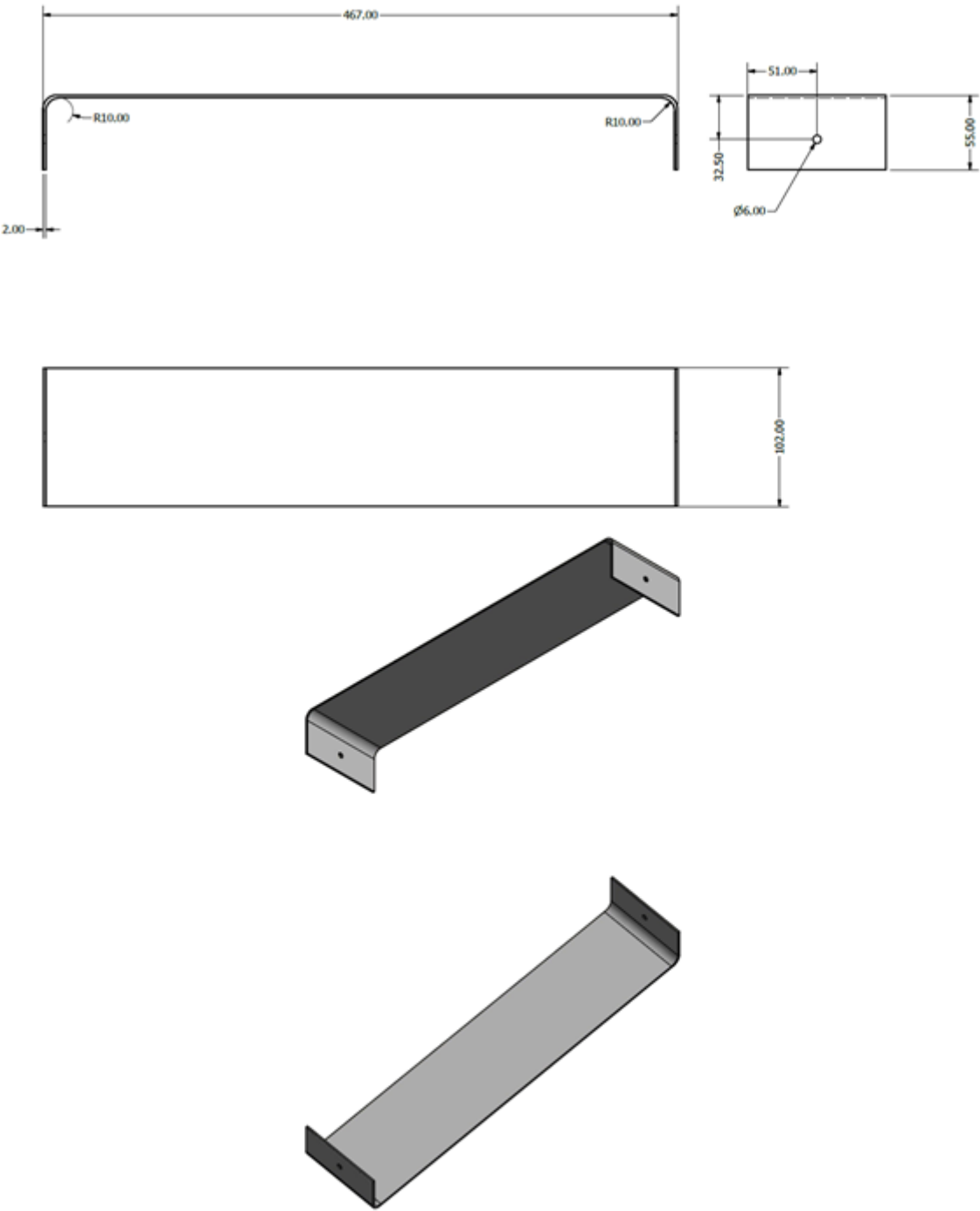
DESIGNED BY Marcelo S. Nogueira		DATE 03/09/2015	ALL DIMENSIONS mm
 CEPOF <small>centro de estudos e pesquisas em física e química</small>	bio <small>tecnologia</small>		
Angles for fixation of laser in the first floor			
2 parts - Aluminum			SHEET 1/1



Appendix LL – Angles for fixation of the computer monitor



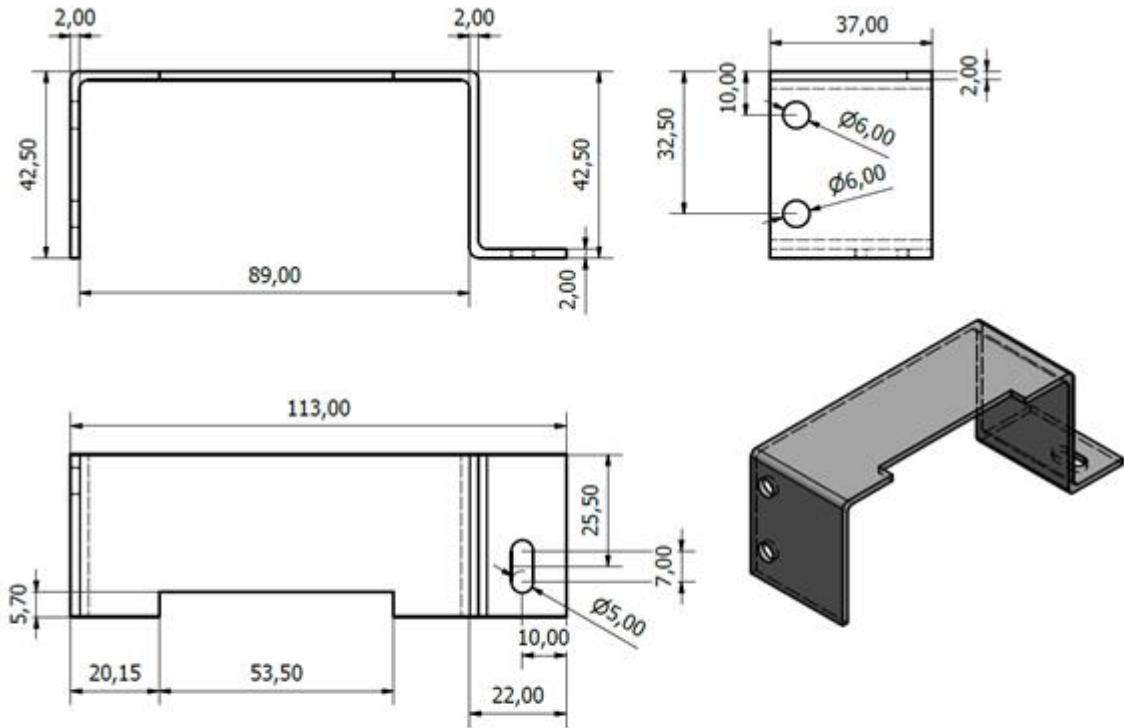
DESIGNED BY Marcelo S. Nogueira		DATE 03/09/2015	ALL DIMENSIONS mm
	Angles for fixation of the computer monitor		
	4 parts - Aluminum		SHEET 1/2



Appendix MM – Support for fixation of the computer monitor



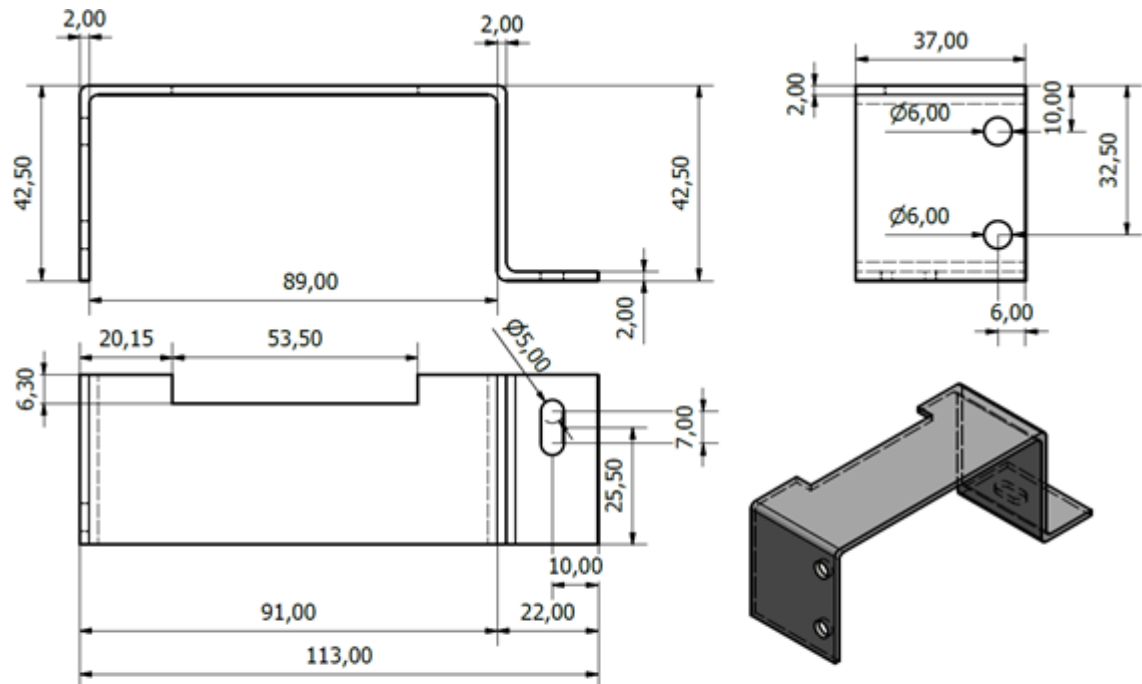
DESIGNED BY Marcelo S. Nogueira			DATE 03/09/2015	ALL DIMENSIONS mm
		Support for fixation of the computer monitor		
		1 part - Aluminum		SHEET 2/2


Appendix NN – Support for fixation of the laser in the second floor – part I



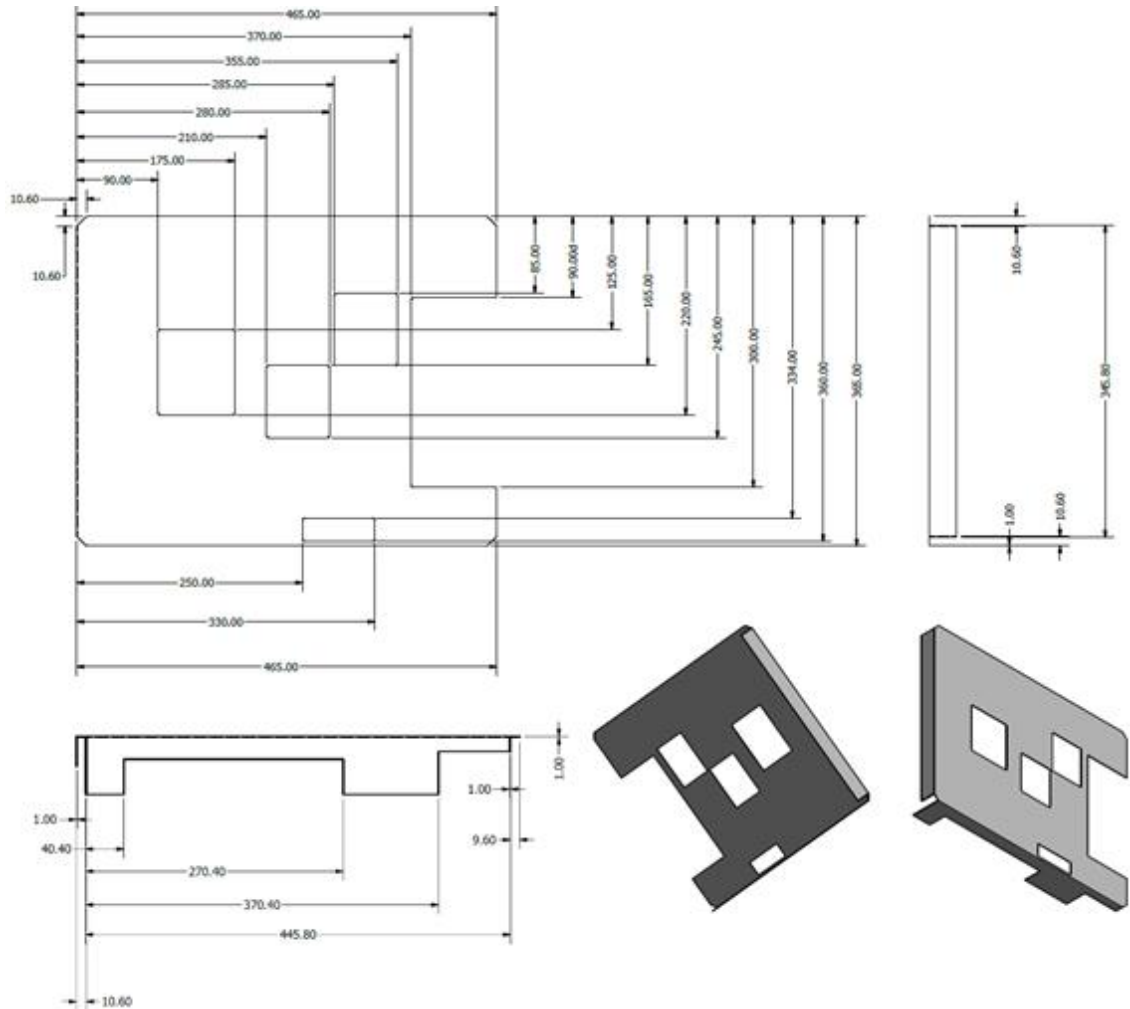
DESIGNED BY Marcelo S. Nogueira		DATE 03/09/2015	ALL DIMENSIONS mm
	Support for fixation of the laser in the second floor – part I		
	1 part - Aluminum		SHEET 1/2



Appendix OO – Support for fixation of the laser in the second floor – part II



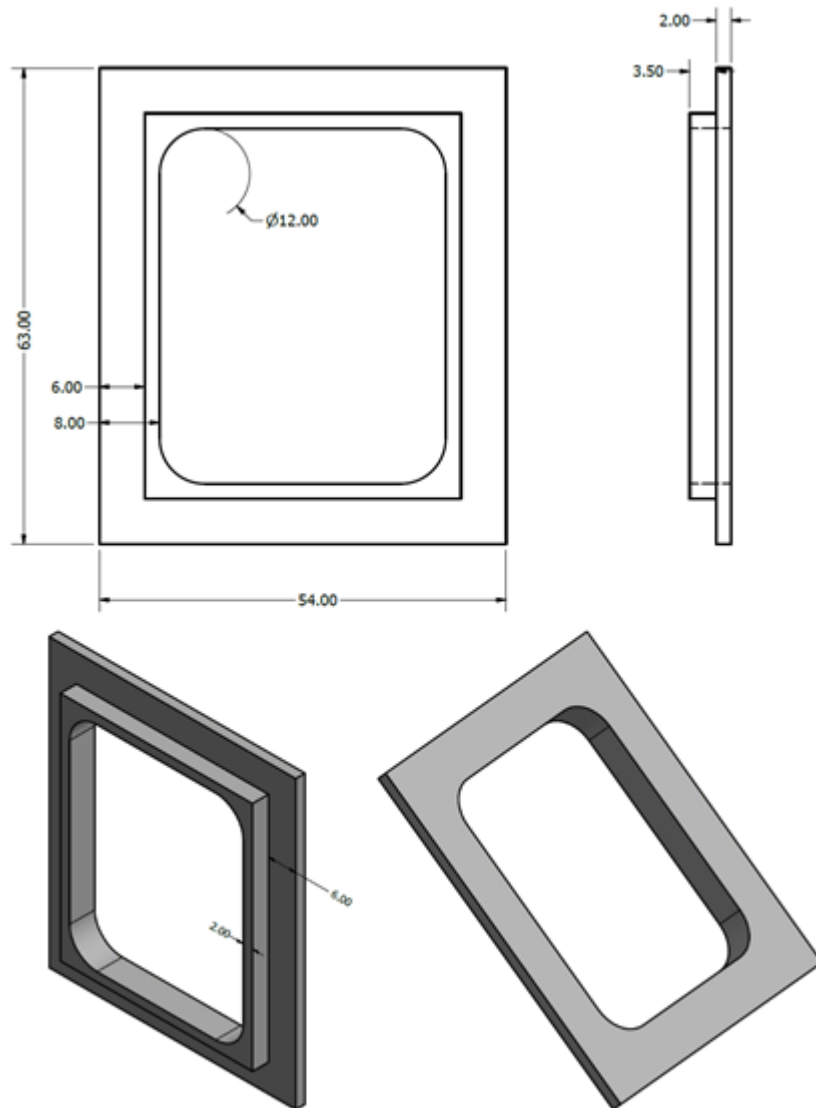
DESIGNED BY Marcelo S. Nogueira		DATE 03/09/2015	ALL DIMENSIONS mm
	Support for fixation of the laser in the second floor – part I		
1 part - Aluminum			SHEET 2/2

Appendix PP – Enclosing and protection part – System front panel



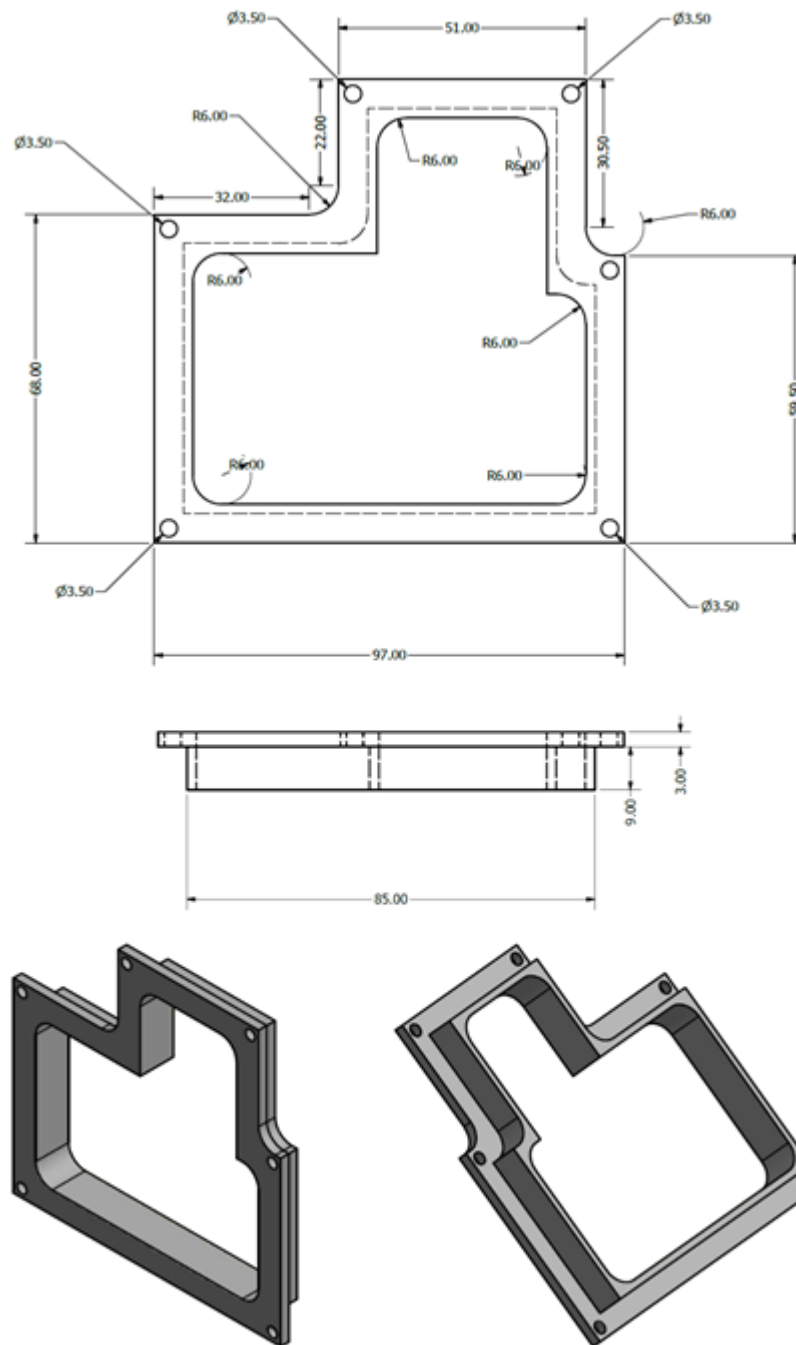
DESIGNED BY		DATE	ALL DIMENSIONS
Marcelo S. Nogueira		05/05/2015	mm
	Enclosing and protection part – System front panel		
	1 part - Aluminum		SHEET 1/1

Appendix QQ – Protection part for laser cooler (first floor)



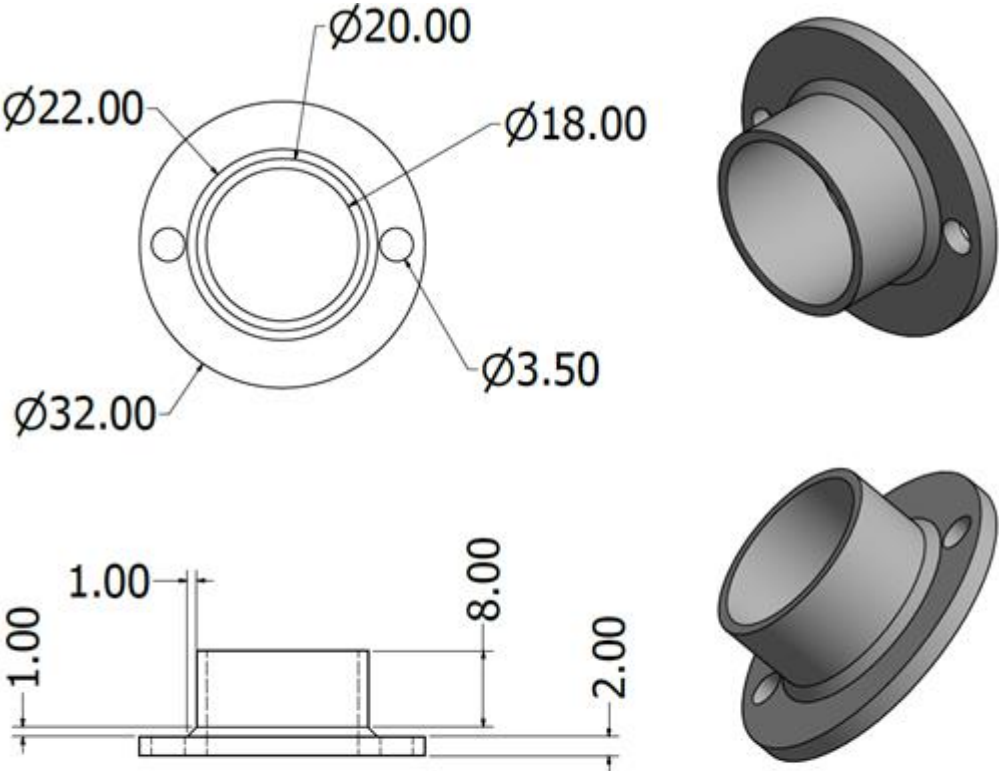
DESIGNED BY Marcelo S. Nogueira		DATE 03/12/2015	ALL DIMENSIONS mm
	Protection part for laser cooler (first floor)		SHEET 1/1
	1 part - Aluminum		



Appendix RR – Protection part for power supply cooler



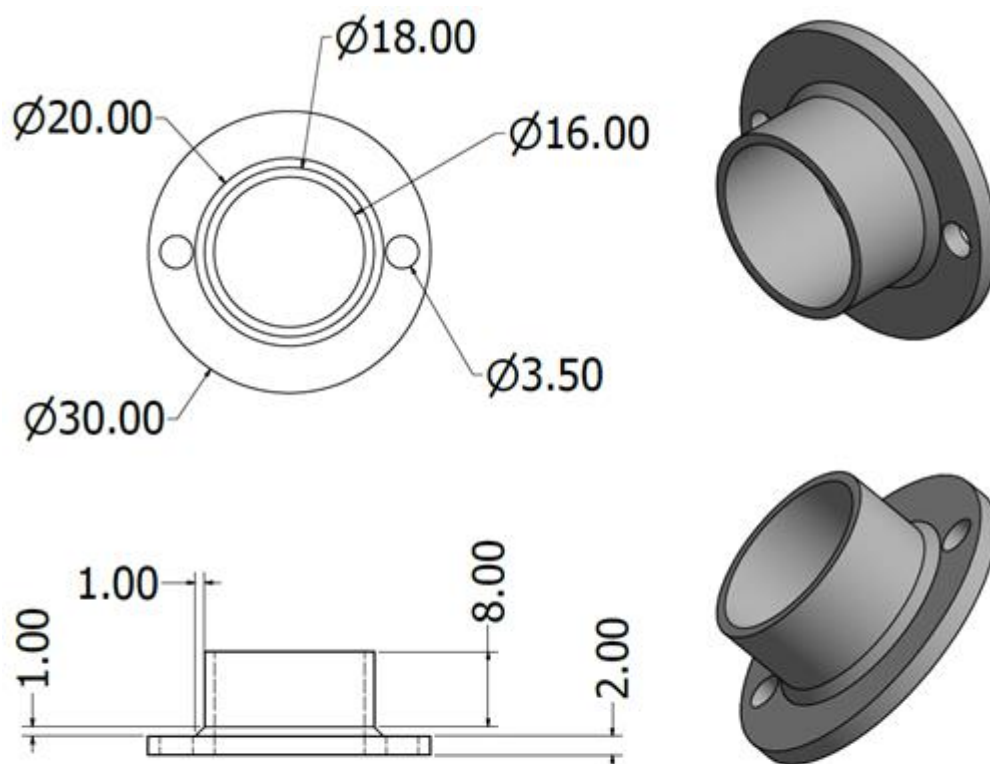
DESIGNED BY Marcelo S. Nogueira		DATE 03/12/2015	ALL DIMENSIONS mm
	Protection part for power supply cooler		
	1 part - Aluminum		SHEET 1/4



Appendix SS – Protection part for filter holder



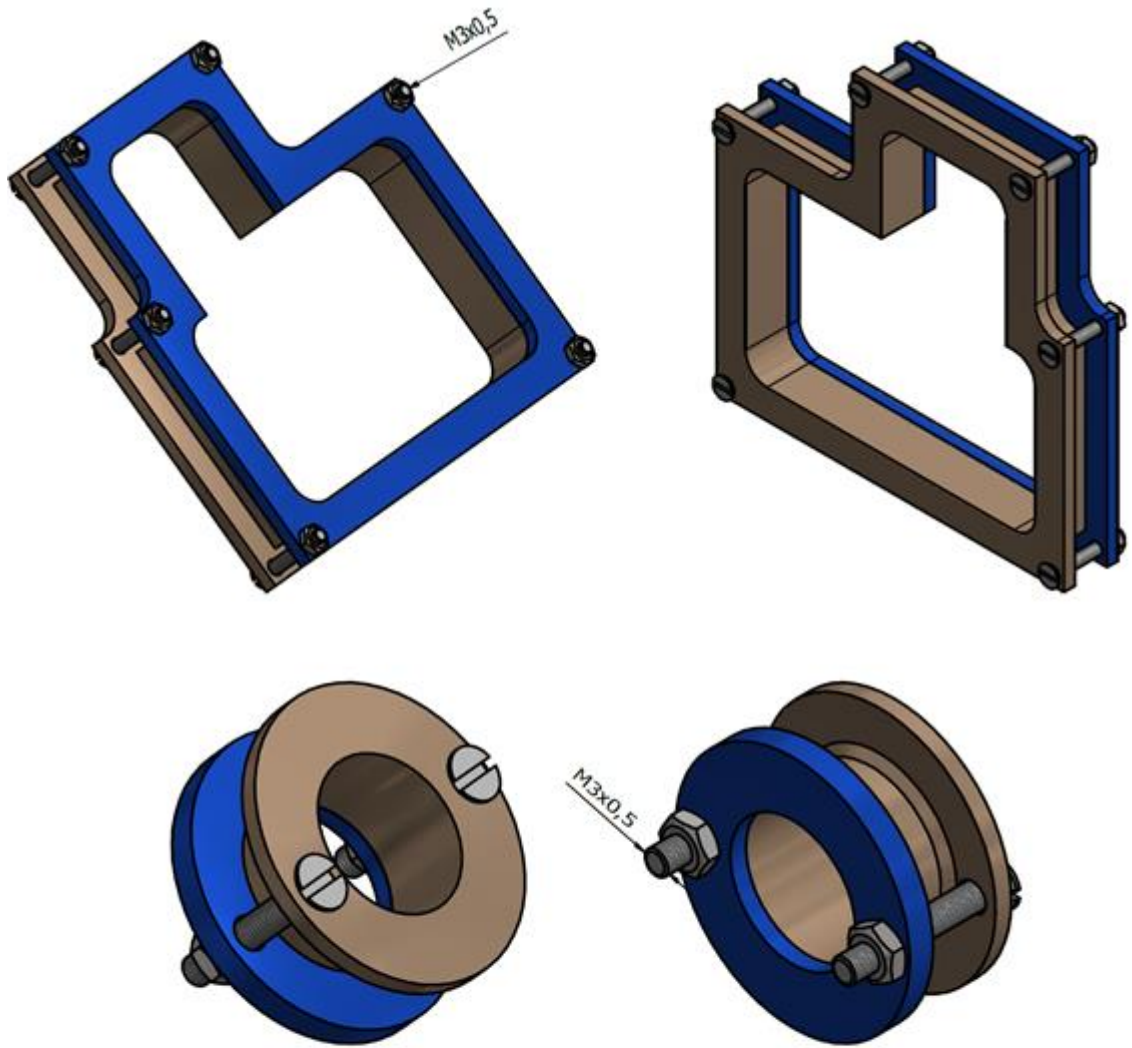
DESIGNED BY Marcelo S. Nogueira		DATE 03/12/2015	ALL DIMENSIONS mm
	Protection part for filter holder		
	1 part - Aluminum		SHEET 2/4



Appendix TT – Protection part for lasers



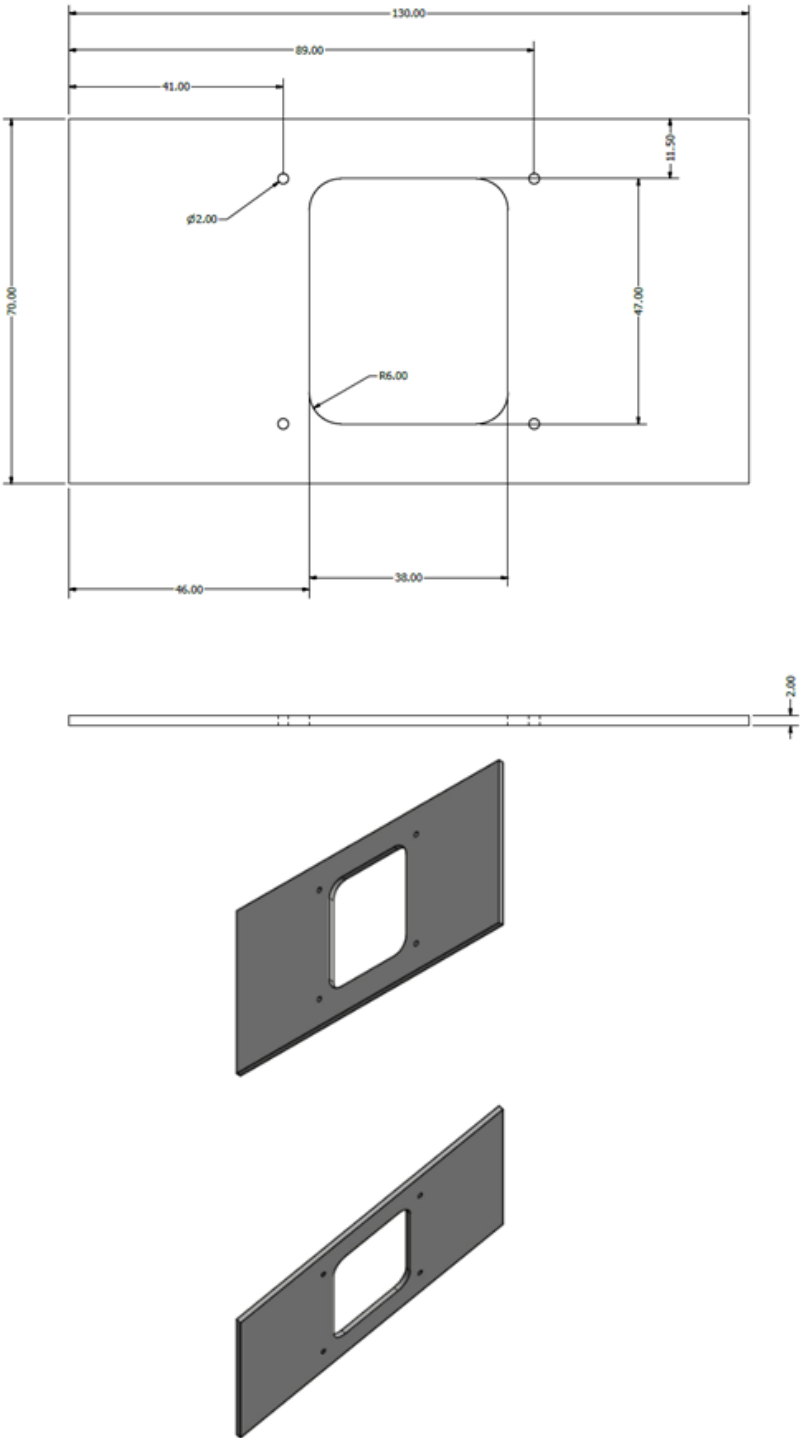
DESIGNED BY Marcelo S. Nogueira		DATE 03/12/2015	ALL DIMENSIONS mm
 CEPOF <small>Centro de Estudos e Pesquisas em Óptica e Fotônica</small>	Protection part for lasers		
	2 parts - Aluminum		SHEET 3/4



Appendix UU – Assembled protection parts



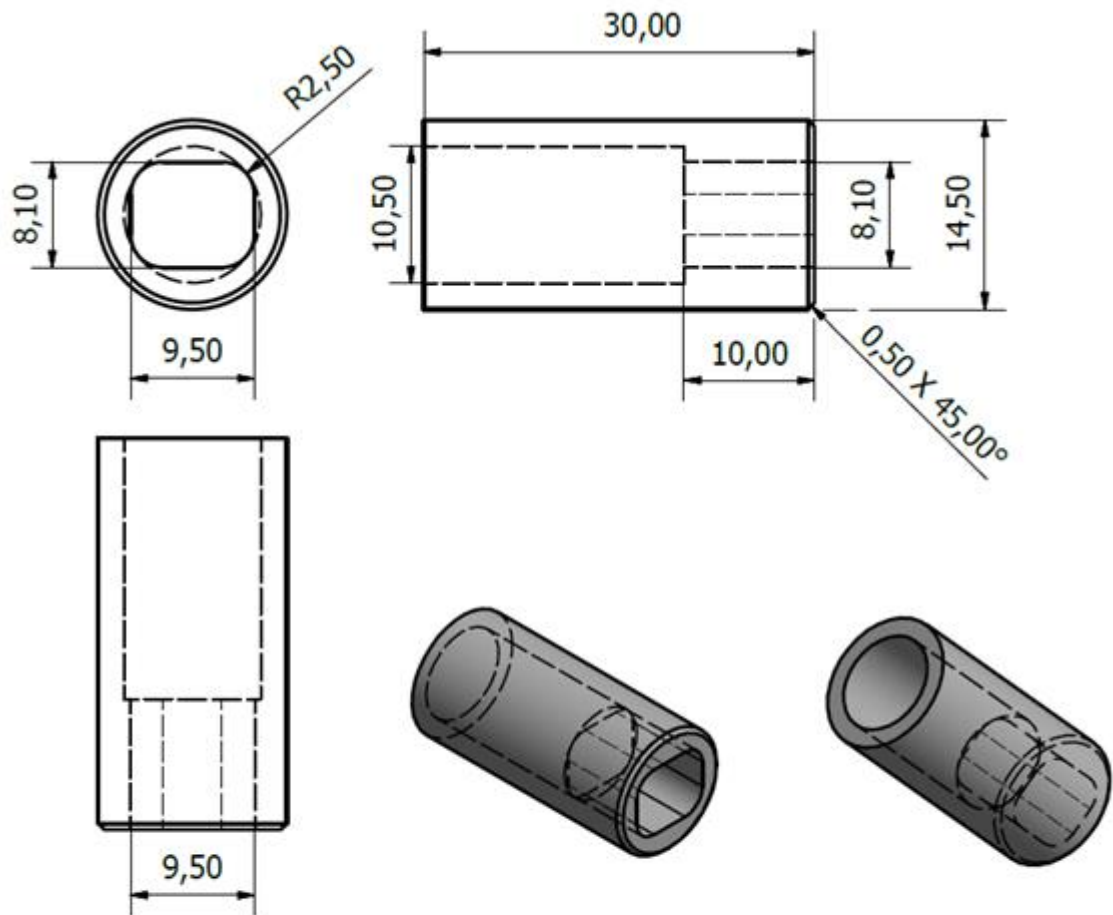
DESIGNED BY Marcelo S. Nogueira		DATE 03/12/2015	ALL DIMENSIONS mm
	Assembled protection parts		SHEET 4/4



Appendix VV – Protection for the laser cooler (first floor)



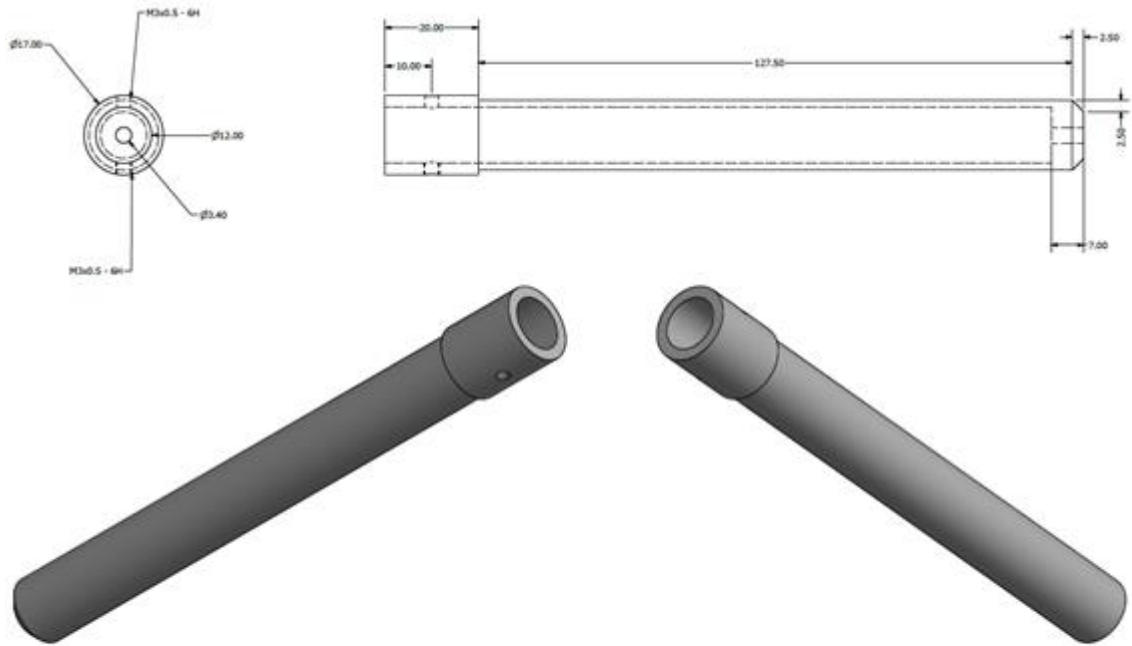
DESIGNED BY		DATE	ALL DIMENSIONS
Marcelo S. Nogueira		03/09/2015	mm
	Protection for the laser cooler (first floor)		
	1 part- Aluminum		SHEET 1/1




Appendix XX – Optical fiber connector



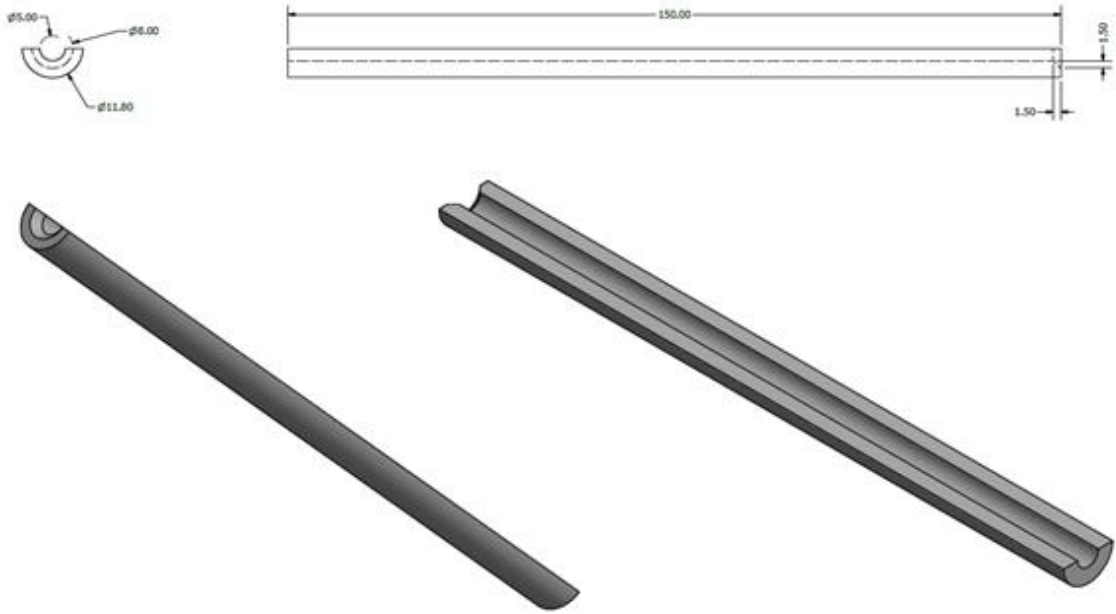
DESIGNED BY Marcelo S. Nogueira		DATE 05/06/2015	ALL DIMENSIONS mm
	Optical fiber connector		
	1 part - Aluminum		SHEET 1/1



Appendix YY – Protection part for fiber probe



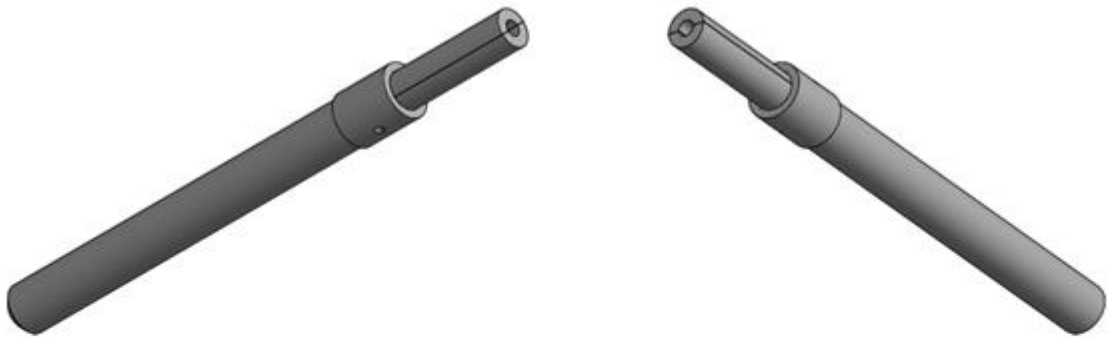
DESIGNED BY Marcelo S. Nogueira		DATE 05/06/2015	ALL DIMENSIONS mm
 	Protection part for fiber probe		
1 part - Aluminum			SHEET 1/3



Appendix ZZ – Fixation part for optical fiber inside the fiber probe



DESIGNED BY Marcelo S. Nogueira			DATE 05/06/2015	ALL DIMENSIONS mm
		Fixation part for optical fiber inside the fiber probe		
		2 parts - Aluminum		SHEET 2/3

Appendix AAA – Assembled fiber probe



DESIGNED BY Marcelo S. Nogueira		DATE 05/06/2015	ALL DIMENSIONS mm
	Assembled fiber probe		SHEET 3/3

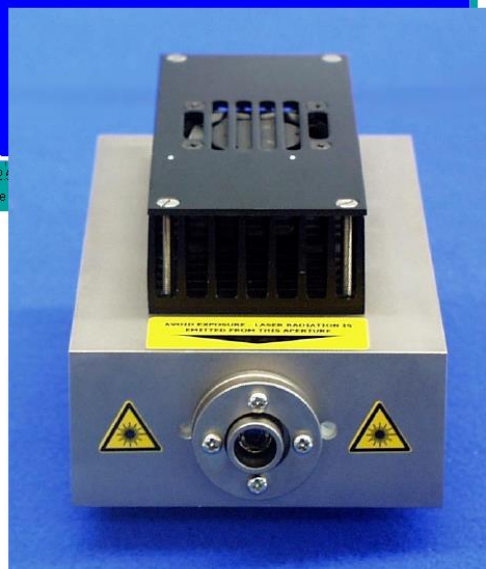
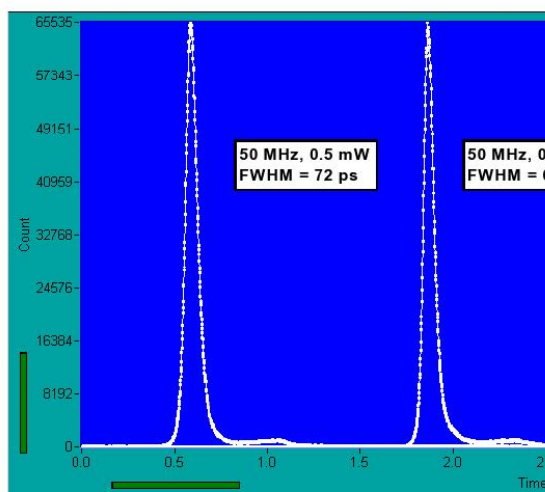
ANNEXES

Annex A – 378 nm laser specifications

BDL-375

Ultraviolet Picosecond Diode Laser

Pulse width down to 60 ps
Repetition rate 20-50-80 MHz
Wavelength 375 nm
Low skew trigger output
Extremely low RF noise
Cooled laser diode
Simple + 9 V to +12V power supply
Compact design - no external controller unit



Luminescence lifetime experiments
Picosecond lifetime microscopy
Fluorescence correlation
Time-correlated single photon counting experiments



Becker & Hickl GmbH
 Nahmitzer Damm 30
 12277 Berlin, Berlin
 Tel. +49 / 30 / 787 56 32
 Fax. +49 / 30 / 787 57 34
 email: info@becker-hickl.com
www.becker-hickl.com



US Representative:
Boston Electronics Corp
tcspc@boselec.com
www.boselec.com



UK Representative:
Photonic Solutions PLC
sales@psplc.com
www.psplc.com

BDL-375

Optical

Repetition Rate	20-50-80 MHz, selectable
Wavelength	370 nm to 380 nm, typ. 375 nm
Pulse Width (FWHM, Power 0.5 mW, 50 MHz)	60 to 90 ps
Peak Power	125 mW ¹⁾
Optical Power	20 MHz: 0.1 mW to 0.3 mW ²⁾
(Average or CW-equivalent power, adjustable)	50 MHz: 0.2 mW to 0.8 mW ²⁾
	80 MHz: 0.3 mW to 0.8 mW ²⁾
Stability of Repetition Rate	± 100 ppm
Pulse-to-Pulse Jitter	< 10 ps
Power and pulse shape stabilisation after 'Laser on' signal	1 µs
Power and pulse shape stabilisation after switch-on	3 min

Trigger Output

Pulse Amplitude	+100 mV (peak) into 50 Ω
Pulse Width	1 ns
Output Impedance	50 Ω
Connector	SMA
Delay from Trigger to Optical Pulse	< 500 ps
Jitter between Trigger and Optical Pulse	< 10 ps

Control Inputs

Frequency 20 MHz	TTL / CMOS high ²⁾
Frequency 50 MHz	TTL / CMOS high ²⁾
Frequency 80 MHz	TTL / CMOS high ²⁾
/Laser Off	TTL / CMOS low ³⁾
External Bias Input	analog input, -10 V to +10 V

Power Supply

Power Supply Voltage	+9 V to +12 V
Power Supply Current	300 mA to 1 A ⁴⁾
Power Adapter	AC-DC power adapter, with key switch and control box in cable

Mechanical Data

Dimensions	160 mm x 90 mm x 60 mm
Mounting Thread	two M6 holes

Maximum Values

Power Supply Voltage	0 V to +15 V
Voltage at Digital Control Inputs	-2 V to +7 V
Voltage at Ext. Bias Input	-12 V to +12 V
Ambient Temperature	0 °C to 30 °C ⁵⁾

1) Typical values, sample tested. Depends on pulse width and selected power.

2) Recommended power adjust range. Lower power gives broader pulses, higher power gives ringing in pulse shape. Power levels above the given range can be selected, but may impair the lifetime of the laser diode.

3) All inputs have 10 kΩ pull-up resistors. Open input is equivalent to logic 'high'.

4) Dependent on ambient temperature. Cooling current changes due to temperature regulation of laser diode.

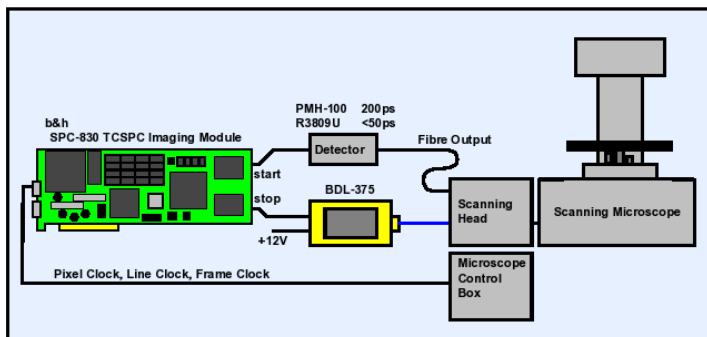
5) Operation below 13 °C may result in unstable power or extended warm-up time.



Caution: Class 3B laser product. Avoid exposure to beam. Light emitted by the device may be harmful to the human eye and skin. Please obey laser safety rules when operating the devices. Complies with US federal laser product performance standards.

Application: TCSPC lifetime imaging with laser scanning microscopes

The BDL-375 laser excites the sample with 50 MHz, 75 ps pulses. The microscope scans the sample in y-x direction, and the SPC-830 TCSPC imaging module records the photon distribution versus time and the coordinates of the scanning area. The setup detects single and double exponential lifetimes down to a few 10ps. Typical applications are ion concentration, pH, or oxygen saturation measurements by fluorescence quenching, FRET experiments and distinguishing of autofluorescence components. Please see www.becker-hickl.com for detailed information.



Becker & Hickl GmbH
Nahmitzer Damm 30
12277 Berlin
Tel. +49 / 30 / 787 56 32
Fax. +49 / 30 / 787 57 34
<http://www.becker-hickl.com>
email: info@becker-hickl.com

Annex B – 445 nm laser specifications

BDL-440-SMC

440 nm Picosecond / CW Diode Laser with Single-Mode Fibre Coupler

60% coupling efficiency into single-mode fibre

TEM₀₀ mode

Wavelength 440 nm

Pulsed and CW operation

Pulse width down to 40 ps

Repetition rate 20-50-80 MHz

Low skew trigger output

Extremely low RF noise

Cooled laser diode

Fast on / off / multiplexing capability

Simple + 9 V to +12V wall-mounted power supply

Compact design - no external controller unit

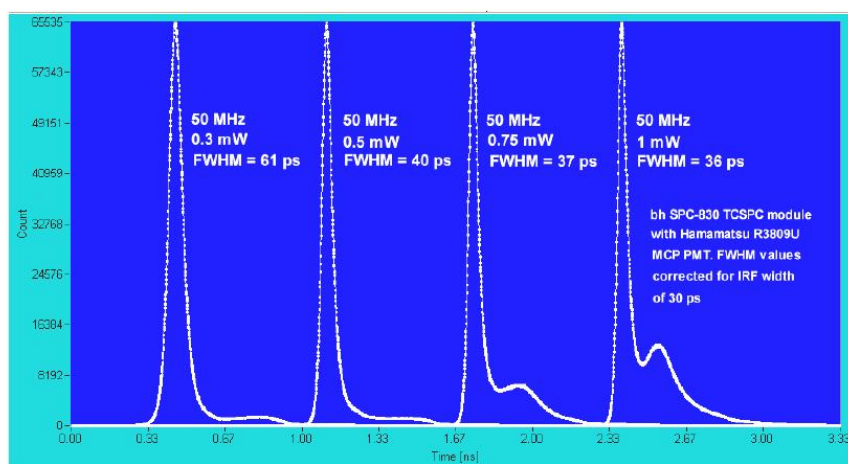
Compatible with all standard 1" footprint fibre couplers

Luminescence lifetime experiments

Laser scanning microscopy

Fluorescence correlation

Time-correlated single photon counting experiments



Designed and manufactured by



Becker & Hickl GmbH
Nahmitzer Damm 30
12277 Berlin, Berlin
Tel. +49 / 30 / 787 56 32
Fax. +49 / 30 / 787 57 34
email: info@becker-hickl.com
www.becker-hickl.com



LASOS Lasertechnik GmbH
Carl-Zeiss-Promenade 10
07745 Jena, Germany
Tel. +49 3641 2944-0
Fax +49 3641 2944-17
info@lasos.com
www.lasos.com



Sales Representatives



US Representative:
Boston Electronics Corp
tcspc@boselec.com
www.boselec.com



UK Representative:
Photonic Solutions PLC
sales@psplc.com
www.psplc.com

BDL-440-SMC

Optical

Repetition Rate	20-50-80 MHz, or CW operation
Wavelength	436 nm to 448 nm, typ. 440 nm
Pulse Width (FWHM, at 1 mW power, 50 MHz)	40 to 90 ps
Peak Power	40 to 250 mW ¹⁾
Average Power	20 MHz: 0.07 mW to 0.2 mW ²⁾
(Average CW equivalent power, user adjustable)	50 MHz: 0.3 mW to 1 mW ²⁾
	80 MHz: 0.4 mW to 1.2 mW ²⁾
	CW mode: 1 mW to 20 mW ²⁾
Beam diameter before coupler	0.7 mm, TEM ₀₀ mode
Polarisation	horizontal
Coupling efficiency into single-mode fibre, typically	60%
Stability of Repetition Rate	± 100 ppm
Pulse-to Pulse Jitter	< 20 ps
Reaction time to 'Laser on' signal (pulsed mode)	1 µs
Reaction time to 'Laser on' signal (CW mode)	3 µs
Power and pulse shape stabilisation after switch-on	3 min ³⁾
Fibre coupler	all 1" footprint couplers: Point Source, Schäfer&Kirchhoff, OZ Optics, Linus

Trigger Output

Pulse Amplitude	+100 to +300 mV (peak) into 50 Ω
Pulse Width	1 ns
Output Impedance	50 Ω
Connector	SMA
Delay from Trigger to Optical Pulse	< 500 ps
Jitter between Trigger and Optical Pulse	< 10 ps

Control Inputs

Frequency 20 MHz	TTL / CMOS high ³⁾
Frequency 50 MHz	TTL / CMOS high ³⁾
Frequency 80 MHz	TTL / CMOS high ³⁾
CW operation	TTL / CMOS high ³⁾
Laser ON / Off	TTL / CMOS low ³⁾
External Power Control	analog input, 0 to + 10V

Power Supply

Power Supply Voltage	+ 9 V to +12 V
Power Supply Current	300 mA to 1 A ⁴⁾
Power Adapter	AC-DC power adapter, with key switch and control box in cable

Mechanical Data

Dimensions	160 mm x 90 mm x 60 mm
Mounting Thread	two M6 holes

Maximum Values

Power Supply Voltage	0 V to +15 V
Voltage at Digital Control Inputs	-2 V to +7 V
Voltage at Ext. Bias Input	-12 V to + 12 V
Ambient Temperature	0 °C to 40 °C ⁵⁾

1) Typical values, sample tested. Depends on pulse width and selected power.

2) Recommended power adjust range. Lower power gives broader pulses, higher power gives ringing in pulse shape. Power levels above the given range can be selected, but may impair the lifetime of the laser diode.

3) All inputs have 10 kΩ pull-up resistors. Open input is equivalent to logic 'high'.

4) Dependent on ambient temperature. Cooling current changes due to temperature regulation of laser diode

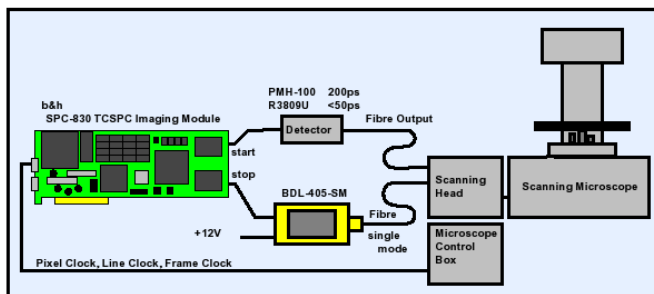
5) Operation below 13 °C may result in extended warm-up time.



Caution: Class 3B laser product. Avoid direct eye exposure. Light emitted by the device may be harmful to the human eye. Please obey laser safety rules when operating the devices. Complies with US federal laser product performance standards.

Application: TCSPC lifetime imaging with laser scanning microscopes

The BDL-405-SM laser excites the sample with 50 MHz, 75 ps pulses. The microscope scans the sample in y-x direction, and the SPC-830 TCSPC imaging module records the photon distribution versus time and the coordinates of the scanning area. The setup detects single and double exponential lifetimes down to a few 10ps. Typical applications are ion concentration, pH, or oxygen saturation measurements by fluorescence quenching, FRET experiments and distinguishing of autofluorescence components. Please see www.becker-hickl.com for detailed information.



Becker & Hickl GmbH
Nahmitzer Damm 30
12277 Berlin
Tel. +49 / 30 / 787 56 32
Fax. +49 / 30 / 787 57 34
<http://www.becker-hickl.com>
email: info@becker-hickl.com

Annex C – Hybrid photomultiplier tube specifications

HPM-100-50

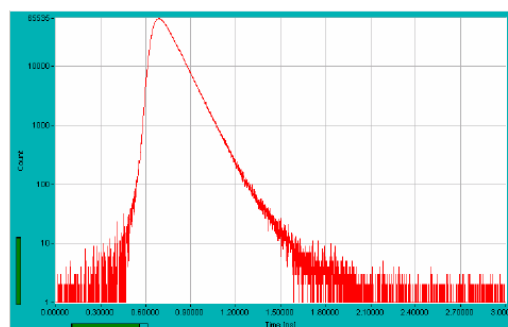
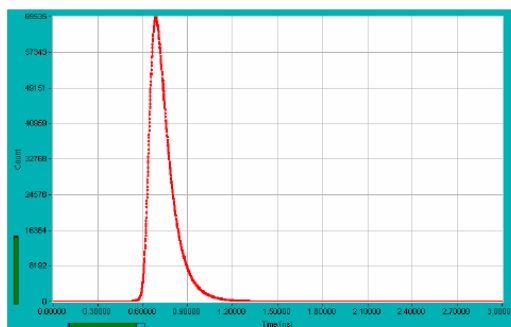
High Speed Hybrid Detector for TCSPC

GaAs cathode: Excellent detection efficiency
Sensitive up to 900 nm
Instrument response function 130 ps FWHM
Clean response, no tails or secondary peaks
No afterpulsing background
Excellent dynamic range of TCSPC measurements
Internal generators for PMT operating voltages
Power supply and control via bh DCC-100 card
Overload shutdown
Direct interfacing to all bh TCSPC systems



The HPM-100-50 module combines a Hamamatsu R10467-50 GaAs hybrid detector tube with the preamplifier and the generators for the tube operating voltages in one compact housing. The principle of the hybrid detector in combination with the GaAs cathode yields excellent timing resolution, a clean TCSPC instrument response function, high detection quantum efficiency up to NIR wavelengths, and extremely low afterpulsing probability. The absence of afterpulsing results in a substantially increased dynamic range of TCSPC measurements. The HPM-100-50 is therefore an excellent detector for NIR fluorescence decay measurements and time-domain diffuse optical tomography.

The HPM-100-50 module is operated via the bh DCC-100 detector controller of the bh TCSPC systems. The DCC-100 provides for power supply, gain control, and overload shutdown. The HPM-100 interfaces directly to all bh SPC or Simple Tau TCSPC systems. It is available with standard C-mount adapters, adapters for the bh DCS-120 confocal scanning FLIM system, and adapters for the NDD ports of the Zeiss LSM 710 NLO multiphoton laser scanning microscopes.



Instrument response function. Left linear scale, right logarithmic scale. FWHM is 130 ps.



Becker & Hickl GmbH
 Nahmitzer Damm 30
 12277 Berlin
 Tel. +49 / 30 / 787 56 32
 Fax. +49 / 30 / 787 57 34
<http://www.becker-hickl.com>
 email: info@becker-hickl.com



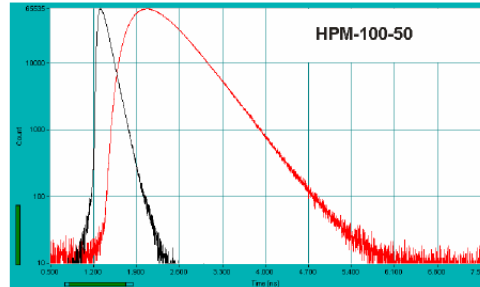
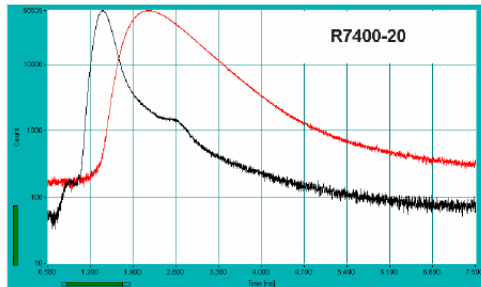
US Representative:
Boston Electronics Corp
tcspc@boselec.com
www.boselec.com



UK Representative:
Photonic Solutions PLC
sales@psplc.com
www.psplc.com

HPM-100-50

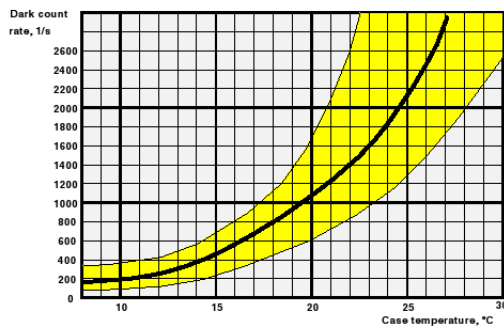
Absence of afterpulsing improves dynamic range of TCSPC measurement



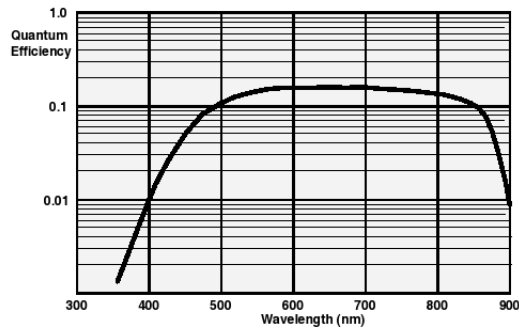
Photon migration curves (red) and IRF (black) recorded with conventional PMT (left) and HPM-100-50 (right). The background signal of the conventional NIR PMT is dominated by afterpulsing. Late photons are lost in the background. Right: The HPM-100-50 is free of afterpulsing. The only background is the thermal emission of the photocathode. The dynamic range is substantially higher than for the conventional PMT.

Dark count rate vs. temperature

Typical values and range of variation



Detection quantum efficiency vs. wavelength



Specifications, typical values

Wavelength Range
 Detector Quantum efficiency, at 600 nm
 Dark Count rate, $T_{case} = 22^\circ C$
 Cathode Diameter
 TCSPC IRF width (Transit Time Spread)
 Single Electron Response Width
 Single Electron Response Amplitude
 Output Polarity
 Output Impedance
 Max. Count Rate (Continuous)
 Overload shutdown at
 Detector Signal Output Connector
 Power Supply (from DCC-100 Card)
 Dimensions (width x height x depth)
 Optical Adapters

400 nm to 900 nm
 15 %
 500 to 3000 s^{-1}
 3 mm
 130 ps, FWHM
 850 ps, FWHM
 50 mV, V_{apd} 95% of V_{max}
 negative
 50 Ω
 > 10 MHz
 > 15 MHz
 SMA
 + 12 V, +5 V, -12V
 60 mm x 90 mm x 170 mm
 C-Mount, DCS-120, LSM 710 NDD port

Related products: HPM-100-40 hybrid detector module, 300 to 700 nm, 45% quantum efficiency

Literature: [1] The HPM-100-50 hybrid detector module: Increased dynamic range for DOT. Application note, www.becker-hickl.com
 [2] The HPM-100-40 hybrid detector. Application note, www.becker-hickl.com



Annex D – SPC-150 Board specifications



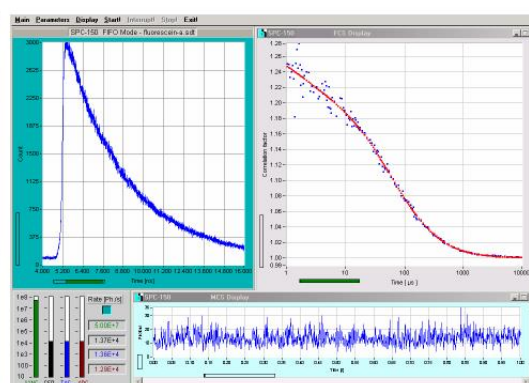
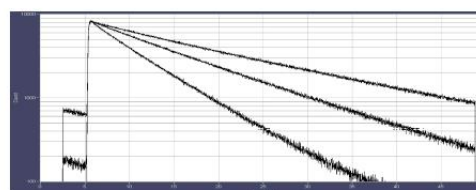
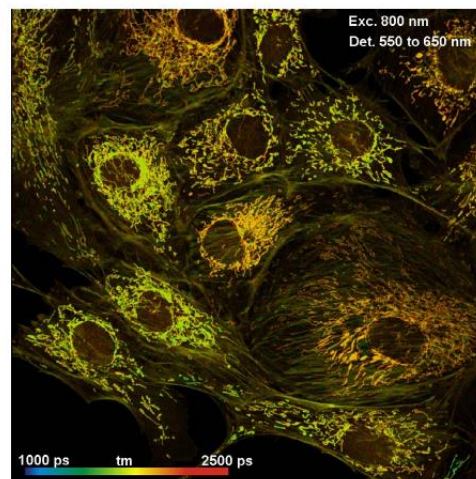
SPC-150

TCSPC / FLIM Module

Time-Correlated Single Photon Counting Module

Picosecond time resolution
 Ultra-high sensitivity
 Multi-detector / multi-wavelength capability
 FLIM by bh Megapixel Technology
 Mosaic FLIM mode
 Multiscaler imaging mode
 Photon distribution and parameter-tag modes
 Unlimited sequential recording of curves or images
 Imaging in histogram mode and in parameter-tag mode
 Time channel width down to 813 fs
 Electrical time resolution (Jitter) 6.6 ps fwhm / 2.5 ps rms
 Reversed start/stop: Laser repetition rates up to 150 MHz
 Saturated count rate 10 MHz
 Total useful recorded count rate up to 5 MHz

Standard fluorescence lifetime experiments
 Multi-wavelength lifetime experiments
 Recording of transient fluorescence lifetime effects
 Single-wavelength FLIM, multi-wavelength FLIM
 Fast-Acquisition FLIM, time-Series FLIM
 Mosaic FLIM, lateral, longitudinal, temporal mosaics
 Simultaneous PLIM and FLIM
 FLITS
 Single and double-exponential FRET imaging
 Recording of Ca^{2+} transients
 fNIRS and NIRS experiments
 Single-molecule spectroscopy
 FCS, FCCS, Photon Counting Histograms
 Anti-bunching experiments



Becker & Hickl GmbH
 Technology Leader in TCSPC
 Nahmitzer Damm 30
 12277 Berlin, Berlin
 Tel. +49 / 30 / 787 56 32
 Fax. +49 / 30 / 787 57 34
 email: info@becker-hickl.com
 www.becker-hickl.com



US Representative:
Boston Electronics Corp
 tcspc@boselec.com
 www.boselec.com



UK Representative:
Photonic Solutions PLC
 sales@psplc.com
 www.psplc.com



Covered by patents DE 43 39 784 and DE 43 39 787



SPC-150

TCSPC / FLIM Module

Photon Channel

Principle
Time Resolution (FWHM / RMS, electr.)
Optimal Input Voltage Range
Min. Input Pulse Width
Threshold
Zero Cross Adjust

Synchronisation Channels

Principle
Optimal Input Voltage Range
Min. Input Pulse Width
Threshold
Frequency Range
Frequency Divider
Zero Cross Adjust

Time-to-Amplitude Converters / ADCs

Principle
TAC Range
Biased Amplifier Gain
Biased Amplifier Offset
Time Range incl. Biased Amplifier
min. Time / Channel
Max. No. of Time Channels
ADC Principle
Diff. Nonlinearity

Data Acquisition (Histogram Mode)

Method
Dead Time
Saturated Count Rate
Useful count rate
Time channels / Pixel
max. Scanning Area
max. Counts / Time Channel
Overflow Control
Collection Time
Display Interval Time
Repeat Time
Sequential Recording
Synchronisation with Scanning
Count Enable Control
Experiment Trigger

Data Acquisition (FIFO / Time-Tag Mode)

Method
Online display
FCS and FCCS calculation
Number of counts of decay / waveform recording
Dead Time
Saturated count rate, peak
Sustained count rate (bus-transfer limited)
Output Data Format (ADC / Macrotime / Routing)
FIFO buffer Capacity (photons)
Macro Timer Resolution, internal clock
Macro Timer Resolution, clock from SYNC input
Curve Control (external Routing)
External event markers
Count Enable Control
Experiment trigger

Data Acquisition, FIFO / Time-Tag Imaging Mode

Method
Online display
Synchronisation with scanner
Detector / Wavelength Channels
Image resolution, 64-bit SPCM software
No. of time channels
No. of pixels, 1 detector channel
No. of pixels, 16 detector channels

Operation Environment

Computer System
Bus Connectors
Used PCI Slots
Total power Consumption
Dimensions

Related Products

SPC-154 4-channel TCSPC modules
Simple-Tau 150 compact TCSPC systems
Simple-Tau 154 compact 4-channel TCSPC systems
DCS-120 confocal scanning FLIM system

HPM-100 GaAsP and GaAs hybrid detectors
PML-SPEC and MW-FLIM multi-wavelength detectors
PMC-100 cooled PMT modules
id-100 SPAD detector modules

DCC-100 detector controller
BDL-SMN and -SMC ps diode lasers
BDS-SM picosecond diode lasers

Related Literature

W. Becker, Advanced time-correlated single photon counting techniques. Springer 2005. Please contact bh for availability.
W. Becker, The bh TCSPC Handbook, 6th edition. Available on www.becker-hickl.com
PML-16-C 16 channel detector head for time-correlated single photon counting. User handbook. Available on www.becker-hickl.com
DCS-120 Confocal Scanning FLIM Systems, user handbook. Available on www.becker-hickl.com
Modular FLIM systems for Zeiss LSM 510 and LSM 710 / 780 / 880 family laser scanning microscopes, handbook. Available on www.becker-hickl.com
BDL-SMN series picosecond diode lasers, user handbook. Available on www.becker-hickl.com
Please see also www.becker-hickl.com, 'Literature', 'Application notes'

Constant Fraction Discriminator (CFD)

6.6 ps / 2.5 ps
- 30 mV to - 1 V
400 ps
0 to - 500 mV
- 100 mV to + 100 mV

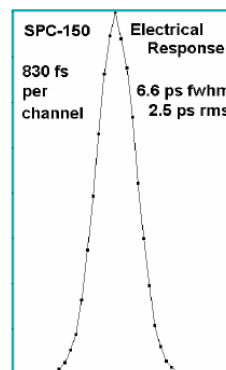
Constant Fraction Discriminator (CFD)

- 30 mV to - 1 V
400 ps
0 to - 500 mV
0 to 150 MHz
1-2-4
-100 mV to + 100 mV

Ramp Generator / Biased Amplifier

50 ns to 5 us
1 to 15
0 to 100% of TAC Range
3.3 ns to 5 us
813 fs
4096

50 ns Flash ADC with Error Correction
< 0.5% rms, typ. < 1% peak-peak



on-board multi-dimensional histogramming process
100ns, independent of computer speed
10 MHz
5 MHz
4096 1024 256 64 16 4 1
16x16 64x64 128 x 128 256x256 512x512 1024x1024 2048x2048
 $2^{16}-1$
none / stop / repeat and correct
0.1 us to 100,000 s
0.1 us to 100,000 s
0.1 us to 100,000 s
Programmable Hardware Sequencer, unlimited recording by memory swapping, in curve mode and scan mode
pixel, line and frame clocks from scanning device
1 bit TTL
TTL

Parameter-tagging of individual photons and continuous transfer into computer

Decay function, FCS, Cross-FCS, PCH, MCS traces
Multi-tau algorithm, online calculation and online fit
unlimited
100 ns
10 MHz
typ. 4 MHz
12 / 12 / 4
2 M
50ns, 12 bit, overflows marked by MTOF entry in data stream
10ns to 100ns, 12 bit, overflows marked by MTOF entry in data stream
4 bit TTL
4 bit, TTL
1 bit TTL
TTL

Buildup of images from time- and wavelength tagged data
up to 8 images in different time and wavelength windows
via Frame Clock, Line Clock, and Pixel Clock pulses
1 to 16

64 256 1024 4096
4096 x 4096 2048 x 2048 1024 x 1024 512 x 512
1024 x 1024 512 x 512 256 x 256 128 x 128

PC Pentium, multi-core CPU recommended or Simple Tau extension box
PCI
1
approx. 12 W from +5V, 0.7 W from +12V
240 mm x 130 mm x 15 mm



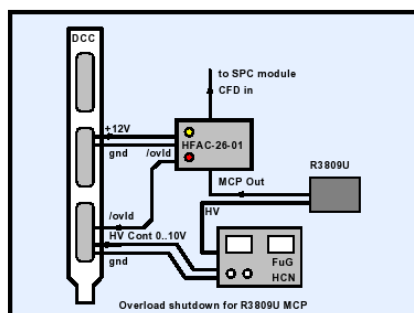
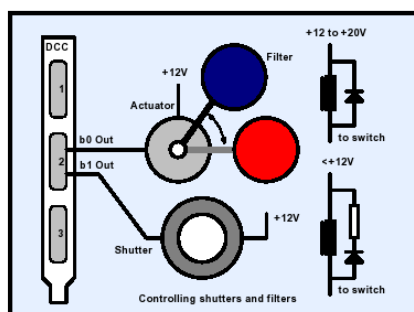
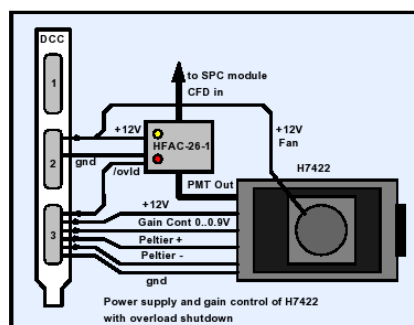
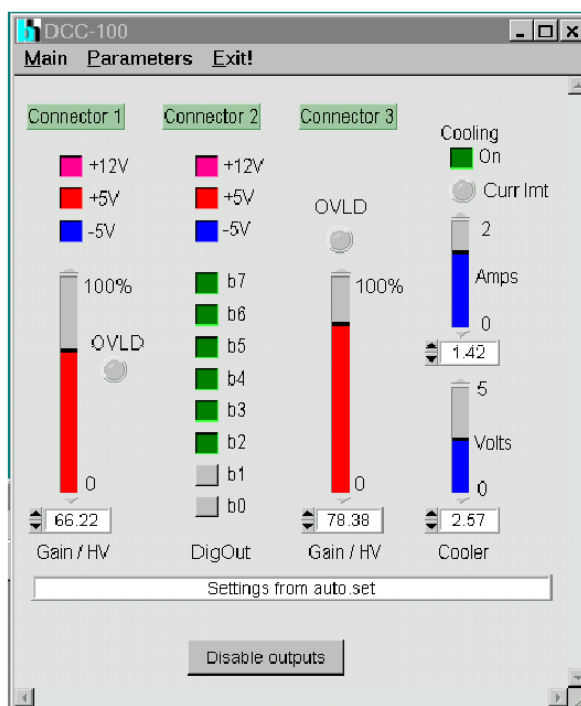
More than 20 years experience in multi-dimensional TCSPC. More than 1500 TCSPC systems worldwide.

Annex E – DCC-100 Board specifications

DCC-100

PCI compatible detector control module for single photon counting experiments

- Power supply and gain control for Hamamatsu H7422, H5783 or H5773 modules
- Gain control for Hamamatsu R3809U MCP via FuG power supplies
- Overload shutdown of detectors in conjunction with bh HFAC-26 preamps
- Power supply for thermoelectric coolers, particularly for H7422
- Short circuit protected +12V, +5V and -5V power supply for preamps and detectors
- Software switched +12V, +5V and -5V power supply outputs for detector on/off control
- High current digital outputs for shutter and filter control
- PCI card, software for Windows 95, 98, 2000 and NT
- Works with any bh photon counting card



Becker & Hickl GmbH
 Nahmitzer Damm 30
 12277 Berlin
 Tel. 030 / 787 56 32 http://www.becker-hickl.com
 Fax. 030 / 787 57 34 email: info@becker-hickl.com

US Representative:
Boston Electronics Corp
 91 Boylston Street, Brookline,
 Massachusetts 02445 USA
 Tel: (800) 347 5445 or (617) 566 3821
 Fax: (617) 731 0935
 www.boselec.com tcspc@boselec.com



DCC-100

Power Supply Outputs (Connectors 1 to 3)

Max. Current at +12 V	100 mA
Short Circuit Current +12 V	50 mA ¹⁾
Time from /OVLD to disable +12V	10 ms ²⁾
Output current in disabled state, +12 V	< 0.5 mA
Max. Current at +5 V	200 mA
Short Circuit Current +5 V	60 mA ¹⁾
Output current in disabled state, +5 V	< 0.5 mA
Max. Current at -5 V	200 mA
Short Circuit Current -5 V	60 mA ¹⁾
Output current in disabled state, -5 V	< 0.5 mA
Max. Current at -12 V	Sum 120 mA, single output 60 mA
Short Circuit Current -12 V	No short protection. Don't short longer than 1s

¹⁾ Foldback Characteristics, don't short several outputs simultaneously for more than 20s

²⁾ Connectors 1 and 3 only. 250 Ω load, time from +12V to +6V output voltage.

Detector Gain Control (Connectors 1 and 3)

Resolution	12 bit
Voltage Range Pin 12	0 to +10 V
Load at Pin 12	min. 1 k Ω
Output Resistance at Pin 12	100 Ω
Voltage Range Pin 13	0 to +0.9 V
Load at Pin 13	min. 1 k Ω
Output Resistance at Pin 13	100 Ω
Output Time Constant	100 ms

Overload Shutdown

Overload inputs at connector 1 and 3	TTL, active Low, Pull-up resistor 10 k Ω
Overload Reset	By Software and at Power-ON

High Current Switches (Connector 2)

Typical 'On' Resistance, 25°C	70 m Ω
Max. Switch Current, Single Switch	2 A
Max. Switch Current, Sum of all Switches	5 A ³⁾
Max. turn-off Voltage at Switch	20 V
Turn-on and turn-off transition time, Load 10 Ω	100 ns
Disable on /OVLD	if configured by jumpers
Disable Transition Time	< 1 μ s
Time from /OVLD to Disable	< 2 μ s

³⁾ Both GND pins used

Supply for Thermoelectric Coolers (Connector 3)

Output Voltage	0 to 5 V
Output Current	0 to 2 A
Resolution of Output Voltage and Current	12 bit
Output Resistance	0.4 Ω ⁴⁾
Output Capacitance	300 μ F
Output Ripple	< 5 mV

⁴⁾ All pins parallel

PC Interface

Dimensions	160 mm x 106 mm x 15 mm
Interface / Connector	PCI
Register Access	I/O only
Supply Current, +5V, No Load, typ. value	0.6 A
Supply Current, +5V, Maximum Load, typ. value	1.2 A
Supply Current, +12V, No Load, typ. value	0.2 A
Supply Current, +12V, Maximum Load, typ. value	1.6 A

Related Products

SPC-300 through SPC-134 TCSPC modules
 MSA-1000, MSA-300, PMS-400, PMM-324 Multiscalers
 HFAC-26 preamplifiers
 Lifetime Kits for LSM-510 and TCS SP2 laser scanning microscopes

For manual, application notes and software please see www.becker-hickl.de



Annex F – Transmission spectra from bifurcated optical fiber



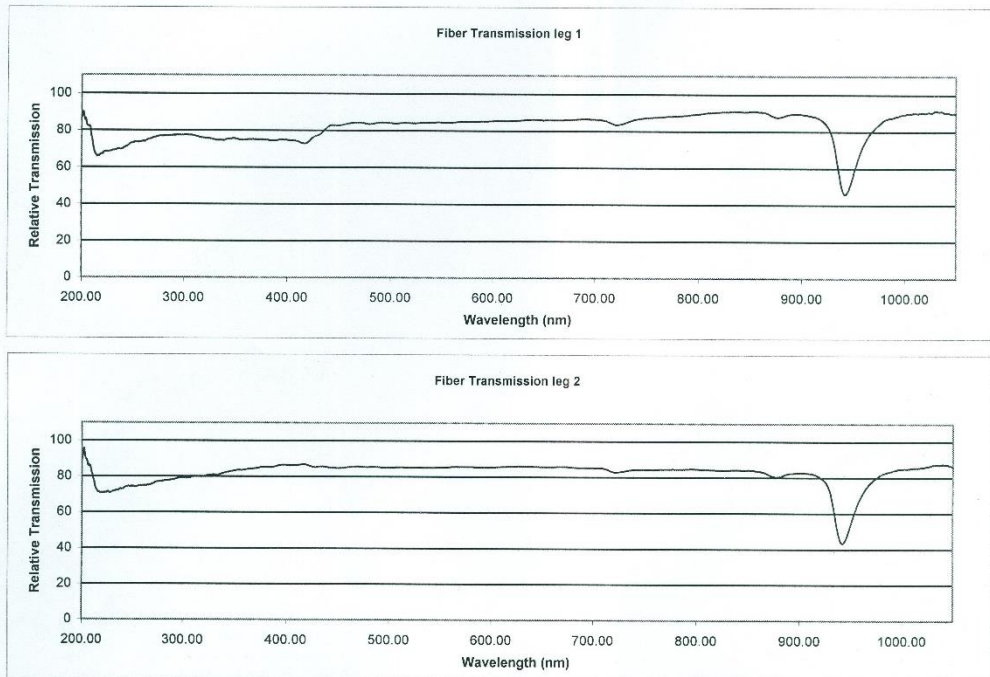
Part #: BIF400-UV-VIS
 Date: September 15, 2013
 Assembly #: OOS-003503-04
 Connector 1 #: SMA-905
 Connector 2 #: SMA-905
 Common #: SMA-905
 Sales Order #: STOCK

www.OceanOptics.com
 Phone: 727-733-2447
 Fax: 727-733-3962
 Info@OceanOptics.com
 830 Douglas Ave.
 Dunedin, FL 34698

Ask about our custom line of Optical Probes and Assemblies.

Fiber Type: UV-VIS
 Fiber Core Diameter: 400um

Jacketing: Zip Tube
 Length (meters): 2.00



Inspection Checklist

Polish: X
 Concentricity: X
 Cap Placement: X
 Labeling: X
 Color Coding: X
 Ferrule length: X



Inspected by: Le Zhang
 Le Zhang

PRODUCT OF OCEAN OPTICS SHANGHAI PRC



RoHS - Compliant

Annex G – Research Ethics Committee approval

 HOSPITAL AMARAL CARVALHO <small>Fundação Amarel Carvalho</small>	FUNDAÇÃO HOSPITAL AMARAL CARVALHO	 Plataforma Brasil												
PARECER CONSUBSTANCIADO DO CEP														
DADOS DO PROJETO DE PESQUISA														
Título da Pesquisa: Espectroscopia de fluorescência para diagnóstico de lesões de pele clinicamente semelhantes														
Pesquisador: ANA GABRIELA SALVIO														
Área Temática: A critério do CEP														
Versão: 3														
CAAE: 38719514.8.0000.5434														
Instituição Proponente: FUNDACAO DOUTOR AMARAL CARVALHO														
Patrocinador Principal: Financiamento Próprio														
DADOS DO PARECER														
Número do Parecer: 1.171.687														
Data da Relatoria: 31/07/2015														
Apresentação do Projeto: Não aplicável.														
Objetivo da Pesquisa: Não aplicável.														
Avaliação dos Riscos e Benefícios: Não aplicável.														
Comentários e Considerações sobre a Pesquisa: Não aplicável.														
Considerações sobre os Termos de apresentação obrigatória: Não aplicável.														
Recomendações: Não aplicável.														
Conclusões ou Pendências e Lista de Inadequações: Foi submetido para análise documentos do qual o mais importante foram alterações no TCLE que trazem alterações que melhoram a qualidade do TCLE e contemplam aspectos éticos necessários.														
<table style="width: 100%; border: none;"><tr><td style="width: 33%;">Endereço: Rua das Palmeiras, 89</td><td style="width: 33%;"></td><td style="width: 33%; text-align: right;">CEP: 17.210-120</td></tr><tr><td>Bairro: VILA ASSIS</td><td></td><td></td></tr><tr><td>UF: SP</td><td>Município: JAU</td><td></td></tr><tr><td>Telefone: (14)3602-1194</td><td>Fax: (14)3602-1207</td><td style="text-align: right;">E-mail: cep.aurea@amaralcarvalho.org.br</td></tr></table>			Endereço: Rua das Palmeiras, 89		CEP: 17.210-120	Bairro: VILA ASSIS			UF: SP	Município: JAU		Telefone: (14)3602-1194	Fax: (14)3602-1207	E-mail: cep.aurea@amaralcarvalho.org.br
Endereço: Rua das Palmeiras, 89		CEP: 17.210-120												
Bairro: VILA ASSIS														
UF: SP	Município: JAU													
Telefone: (14)3602-1194	Fax: (14)3602-1207	E-mail: cep.aurea@amaralcarvalho.org.br												

Página 01 de 02



FUNDAÇÃO HOSPITAL
AMARAL CARVALHO



Continuação do Parecer: 1.171.687

Situação do Parecer:

Aprovado

Necessita Apreciação da CONEP:

Não

Considerações Finais a critério do CEP:

O colegiado acompanha o parecer do relator.

Solicitamos que antes de iniciar a pesquisa, o pesquisador encaminhe-se ao RH para providenciar o crachá para que seja permitida a sua entrada no Hospital.

Informamos que nenhum dos pesquisadores envolvidos no estudo participou da votação.

Aproveito para recordar-lhe do compromisso de enviar relatórios semestrais referentes à evolução do estudo.

JAU, 05 de Agosto de 2015

Assinado por:
Oswaldo Contador Junior
(Coordenador)

Endereço: Rua das Palmeiras, 89

Bairro: VILA ASSIS

CEP: 17.210-120

UF: SP

Município: JAU

Telefone: (14)3602-1194

Fax: (14)3602-1207

E-mail: cep.aurea@amaralcarvalho.org.br

Annex H – Confidentiality Agreement

TERMO DE CONFIDENCIALIDADE

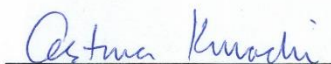
Eu, Ana Gabriela Salvio do RG nº 23.881.810-x e do CPF nº 245.869.848-48, Dermatologista do Hospital Amaral Carvalho de Jahu, CRM 93709-SP, residente na cidade de Jahu, que este subscreve, comprometo-me a manter o sigilo das informações contidas nos prontuários médicos que estarei acessando como nome e demais dados pessoais, para fins do Projeto de Pesquisa Intitulado: "Espectroscopia de fluorescência para diagnóstico de lesões de pele clinicamente semelhantes", bem como a manter o sigilo das informações contidas no banco de dados, trabalhando conforme os preceitos éticos da pesquisa.

Por fim, declaro estar ciente dos fins para os quais as informações serão utilizadas e assumo a responsabilidade civil, administrativa e criminal pela confidencialidade destas informações, a partir desta data, inclusive perante terceiros, respondendo judicialmente pelos prejuízos causados devido ao uso inadequado ou eventual má fé na divulgação e / ou utilização das mesmas, que constituem crimes previstos no Código Penal Brasileiro.

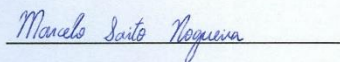
Jahu, 08 agosto 2014.



Ana Gabriela Salvio
Dermatologista- CRM 93709-SP



Cristina Kurachi
Professora Doutora do Instituto
de Física de São Carlos/USP



Marcelo Saito Nogueira
Mestrando do Instituto de Física de São Carlos/USP

**Annex I – Letter for the analysis of the project sent to the Research Ethics
Committee of Amaral Carvalho Hospital**

Ofício de Encaminhamento

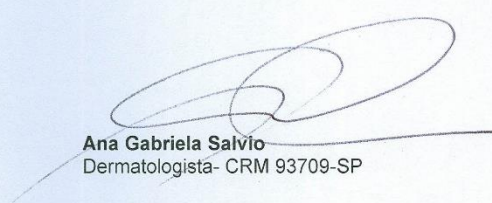
Jahu, 22 de setembro de 2014

Ilmo. Dr.
Éderson Roberto de Mattos
Coordenador do Comitê de Ética em Pesquisa
Fundação Hospital Amaral Carvalho

Prezado Doutor,

Sirvo-me do presente para encaminhar o Projeto de Pesquisa intitulado "Espectroscopia de fluorescência para diagnóstico de lesões de pele clinicamente semelhantes", de minha autoria, sob a orientação de Ana Gabriela Salvio, para análise deste Comitê de Ética em Pesquisa.

Atenciosamente,



Ana Gabriela Salvio
Dermatologista- CRM 93709-SP

Annex J – General data about the research project at Amaral Carvalho Hospital



MINISTÉRIO DA SAÚDE - Conselho Nacional de Saúde - Comissão Nacional de Ética em Pesquisa – CONEP

FOLHA DE ROSTO PARA PESQUISA ENVOLVENDO SERES HUMANOS

1. Projeto de Pesquisa: Espectroscopia de fluorescência para diagnóstico de lesões de pele clinicamente semelhantes		2. Número de Participantes da Pesquisa: 70	
3. Área Temática:			
4. Área do Conhecimento: Grande Área 1. Ciências Exatas e da Terra			
PESQUISADOR RESPONSÁVEL			
5. Nome: ANA GABRIELA SALVIO			
6. CPF: 245.869.848-48		7. Endereço (Rua, n.º): BENEDITO FERRAZ DE ALMEIDA PRADO JARDIM SANTA ROSA 301 JAU SAO PAULO 17209620	
8. Nacionalidade: BRASILEIRO		9. Telefone: (14) 3626-6190	10. Outro Telefone: 11. Email: gasalvio@hotmail.com
12. Cargo:			
<p>Termo de Compromisso: Declaro que conheço e cumprirei os requisitos da Resolução CNS 466/12 e suas complementares. Comprometo-me a utilizar os materiais e dados coletados exclusivamente para os fins previstos no protocolo e a publicar os resultados sejam eles favoráveis ou não. Aceito as responsabilidades pela condução científica do projeto acima. Tenho ciência que essa folha será anexada ao projeto devidamente assinada por todos os responsáveis e fará parte integrante da documentação do mesmo.</p> <p>Data: 25 / 09 / 14</p> <p style="text-align: right;">Assinatura</p>			
INSTITUIÇÃO PROPONENTE			
13. Nome: FUNDACAO DOUTOR AMARAL CARVALHO		14. CNPJ: 50.753.755/0001-35	
15. Unidade/Órgão:			
16. Telefone: (14) 3602-1200		17. Outro Telefone:	
<p>Termo de Compromisso (do responsável pela instituição): Declaro que conheço e cumprirei os requisitos da Resolução CNS 466/12 e suas Complementares e como esta instituição tem condições para o desenvolvimento deste projeto, autorizo sua execução.</p> <p>Responsável: Antonio Luis C. de Moraes Nobre CPF: 044.878.668-04</p> <p>Cargo/Função: Diretor Superintendente</p> <p>Data: 02 / 10 / 14</p> <p style="text-align: right;">Assinatura</p>			
PATROCINADOR PRINCIPAL			
Não se aplica.			

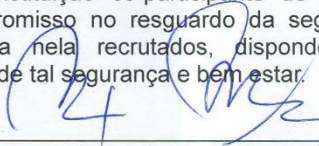
Annex L – Authorization for the development of the proposed research project

Jahu, 08 de agosto de 2014.

Ao
Comitê de Ética em Pesquisa da Fundação Hospital Amaral Carvalho
Autorização para realização de pesquisa

Eu, Ary Assumpção Júnior do RG nº 8261930-X e do CPF nº 077.119.378-57, Cirurgião Plástico do Departamento de Pele e Partes Moles, Jahu, venho por meio desta informar a V. Sa. que autorizo a pesquisadora Dra. Ana Gabriela Salvio desenvolver a pesquisa intitulada **"Espectroscopia de fluorescência para diagnóstico de lesões de pele clinicamente semelhantes"**.

Declaro conhecer e cumprir as Resoluções Éticas Brasileiras, em especial a Resolução CNS 196/96. Esta instituição está ciente de suas co-responsabilidades como instituição co-participante do presente projeto de pesquisa, e de seu compromisso no resguardo da segurança e bem-estar dos sujeitos de pesquisa nela recrutados, dispondo de infra-estrutura necessária para a garantia de tal segurança e bem-estar.



"Assinatura e carimbo do chefe do serviço"